Vol.
1
1961

INFRARED PHYSICS

AN INTERNATIONAL RESEARCH JOURNAL

VOLUME 1 1961

Editors:

P. Goerlich : M. Migeotte : T. S. Moss
S. Passman : W. K. Weihe

Supported by an International
Advisory Editorial Board

Copyright © 1961
Pergamon Press Ltd.

Pergamon Press

OXFORD · LONDON · NEW YORK · PARIS

INFRARED PHYSICS

Board of Editors

P. GOERLICH — Director for Research and Development, VEB Carl Zeiss, Jena, Germany.
M. MIGEOTTE — Université de Liège, Institut d'Astrophysique, Cointe-Solessin, Belgium.
T. S. MOSS — Royal Aircraft Establishment, Radio Department, Ambarrow Court, Lower Sandhurst Road, near Camberley, Surrey, England.
S. PASSMAN — The RAND Corporation, 1700 Main Street, Santa Monica, California, U.S.A.
W. K. WEIHE — U.S. Army Engineer Research and Development Laboratories, Fort Belvoir, Virginia, U.S.A.

Honorary Editorial Advisory Board

ARTHUR ADEL, Flagstaff
BØRGE BAK, Copenhagen
STANLEY S. BALLARD, Gainesville
PIERRE BARCHEWITZ, Paris
R. BOWLING BARNES, Stamford, Connecticut
ELY E. BELL, Columbus
G. A. BOUTRY, Paris
E. F. DALY, Cambridge
G. F. J. GARLICK, Hull
H. A. GEBBIE, Teddington
L. GENZEL, Freiburg, i.Br.
LEO GOLDBERG, Cambridge, Massachusetts
R. M. GOODY, Cambridge, Massachusetts
JOHN HAMPSON, Quebec
C. HILSUM, Baldock
J. T. HOUGHTON, Oxford
J. H. JAFFE, Rehovoth
R. CLARK JONES, Cambridge, Massachusetts
R. V. JONES, Aberdeen
J. LECOMTE, Paris
HENRY LEVINSTEIN, Syracuse, New York
R. MECKE, Freiburg i.Br.
G. A. MORTON, Princeton
L. G. MUNDIE, Ann Arbor
R. PENNDORF, Wilmington, Massachusetts
R. L. PETRITZ, Dallas
GILBERT N. PLASS, Newport Beach, California
DAVID Z. ROBINSON, Washington, D.C.
J. H. TAYLOR, Memphis, Tennessee
HIROSHI YOSHINAGA, Osaka
GEORGE J. ZISSIS, Ann Arbor

Publishing Offices

Pergamon Press Limited, Headington Hill Hall, Oxford, England;
Pergamon Press, Inc., 122 East 55th Street, New York 22, N.Y.

Annual Subscription Rates

(A) For libraries, government establishments, research laboratories, etc.: £7 ($20.00)
(B) For individuals who place their orders directly with the publisher and certify that the journal is for their personal use: £3 10*s*. ($10.00)

Copyright © 1961
Pergamon Press Ltd.

PERGAMON PRESS LIMITED

HEADINGTON HILL HALL, OXFORD

122 EAST 55TH STREET, NEW YORK 22, N.Y.

Vol 1 196

Vol.
1
1961

VOLUME 1

NUMBER 1/2

E. SCOTT BARR: The infrared pioneers—I. Sir William Herschel 1

N. C. BEESE: Light sources for optical communication 5

D. F. EDWARDS and M. MERCADO: Ultimate sensitivity and practical performance of the tellurium photoconductive detector 17

S. NIELSEN, W. D. LAWSON and A. F. FRAY: Some infrared transmitting glasses containing germanium dioxide 21

P. BRATT, W. ENGELER, H. LEVINSTEIN, A. MACRAE and J. PEHEK: A status report on infrared detectors 27

H. HAPP und L. GENZEL: Interferenz-Modulation mit monochromatischen Millimeter-Wellen 39

P. A. LAPP and H. S. KERR: Sunseeker for high-altitude infrared solar spectra 49

H. KALLMANN, J. RENNERT and M. SIDRAN: Infrared photography using persistent internal polarization in phosphor plates 58

C. HILSUM and W. R. HARDING: The theory of thermal imaging, and its application to the absorption-edge image-tube 67

R. BEER and J. RING: A high-pressure scanning Fabry–Perot interferometer for the infrared . . 94

T. S. MOSS and A. G. PEACOCK: Infrared optical properties of lead halides (Research Note) . . 104

R. H. TOURIN: Infrared spectral emissivites of CO_2 in the 2·7 micron region 105

T. S. MOSS and T. D. F. HAWKINS: Infrared absorption in gallium arsenide 111

J. S. SEELEY and J. T. HOUGHTON: Spectroscopic observations of the vertical distribution of some minor constituents of the atmosphere 116

J. A. JAMIESON: Inference of two-dimensional Wiener spectra from one-dimensional measurements 133

J. J. MCARDLE: Effect of cooled apertures in PbS detectors 146

R. V. JONES: Infrared detection in British air defence, 1935–38 153

N. C. ANDERSON: Comparative performance of cooled infrared photoconductors 163

NUMBER 3

P. S. MCDERMOTT, R. L. POWELL and E. R. STACK: Infrared measurements of the optical constants of the low melting temperature glass system of 30% Arsenic—34% Sulfur—36% Thallium . 167

A. F. FRAY and S. NIELSEN: Germanate glasses: Removal of OH absorption bands 175

E. R. STEPHENS: Long-path infrared spectroscopy for air pollution research 187

H. P. WURTZ: Complete liquefaction cryostat 197

R. R. BILLUPS and W. L. GARDNER: Radiation damage experiments on PbS infrared detectors . 199

G. F. J. GARLICK and H. CHECINSKA: Recombination radiation and photoconduction efficiency in lead sulphide layers 209

R. P. DAY, R. A. WALLNER and E. A. LODI: An experimental study of energetic proton radiation effects on IR1 lead sulfide infrared detectors 212

Book Review 225

AUTHOR INDEX TO VOLUME I

Anderson N. C., 163
Beer R., 94
Beese N. C., 5
Billups R. R., 199
Bratt P., 27
Checinska H., 209
Day R. P., 212
Edwards D. F., 17
Engeler W., 27
Fray A. F. 21, 175
Gardner W. L., 199
Garlick G. F. J., 209
Genzel L., 39
Happ H., 39
Harding W. R., 67
Hawkins T. D. F., 111
Hilsum C., 67
Houghton J. T., 116
Jamieson J. A., 133
Jones R. V., 153
Kallmann H., 58
Kerr H. S., 49
Lapp P. A., 49
Lawson W. D., 21
Levinstein H., 27
Lodi E. A., 212
MacRae A., 27
McArdle J. J., 146
McDermott P. S., 167
Mercado M., 17
Moss T. S., 104, 111
Nielsen S., 21, 175
Peacock A. G., 104
Pehek J., 27
Powell R. L., 167
Rennert J., 58
Ring J., 94
Scott Barr E., 1
Seeley J. S., 116
Sidran M., 58
Stack E. R., 167
Stephens E. R., 187
Tourin R. H., 105
Wallner R. A., 212
Wurtz H. P., 197

Vol
1
196

Infrared Physics, 1961, Vol. 1, pp. 1–4. Pergamon Press Ltd., Printed in Great Britain.

THE INFRARED PIONEERS—I. SIR WILLIAM HERSCHEL

E. SCOTT BARR

Department of Physics, University of Alabama, U.S.A.

THE discovery that radiation existed outside the visible spectral region was made by Sir William Herschel in the spring of the year 1800. While it would be wrong to describe the discovery as accidental, it was without doubt a by-product, for Herschel was involved in a search for a solution to an astronomical problem. In order to facilitate his studies of sunspots, he was seeking some filtering technique which would give adequate light for seeing, without undesirable heating.

His first step toward the design of such a filter was to undertake a careful survey of the distribution of thermal energy in the visible solar spectrum. To do this he formed a prismatic spectrum on a table top in a dark room and placed one of two identical sensitive thermometers at various positions in the spectrum, in each case comparing the equilibrium temperature reached with that of the other thermometer which was unilluminated. The arrangement is seen in Fig. 1.

He found that the thermometer rise increased as he went from the violet to the red, and that, I quote, "it appears that the maximum of the full red falls still short of the maximum of heat; which perhaps lies even a little beyond visible refraction. In this case, radiant heat will at least partly, if not chiefly, consist, if I may be permitted the expression, of invisible light". [1]

Immediately following this report is to be found the first paper devoted to an infrared investigation. [2] This paper discusses the measurements he made in the region adjoining the red end of the spectrum and which led him to the conclusion that the radiation found there was of the same nature as visible light.

The methodical thoroughness which was so characteristic of Herschel impelled him to go further into the matter and he undertook a comprehensive study of the radiation from a candle, from a fireplace fire, and from a hot poker, to supplement his solar measurements. [3] While he found in every case that the invisible radiation obeyed the same laws of reflection and refraction that governed visible light, his quantitative comparison of visible radiation and thermal radiation in the solar spectrum brought out the fact that the regions which were brightest were not the regions of greatest observed heating. Herschel examined objects placed in various parts of the spectrum and made subjective judgments as to the relative illuminating capabilities of the different colors of light. His opinions as to the "relative luminosity" gave the curve marked *R* in Fig. 3, where the visible is subdivided according to the domains designated by Newton. The curve *S*, bounding the shaded area, shows the relative heating effects observed by him. We see that if one makes allowance for the fact that Herschel's curve of "luminosity" was entirely subjective, and that he had no way of measuring wavelengths, it is apparent that his values are not greatly in disagreement with the correct distribution curve for energy as a function of wavelength. At the same time his "thermal" curve appears entirely discordant due to the fact that the prismatic spectrum

has increasingly poor dispersion as we go toward longer wavelengths, with the result that a detector with a fixed intercept area collects the energy of progressively larger wavelength spans. This situation was, of course, entirely unknown to scientists at that time, for the first measurements of the wavelengths of light were just being achieved at that same time by Thomas Young. Thus we can understand how Herschel felt compelled to relinquish his belief that the visible and infrared radiations were of the same nature. To quote him again, "A mere inspection of the two figures, which have been drawn as lying upon one another, will enable us now to see how very differently the prism disperses the heat-making rays, and those which occasion illumination. . . . These rays neither agree in their mean refrangibility, nor in the situation of their maxima. At *R*, where we have the most light, there is little heat; and at *S*, where we have most heat, we find no light at all!" [3]

Of Herschel's papers only two others were concerned with infrared [4] for astronomy had been and remained his consuming interest. It was sufficient to him to have found a solution to his problem of viewing the sun, through the discovery that a "darkening glass" could be advantageously replaced by a layer of water tinted with ink. Apparently he gave little further thought to this momentarily distracting aspect of nature, which probably seemed unlikely to be of importance to his work. The same failure to recognize the importance of his discovery of the infrared region is surprisingly evidenced by the fact that no mention is made of his discovery in the *Encyclopaedia Britannica* sketch of his career!

When Friedrich Wilhelm Herschel was born on 15 November 1738, in Hanover, Germany, as the fourth child (of ten, two girls and four boys surviving childhood) in a Jewish family that had adopted the Protestant faith, his future prospects could not have been considered bright. His father was a music teacher and oboe player in the band of the Hanoverian Foot Guards, who saw to it that his children also became good musicians. By the age of fourteen William was an able performer on both oboe and violin, and he, too, joined the band, going with the Guards to visit England in 1755. After his return, the hardships of campaigning during the Seven Years' War resulted in his health being undermined, and his parents decided that it would be best for him to leave the Guards and go to England to try to earn a living there as a music teacher. His brother Jacob, who was four years older than William, also went to England, both arriving in 1757 with no funds, but neither was able to do much in the way of helping the other.

His first few years in England were a continual struggle with poverty, despite the fact that he was both a good teacher and performer, and an adequate composer. He finally became established as an organist at Bath and by about 1766 he had achieved a degree of security and an established position. After teaching 14 to 16 hours a day, he found relaxation with his books and devoted much time to educating himself. He studied Latin, Italian, French, English, and Greek. His study of harmony led him to a study of mathematics; this in turn led him to optics, and optics to astronomy—which he found of consuming interest. After first renting a small Gregorian telescope and having a taste of the wonders of the sky, he decided to make a better one of his own. Fortunately his brother Alexander (who was a violoncello player and who had joined William at Bath in 1770) was an able mechanical assistant. They undertook between them the casting of speculum metal blanks and the grinding of mirror surfaces into them. A second helper was found in his sister Caroline Lucretia (1750–1848) who was to become his invaluable lifelong assistant. (She had been cast by her mother in the role of housekeeper at home and had generally led the life of a slavey before being rescued by the brother she adored. He, in turn, agreed to send to his mother regular remittances sufficient to hire a servant to replace Caroline.) From her

Vol 1 196

Vol.
1
1961

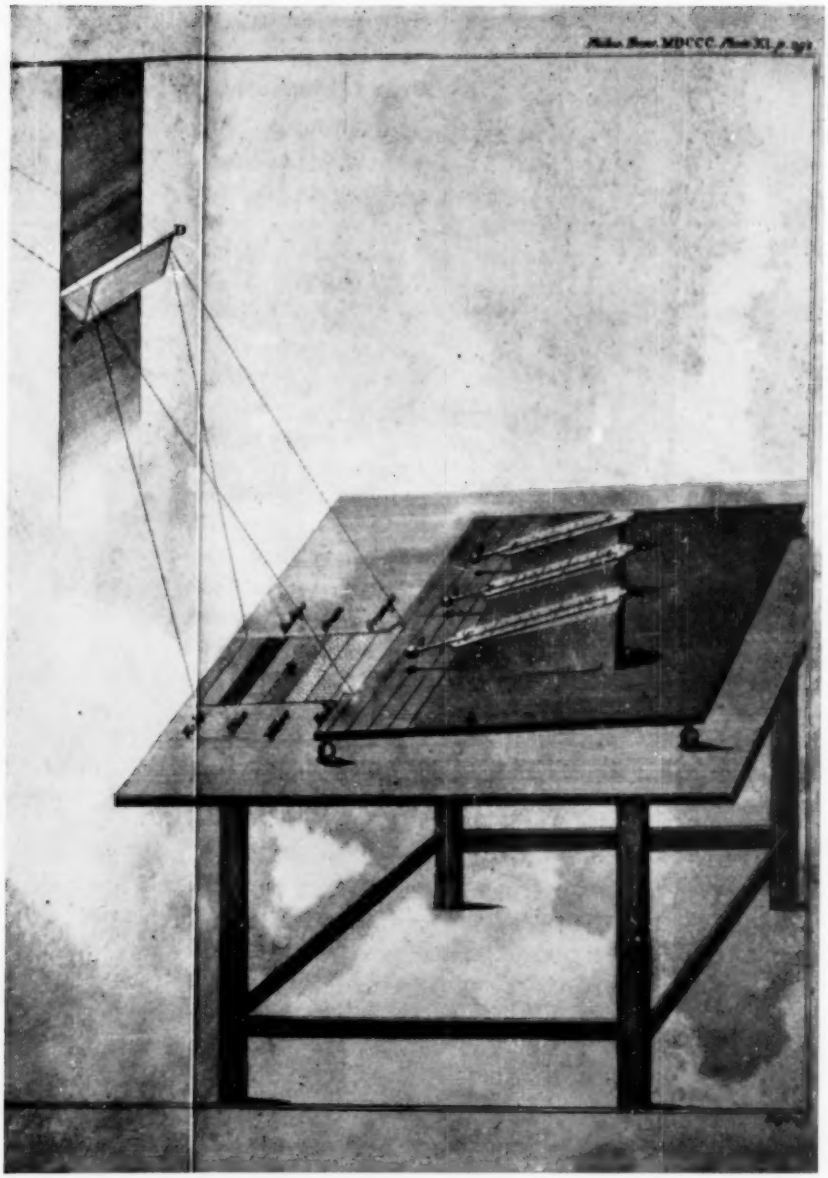

FIG. 1. Herschel's experimental arrangement, from *Phil. Trans.* Pt. II, **90**, 292 (1800).

Facing Page 2

XIV. *Experiments on the Refrangibility of the invisible Rays of the Sun.* *By* William Herschel, *LL. D. F. R. S.*

Read April 24, 1800.

In that section of my former paper which treats of radiant heat, it was hinted, though from imperfect experiments, that the range of its refrangibility is probably more extensive than that of the prismatic colours: but, having lately had some favourable sunshine, and obtained a sufficient confirmation of the same, it will be proper to add the following experiments to those which have been given.

I provided a small stand, with four short legs, and covered it with white paper.* On this I drew five lines, parallel to one end of the stand, at half an inch distance from each other, but so that the first of the lines might only be $\frac{1}{4}$ of an inch from the edge. These lines I intersected at right angles with three others; the 2d and 3d whereof were, respectively, at $2\frac{1}{2}$ and at 4 inches from the first.

The same thermometers that have before been marked No. 1, 2, and 3, mounted upon their small inclined planes, were then placed so as to have the centres of the shadow of their balls thrown on the intersection of these lines. Now, setting my little stand upon a table, I caused the prismatic spectrum to fall with its extreme colour upon the edge of the paper, so that none might advance beyond the first line. In this arrangement,

* See Plate XI.

FIG. 2. The first page of Herschel's original investigation of the infrared region, *Phil. Trans.* Pt. II, **90**, 284 (1800).

arrival in 1772 until his death, she was his indispensable assistant in his astronomical work.

The lack of equipment and the lack of instruction were formidable barriers, but after about 200 partial failures, Herschel achieved a satisfactory mirror for his first telescope in 1774, a 5·5 ft focal length instrument. From then on Herschel led a double life, teaching music in the day and sweeping the sky at night even when the temperature was down to 11 °F, meanwhile making more and more perfect mirrors whenever the opportunity arose. His sister recorded one occasion when he polished a mirror for 16 consecutive hours, never taking his hands from the speculum, while she fed him and read to him.

During the course of one of his observation nights (13 March 1781 to be exact) he noted an object which seemed too diffuse to be a star, and after testing by changing magnifications of the eyepiece, he decided that he had discovered a comet. The discovery was reported in his paper, "Account of a Comet" which appeared in the *Philosophical Transactions of the Royal Society of London* of that year. Further careful study revealed the exciting truth: Herschel's "comet" was actually a new planet—URANUS! Herschel's great skill as an observer, and the quality of his telescope, are indicated by the fact that this same heavenly body had been observed seventeen times previously since 1690, but had always been taken to be a star.

Vol. 1 1961

The discovery revolutionized Herschel's life almost overnight. Later that same year he was awarded the Copley Medal by the Royal Society of London and made a Fellow of that body. The next year he was appointed Royal Astronomer to George III (in whose honour Herschel wished to name the new planet Georgium Sidus) at a salary of £200 a year, with an extra £50 for Caroline as his assistant. As it was put by Dr. William Watson, "Never before was honour purchased by a monarch at so cheap a rate." With this income to rely upon, Herschel turned from music to devote his full energy to astronomy, leaving Bath and moving to Slough, near Windsor.

There he perfected his skill as a mirror maker. Actually, with him it was something nearer an art, for he had the equivalent of a gardener's green thumb. His mirror surfaces were not computed, but given their final adjustments on the basis of their performance in actual use. Although he did once use a glass mirror backed with black velvet to look at the sun, most of his mirrors were formed from tin–copper alloy blanks. His fame as a telescope maker spread rapidly and widely, and between 1788 and 1795 he supplied 200 7-ft, 150 10-ft, 80 20-ft, and many smaller telescopes. His 10-ft ones sold for 600 guineas and a 25-ft one brought him £3150 in 1796. His greatest achievement was a mirror weighing 1900 lb, 48 in. in diameter, $3\frac{1}{2}$ in. thick and with a 40 ft focal length, which was finished in 1789. His instruments were remarkable in terms of the perfection of their figuring, which made it possible to use high power eyepieces with them. For some of his observations, Herschel used magnifications of slightly above 6000×. His telescopes were designed for viewing rather than measurement, however, and even the largest ones were mounted on simple frameworks. For the 40-ft telescope, observations were made from a 50-ft ladder. Herschel, by the way, introduced his own mounting, in which he tilted the mirror slightly so as to bring the focal point to the edge of the tube at the front end for observation there, so as to avoid the loss of light implicit in the Newtonian, Gregorian, or Cassegranian mounts.

Life at Slough was a happy one for Herschel despite the fact that he spent his energy prodigally. Between dark and dawn he sometimes observed as many as 400 objects, calling off their locations and descriptions to Caroline who sat by a shaded lamp nearby. He once worked on his mirrors and observed continuously for three days and nights, then slept for

twenty-six hours. His work was reported chiefly in sixty-nine memoirs published in the *Philosophical Transactions*, and cannot be treated here in detail. He devoted much attention to sunspots, the sun and its motion relative to the other stars, double stars, and nebulae (increasing the known number of them from ninety-six to more than 2500). He also identified the ice caps of MARS as such.

When he was naturalized in 1793, he took the name William Herschel: he was knighted in 1816. His marriage in 1788 to the widow of a wealthy London merchant relieved him of all financial worries. Their only child, John Frederick William (1792–1871) became famous in his own right in the fields investigated earlier by his father, as well as in others. Honours came to Herschel from all sides and his home became a scientific Mecca. As an individual he was characterized by faithfulness to his friends, strong family affections, and social charm. Throughout all his life music remained his recreation. His health remained good until he suffered a severe illness when sixty-nine, and at seventy-six was described as "fresh and stout". He continued to work until he was eighty, when increasing physical weakness brought an accompanying lowering of his spirits, although his intellect remained clear. Finally, as a result of a bilious fever, he died on 25 August 1822, at Slough.

To persons wishing a more detailed treatment of his life, I recommend, *William Herschel. Explorer of the Heavens*, by J. B. SIDGWICK (Faber and Faber Ltd., London, 1953) and the sketch in the *Dictionary of National Biography*. Mention should also be made of the fact that good, inexpensive reproductions of an engraved portrait of Herschel (9·6 cm by 10·5 cm) are available from Gauthier-Villars, Paris.

Vol 1 196

REFERENCES

1. HERSCHEL, W., *Phil. Trans.* Pt. II, **90**, 255 (1800).
   Reprinted in full in *Phil. Mag.* **7**, 311 (1800).
2. HERSCHEL, W., *Phil. Trans.* Pt. II, **90**, 284 (1800).
   Reprinted in full in *Phil. Mag.* **8**, 9 (1800).
3. HERSCHEL, W., *Phil. Trans.* Pt. II, **90**, 293 and 437 (1800).
4. HERSCHEL, W., *Phil. Trans.* **91**, 265 and 354 (1800).

Vol.
1
1961

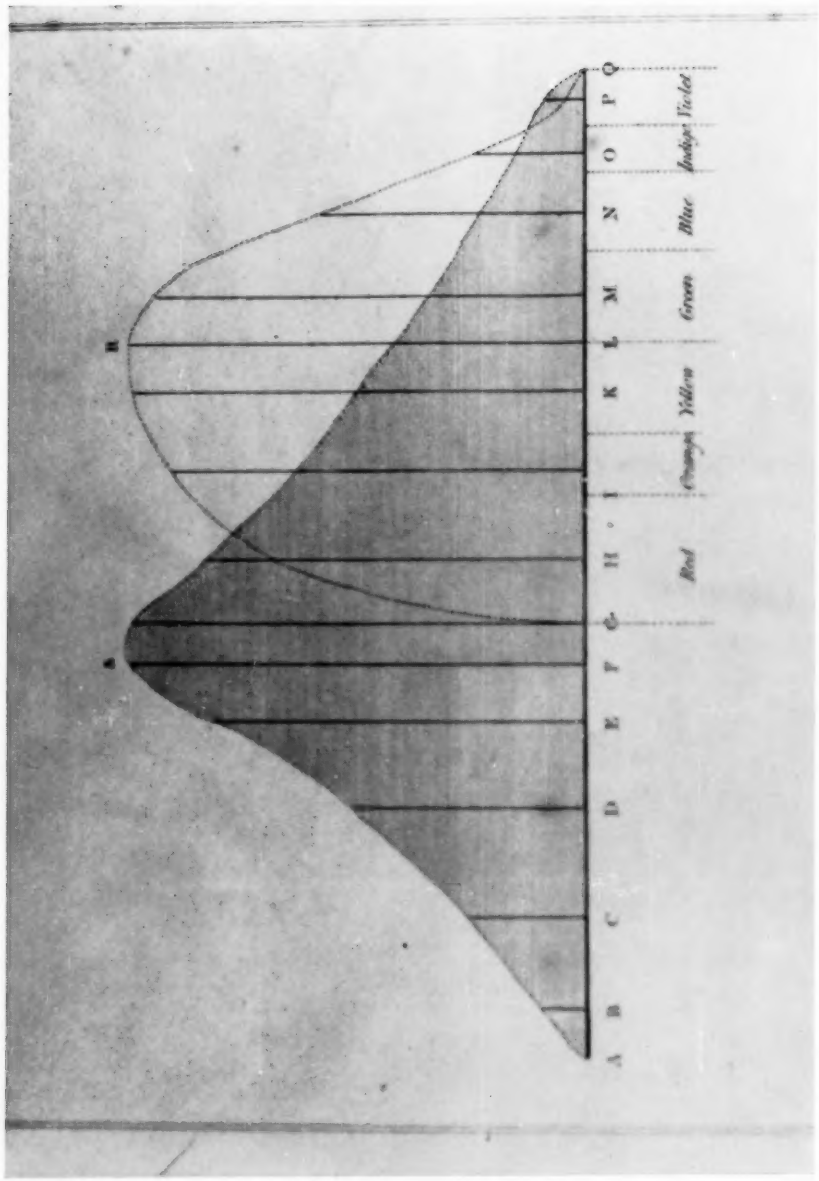

FIG. 3. Herschel's curves for the comparison of "luminosity" with heating effect. *Phil. Trans.* Pt. II, **90**, 538 (1800).

Facing Page 4

FIG. 4. William Herschel, reproduced through the courtesy of the publisher Gauthier-Villars, Paris.

FIG. 5. William Herschel; portrait by Lemuel Abbott in the National Portrait Gallery at South Kensington, from *Illustrated London News* **58**, 485 (1871).

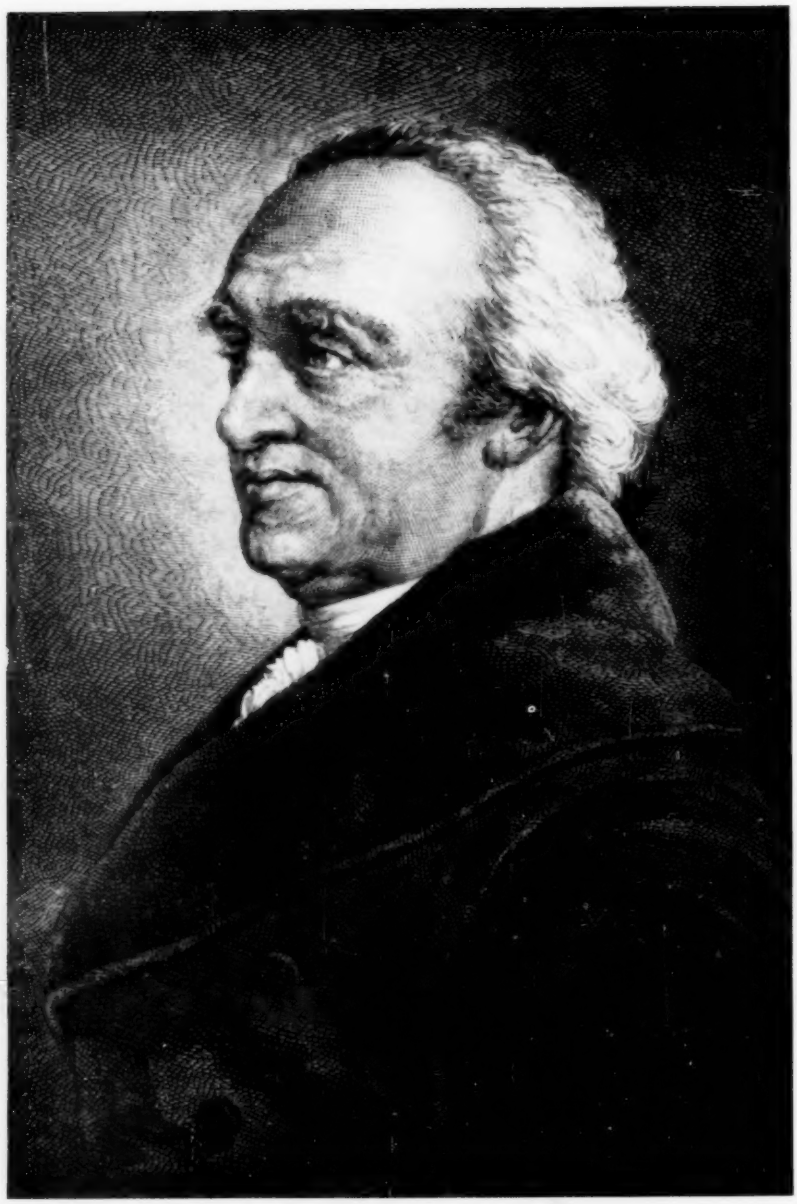

FIG. 6. William Herschel, from the engraving by Henry Velten after a drawing by H. Grevedon in the British National Gallery, from *Century* **30**, 181 (1885).

Vol.
1
1961

Infrared Physics, 1961, Vol. 1, pp. 5–16. Pergamon Press Ltd., Printed in Great Britain.

LIGHT SOURCES FOR OPTICAL COMMUNICATION

N. C. BEESE

Westinghouse Electric Corporation, Bloomfield, N.J., U.S.A.

Abstract—Several modulated light sources of historical nature are described which have been used in transmitting intelligence to distant points. Some of the characteristics of cesium-vapor lamps and high-intensity short-arc xenon lamps are described. The phenomenon of acoustical resonance in enclosed arcs is discussed.

ol.
1
961

FOR centuries man has used light as a means of communication over distances greater than those over which his voice could be heard. American Indians used fires at night and smoke signals by day to transfer news to their distant friends. Such signals are simple, slow in execution, and very limited in range of usefulness.

Sailors use a blinker system of long and short flashes of light from a searchlight beam by means of which letters and words may be transmitted to a distant observer. While any message may be relayed in this manner, the speed is relatively slow—of the order of 6–8 words/min. The chief advantage of this system is simplicity of operation, since it consists merely of a shutter in front of a searchlight for the transmitter and the eyes of the observer for the receiver. By interrupting or "keying" the current through special incandescent lamps filled with hydrogen gas, and by using thyratron-controlled electrical circuits, one may obtain a speed of about 10–12 words/min.[1] This is limited by the heating and cooling times of the filament.

Accustomed to high-speed voice communication over telephone lines or radio, we would like to transmit speech over a searchlight beam as an improvement over the present blinker system. This idea is not new, for in 1880 Dr. Alexander Graham Bell, inventor of the telephone, described two methods of modulating a beam of light from a steady source with voice frequencies.[2] Sunlight was the light source, while his stethoscope was the receiver. These ideas were not developed into a practical device because of the mechanical difficulties involved. Bell's early experiments were limited to a range of several hundred yards. Optical systems have greater security than radio, which is very important in military applications. A searchlight beam is limited to horizon distances and cannot be intercepted or interrupted by unauthorized persons. Visual security is readily obtained with visibly-opaque but infrared-transparent filters.

MAJOR REQUIREMENTS FOR SPEECH TRANSMISSION

To transmit speech by light, three major requirements must be fulfilled. First, it is necessary to modulate a beam of light so that it varies in intensity and frequency with voice vibrations. Second, these variations in light intensity must be picked up at a distant station and transformed back into audible sounds by electric means. Third, the atmosphere must be sufficiently transparent to permit the transmission of radiant energy.

We have a choice of many light sources at our disposal, depending upon what auxiliary mechanical and electrical equipment is used. A vapor or gas-discharge lamp may be

modulated with audio-frequency currents superimposed upon the normal direct current with good efficiency because of its low thermal inertia. In this scheme the source of light itself is modulated. An incandescent tungsten filament lamp of the common 120 V household type can be current-modulated with audio frequencies, but it has relatively poor efficiency, especially at the higher frequencies because of the relatively high heat-capacity of the filament. One may also modulate the flux of light emitted by any source of constant intensity—artificial or sunlight—with suitable mechanical or optical systems of small inertia. In this method the light beam is modulated after it leaves the source.

Modern photocells of the photoemissive or photoconductive types, with suitable electronic amplification, make satisfactory receivers. The most common are silver–oxygen–cesium vacuum or gas-filled phototubes, and selenium, thallous sulfide, and lead sulfide photoconductive cells.[3]

Between the light source and the receiver is the atmosphere that scatters, absorbs and transmits the signals with variable degrees of efficiency. This is a factor of great importance, but is generally neglected for short ranges of transmission. Even a small amount of smoke or fog greatly reduces both the visibility and the transmission of infrared energy. There is also the molecular absorption of water vapor and carbon dioxide gas in the air that limits long-range operations to a few isolated wavelength bands or windows in the infrared.[4]

Up to the present time the most useful spectral band of infrared energy for optical communication is in the zone between 8000 Å and 12,000 Å. A number of available-light sources and phototube detectors have good efficiency in this region, and there are also several filters that can be used to screen out the unwanted visible light, yet transmit this near-infrared energy very efficiently.[5] A serious objection to using this atmospheric window is that the near-infrared energy is readily detected with infrared image-converter tubes.[6] A more desirable communication system would be one that utilizes longer wavelengths in the infrared.

For low-power portable devices it might be desirable to use infrared-emitting phosphors excited by cathode rays as a source of pre-selected infrared energy.[7] In this system one of the longer-wave atmospheric windows could be utilized. Lead sulfide or lead selenide phototubes might then be used as detectors.

MODULATED GAS FLAMES

Almost 100 years ago Koenig demonstrated that a small gas flame could be modulated with audio frequencies. He used a device called a manometric capsule (Fig. 1) which consisted

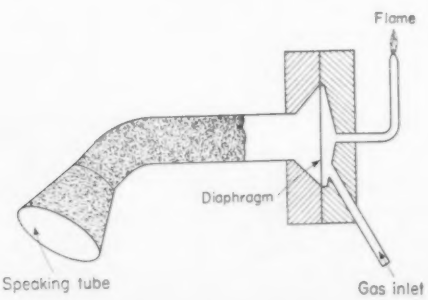

FIG. 1. Koenig's manometric capsule involving modulation of a gas flame.

of a shallow cavity in a block of wood, one side of which was covered with a flexible diaphragm.[8] Two pipes were connected with the cavity, one leading to the gas supply and the other to a lighted gas jet that formed a flame about 2 cm high. When words were spoken into the speaking tube, the gas in the small chamber changed its pressure rapidly and caused fluctuations in the height and brightness of the flame. Changes in light intensity were observed as reflections on the rotating mirror. Even with a modern photocell for a detector the quality of the sound emitted by this source is poor.

PHOTOPHONE

During 1916 Professor Rankine developed his photophone,[9] a device which could carry speech over a light beam to a distance of several miles. The theory of its operation is sketched in diagrammatic form in Fig. 2. A source of light, either artificial or sunlight, was focussed by a lens upon a small concave mirror that was mechanically coupled to a

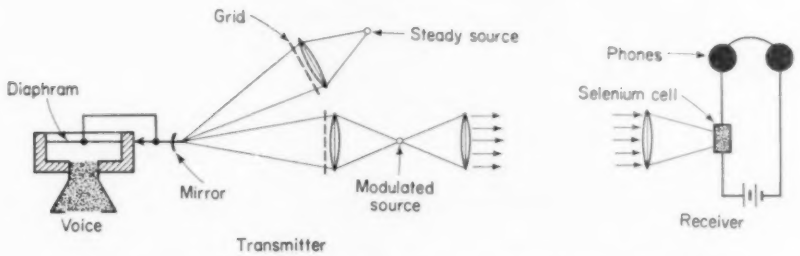

FIG. 2. Rankine's photophone involving voice transmission by modulated light.

telephone-transmitter diaphragm. The mirror reflected the incident light to another similar lens and produced a real image of the source behind it. Similar grids of equally spaced opaque and transparent bars were mounted in front of each lens. When the mirror oscillated under the excitation of speech vibrations, the image of the first grid moved over the second grid and thus produced variations in the light intensity that emerged from the searchlight beam. This accomplished what Dr. Bell failed to do, in using a grid without inertia. In this system only half of the light is usable, since half is wasted by the opaque grids. Signals were received at a distant station on a selenium photocell that converted the light pulses into sounds. This device had not been developed to a practical state during World War I. A by-product of Rankine's research was the recording of sound by photographic means on a moving ribbon of film and the reproduction of the sound at a later time. This development added sound to silent movies.

GERMAN LICHTSPRECHERS

Since 1935 the German Army has used light-beam communication equipment which employed novel optical components.[10] As shown in Fig. 3, light from a small low-wattage tungsten-filament lamp is reflected from the inner surfaces of the glass prism and then out through the objective lens of the searchlight. Voice modulation is produced by rocking the small prism against the larger one. When the small prism is in contact with the large one, light passes through the interface to the observation tube. When removed by only about one wavelength of light (1/25,000 in.) practically all the light is transmitted by internal reflection to the searchlight objective lens. This system gives nearly 100 per cent light

modulation in the beam. Fig. 4 illustrates the optical system of another *Lichtsprecher*. Here the opaque grids of Rankine's photophone are replaced by prisms of high optical performance. These devices are illustrations that the flux of light from a source of constant intensity can be modulated by mechanical–optical methods. With suitable filters these

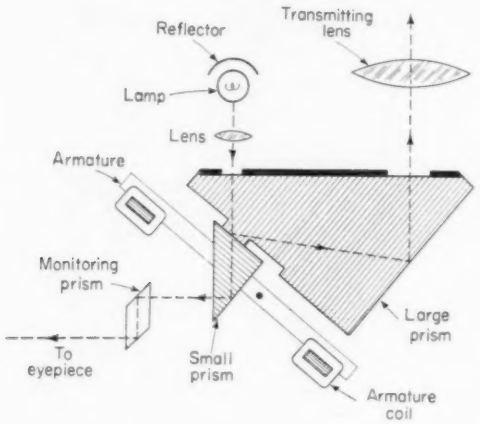

FIG. 3. Modulator system of German *Lichtsprecher*.

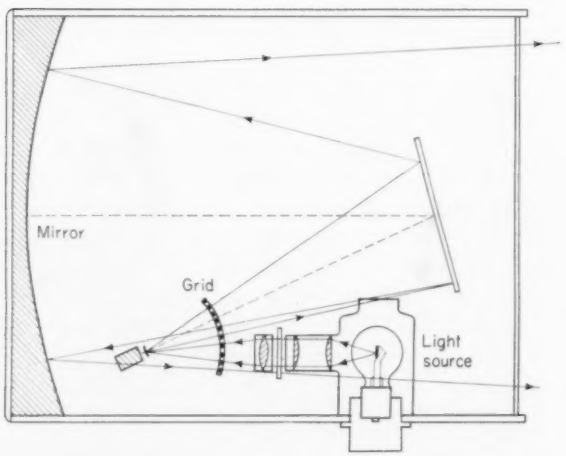

FIG. 4. Transmitter optics of long-range German *Lichtsprecher*.

instruments could be turned into secret communication systems using only infrared radiation. The detectors were lead sulfide photoconductive cells cooled with dry ice to obtain increased sensitivity.

CESIUM-VAPOR LAMPS

During 1944 the U.S. Navy sponsored researches in industrial and university laboratories that led to the development of a successful wireless-telephone system in which conversations

Vol. 1 1961

were carried by a beam of infrared light. The assignment involved the development of the cesium-vapor arc into a practical light source.[11] Cesium vapor was selected because of the location of its resonance spectral lines at 8521 and 8944 Å. It was known that this type of radiation could be generated very efficiently; e.g. the yellow *D* lines of sodium vapor produce one of our most efficient light sources, and the 2537 Å resonance radiation of mercury vapor produces our most efficient ultraviolet source. This radiation is used for energizing fluorescent lamps and bactericidal lamps. By analogy with sodium and mercury vapor, cesium vapor should produce near-infrared rays very efficiently under suitable conditions. As a result of the use of a vapor, the lamp had high modulability for voice frequencies.

The research program resulted in the development of the CL–2 lamp shown in outline in Fig. 5. The source of light is the inner bulb, 1·37 in. in diameter and 5 in. long, with an arc length of 3 in. between electrodes. This size produced a 25° beam spread in a 15 in. reflector. The bulb has two electrodes to anchor the arc to its center. The lamp contains argon gas at about 20 cm of mercury pressure and several tenths of a gram of cesium metal. The partial pressure of cesium vapor during normal operation was about 3 mm of mercury pressure. An outer evacuated envelope is used to conserve heat, for the inner bulb operates at a temperature of about 325 °C. Spectrograms show that most of the useful energy radiated by this lamp is in the resonance lines, 8521 and 8944 Å. At a steady current of 5·5 A the useful life is over 500 hr. About 21 per cent of the power supplied to the lamp is

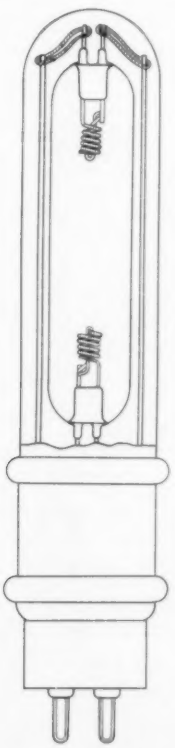

FIG. 5. 100 W cesium-vapor lamp.

radiated as near-infrared radiation. At 6 A and 17 V (102 W), it would require a 675 W tungsten-filament lamp to give the same total amount of infrared, as measured with a cesium photocell through filters that give the same visual security to the lamps. Throughout the life of the lamp the intensity of the infrared radiation remains practically constant. The end of life occurs when the infrared intensity drops very abruptly to a low value, as a result of the absorption of the cesium by the glass bulb. The discharge then becomes essentially an argon arc with very low infrared intensity.

Figure 6 shows how a cesium-vapor lamp is incorporated into a communication system. The lamp is mounted in a reflector with an infrared filter on the front to give visual security.

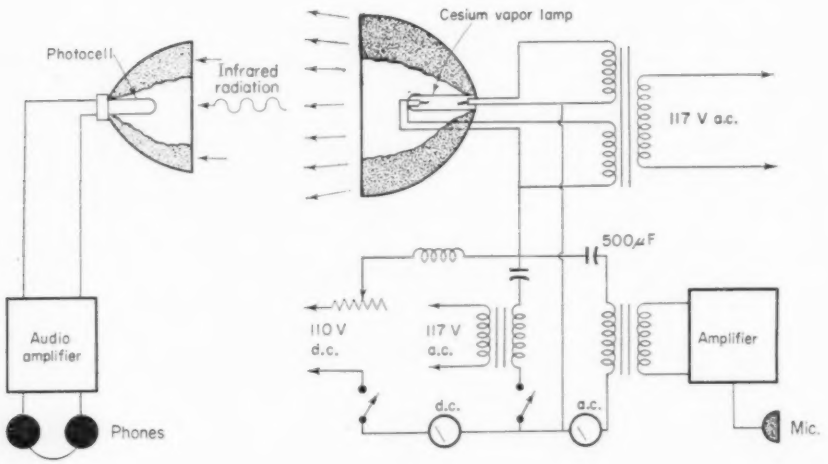

FIG. 6. Apparatus for transmitting speech over a light beam.

It operates on d.c. with amplified voice frequencies superimposed on the lamp current. The modulated light is picked up at a distant station with a thallous sulfide photocell, the current from which is amplified and converted to sound, which duplicates with excellent quality the original spoken words.

Both larger and smaller cesium-vapor lamps were made. A 50 W size, produced for the Air Force, operated on a 24 V supply, had good life, and an efficiency slightly less than the larger 100 W size because of the shorter arc length. Lamps of 500 W rating were made for use without optics to give 360° horizontal coverage. The efficiency of these lamps was greater; about 35 per cent of the power supplied to the lamps was converted into useful near-infrared radiation.

A study was also made of lamps having a power consumption of 10–20 W. They were similar to the larger sizes, but were mounted in sealed-beam automotive-type headlamps. Fig. 7 shows the general outline of the lamp. The bulb enclosing the light source is surrounded by a nichrome-wire heating element that forms part of the ballast for operating the lamp on a 12 V storage battery. The lens and the reflector of the sealed-beam lamp are cemented together with a thermosetting plastic cement, since fusing the edges of the lamp together, as is common practice in the production of automotive lamps, would be deleterious to the cesium lamp.

Vol. 1 1961

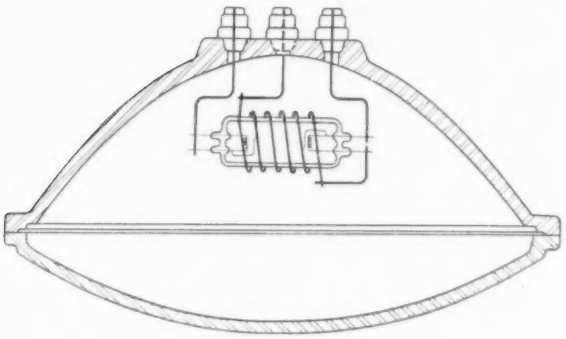

FIG. 7. Sealed-beam type of low-wattage cesium-vapor lamps.

Figure 8 shows a circuit used in our laboratory for operating the lamps on a 12 V storage battery. The battery is tapped at 8 V to supply the preheat current of 1·5 A through the cathode and ballast resistor, which is allowed to run for several minutes before the starting circuit of 150 V a.c. is turned on. After another 1–3 min the arc concentrates between the

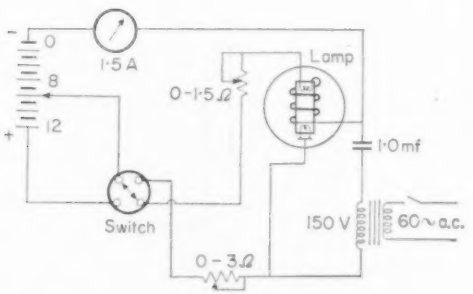

FIG. 8. Circuit for operating small cesium-vapor lamps on 12 V battery.

electrodes, at which time the starting circuit can be disconnected and the lamp operated on the 12 V supply. Some lamps have burned with practically constant infrared output for 250 hr under these conditions.

HIGH-INTENSITY SHORT-ARC LAMPS

During and after World War II Professor Paul Schulz in Germany developed the high-intensity short-arc xenon lamp which has an operating pressure of 20–40 atm.[12] The xenon lamps emit radiations of almost constant spectral intensity throughout the visible region, and strong radiations in both near-infrared and near-ultraviolet regions.[13] These lamps are

now being used in Europe as replacements for carbon arcs in small and medium size movie theatres.

Experimental lamps were made with heavy-wall quartz bulbs and were filled with mercury vapor, xenon gas, and combinations of mercury and xenon for power ratings of 500–2000 W. The electrodes were machined from solid tungsten rods. The cathodes supplied heavy currents largely by field emission rather than by thermionic emission and were made with pointed conical tips. The anodes had to be quite massive to dissipate the large amount of heat generated at that electrode. Fig. 9 is a sketch of an experimental high-intensity

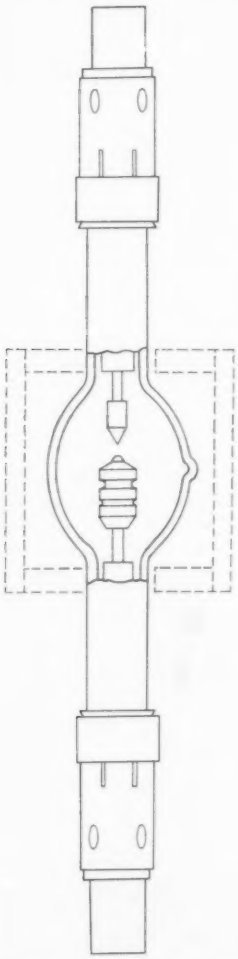

FIG. 9. Short-arc xenon lamp.

short-arc xenon lamp. The lamp is enclosed in a heavy-wall plastic housing during handling and storage to prevent a dangerous explosion since it is filled to several atmospheres pressure.

Spectral energy distributions were made with a Perkin–Elmer infrared spectrometer in

Vol. 1 1961

the region between 0·8 and 1·7 μ. A high-pressure xenon lamp emits ten to twelve strong spectral lines in the zone between 0·8 and 1·0 μ and a small amount of continuous energy throughout the near-infrared region. A high-pressure mercury lamp emits a strong spectrum line at 1·01 μ and six other lines of lesser intensities between this line and 1·7 μ, and also some continuous energy throughout this region. A composite mercury–xenon lamp with high pressures of both components exhibits the combined spectra of both elements with good intensity. This is quite different from low-pressure discharges in which only the spectrum of the metallic element is recorded. The relatively high intensity of the xenon arc lines makes this a desirable source for those applications where a small, intense, efficient and readily modulable source of radiant energy is desired.

Xenon lamps operate at higher currents and lower voltages than mercury vapor lamps of similar structure. Mercury–xenon lamps have intermediate operating characteristics that depend upon the partial pressures of the two components. Some of our experimental high-intensity xenon lamps with a spacing of 4 mm between the electrodes have operated at 25 ± 2 V over a current range of 25 A to 75 A. Because of the strong convection currents inside the lamps, it is desirable to burn the lamps in a vertical position, anode end on top, to attain stable, constant light intensity.

DUDDELL'S SPEAKING ARC

An electric arc operated in air may be modulated with voice frequencies and so produce sounds directly. Duddell in 1901 operated an arc light on direct current and then superimposed audio frequencies by the scheme indicated in Fig. 10.[14] In this case the light emitted by the arc is of secondary importance since it is not used or wanted. The variations

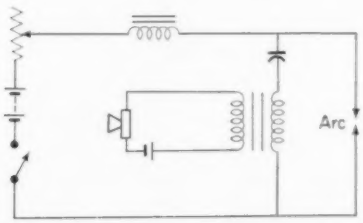

FIG. 10. Duddell's speaking arc.

in air pressure caused by changes in current through the arc produce the sound vibrations. The arc emits sounds of sufficient intensity to be audible to several hundred people in an auditorium of moderate size. If the arc is enclosed in an outer jacket or bulb, the sound energy is confined within the lamp. We would like to use the light of a modulated arc lamp and discard the accompanying sound energy.

STANDING SOUND WAVES IN ARC LAMPS

Enclosed arc lamps operated on a.c. power in the audio-frequency range or on d.c. and modulated by a.c. currents may cause sound vibrations to be produced within the arc chamber. They are caused by thermally induced variations in gas pressure that result from changes in current density in the arc. At certain critical frequencies resonance of appreciable intensity is built up by reflections from the bulb walls. The size and shape of bulb, kind of gas or vapor filling, temperature and operating conditions determine the frequency of the

plasma oscillations that are similar to standing sound waves in the discharge. Ordinarily this phenomenon is not observed because lamps are operated on d.c. or low-frequency a.c. with sufficient ballast to insure stable operation. In long tubes the discharges assume a constricted, snakelike appearance at the critical frequencies and are caused by sound energy reflected from the ends of the bulb. In a spherical bulb the sound waves spread to the bulb walls and are then focused back upon the arc to produce instability at the electrodes.

The simple lamp structures shown in Fig. 11 illustrate the acoustical resonance phenomena.

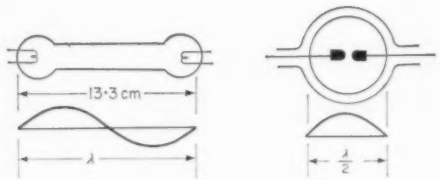

FIG. 11. Illustration of standing sound waves in experimental lamps.

Vol. 1 1961

The lamp at the left is about 1·5 cm in diameter, 13·3 cm long and contains xenon gas at 34 mm mercury pressure at room temperature. When operated on 3 A d.c. current with 2 A a.c. modulation superimposed, the arc showed violent distortions at 2250 c/s, but was quiescent at 2000 and 2500 c/s. With 5 A d.c. and 3 A a.c. modulation at 2500 c/s, the discharge again showed pronounced disturbances, but was stable at 2300 and 2700 c/s. The instability may start at either electrode, whereupon the discharge constricts into a thin luminous ribbon with sinusoidal shape, and the voltage increases because of increased arc length. Harmonics of the fundamental frequency may also be observed.

The following theory applies to this phenomenon. Laplace showed that the velocity of sound in a gas is determined by the equation $V = \sqrt{(\gamma p/d)}$. From the universal gas law $pv = RT$ and the definition of density $d = m/v$ one can rewrite Laplace's equation with equivalent quantities as $V = \sqrt{(\gamma RT/M)}$. V is the velocity at absolute temperature T, R is the universal gas constant $8{\cdot}3 \times 10^7$ ergs/degree, M is the mass in grams of one mole of gas, γ is the ratio of the specific heats of the gas and is a constant, e.g. 1·42 for air and 1·66 for argon, xenon and mercury vapor.

Assuming an effective temperature of 600 °C (= 873 °K) for xenon gas in the first illustration above, one obtains a value of 30,300 cm/sec as the velocity of sound in the lamp. Since velocity = frequency × wavelength, in the above example the wavelength of the sound produced inside the lamp bulb would be:

$$\lambda = \frac{30{,}300 \text{ cm/sec}}{2250 \text{ c/s}} = 13{\cdot}5 \text{ cm}$$

This is approximately the length of the lamp. In this lamp standing sound waves one wavelength long have nodes at the ends and center of the lamp, illustrated with a sine wave in Fig. 11. With the higher current rating and acoustical resonance at 2500 c/s, assuming a gas temperature of 800 °C, one finds that the velocity should be 33,500 cm/sec and the generated wavelength to be 13·4 cm. Having observed the relationship between bulb dimensions and acoustical resonance, one can estimate the temperatures of the gas or vapor in a discharge lamp by this method.

In a spherical bulb with electrodes at the center (Fig. 11) acoustical resonance occurs when the bulb diameter is equal to one-half wavelength. It was found that the mirror-like reflections of sound energy from spherical bulb walls could be minimized by locating the arc below the center of the bulb. This defocuses the echoes of the sound energy so that some is dissipated at the electrodes or on the bulb walls. An arc centered in a spherical bulb will literally "blow itself out" by its own sound waves, if any of the strong resonance frequencies are applied to the lamp for any appreciable time. A narrow enlarged band formed on a cylindrical shaped envelope directly opposite the constricted arc also defocuses the echo sound waves. These simple modifications can be used to improve the stability of modulated high-intensity arcs.

An experimental lamp was made to study standing waves in a low-pressure discharge containing argon gas at several mm pressure and mercury vapor. A diagram of the lamp is shown in Fig. 12 as well as the characteristic relations of current, gas pressure and light output on both a.c. and modulated d.c. power. The lamp was 1·5 in. in diameter, 28 in.

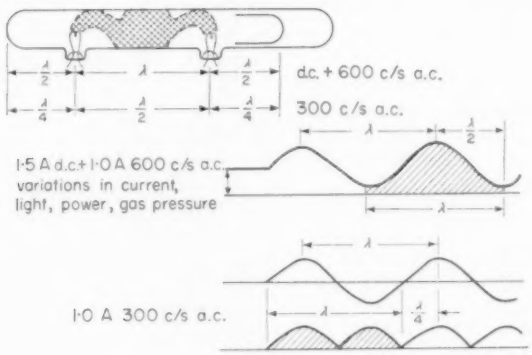

FIG. 12. Demonstration of acoustical resonance.

long and had a spacing of 12 in. between electrodes. A movable glass sleeve, closed at one end, permitted tuning of the resonating cavity at one end of the lamp. A resonant frequency of about 600 c/s was established with 1·5 A d.c. flowing through the lamp and 1·0 A a.c. superimposed. If the movable end-chamber was placed 6 in. from the electrode, both electrode regions showed a symmetric pattern of constricted arc as shown by the cross-hatched area inside the lamp. An audible 600 c/s tone was heard several feet from the lamp during this condition of operation. Sound generated inside the lamp was transmitted through the bulb walls to the air in the room. If the movable end-chamber was placed closer to or further from the electrode the disturbance at that electrode was minimized or disappeared completely with 600 c/s excitation while the constricted pattern of arc disturbance did not change at the other electrode.

In this low-pressure discharge lamp, assuming an average gas temperature of 250 °C, the velocity of sound in mercury vapor was 19,000 cm/s calculated by Laplace's formula.

$$\text{The wavelength} = \frac{\text{velocity}}{\text{frequency}} = \frac{19{,}000 \text{ cm/sec}}{600 \text{ c/s}} = 31{\cdot}7 \text{ cm}$$

This is very close to the electrode spacing of 30·5 cm or 12 in. With a d.c. bias and audio-frequency modulation there is a single light pulse and a single pressure pulse in each wavelength. Maximum disturbance or turbulence at the electrodes occurs at $\lambda/2$ from the nodes which are at the ends and center of the lamp.

When the lamp was excited with 1–2 A a.c., with no d.c. bias, the critical frequency required to cause pronounced disturbance or turbulence at the electrodes occurred at about 300 c/s. This was just half the preceding frequency with d.c. bias. In this case there are two pressure pulses for each wavelength and the spacing between electrodes is equal to a half wavelength for the resonant frequency.

$$\lambda = \frac{19{,}000 \text{ cm/sec}}{300 \text{ c/s}} = 63{\cdot}3 \text{ cm}$$

The distance between a node at the end of the lamp and the electrode would again be about 16 cm for maximum disturbance. This simple discharge tube readily demonstrates the phenomenon of acoustical resonance.

REFERENCES

1. FLUKE, J. M., and N. E. PORTER, *Proc. Inst. Radio Engrs., N.Y.* **34**, 876 (1946).
2. BELL, A. G., *Publ. Amer. Ass. Advanc. Sci.* **29**, 115 (1881).
3. CASHMAN, R. J., *Proc. Inst. Radio Engrs., N.Y.* **47**, 1471 (1959).
4. ELDER, T., and J. STRONG, *J. Franklin Inst.* **255**, 189 (1953).
5. BLOUT, AMON, SHEPHERD, THOMAS, WEST, LAND, *J. Opt. Soc. Amer.* **36**, 460 (1946).
6. MORTON, G. A., and L. E. FLORY, *RCA Rev.* **7**, 385 (1946).
7. GARLICK, G. F. J., and M. J. DUMBLETON, *Proc. Phys. Soc. Lond.* B **67**, 442 (1954).
8. STEPHENSON, R. J., and G. K. SCHOEPFLE, *Amer. J. Phys.* **14**, 294 (1946).
9. RANKINE, A. O., *Proc. Phys. Soc. Lond.* **31**, 242 (1919).
10. HUXFORD, W. S., and J. R. PLATT, *J. Opt. Soc. Amer.* **38**, 253 (1948).
11. BEESE, N. C., *J. Opt. Soc. Amer.* **36**, 555 (1946).
12. SCHULZ, P., *Ann. Phys., Lpz.* **6**, 95 (1947).
13. FRÜHLING, H. G., W. MÜNCH, and M. RICHTER, *Die Farbe* **5**, 41 (1956).
14. DUDDELL, W., *J. Instn. Elect. Engrs.* **30**, 232 (1900).

Vol
1
196

Infrared Physics, 1961, Vol. 1, pp. 17–20. Pergamon Press Ltd., Printed in Great Britain.

ULTIMATE SENSITIVITY AND PRACTICAL PERFORMANCE OF THE TELLURIUM PHOTOCONDUCTIVE DETECTOR*

D. F. EDWARDS and M. MERCADO†

The University of Michigan, Willow Run Laboratories,
Ann Arbor, Michigan, U.S.A.

Abstract—Calculations of the ultimate sensitivity and measurements of the practical performance have been made for the tellurium photoconductive detector. For the condition that detector sensitivity is limited by fluctuations of background radiation, the theoretical NEP (noise equivalent power) at the peak of spectral sensitivity ($\lambda = 3{\cdot}4\,\mu$) was calculated to be $5{\cdot}1 \times 10^{-13}$ W. For the "best" tellurium detector the measured value of NEP was $3{\cdot}1 \times 10^{-13}$ W at the same wavelength and at the optimum chopping frequency. These values indicate that the tellurium photoconductive detector is background limited and therefore is ideal.

Vol.
1
1961

INTRODUCTION

THE purpose of this paper is to report the results of calculations of the ultimate sensitivity of the tellurium detector and of measurements of sensitivity for a select few of these detectors as prepared by Suits *et al.* The results indicate that the tellurium detector is an ideal detector. The fact that only one of six detectors measured approached the ultimate sensitivity indicates the need for continued development. Of the other five, two detectors had an NEP (noise equivalent power) at $3{\cdot}4\,\mu$ within a factor of about ten of the ideal. For the ideal detector, i.e., one that is background-radiation limited, the addition of a cooled radiation shield to match the aperture of the detector to that of the optics should increase the detector sensitivity by as much as a factor of ten.

The use of tellurium as a photoconductor was first investigated in 1949 by Moss,[1, 2] who used evaporated thin films. The most sensitive cell that he reported, when cooled to liquid-nitrogen temperature, had a signal equal to the r.m.s. (root mean square) noise in 1 c/s bandwidth for incident radiation of $1{\cdot}2 \times 10^{-10}$ W of monochromatic radiation at $1\,\mu$. This quantity is called the NEP and is defined as the incident radiation necessary to produce a signal equal to the r.m.s. noise. This same tellurium film was only moderately sensitive (NEP $= 10^{-6}$ to 10^{-7} W, at $1\,\mu$ and 1 c/s bandwidth) at room temperature. Loferski[3] in 1954 made photoconductivity measurements on single crystals of tellurium with about the same results as those obtained for evaporated films. Loferski's data were extrapolated and the NEP was found to be about 10^{-8} to 10^{-9} W for the most sensitive photoconductor when cooled to liquid-oxygen temperature. The single-crystals used for Loferski were cut or cleaved from large tellurium crystals, ground, polished, and sometimes etched to the desired dimensions.

Suits[4] in 1957 found that thin hexagonal single-crystal prisms of tellurium when cooled to liquid-nitrogen temperature had sensitivities and response times comparable to those of the lead salt detectors. These thin single-crystal prisms were grown from the vapor phase in

* This work was conducted by Project MICHIGAN under Department of the Army Contract (DA-36-039-78801) administered by the U.S. Army Signal Corps.

† Presently employed at Bendix Aviation Corporation Systems Division, Ann Arbor, Michigan.

a low-pressure hydrogen atmosphere, starting with 99·999+ per cent pure material*. The electrical contacts were made by welding a hot wire, in most cases platinum, to the tellurium. The crystals were then mounted in a more or less standard glass dewar with a sapphire window.

ULTIMATE SENSITIVITY

The ultimate sensitivity was calculated for the tellurium detector for the condition that fluctuation in the background radiation is the fundamental limitation of detector sensitivity. Recently, several articles have been published [5–8] that describe methods for calculating the ultimate sensitivity of a photoconductor for the background-limited condition. The calculations reported in the present paper follow closely those of Moss. [6]

The background radiation is taken as a 300 °K blackbody with the spectral distribution given in Fig. 1, curve (a). Only that radiation that lies within the sensitive spectral region of

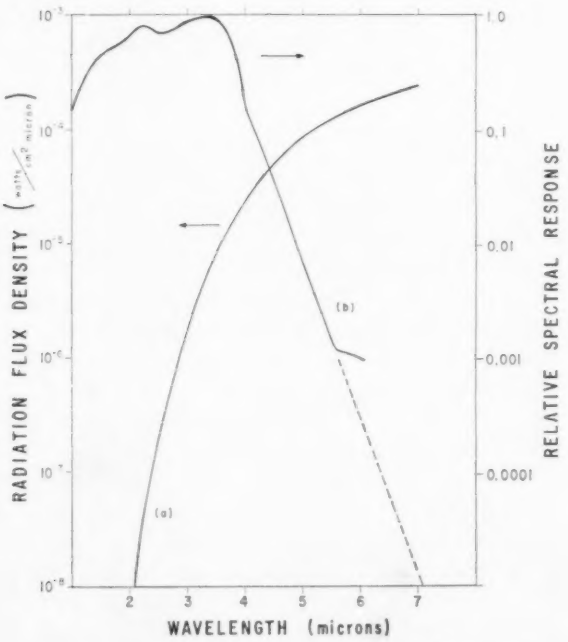

FIG. 1. Curve (a) Spectral distribution for a 300 °K blackbody. Curve (b) Relative spectral response of the tellurium detector.

the detector will affect the ultimate sensitivity. The relative spectral response of the tellurium detector at 77 °K is given in Fig. 1, curve (b). The product of these two curves is the spectral distribution of the effective radiation incident on the detector (Fig. 2). It is seen that the effective wavelengths are limited to a narrow band centered at 3·7 μ. For purposes of calculations, it is assumed to a good degree of approximation that the effective radiation is monochromatic with the wavelength of the peak 3·7μ. The area under this

* American Smelting and Refining Co., South Plainfield, New Jersey.

Vol. 1 1961

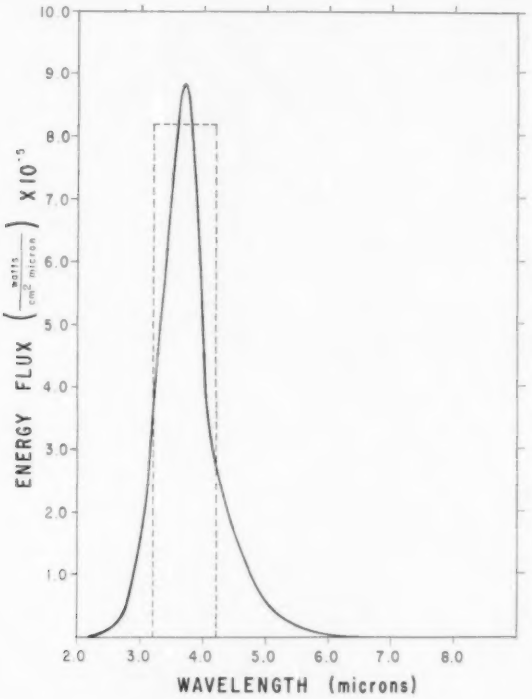

FIG. 2. Spectral distribution of effective radiation incident on detector.

curve is the equivalent energy falling on the detector and equals 82·2 μW/cm². This corresponds to $N_0 = 1{\cdot}5 \times 10^{15}$ quanta/cm²/sec at 3·7 μ. The number of absorbed quanta producing a detector signal, N_s, will depend on the absorption properties of the material, the quantum efficiency, and the diffusion length of the free carriers. The relation between N_s and N_0 has been given by Moss [6] as

$$N_s^2 = 2AN_0\Delta f(1 - r - t),$$

where A is the sensitive area of the detector, Δf the bandwidth of the measuring equipment, and r and t are the reflexion and transmission coefficients. For a detector with $A = 0{\cdot}0025$ cm² and $\Delta f = 5$ c/s, $N_s = 9{\cdot}55 \times 10^6$ quanta/sec at 3·7 μ. The reflexion coefficient $r(= 0{\cdot}48)$ was calculated from the weighted average for the index of refraction,[9] $\bar{n} = 5{\cdot}5$. The transmission coefficient $t(= 0{\cdot}10)$ was calculated from the absorption coefficient value of Loferski [3] and the sample thickness. This calculated value of N_s corresponds to a theoretical NEP (3·4 μ) = $5{\cdot}1 \times 10^{-13}$ W at the peak of the spectral response ($\lambda = 3{\cdot}4\,\mu$) and represents the ultimate sensitivity of the tellurium detector for the background-radiation limited condition.

PRACTICAL PERFORMANCE

The absolute spectral sensitivity of the "best" tellurium photoconductor measured is shown in Fig. 3. The measured NEP at 3·4 μ is $(3{\cdot}1 \pm 0{\cdot}8) \times 10^{-13}$ W. This was measured

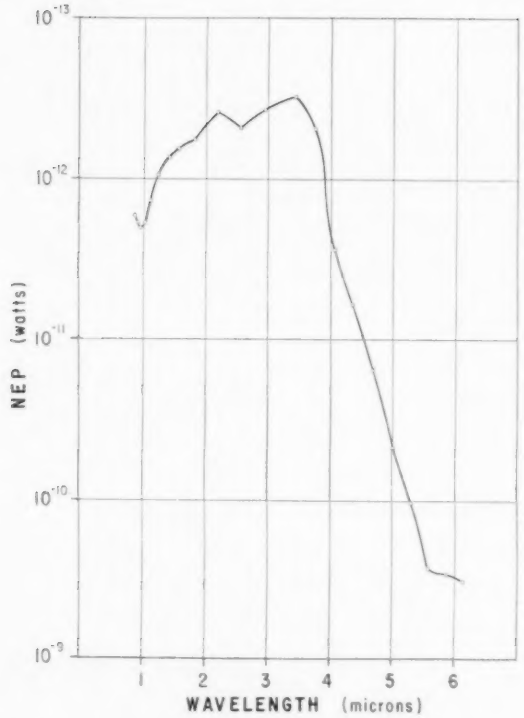

FIG. 3. Absolute spectral sensitivity of the tellurium detector at 77 °K with a chopping frequency of 5000 c/s and a 5 c/s bandwidth.

for radiation chopped at 5000 c/s and 5 c/s bandwidth. The assumptions used in the calculation of the ultimate sensitivity result in the value of the ideal NEP being larger than the measured value. A more refined calculation does not seem warranted at this time. The monochromatic radiation calibration was made with a Reeder* thermocouple that had been calibrated with a 500 °K standard blackbody† and checked with a National Bureau of Standards calibrated lamp. The r.m.s. values of noise and signal voltages were calibrated with a Weston a.c. thermocouple.

REFERENCES

1. MOSS, T. S., *Proc. Phys. Soc., Lond.* A **62**, 264 (1949).
2. MOSS, T. S., *Photoconductivity in the Elements*, Butterworth, London (1952).
3. LOFERSKI, J. J., *Phys. Rev.* **93**, 707 (1954).
4. SUITS, G. H., "Tellurium Infrared Detector," University of Michigan, Internal Report (1957).
5. BURSTEIN, E., and G. S. PICUS, "Background Limited Infrared Detection," Naval Research Laboratory Internal Report (1958).
6. MOSS, T. S., *J. Opt. Soc. Amer.* **40**, 603 (1950).
7. PETRITZ, R. L., *Photoconductivity Conference, Atlantic City*. John Wiley, New York (1956).
8. SMITH, R. A., F. E. JONES, and R. P. CHASMAR, *The Detection and Measurement of Infrared Radiation*. Oxford University Press, London (1957).
9. HARTIG, P. A., and J. J. LOFERSKI, *J. Opt. Soc. Amer.* **44**, 17 (1954).

* Charles M. Reeder Co., Detroit 3, Michigan.
† Models RS–1A Blackbody, Barnes Engineering Co., Stamford, Connecticut.

Vol. 1 1961

Infrared Physics, 1961, Vol. 1, pp. 21–26. Pergamon Press Ltd., Printed in Great Britain.

SOME INFRARED TRANSMITTING GLASSES CONTAINING GERMANIUM DIOXIDE

S. NIELSEN, W. D. LAWSON and A. F. FRAY

Royal Radar Establishment, Malvern, England

Abstract—We report here the glass forming regions of the ternary systems containing GeO_2, PbO, and (a) AlF_3, (b) PbF_2, (c) TiO_2, (d) As_2O_3, (e) Sb_2O_3, (f) Bi_2O_3, (g) TeO_2. The infrared transmission of these glasses is similar to that of germanium dioxide itself, but other properties, softening point, strength, resistance to chemical attack etc., are altered. A strong, weather-resistant glass containing only 15 per cent GeO_2 can be prepared.

Vol. 1 1961

INTRODUCTION

GERMANIUM dioxide, GeO_2, forms a glass having good transmission in the infrared to about 6 μ,[1] but is expensive and poorly resistant to chemical attack. Various modifiers can be added to GeO_2 to produce glasses which are stronger, more resistant to chemical attack, and have similar transmission spectra in the infrared. Lead dioxide is a very suitable modifier[2] and glasses containing up to 50 mol. per cent PbO can be obtained. We note, however, in agreement with Merker and Wondratschek,[3] that the 50 mol. per cent mixture only forms a glass if traces of impurity are present. In the presence of a third component the mol. per cent of PbO can be substantially increased.

Blau[4] indicated that glasses with compositions GeO_2 (18–99%), PbO (traces–79%), and ZrO_2 or La_2O_3 (3–5%), formed glasses with high transmittance in the infrared. He also recommended the addition of small quantities of MnO_2 and Li_2O in these glasses.

Florence, Glaze and Black[5] measured the transmission spectra of glasses with compositions GeO_2 (42·7%), PbO (57·3%); GeO_2 (53·7%), PbO (7·7%), BaO (37·2%), BeO (1·4%); GeO_2 (11·3%), CaO (49·5%), Al_2O_3 (39·2%); and GeO_2 (36%), PbO (58%), La_2O_3 (6%).[6] Hafner, Kreidel and Wiedel[7] mention the addition of GeO_2 to some calcium aluminate glasses and Stanworth[8] to glasses containing TeO_2.

We have extended these observations and in particular report the glass forming regions of some ternary systems containing GeO_2 and PbO, together with preliminary results indicating the effect of the various modifiers on the melting point, resistance to boiling water, and transmittance in the infrared. We also record in Table 1 comments on other compositions containing GeO_2.

APPARATUS AND METHOD

Glasses were prepared in the apparatus illustrated in Fig. 1, except for those containing As_2O_3 which were prepared in sealed evacuated silica tubes. The platinum crucible was used as a resistance heater, current being supplied through water cooled terminals. The crucible was enclosed by an 8-in. diameter bell jar supported on a paxolin base plate and the glasses were prepared in an atmosphere of dry nitrogen. A platinum–rhodium thermocouple, suspended in the melt, was used for measuring and controlling the temperature of the melt and also for stirring.

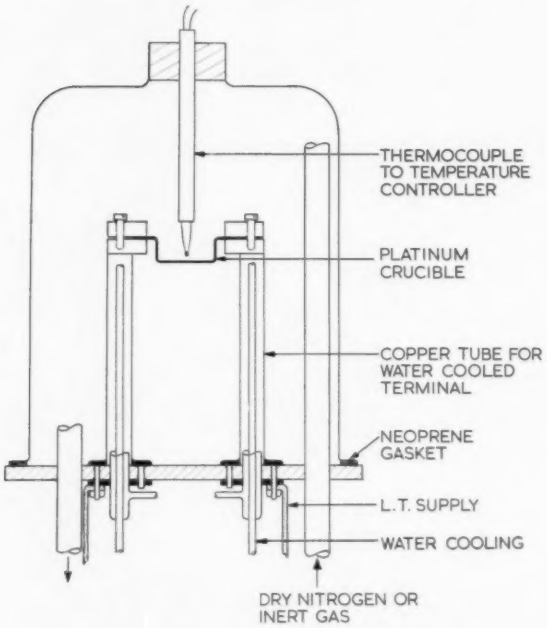

FIG. 1

Weighed amounts of commercial high purity oxides and fluorides were fused in a previously weighed platinum crucible to a temperature about 100 °C above the melting point. After about 30 min at this temperature, the heating current was switched off, giving a rapid quenching. Mixtures which produced glasses were then annealed for some 30 min at a temperature below the melting point. Where evaporation was observed the loss of the more volatile component was assumed to be the difference between the initial and final weights.

Transmission spectra were obtained from polished specimens of the glasses using a double beam infrared spectrometer. The "melting" point was measured as that temperature at which the thermocouple could just be moved in the glass. A measure of the resistance of the glass to water was obtained by immersing the specimen in boiling water and estimating the change in weight per square centimetre per hour by direct weighing.

RESULTS AND DISCUSSION

The glass forming regions in the systems GeO_2, PbO, with (a) AlF_3, (b) PbF_2, (c) TiO_2, (d) As_2O_3, (e) Sb_2O_3, (f) Bi_2O_3, and (g) TeO_2 are shown in Figs. 2–8; mixtures forming clear glasses are indicated by ○, those almost forming glasses as ⊗ and those not forming glasses ●. These show that glasses containing as little as 15 mol. per cent of GeO_2 (Fig. 2) can be prepared. Various other modifiers can be used (Table 1). Preliminary results suggest that only small percentages of univalent fluorides can be used, but larger percentages of the bivalent fluorides are possible.

Results show that the modifiers used have no effect on transmission in the infrared; modifiers used include PbO, Bi_2O_3, ZnO, As_2O_3, Sb_2O_3, TeO_2, TiO_2, NaF, CaF_2, SrF_2, PbF_2, AlF_3. Some typical spectra are shown in Figs. 9–12. These spectra show a pronounced

Vol. 1 1961

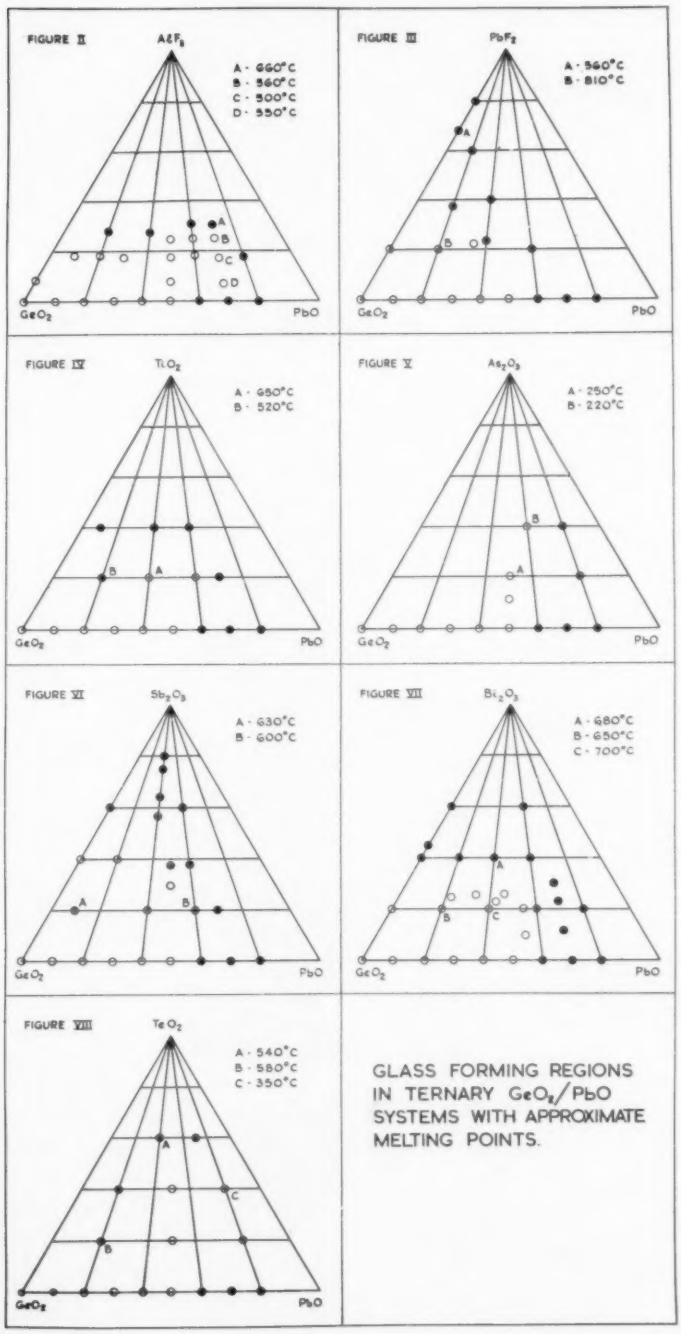
FIGURE II
AlF_3
A - 660°C
B - 560°C
C - 500°C
D - 550°C
GeO_2
PbO
FIGURE III
PbF_2
A - 560°C
B - 810°C
GeO_2
PbO
FIGURE IV
TiO_2
A - 650°C
B - 520°C
GeO_2
PbO
FIGURE V
As_2O_3
A - 250°C
B - 220°C
GeO_2
PbO
FIGURE VI
Sb_2O_3
A - 630°C
B - 600°C
GeO_2
PbO
FIGURE VII
Bi_2O_3
A - 680°C
B - 650°C
C - 700°C
GeO_2
PbO
FIGURE VIII
TeO_2
A - 540°C
B - 580°C
C - 350°C
GeO_2
PbO
GLASS FORMING REGIONS IN TERNARY GeO_2/PbO SYSTEMS WITH APPROXIMATE MELTING POINTS.

FIGS. 2–8

TABLE 1. ADDITIONAL GeO_2 GLASS COMPOSITIONS

Composition	Approx. Softening point	Colour	Comments
GeO_2 46% PbO 46% NaF 8%	~ 550 °C	Clear	8% NaF (or other univalent fluorides) appears to be maximum amount permissible in the glass
GeO_2 70% CaF_2 30%	>1000 °C	Clear	CaF_2 appears to increase hardness. Much evaporation during preparation
GeO_2 70% SrF_2 30%	~1000 °C	Clear	SrF_2 appears to increase hardness and resistance to thermal shock
GeO_2 62% SrF_2 38%	~1000 °C	Clear	38% SrF_2 represents a maximum permissible amount in the glass
GeO_2 45% Sb_2O_3 10% ZnO 10%	~ 900 °C	Clear	This glass seemed fairly hard
GeO_2 40% Sb_2O_3 56% PbF_2 4%	~ 800 °C	Clear	These glasses proved very difficult to prepare in our apparatus due to evaporation of Sb_2O_3
GeO_2 45% Sb_2O_3 42% PbF_2 13%	~ 800 °C	Clear	
GeO_2 50% Sb_2O_3 25% PbF_2 25%	~ 750 °C	Clear	

water absorption band at 3 μ, which often reduces transmission considerably. Attempts to remove water from these and similar glasses will be discussed in a subsequent paper.

The properties of these glasses, other than the transmission spectra, have received little attention as yet. However, some qualitative observations may be of interest.

The "melting" point of GeO_2 glass was lowered 200–300 °C by addition of PbO, and lowered a further 200–300 °C by addition of PbO plus TeO_2, As_2O_3, or Sb_2O_3, but addition of PbO plus TiO_2, AlF_3, or PbF_2 did not produce a further lowering of the melting point.

The GeO_2/PbO glasses had a pale yellow colour when prepared in an atmosphere of oxygen, but were almost colourless when prepared in an atmosphere of nitrogen. The colour intensified when higher melt temperatures were used. Glasses containing only GeO_2 and Bi_2O_3 had a red colour; these glasses were difficult to prepare due to decomposition of Bi_2O_3 at temperatures above about 700 °C. The GeO_2/PbO glasses containing As_2O_3 were a yellow colour and those containing TeO_2 a yellow-green, but those containing Sb_2O_3, TiO_2, AlF_3 or PbF_2 were colourless.

The relative ease of grinding and polishing specimens suggested that additions of TiO_2, PbF_2, or AlF_3 to the GeO_2/PbO glasses, gave a harder and more brittle glass, while additions of TeO_2, As_2O_3, or Sb_2O_3 had the opposite effect. The harder glasses were also more resistant to boiling water (Table 2).

Vol. 1 1961

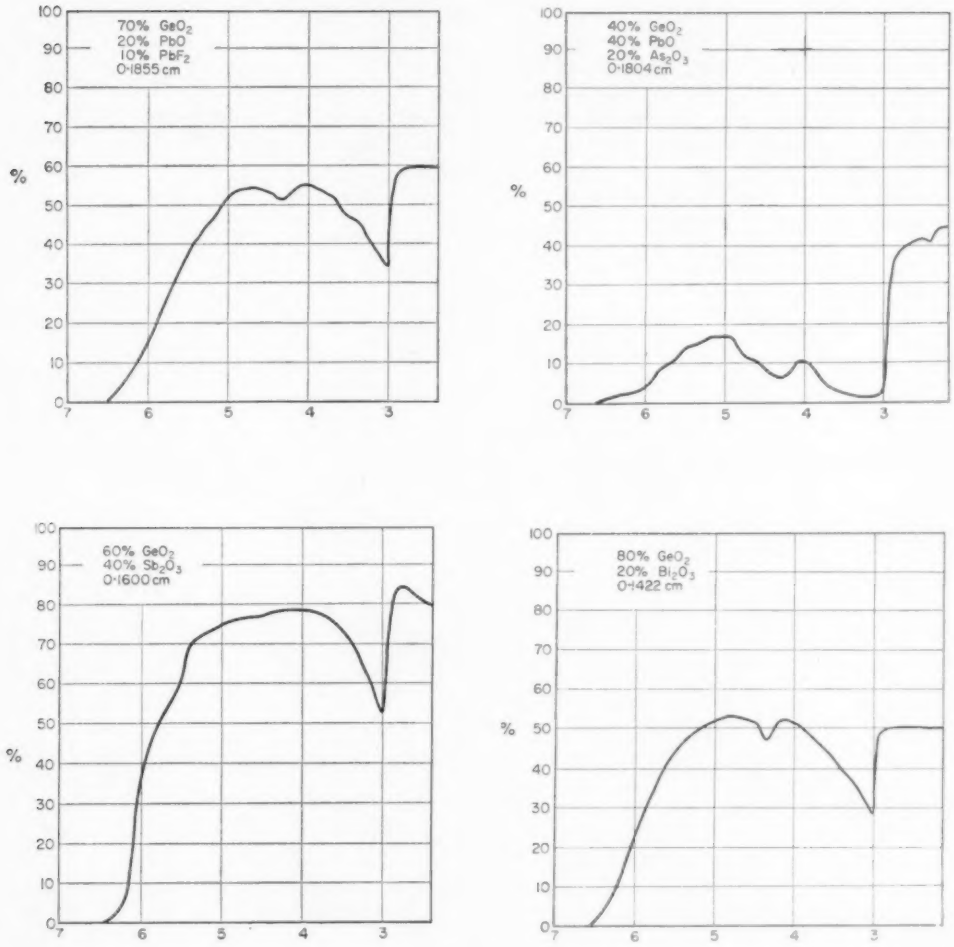

FIGS. 9–12

TABLE 2. RESISTANCE OF GLASSES TO BOILING WATER

Composition (mol.%)	loss/hr/cm²
80% GeO_2, 20% Bi_2O_3	> 2 mg.
6% GeO_2, 47% ZnO, 47% TeO_2	~ 0·2 mg.
30% GeO_2, 30% PbO, 40% TeO_2	~ 0·1 mg.
70% GeO_2, 30% PbO	~ 0·01 mg.
70% GeO_2, 24% PbO, 6% PbF_2	< 0·01 mg.
32% GeO_2, 48% PbO, 20% AlF_3	~ 0
32% GeO_2, 48% PbO, 20% TiO_2	~ 0

Acknowledgement—Acknowledgement is made to the Controller, Her Majesty's Stationery Office, for permission to publish this paper.

REFERENCES

1. COHEN, A. J., and H. L. SMITH, *Phys. and Chem. Solids* **7**, 301 (1958).
2. SPERANSKAYA, E. I., *Chem. Abstr.* **53**, 11971 (1959).
3. MERKER, L., and H. WONDRATSCHEK, *Glastech. Ber.* **30**, 471 (1957).
4. BLAU, H. H. (Ohio State University Research Foundation), *U.S. Pat.* 2,701,208 (1955).
5. FLORENCE, J. M., F. W. GLAZE, and M. H. BLACK, *J. Res. Nat. Bur. Stand.* **55**, 231 (1955).
6. GLAZE, F. W., *Bull. Amer. Ceram. Soc.* **34**, 291 (1955).
7. HAFNER, H. C., N. J. KREIDEL, and R. H. WIEDEL, *J. Amer. Ceram. Soc.* **41**, 315 (1958).
8. STANWORTH, J. E., *J. Soc. Glass Technol.* **36**, 3 (1952).

Vol.
1
1961

Infrared Physics, 1961, Vol. 1, pp. 27–38. Pergamon Press Ltd., Printed in Great Britain.

A STATUS REPORT ON INFRARED DETECTORS*

P. BRATT,† W. ENGELER, H. LEVINSTEIN, A. MAC RAE‡ and J. PEHEK

Department of Physics, Syracuse University, U.S.A.

Abstract—Infrared photon detectors may be placed into two categories: intrinsic and impurity activated detectors. Intrinsic detectors include film detectors PbS, PbSe, PbTe, and single crystal detectors InSb and InAs. Their spectral response generally rises linearly to the spectral peak, then drops sharply. Typical PbS detectors operated at room temperature have a long wavelength threshold at 3 μ and a detectivity of 10^{11} cm c/s$^{1/2}$ W^{-1} at 2 μ, their spectral peak. Time constants are of the order of 100 μsec. PbSe and PbTe detectors when operated at liquid nitrogen temperature have a detectivity of about 2×10^{10} cm c/s$^{1/2}$ W^{-1} at their spectral peak between 4 and 6 μ. Time constants vary between 20 and 100 μsec. InSb detectors, when cooled to liquid nitrogen temperature, have a spectral peak in the vicinity of 5 μ and a detectivity of about 4×10^{10} cm c/s$^{1/2}$ W^{-1}. Their time constants are of the order of 1 μsec.

Impurity activated detectors include Ge and Ge–Si single crystals with impurities such as Au, Cu, Zn, Sb. The spectral response of Ge with the peak at 1·5 μ and a cut-off at 1·8 μ is superimposed on the response characteristic of the impurity. Gold extends the response to 9 μ, Cu to 30 μ, Zn to 40 μ, and Sb to 120 μ. When these detectors are cooled until they are background limited, their detectivity is about 2×10^{10} cm c/s$^{1/2}$ W^{-1} at spectral peak. Time constants of Ge : Au and Ge : Zn detectors are less than 0·1 μsec.

Evaluation of the theoretical limit of detectivity indicates that most currently available single crystal detectors approach the theoretical limit to within a factor of two–three; average film detectors, however, differ by a greater amount.

INTRODUCTION

INFRARED photon detectors may be grouped into two categories: intrinsic detectors and extrinsic, or impurity activated detectors. Intrinsic detectors include PbS, PbSe, PbTe, InSb, and InAs. The first three materials show sensitivity only when prepared in thin evaporated or chemically deposited layers, carefully sensitized by various "cook-book" techniques. InSb and InAs detectors employ sections of single crystals grown by the conventional techniques. InSb detectors may be either of the photoconductive or the photovoltaic type; InAs detectors, still in the developmental stage, are of the photovoltaic type. Impurity activated detectors[1] include Ge with such impurities as gold, zinc, copper, antimony,[2] and Ge–Si alloys[3] with the same impurities. They are of the photoconductive type consisting of Ge single crystals to which the impurity is added either during the crystal growth process or later by diffusion.

All current intrinsic infrared detectors consist of compounds containing two components in stoichiometric proportions. Photoconductivity is produced when photons liberate charge carriers from atoms of the compound. All the intrinsic detectors available today have a long wavelength threshold at wavelengths shorter than 7 μ (activation energy of currently used intrinsic materials is greater than 0·18 eV). When response to longer wavelengths is

* This work has been supported by the Air Research and Development Command, U.S. Air Force.
† Now at Raytheon Manuf. Co.
‡ Now at Bell Telephone Laboratories.

desired, impurity activated detectors provide at present the only solution. While the energy required to free a charge carrier from the Ge–Ge covalent bond is about 0·7 eV, the activation energy of charge carriers from impurities placed substitutionally in the Ge lattice may be considerably less and depends on the type of impurity.

When in use, a photoconductive detector is placed in a circuit containing a load resistor and a bias battery. Voltage variations across the load resistor, produced by resistance changes of the detector element when exposed to signal radiation, are amplified as required. Photovoltaic detectors generate their own potential difference when carriers liberated by the radiation are collected at the p–n junction. This output is generally connected through a step-up transformer or a transistorized preamplifier[4] to an amplifier. Under certain conditions, photovoltaic detectors may be operated in conjunction with a bias battery, connected to the sensitive element with the proper polarity (back bias operation). They may then be used in a manner similar to photoconductive detectors. Fig. 1 shows a typical circuit for photoconductive and photovoltaic detectors.

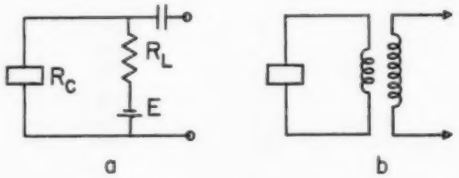

FIG. 1. Electrical connections for photoconductive (a), and photovoltaic (b) detectors.

PHYSICAL CHARACTERISTICS OF DETECTORS

Signal

The signal voltage S, obtained from a detector may be expressed in terms of the circuit parameters and the physical properties of the photosensitive device. When the detector is of the photoconductive type and if one type of charge carrier predominates in the conduction process

$$S = \frac{ER_CR_L}{(R_C + R_L)^2} \frac{\Delta n}{n} \tag{1}$$

where R_C and R_L represent detector and load resistance, respectively, E is the EMF of the bias battery, n is the number of free charge carriers within the detector element, and Δn is the change in the number of charge carriers produced by the signal radiation.

But

$$\Delta n = \eta Q_s A \tau \tag{2}$$

where Q_s is the photon flux density incident on the detector of area A, η is the efficiency with which this flux is transformed into free charge carriers. For simplicity it is assumed to be constant within the spectral range of the detector. (η has a maximum value of one when each incident photon produces one free charge carrier.) τ, the time constant of the material, is the length of time a charge carrier remains free after being generated by a photon. When the amplitude of the signal has a sinusoidal time dependence, the r.m.s. signal, V_s, may be written as

$$V_s = \frac{E\,R_C R_L}{(R_C + R_L)^2}\,\frac{\eta Q_s A \tau}{n}\,\frac{1}{(1+\omega^2\tau^2)^{1/2}} \tag{3}$$

where Q_s is the r.m.s. photon flux (at wavelengths shorter than the long wavelength cut-off of the detector).

Noise

Noise produced in a detector may be due to several sources:

(1) *Johnson noise*. This is due to the random motion of charge carriers. It is present in all conducting solids but is generally negligible in comparison to the other types of noise in semiconductors.

(2) $1/f$ *noise*. This is the type of noise whose power varies inversely with frequency. It appears to be due to surface effects[5] and its magnitude may be controlled by proper production techniques. Well constructed detectors show little $1/f$ noise above frequencies of 100 c/s.

(3) *Noise due to the fluctuations in generation and recombination rates of charge carriers.*[6] This type of noise is given by the expression

$$V_n = 2\,\frac{E\,R_C R_L}{(R_C + R_L)^2}\left(\frac{\tau}{<\Delta n^2>}\right)^{1/2} \Delta f^{1/2}\,\frac{1}{(1+\omega^2\tau^2)^{1/2}} \tag{4}$$

where Δf represents the bandwidth of the amplifier and $<\Delta n^2>$ is the variance in n. When the number of charge carriers is due to thermal generation by lattice vibrations, this noise is then designated as generation–recombination (G–R) noise and $<\Delta n^2> = n$. When the number of charge carriers is determined by the background radiation, this noise is designated as photon noise and

$$<\Delta n^2> = \sum_{\lambda} n_\lambda \left(1 + \frac{1}{\exp\,(hc/\lambda kT) - 1}\right).$$

For a background at a temperature of 300 °K or less and wavelengths shorter than 20 μ, $\{[1/\exp\,(hc/\lambda kT) - 1]\} \ll 1$ and $<\Delta n^2> = n$ as in the case of G–R noise. This type of noise in photovoltaic detectors is less by the factor $\sqrt{2}$, since charge carriers are all collected at the p–n junction such that fluctuations occur only in the generation process.

Detectivity

The performance of a detector may be described by giving its signal to noise ratio for a given incident power. This quantity is designated as the detectivity, D

$$D = \frac{V_s/V_n}{H_s A} \tag{5}$$

where H_s is the r.m.s. power density at the detector. D is dependent on the area of the detector. Frequently its reciprocal, the noise equivalent power (NEP), is specified. In the comparison of different types of detectors it is desirable to normalize all detectors to the

same area (generally 1 cm²). With certain assumptions, $DA^{1/2} = \text{constant}$,[7] this leads to the area independent quantity

$$D^*(T\ ^\circ\text{K},\ X\ \text{c/s}) = \frac{V_s/V_n(\Delta f)^{1/2}}{H_s\sqrt{A}} \tag{6}$$

where the amplifier bandwidth Δf has been reduced to 1 c/s. The quantities in parenthesis refer to the conditions of measurement, T °K the temperature of the blackbody which supplies the power H_s, and X c/s the frequency at which the signal is modulated. In terms of equations (3) and (4)

$$D^* = \tfrac{1}{2}\eta A\left(\frac{\tau}{n}\right)^{1/2}\frac{Q_s}{H_s} \tag{7}$$

where the $<\Delta n^2>$ term in equation (4) has been replaced by n.

Theoretical Limits of D*

The number of free charge carriers in a detector is determined by the number of charge carriers liberated by lattice vibrations, n_{TH}, and those (n_B) freed by background radiation. Under ideal conditions a detector is operated at a sufficiently low temperature where $n_{TH} \ll n_B$. Then $n = n_B$ and the detector is said to be background limited.

Now

$$n_B = \eta A Q_B \tau \tag{8}$$

where Q_B is the background photon flux for wavelengths shorter than the long wavelength cut-off of the detector.

Thus for a photoconductive detector

$$D^*(T\ ^\circ\text{K}) = \tfrac{1}{2}\left(\frac{\eta}{Q_B}\right)^{1/2}\frac{Q_s}{H_s}. \tag{9}$$

Under ideal conditions, η is taken as unity.

$$Q_B = 2\pi c \sin^2\frac{\theta}{2}\int_0^{\lambda_m}\frac{1}{\lambda^4}\,\frac{d\lambda}{\exp(hc/\lambda kT) - 1} \tag{10}$$

where θ is the angular field of view of the detector element, h Plank's constant, k the Boltzmann constant, and c the velocity of light. The value of the integral is given in the tables by Lowan and Blanch (*J. Opt. Soc. Amer.* **30**, 1940). In order to calculate the detectivity D^*_λ at wavelength λ, H_s in equation (9) is replaced by $(hc/\lambda)Q_s$. Then

$$D^*_\lambda = \frac{1}{2hc}\left(\frac{\eta}{Q_B}\right)^{1/2}\lambda.$$

Vol. 1 1961

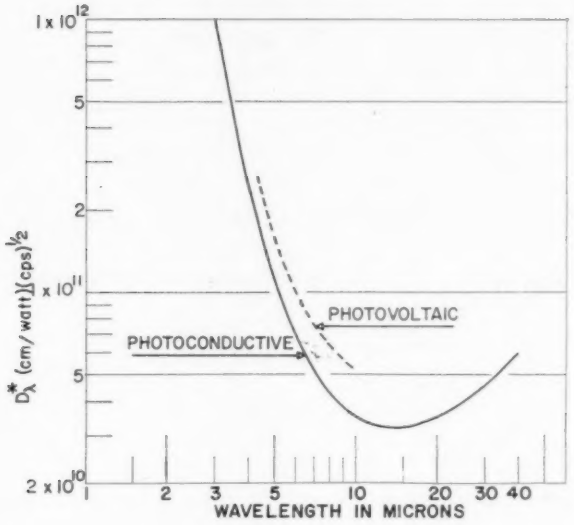

FIG. 2. Variation of detectivity at spectral peak as a function of the long wavelength threshold of background limited detectors (angular field of view 180°, background temperature 300 °K).

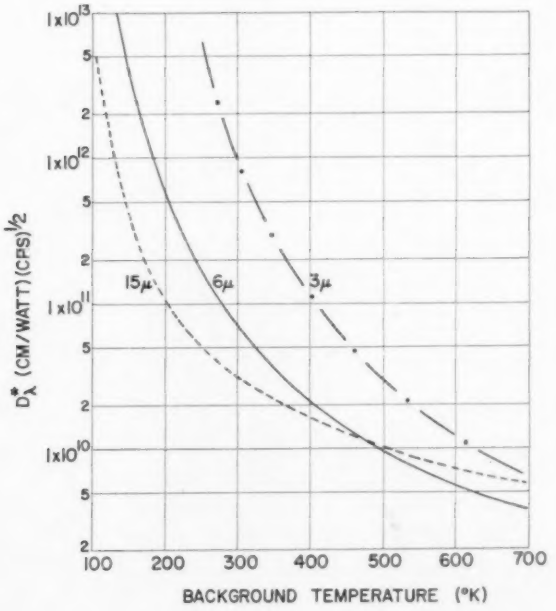

FIG. 3. Variation of detectivity at spectral peak as a function of background temperature for 3, 6, and 15 μ detectors.

Figure 2 shows the variation of D^*_λ; at the spectral peak of a detector as a function of the threshold wavelength of the detector for the ideal detector. Background radiation for these calculations is assumed to come from a 300 °K hemispherical blackbody surrounding the sensitive element. Improvement in D^* can come only by reducing the background radiation. This may, of course, be accomplished by operating the detector in a location where the background temperature is lower. Fig. 3 shows the effect of varying background temperature on D^*_λ; of detectors with a 3, 6, and 15 μ long wavelength threshold. More practically, background radiation may be reduced either by limiting the angular field of view which the detector "sees" or by narrowing the range of spectral sensitivity of the detector. The former is accomplished by the use of a cooled aperture, the latter by means of a cooled filter which eliminates background radiation from spectral regions in which the detector need not respond.

INTRINSIC DETECTORS

Film Type

Included in this list are PbS, PbSe, and PbTe.[8] Typical absolute spectral response curves of these detectors are shown in Fig. 4. PbS detectors are generally operated at room

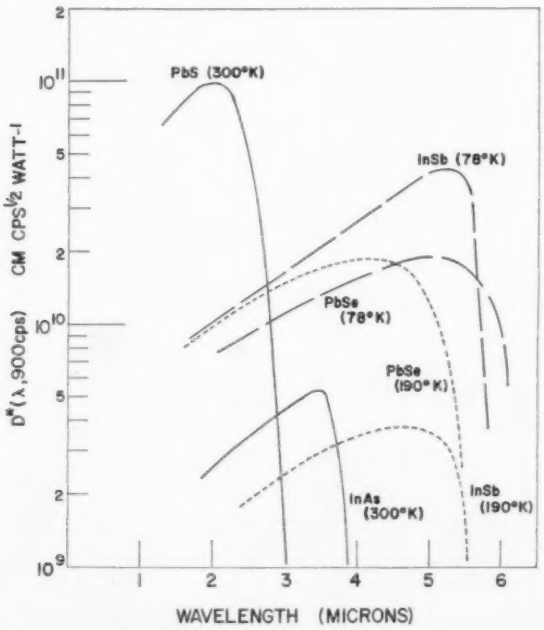

FIG. 4. Spectral response of intrinsic detectors.

temperature. The thin layer of PbS is deposited on a glass slide,[9] the sensitive element being covered with a protective coating. Time constants vary between 100 and 1000 μsec. When the detector is cooled to 78 °K, its response is shifted to longer wavelengths (cut-off at about 4 μ). In addition the detectivity at spectral peak may be greater. Commercial suppliers include Eastman Kodak, Electronics Corporation of America, Infrared Industries, and the Bulova Watch Company.

Vol. 1 1961

PbSe detectors may be obtained for cooling at 78 °K or 190 °K. Detectivity at spectral peak is similar for the two types. When PbSe detectors are operated at room temperature, their detectivity is lowered considerably. Time constants of the cooled PbSe detectors vary between 10 and 100 μsec. The 78 °K detector differs from the 190 °K detector by its higher resistance (50–100 MΩ/square) and its spectral response (see Fig. 4). Commercial supplier for the 190 °K detector is the Santa Barbara Research Center. PbSe detectors for use at room temperature and 78 °K may be obtained from Eastman Kodak and the Santa Barbara Research Center.

Considerable improvement in D^* has been obtained at the Santa Barbara Research Center for the chemically deposited detectors at liquid nitrogen temperature upon reduction of background radiation. This has been accomplished by reducing the angular field of view and by using a thin cooled quartz layer as a filter directly over the PbSe film. Such techniques, however, increase the time constant to values ranging between 100 and 1000 μsec, depending on the amount of background which has been suppressed.

PbTe detectors are produced by evaporation of PbTe and subsequent sensitization of the layer with oxygen.[10] Their characteristics are similar to PbSe. While these detectors can be prepared with considerable ease in the laboratory, considerable difficulty has been encountered in manufacturing large quantities of these detectors reproducibly and of high quality. Commercial detectors of this type are available from ITT, Minneapolis Honeywell, and Mullard International Electronics Corporation.

Single Crystal Intrinsic Detectors

Single crystal photoconductive InSb detectors[11] are prepared by combining In and Sb in stoichiometric proportions, purifying the resulting compound and then growing it in the form of a single crystal. For best results, the crystal must contain as few impurities as possible but must be slightly "p" type at liquid nitrogen temperature. The crystal is then cut into thin slices of the desired dimensions, leads are attached to the slice and it is mounted on the inside of a dewar type container. A typical spectral response of an experimental detector prepared at Syracuse University is shown in Fig. 3. Since the detector is background limited at 78 °K, considerable increase in D^*_λ; may be obtained when the angular field of view is reduced. Time constants of these detectors are of the order of 1 μsec. This is increased to values as large as 10 μsec as the angular field of view is reduced. When the detector is to be operated at dry ice temperature, the starting InSb must be prepared with greater "p" type impurity concentration. Detectors of this type are available commercially from Radiation Electronics.

Photovoltaic InSb detectors are prepared either by producing a p–n junction during crystal growth,[12] or by starting with a single crystal and then producing a p–n junction at the surface either by an alloying[13] or a diffusion technique. Their spectral response varies somewhat with the preparation of the surface of the crystal. Average commercial detectors have a spectral curve similar to that shown in Fig. 4. These detectors have a time constant of about 1 μsec and must be operated in the vicinity of liquid nitrogen temperature. Since conditions involved in the production of these detectors may be controlled, considerable improvement in the response of the average detector should be achieved in the near future such that even the average detectors will approach the theoretical value given in Fig. 2. Among commercial suppliers for these detectors are Philco Corporation, Texas Instruments, and the Santa Barbara Research Center.

IMPURITY ACTIVATED GERMANIUM DETECTORS

The spectral response of these detectors consists of the response of Ge with a peak at 1·5 μ and a cut-off at 1·8 μ superimposed on the response characteristic of the impurity.

Gold in Germanium

Gold atoms are added to germanium during the growth process of a single crystal. Photons of energy greater than 0·14 eV are required to free charge carriers.[14, 15] This leads to a spectral response extending to 9 μ, superimposed on the spectral response of pure Ge which extends to about 1·8 μ. Ge : Au detectors become background limited at 60 °K. Because of the lack of a convenient coolant, they are generally operated at 78 °K, the boiling point of liquid nitrogen, at a considerable loss in detectivity. Fig. 5 shows the

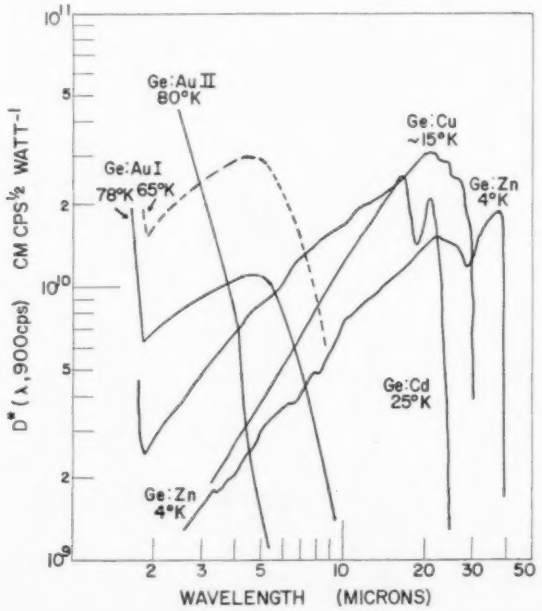

FIG. 5. Spectral response of impurity activated Ge detectors.

spectral response of an experimental Ge : Au detector prepared at Syracuse University at the two temperatures. Commercial detectors of this type are available from Westinghouse, Raytheon, Philco, R.C.A., and Santa Barbara Research Center. Time constants for different detectors vary between 0·01 and 1 μsec. Ge : Au crystals are generally mounted in an integration sphere. This increases the efficiency of the element by reflecting back into the crystal much of the infrared radiation which has not been absorbed during the first passage of the radiation through the crystal. When the detector is background limited, the integration sphere at liquid nitrogen temperature further increases the detectivity by limiting the angular field of view of the detector, thereby reducing the background radiation.

The absorbing centers in Ge : Au detectors are neutral gold atoms. Generally donor impurities are present which supply electrons to these atoms, thereby decreasing the number of absorbing centers. When each Au atom receives one additional electron to become a

Vol. 1 1961

negative ion, the response no longer extends to 9 μ. Further addition of donor impurities produces a double negative charge on the gold atom. Donor impurities such as Sb or As are incorporated during crystal growth. The energy required to free the second electron is 0·2 eV. This leads to a detector with spectral response extending to 6 μ (Fig. 5). Detectors of this type are commercially available from Philco. Their time constant, in contrast to the 9 μ detector, varies anywhere between 50 and 2000 μsec.[16] Because of the larger activation energy, these detectors may be operated at 90 °K.

Cadmium in Germanium

The addition of Cadmium to Ge produces a detector with a long wavelength threshold at 25 μ. The spectral curve of such a detector with a 60° angular field of view prepared at Syracuse University is shown in Fig. 5. Since the energy required to free charge carriers (holes) from the Cd atoms is only 0·05 eV, the detector must be cooled to about 25 °K before it becomes background limited. Liquid hydrogen is thus a suitable coolant. Above 25 °K, the detectivity decreases rapidly with increasing temperature and approaches zero as lattice vibrations free more and more charge carriers from the Cd atoms.

Copper in Germanium

Copper may be added to Ge by a diffusion process after the crystal has been grown. The spectral response of a 60° field experimental detector prepared at Syracuse University is shown in Fig. 5. Similar detectors are available commercially from the Santa Barbara Research Center and Texas Instruments. Since the energy to free holes from Cu atoms is only 0·04 eV, the detector must be cooled to about 18 °K before it becomes background limited.

Zinc in Germanium

Zinc impurities are added to intrinsic Ge while the Ge crystal is grown. Since the energy to free charge carriers is only about 0·03 eV, the long wavelength threshold of this detector is at about 40 μ.[17, 18] Zinc may be added to Ge in greater amounts than either Au or Cu. This makes possible the use of thinner samples. An integration sphere when used, merely serves to reduce background radiation. Fig. 5 shows the typical spectral response of such an experimental Ge : Zn detector with an angular field of view of 60° cooled to about 5 °K. Commercial units of this type are available from the Perkin–Elmer Corporation. This detector must be cooled to at least 10 °K before it becomes background limited. Because of the convenience of liquid helium, the sample is generally mounted in a double dewar containing chambers for liquid nitrogen and liquid helium.

A second type of Ge : Zn detector is obtained when all Zn atoms are singly ionized. This is accomplished by adding Sb or As atoms in number equal to Zn during the crystal growth process. Holes must now be freed from the singly charged Zn ions. This process requires more energy and leads to a detector which has a spectral response to only 15 μ but requires cooling to only 40 °K. Since no convenient coolant is available for that temperature, this detector has not as yet been fully developed.

Antimony in Germanium

The addition of Sb to the Ge melt produces detectors which have the longest wavelength response of any photon detector.[19] The energy required to free electrons from Sb atoms in Ge is about 0·01 eV, leading to a long wavelength threshold at about 130 μ. Such a detector

requires cooling to about 2 °K before it becomes background limited. Experimental detectors of this type have been prepared at the Radar Research Establishment at Malvern, England, and at Syracuse University.

Impurity Activated Ge : Si *Detectors*

The temperature at which a detector becomes background limited depends strongly on the activation energy of the charge carriers. In the case of impurities in Ge, this number depends on the type of impurity atom. When silicon is added to the Ge lattice, the activation energy for a particular impurity becomes variable and depends on the relative amounts of Ge and Si. It is thus possible to adjust the activation energy of a particular impurity until it may be used in conjunction with available coolants. Detectors of this type with various impurities are in the developmental stage at R.C.A. Of special interest is a Ge : Si alloy detector containing singly charged zinc ions. This detector has a spectral cut-off at about 14 μ and may be operated by using liquid air whose temperature is lowered to between 50° and 60 °K by rapidly reducing the pressure over the liquid.

DETECTOR ANALYSIS

The theoretical limit of the detectivity has been given by equations (9) and (10).

During recent years, considerable progress has been made in obtaining an understanding of the conduction processes in single crystals. This has made it possible to evaluate the performance of most single crystal detectors in order to see how this limit may be approached. The following analysis of Ge : Au detectors may be applied with minor modifications to all impurity activated detectors and an analysis along similar lines may be performed on intrinsic detectors such as InSb and InAs. In the case of Ge : Au, incoming photons free charge carriers (holes) from the neutral gold atoms. These charge carriers travel through the crystal at thermal velocities until they are captured by singly ionized gold centers. The time constant, τ, of the detector is given by

$$\tau = \frac{1}{N_D v \sigma} \tag{11}$$

where N_D represents the number of singly ionized gold centers (these are atoms which have accepted an extra electron from donor impurities), v is the thermal velocity of the charge carriers, and σ is the capture cross section of the negative gold ions for positive holes. Since $N_D \sim 10^{14}/\text{cm}^3$, $v \sim 10^7$ cm/sec, and $\sigma \sim 10^{-13}$ cm^2. τ turns out to be about 0·01 μsec. This value may be increased or decreased by varying N_D.

D^* given by equation (7) depends on the number of photons which are absorbed and on the number of free charge carriers in the sensitive element. The efficiency of absorption is given by the relation

$$\eta = \frac{(1 - R)(1 - e^{\alpha t})}{1 - R\, e^{-\alpha t}} \tag{12}$$

where R is the fraction of radiation reflected from the surface of Ge, α the absorption coefficient, and t the thickness of the sensitive crystal. For $\alpha t \ll 1$, as is the case in the Ge : Au sample, $\eta \propto \alpha t$. α is proportional to the number of those gold centers which interact with incoming photons. These are the neutral gold atoms. Their number is equal to

Vol. 1 1961

the gold atoms (N) originally incorporated in the crystal minus those (N_D) which have accepted an electron. Thus, $\eta \propto (N - N_D)t$.

The number of free charge carriers in the crystal depends on the temperature of the crystal and the amount of background radiation falling onto the crystal. When the detector is background limited, the background radiation determines the charge carrier concentration and D^* may be obtained by substituting $(N - N_D)t$ for η in equation (9) giving

$$D^* \propto \frac{[(N - N_D)t]^{1/2}}{(Q_B)^{1/2}}. \tag{13}$$

At higher temperatures, in the absence of a signal, lattice vibrations are mainly responsible for freeing charge carriers. When their number is much less than N_D, as is the case for photoconductive detectors

$$n_{TH} = 2V\left(\frac{N - N_D}{N_D}\right)\left(\frac{2\pi m^* kT}{h^2}\right)\exp(-\Delta\epsilon/kT) \tag{14}$$

where V is the crystal volume, m^* the effective mass of the charge carriers, and $\Delta\epsilon$ the activation energy (0·14 eV for Au in Ge). Substituting

$$V\left(\frac{N - N_D}{N_D}\right)\exp(-\Delta\epsilon/kT) \text{ for } n, \quad \frac{1}{N_D} \text{ for } \tau, \text{ and } (N - N_D)t \text{ for } \eta$$

in equation (7), one obtains

$$D^* \propto [(N - N_D)t]^{1/2}\exp(\Delta\epsilon/2kT) \tag{15}$$

For practical Ge : Au detectors this value at 78 °K is lower than D^* at 60 °K (by a factor of about three). The number of gold atoms which can be added to Ge generally does not exceed $5 \times 10^{15}/\text{cm}^3$ of Ge. Thus N_D, the number of donor impurities, should not exceed 10^{14}. In the case where time constants much shorter than 0·1 μsec are required, this value might be increased safely to 5×10^{14}. When an integration sphere is used, an additional factor (depending on the amount of integration) should be incorporated in equations (13) and (15). D^*, of course, can never exceed the value given by expression (9) when η is taken as unity.

REFERENCES

1. This technique was first suggested by E. BURSTEIN at W. Nottingham Photoconductivity Conference, March, 1949.
2. NEWMAN, R., and W. W. TYLER, *Solid-State Physics*, Vol. VIII, p. 49. Academic Press, New York.
3. MORTON, G. A., M. L. SCHULTZ, and W. E. HARTY, *R.C.A. Rev.* **20**, p. 599 (1959).
4. PRUETT, G. R., and R. L. PETRITZ, *Proc. Inst. Radio Engrs.* **47**, 1524 (1959).
5. MAC RAE, A. U., and H. LEVINSTEIN, *Phys. Rev.* **119**, 62 (1960).
6. VAN VLIET, K. M., *Proc. Inst. Radio Engrs.* **46**, 1004 (1958).
7. JONES, R. C., *Proc. Inst. Radio Engrs.* **47**, 1498 (1959).
8. MOSS, T. S., *Proc. Inst. Radio Engrs.* **43**, 1869 (1955).
9. CASHMAN, R. J., *Proc. Inst. Radio Engrs.* **47**, 1471 (1959).

10. BODE, D. E., and H. LEVINSTEIN, *Phys. Rev.* **96**, 259 (1954).
11. GOODWIN, D. W., *J. Sci. Instr.* **34**, 367 (1957).
12. MITCHELL, G. R., A. E. GOLDBERG, and S. W. KURNICK, *Phys. Rev.* **97**, 239 (1955).
13. LASSER, M. E., P. CHOLET, and E. C. WURST, *J. Opt. Soc. Amer.* **48**, 468 (1958).
14. MORTON, G. A., E. E. HAHN, and M. L. SCHULTZ, Photoconductivity Conference, John Wiley, New York (1956).
15. DUNLAP, W. C., *Phys. Rev.* **91**, 1282 (1953); **97**, 614 (1955).
16. JOHNSON, L., and H. LEVINSTEIN, *Phys. Rev.* **117**, 1191 (1960).
17. E. BURSTEIN, J. W. DAVISON, F. E. BELL, W. J. TURNER, and H. G. LIPSON, *Phys. Rev.* **93**, 65 (1954).
18. PICUS, G., and S. F. JACOBS, 5th Conference of the International Commission for Optics, Stockholm, August 1959.
19. FRY, S. J., and C. F. OLIVER, *J. Sci. Instrum.* **36**, 195 (1959).

Vol.
1
1961

Infrared Physics, 1961, Vol. 1, pp. 39–48. Pergamon Press Ltd., Printed in Great Britain.

INTERFERENZ-MODULATION MIT MONOCHROMATISCHEN MILLIMETER-WELLEN

H. HAPP und L. GENZEL

Physikalisches Institut der Universität, Frankfurt/Main, Deutschland

Abstract—The work reported here relates to a millimeter-wave investigation of the principal features of a periodically working Interference-Modulator (I.M.). Its characteristic spectral function $B_n(\lambda)$ could immediately be obtained with the help of monochromatic radiation and scanning the I.M. through its wavelength scale, the radiation being produced by microwave techniques. Furthermore we have studied the resulting signal when several discrete wavelengths were present, this being a first step in the direction of employing continuous radiation. To improve the spectral purity of the I.M. a process usually called apodization was applied to the I.M.-signal. The experimental results are discussed and compared with theory.

EINLEITUNG

IN einigen vorausgegangenen Publikationen[1, 2, 3] wurde die Theorie der Interferenzmodulation für Zweistrahl-Interferenzen dargelegt und ein periodisch arbeitender Interferenzmodulator (I.M.) für das Gebiet von 0,2–4 mm Wellenlänge, sowie seine spektroskopischen Eigenschaften beschrieben[4]. Die vorliegende Arbeit befasst sich mit der experimentellen Prüfung dieses I.M. mittels monochromatischer Mikrowellenstrahlung. Die Benutzung dieser Strahlung eröffnet die Möglichkeit, die prinzipiellen Züge der Theorie in durchsichtiger Weise zu prüfen und festzustellen, in wieweit die technische Ausführung des I.M. den von der Theorie gestellten Forderungen genügt.

Zum besseren Verständnis der Untersuchung sollen zunächst noch einmal die wichtigsten, theoretisch zu erwartenden Eigenschaften des I.M. zusammengestellt werden.

Der hier betrachtete I.M. besteht im wesentlichen aus einem Laminargitter, Fig. 1, das

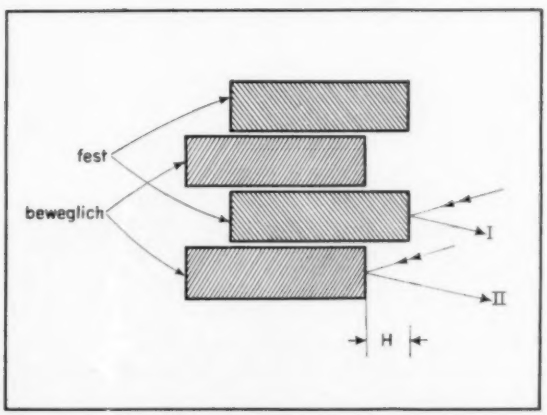

FIG. 1. Ausschnitt aus dem Laminargitter-I.M. in schematischer Darstellung. I und II repräsentieren die interferierenden Bündel.

aus einem feststehenden und einem beweglichen System von Stäben zusammengesetzt ist und im Spektrum O. Ordnung seiner Gitterbeugung arbeitet[4]. Die mit der Intensität $dI_0 = E(\lambda)d\lambda$ im Wellenlängenbereich $d\lambda$ auffallende Strahlung wird in zwei intensitätsgleiche Bündel I und II zerlegt, die nach Reflexion bei nahezu Autokollimation einen Gangunterschied $\gamma = 2H$ bzw. einen Phasenunterschied $\varphi = 2\pi\gamma/\lambda$ haben. Die Intensität am Interferenzort, an dem sich der Strahlungsempfänger befindet, ist dann abhängig von φ in der Form

$$dI(\lambda) = \tfrac{1}{2}E(\lambda)\, d\lambda\, (1 + \cos\varphi) \tag{1}$$

Das bewegliche System des I.M. bewegt sich in der Zeit T_0 zeitlinear (abgesehen von den Umkehrstellen) von $H = 0$ nach $H = H_{\max}$ und zurück. Dieser Zyklus wiederholt sich periodisch. Innerhalb des Zeitbereiches $-\,T_0/2 \leq t \leq T_0/2$ ändert sich φ in der Form

$$\varphi = \pi \frac{\gamma_{\max}}{\lambda/2} \frac{|t|}{T_0/2} = \omega_0 \mu |t| \tag{2}$$

wobei

$$\omega_0 = 2\pi/T_0; \quad \mu = 2\gamma_{\max}/\lambda; \quad \gamma_{\max} = 2H_{\max}$$

ist.

Das $dI(\lambda)$ proportionale Empfängersignal ist dann in diesem Zeitintervall zeitlich veränderlich entsprechend der Modulationsfunktion

$$F(t) = 1 + \cos\omega_0\mu t \tag{3}$$

$F(t)$ ist periodisch mit ω_0. Seine Fourierreihe lautet:

$$F(t) = \frac{B_0}{2} + \sum_m B_m \cos m\omega_0 t \tag{4}$$

Die Koeffizienten ergeben sich zu

$$B_0(\mu) = 2\left(1 + \frac{\sin\pi\mu}{\pi\mu}\right) \tag{5}$$

$$B_m(\mu) = \frac{2}{\pi}\cos\pi m \frac{\sin\pi\mu}{\mu - \dfrac{m^2}{\mu}} \tag{6}$$

Diese Koeffizienten, und damit die Form von $F(t)$, hängen von μ ab. Man sieht leicht ein, dass für $\mu = m$, $m = 1, 2, 3, \ldots$. $F(t)$ die einfache Form

$$F(t) = 1 + \cos m\omega_0 t \tag{7}$$

annimmt, während für nicht ganzzahliges μ die volle Fourierreihe auftritt.

Das Empfängersignal wird einer Fourieranalyse unterworfen, im vorliegenden Fall realisiert durch einen selektiven Verstärker, der nur die Modulationsfrequenz $n\omega_0$ durchlässt und verstärkt. n ist ein spezieller Wert für m. Ueber das den Analysator verlassende Signal S kann man folgende Aussage machen.

Vol. 1 1961

Hält man γ_{max} fest, so gibt es gewisse Wellenlängen λ_m, für die $\mu = m$ ist. Die diesen Wellenlängen zugeordneten Modulationsfunktionen besitzen die einfache Form (7). Wären nur diese Wellenlängen in der Strahlung vorhanden, so wäre eine exakte spektrale Zerlegung möglich, da nur die Wellenlänge λ_n mit $m = n$ zu S beiträgt.

Die Wellenlängen mit $\mu \neq m$ liefern aber auch einen Beitrag zur Modulationsfrequenz $n\omega_0$, und somit zu S, weil ihre volle Fourierreihe auftritt. Diese Beiträge stellen eine spektrale Verunreinigung des Signales für λ_n dar.

Es ist somit

$$S \sim \int_{\lambda} B_n \left(\frac{2\gamma_{max}}{\lambda}\right) E(\lambda) d\lambda \tag{8}$$

$B_n\,(2\gamma_{max}/\lambda)$ gibt also bei festem γ_{max} in Abhängigkeit von λ den relativen Beitrag an, den die Strahlung der Wellenlänge λ zum Signal S liefert.

Die Tatsache, dass B_n von μ, also dem Verhältnis $2\gamma_{max}/\lambda$ abhängt, gibt nun die Möglichkeit, diese Funktion experimentell zu bestimmen. Man kann ja auch μ dadurch variieren, dass man monochromatische Strahlung mit fester Wellenlänge $\lambda^{(i)}$ benutzt und γ_{max} variiert. Dann ist

$$S \sim B_n \left(\frac{2\gamma_{max}}{\lambda^{(i)}}\right) \tag{9}$$

entgegen (8), wo B_n im Integral auftritt. Für diese Untersuchung ist natürlich mikrowellentechnisch erzeugte Strahlung besonders geeignet. Darüber hinaus kann man durch diese Technik Strahlung herstellen, die mehrere diskrete Wellenlängen $\lambda^{(i)}$ enthält, wobei dann

$$S \sim \sum_i B_n \left(\frac{2\gamma_{max}}{\lambda^{(i)}}\right) J_i \tag{10}$$

wird. J_i bezeichnet die Strahlungsintensität der diskreten Wellenlänge $\lambda^{(i)}$. (10) ist die einfache Form, auf die sich das Integral (8) bei Vorhandensein einiger diskreter Wellenlängen reduziert.

EXPERIMENTELLES

Die optische Anordnung, in der der I.M. arbeitet, entspricht weitgehend der in [6] gegebenen*. Der Strahlungsempfänger ist ein Bolometer, dessen Signal einem selektiven 12,5 Hz—Verstärker mit 0,2 Hz Bandbreite zugeführt wird. Nach Verstärkung und linearer Gleichrichtung wird das Signal registriert. Die Erzeugung der Mikrowellenstrahlung erfolgt durch die übliche Vervielfachertechnik [5, 6]. Die Vervielfacheranordnung wurde mit einem 12,5 mm Klystron betrieben, die Vervielfacherdiode war eine Ge–W Kombination. Von den auftretenden Harmonischen wurde die 4.–7. bei $\lambda^{(i)} = 3{,}085,\ 2{,}470,\ 2{,}058,\ 1{,}763$ mm verwendet. Für die Untersuchung, bei der nur eine Wellenlänge erwünscht war, konnten die übrigen Harmonischen durch geeignete Abstimmung des Vervielfachers weitgehend unterdrückt werden.

* Das Glanzwinkel–Echelette–Gitter wurde durch den I.M. ersetzt und der Strahlengang in Autokollimation benutzt.

UNTERSUCHUNG DER FUNKTION $B_n(\mu)$ MIT MONOCHROMATISCHER STRAHLUNG

Die Vervielfacheranordnung wurde auf die 5. Harmonische der Klystronstrahlung abgestimmt, deren Wellenlänge $\lambda^{(5)} = 2{,}470$ mm betrug. Die übrigen Harmonischen hatten höchstens 10 Prozent der Intensität dieser Strahlung. Für die Fourieranalyse wurde $n = 25$ gewählt, und $n\omega_0 = 2\pi$ 12,5 Hz.

Beim vorliegenden I.M. kann γ_{max} stetig mit einer Geschwindigkeit, die klein ist gegen die Bewegungsgeschwindigkeit des Gitters, verändert werden. Jedem γ_{max} ist formal durch die Beziehung $\mu = n$ eine Wellenlänge λ_n zugeordnet.

$$\lambda_n = \frac{2\gamma_{max}}{n} \tag{11}$$

Diese Wellenlänge λ_n ist die zu der gerade vorhandenen Einstellung von γ_{max} "passende" Wellenlänge, die also ein rein mit $n\omega_0$ cos-förmig moduliertes Signal ergeben würde. Anstelle einer γ_{max}—Skala ist der I.M. mit einer λ_n—Skala versehen. Mit λ_n formuliert ist im vorliegenden Fall $\mu = n\lambda_n/\lambda^{(5)}$ und

$$B_n = B_n\left(n\frac{\lambda_n}{\lambda^{(5)}}\right) \tag{12}$$

Das experimentelle B_n wird dementsprechend über einer λ_n—Skala aufgetragen. Die zugehörigen Werte von μ sind ebenfalls angegeben. Gemäss (6) und früherer Ausführungen[3, 4] erwartet man in dieser Darstellung folgendes prinzipielles Aussehen von $B_n(\mu)$, siehe Tabelle 1):

TABELLE 1

μ	λ_n	$B_n(\mu)$
n	$\lambda^{(5)}$	1
$n \pm k$	$\frac{(n \pm k)\cdot\lambda^{(5)}}{n}$	0
$n \pm k \pm \frac{1}{2}$ (k ganzzahlig)	$\frac{(n \pm k \pm \frac{1}{2})\lambda^{(5)}}{n}$	$\approx \frac{2}{\pi(2k+1)}$

Der Maximalwert von B_n ist 1 und liegt bei $\mu = n$. Zwischen den Nullstellen von B_n liegt je ein Nebenmaximum näherungsweise bei $n \pm k \pm \frac{1}{2}$. Für grosse n hat B_n dort die oben angegebenen Werte. Die Nullstellen liegen äquidistant mit dem Abstand $\lambda^{(5)}/n$ auf der λ_n—Skala. Fig. 2 zeigt das experimentelle Ergebnis bei Einstrahlung der 5. Harmonischen der Klystronstrahlung. Das Hauptmaximum liegt bei $\lambda_n = \lambda^{(5)} = 2{,}47$ mm, da dort die eingestrahlte Wellenlänge "passt". Die senkrechten Striche unterhalb der Skala bedeuten die theoretische Lage der Nullstellen, gekennzeichnet durch $\mu = m$, die gestrichelte Kurve die Enveloppe der Beträge der Nebenextrema. Die $\pm$ Zeichen bedeuten die Vorzeichen von B_n.

Vol. 1 1961

DISKUSSION

Im allgemeinen entspricht das experimentelle B_n den Erwartungen. Die Unstimmigkeiten auf der langwelligen Seite sind sehr wahrscheinlich mechanischen Unzulänglichkeiten des I.M. zuzuschreiben, die später noch erörtert werden. Die 6. und 7. Harmonische der Klystronstrahlung mit $\lambda^{(6)} = 2{,}058$ mm und $\lambda^{(7)} = 1{,}763$ mm machen sich noch etwas bemerkbar und beeinflussen die Funktion auf der kurzwelligen Seite des Hauptmaximums.

Geht man auf die eingangs dargelegte Deutung von B_n bei Vorhandensein kontinuierlicher Strahlung zurück, so übersieht man durch die Fig. 2, welche Beiträge die einzelnen

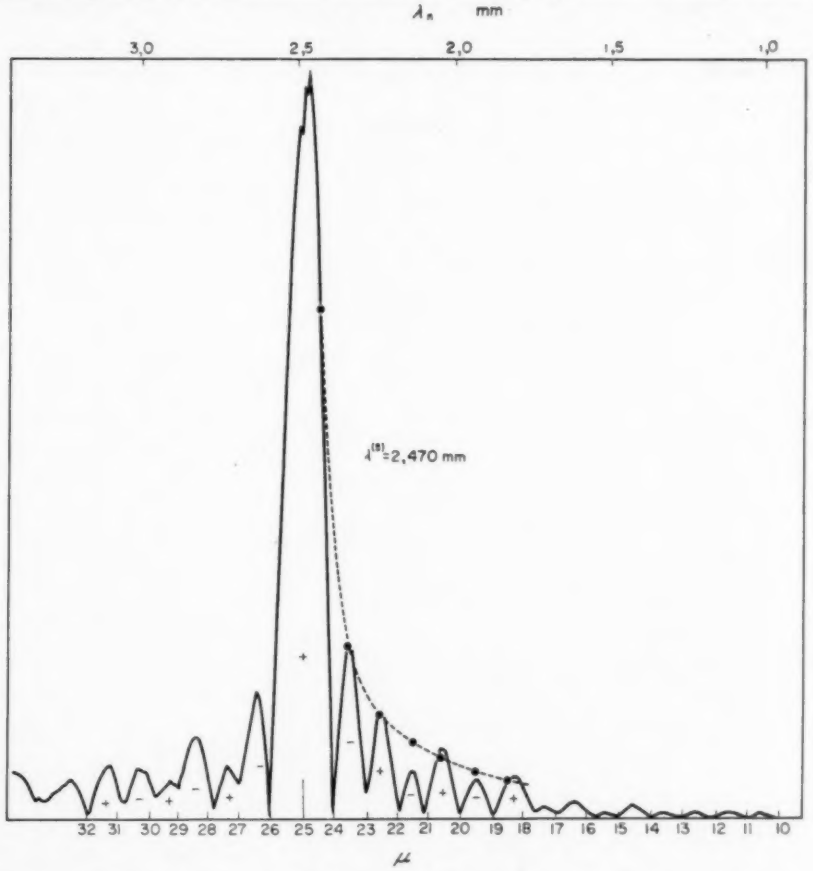

FIG. 2. Registrierung des I.M.-Signals bei Einstrahlung von $\lambda^{(5)} = 2{,}47$ mm. Diese Kurve repräsentiert im Idealfall $\left| B_{25}\left(\frac{\lambda_n}{\lambda^{(5)}}\right)\right|$.

Stellen des Strahlungsspektrums, gekennzeichnet durch ihr μ, zum Signal S geben. Allerdings ist zu berücksichtigen, dass in diesem Falle S durch das Integral (8) über B_n gegeben ist und wegen der Vorzeichenweschel sich die Beiträge der einzelnen Wellenlängenbereiche am Empfänger teilweise kompensieren. Für den Fall $E(\lambda) = \text{const.}$ ist dem Anhang der Arbeit[3] eine Abschätzung des Beitrages der Wellenlängen ausserhalb der 1. Nullstellen zu S entnehmbar. Er beträgt danach ungefähr 20 Prozent.

SIGNAL S BEI VORHANDENSEIN MEHRERER HARMONISCHER

Figur 3 zeigt eine Registrierung, bei der die 4.–7. Harmonische der Klystronstrahlung vorhanden war. Ist $\lambda^{(0)}$ die Wellenlänge der Grundstrahlung, so ist die Wellenlänge der der i.—Harmonischen $\lambda^{(i)} = \lambda^{(0)}/i$. Unter der Voraussetzung, dass die Lage der starken 4. Harmonischen korrekt sei, ist die theoretische Lage der Hauptmaxima der anderen Harmonischen auf der λ_n—Skala angegeben. Man erkennt, dass die grösseren Maxima nicht nur von diesen Harmonischen herrühren können, da sie nicht an den geforderten Stellen liegen. Ist der I.M. z.B. auf die 5. Harmonische eingestellt, so existieren an dieser Stelle natürlich auch Signale der übrigen Harmonischen gemäss Fig. 2. Das Signal S wird also durch den Ausdruck (10) angegeben, wobei durch die Vorzeichen der B_n $(n\lambda_n/\lambda^{(i)})$ teils Verminderung, an anderen Stellen Vermehrung des Signals der 5. Harmonischen auftreten kann. Aus der Fig. 3, in der auch die Nullstellen von B_n $(n\lambda_n/\lambda^{(4)})$ angegeben sind, ersieht

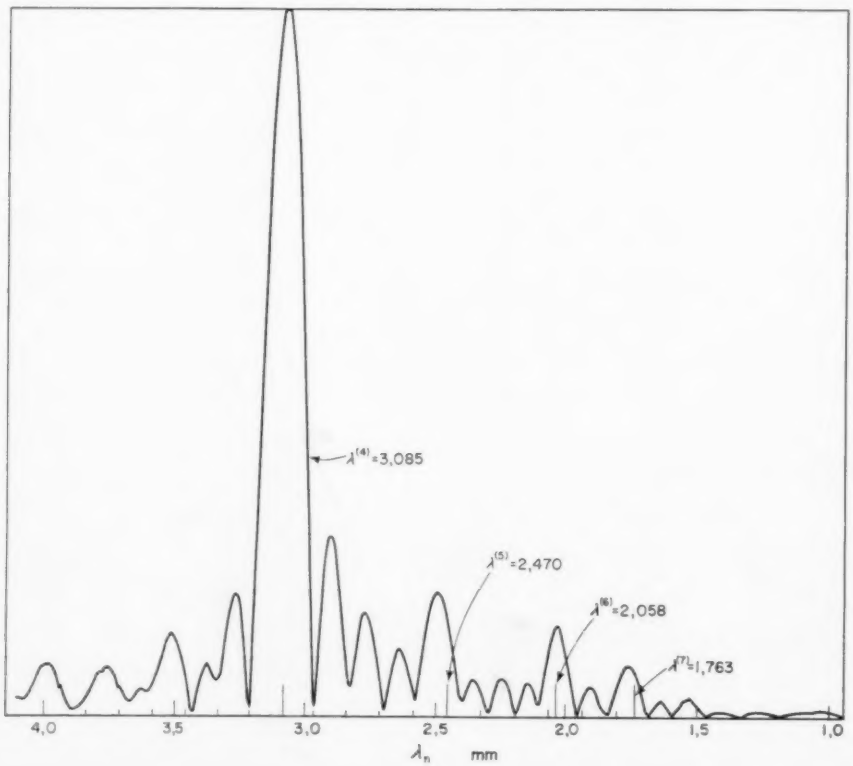

FIG. 3. Registrierung des I.M.-Signals bei Einstrahlung der 4.–7. Mikrowellen-Harmonischen.

man z.B., dass das Hauptmaximum der 5. Harmonischen mit einer Nullstelle des zu $\lambda^{(4)} = 3{,}085$ gehörenden B_n zusammenfällt. Dieses B_n wechselt dort aber sein Vorzeichen, wird also auf der langwelligen Seite der Nullstelle das Signal der 5. Harmonischen verstärken, auf der kurzwelligen Seite vermindern, so dass scheinbar eine Verrückung des Hauptmaximums der 5. Harmonischen auftritt. Das Bild wird überhaupt stark durch die 4. Harmonische bestimmt. Dividiert man den Abstand der Harmonischen durch den

Vol. 1 1961

Abstand der Nullstellen der 4. Harmonischen, so ergibt sich, dass letztere 4 Nebenmaxima zwischen ihrem Hauptmaximum und der 5. Harmonischen besitzt und 3 zwischen der 5. und 6. Die auftretenden Maxima sind also wesentlich durch die 4. Harmonische bedingt.

APODIZATION

Die Tatsache, dass zum Signal S ausser der passenden auch die übrigen Wellenlängen des Spektrums beitragen und dadurch unter Umständen Bereiche geringerer Intensität von solchen grosser Intensität ernsthaft gestört werden, legt den Versuch nahe, den Einfluss nichtpassender Wellenlängen herabzudrücken. Ein derartiges Vorgehen ist unter dem Namen Apodisation bekannt[7]. Im vorliegendem Falle führt folgende Ueberlegung zum Ziel: Gewünscht wird, dass die Modulationsfunktion für $\mu \neq n$ ein möglichst kleines B_n enthält. Mit dieser Absicht wird die Strahlungsintensität primär zusätzlich mit einer Funktion $C(t)$ moduliert, so dass die wirksame Modulationsfunktion lautet

$$F^*(t) = F(t)\, C(t) \tag{13}$$

$F(t)$ ist die Funktion (3), $C(t)$ sei periodisch mit ω_0 und es gilt $0 \leq C(t) \leq 1$.

Für $F^*(t)$ und $C(t)$ werden folgende Fourierreihen angesetzt

$$F^*(t) = \frac{B_0^*}{2} + \sum_m B_m^* \cos m\omega_0 t \tag{14}$$

Alle B sind wieder Funktionen von μ.

$$C(t) = \frac{C_0}{2} + \sum_{k=1}^{\infty} C_k \cos k\omega_0 t \tag{15}$$

Der interessierende Fourierkoeffizient B_n^* der Entwicklung (14) ergibt sich aus

$$B_n^*(\mu) = \frac{2}{T_0} \int_{-T_0/2}^{+T_0/2} F(t)\, C(t) \cos n\omega_0 t \, dt \tag{16}$$

Einführung von (15) in (16) führt zu der Darstellung

$$B_n^*(\mu) = \frac{B_0}{2} C_n + B_n \frac{C_0}{2} + \sum_{k=1}^{\infty} \frac{C_k}{2} B_{n+k} + \sum_{\substack{k=1 \\ k \neq n}}^{\infty} \frac{C_k}{2} B_{|n-k|} \tag{17}$$

Setzt man als einfachste Möglichkeit $C_i = 0$ für $i > 1$, so hat man

$$C(t) = \frac{C_0}{2} + C_1 \cos \omega_0 t \tag{18}$$

und

$$B_n^*(\mu) = B_n \frac{C_0}{2} + \frac{C_1}{2} (B_{n-1} + B_{n+1}) \tag{19}$$

Ist $\mu = n$, so ist $B_{n+1}(n) = 0$ und $B_n^* = B_n \cdot (C_0/2)$ Das passende Signal wird also um den Faktor $C_0/2$ reduziert.

Ist $\mu \neq n$, so kann durch geeignete Wahl von C_0/C_1 $B_n^* = 0$ gemacht werden für ein bestimmtes μ, wobei auch eine Verkleinerung von B_n^* für andere μ resultiert. Für $\mu = n \pm 1$ ist $B_n = 0$ und es bleibt das Glied mit C_1 übrig, das heisst, die beiden ersten Nullstellen neben der passenden Wellenlänge verschwinden, das Hauptmaximum wird durch die Apodisation notwendig breiter. Fig. 4(b) zeigt ein $B_n^*(\mu)$, welches mit einem gemäss (18) festgelegten $C(t)$ konstruiert wurde. Fig. 4(a) enthält die einzelnen Glieder von (19). In dem

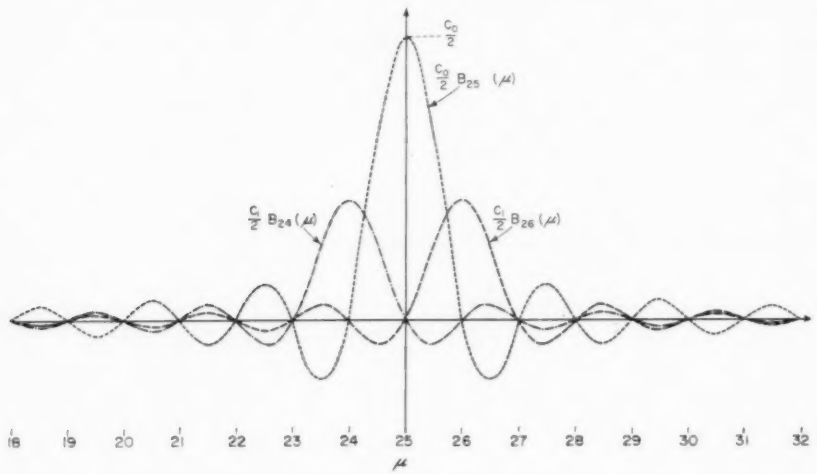

(a)

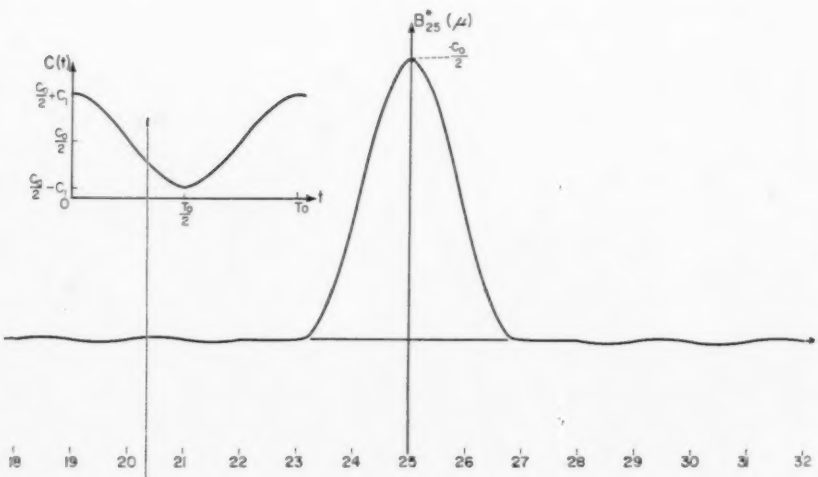

(b)

FIG. 4. Apodisation von B_{25} mit Hilfe von B_{24} und B_{26}; (a) Verlauf der B-Funktionen, multipliziert mit geeignet gewählten Konstanten C_0 und C_1. (b) Resultierendes $B_{25}^*(\mu)$ und Apodisationsfunktion $C(t)$.

Vol. 1 1961

gezeichneten Fall wurde B_n^* gleich 0 gesetzt für $\mu = 27{,}5$, wobei es aus Symmetriegründen auch für $\mu = 22{,}5$ gleich 0 ist. Man erkennt aus der Darstellung, dass B_n^* ausserhalb des Hauptmaximums nur noch etwa 1 Prozent des Wertes im Hauptmaximum hat.

Figur 5 zeigt eine Registrierung derselben Harmonischen wie in Fig. 3 mit Apodisation. Die Harmonischen sind jetzt recht gut isoliert und ihre Lagen auf der Skala stimmen annähernd mit den theoretischen Lagen überein, abgesehen von der Harmonischen bei 2,47 mm, die immer noch etwas von $\lambda^{(4)} = 3{,}085$ beeinflusst ist. Die Apodisation wurde aus technischen Gründen durch Variation des Verstärkungsgrades des Verstärkers entsprechend $C(t)$ vor den selektiven Stufen durchgeführt, was der Intensitätsmodulation äquivalent ist. Ganz allgemein lässt sich sagen, dass die Apodisation, also die Multiplikation der Modulations-Funktion $F(t)$ mit der Funktion $C(t)$, im Empfangsteil der Apparatur hinter der massgebenden Rauschquelle und vor der Fourierzerlegung zu erfolgen hat, um das Signal—Rausch Verhältnis nicht zu verschlechtern.

DISKUSSION DER RESULTATE

Die Resultate zeigen, dass der untersuchte I.M. die prinzipiellen Züge der Theorie richtig realisiert, und durch die Apodisation eine wesentliche Verbesserung der spektralen Reinheit zu erzielen ist. Allerdings erscheinen die feineren Details noch unbefriedigend.

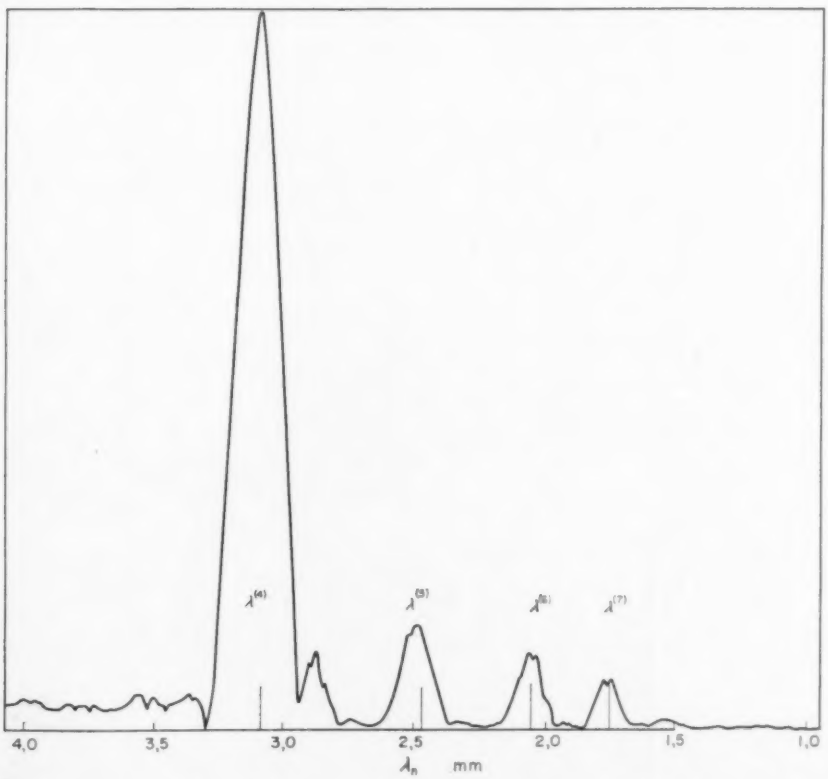

FIG. 5. Registrierung des I.M.-Signals bei Einstrahlung der 4.–7. Mikrowellen-Harmonischen mit Apodisation. Die Apodisationsfunktion entspricht etwa der in Fig. 4(b) gezeigten.

Diese Unstimmigkeiten sind bedingt durch die mechanischen Toleranzen des Instrumentes, die nicht vermieden werden konnten. Insbesondere ist kritisch, dass die Spiegelposition $H = 0$ exakt erreicht wird, was im vorliegenden Falle schwierig ist, da dort die Umkehrstelle der sonst zeitlinearen Bewegung ist, also grosse Trägheitskräfte auftreten. Nimmt man an, dass der Umkehrpunkt der Gitterbewegung nicht bei $H = 0$, sondern bei $H = h_0$ erfolgt, so entspricht dies einem Fehler im Gangunterschied $\gamma_0 = 2h_0$. Gemäss den Genauigkeitsansprüchen bei Zweistrahlinterferenzen muss $\gamma_0 \ll \lambda/4$ sein. Nach unserer Erfahrung ist $\gamma_0 \approx \lambda/10$ ausreichend. Für $\lambda = 0{,}2$ mm, der unteren Grenze des Arbeitsbereiches des untersuchten I.M., bedeutet dies eine Toleranz $h_0 \approx 0{,}01$ mm.

Die Rechnung zeigt, dass sich dann, wenn H am Umkehrpunkt des I.M. nicht genau 0 wird, die Lage des Hauptmaximums auf der λ_n—Skala verschiebt. Weiterhin braucht der Abstand der Nullstellen von B_n auf der λ_n—Skala nicht mehr konstant zu sein und die Höhen der Nebenmaxima nehmen nicht monoton ab. Dieser Effekt ist insbesondere auf der langwelligen Seite der Registrierungen der Harmonischen zu erkennen.

Die Untersuchung zeigt aber, dass der I.M., wenn die Spiegelpoisition z.B. nicht Umkehrpunkt der Bewegung ist, sondern die Bewegung symmetrisch um diese erfolgt und die mechanischen Toleranzen reduziert werden, den theoretischen Erwartungen voll entspricht. Hinsichtlich der Anwendung für spektroskopische Zwecke stellen wir in Übereinstimmung mit den in[2] gegebenen Ausführungen fest, dass der I.M., obgleich bereits allein zur spektroskopischen Zerlegung von Strahlen geeignet, in Verbindung mit einem Glanzwinkel–Echelette–Gitter die gegenwärtig günstigste Monochromatoranordnung für das ferne Ultrarot zu sein scheint.

Anerkennung—Wir danken Herrn Professor M. Czerny für sein förderndes Interesse an dieser Arbeit sowie fur die Bereitstellung von Institutsmitteln. Der Deutschen Forschungsgemeinschaft sind wir zu grossem Dank verpflichtet für die Mittel zum Aufbau des I.M.-Spektrometers und der Mikrowellen-Einrichtung.

LITERATUR

1. STRONG, J., *J. Opt. Soc. Amer.* **47**, 354 (1957).
2. GENZEL, L., und R. WEBER, *Z. angew. Phys.* **10**, 127 (1957).
3. GENZEL, L., *J. Mol. Spectro.*, **4**, 241 (1960).
4. GENZEL, L., und R. WEBER, *Z. angew. Phys.* **10**, 195 (1958).
5. KING, W. C., und W. GORDY, *Phys. Rev.* **93**, 407 (1954).
6. GENZEL, L., H. HAPP, und R. WEBER, *Z. Phys.* **154**, 1 (1959).
7. JACQUINOT, P. Apodization, Appendix E to STRONG, J.: *Concepts of Classical Optics*. Freeman, San Francisco, 1958.

Vol. 1 1961

Infrared Physics, 1961, Vol. 1, pp. 49–57. Pergamon Press Ltd., Printed in Great Britain.

SUNSEEKER FOR HIGH-ALTITUDE INFRARED SOLAR SPECTRA

P. A. LAPP and H. S. KERR

The De Havilland Aircraft of Canada, Limited, Special Products Division,
Downsview, Ontario, Canada

Abstract—A Sunseeker System is described which is installed in the wing-tip tank of a CF–100 aircraft. The instrument is capable of maintaining the solar image on the slit of a spectrometer contained within the tank to an accuracy of $\pm 4'$ of arc, thereby removing the effects of random angular motions of the aircraft. Factors leading to the optical and mechanical design of the equipment are presented, together with the overall systems considerations necessary for the successful operation of the instrument remotely by the flight crew of the aircraft. The equipment is primarily intended to be used for recording solar spectra through long atmospheric paths, so that the instrument is capable of operating up to an altitude of 45,000 ft and at sun elevations as low as $-2°$. Sample recordings are included which indicate the actual performance of the system under operational conditions, and which reveal that the $\pm 4'$ requirement on solar image stabilization was obtained. The Sunseeker System was developed for use by the Canadian Armament Research and Development Establishment in connection with their high-altitude infrared measurement program.

INTRODUCTION

THE equipment to be described is part of an overall research program by the Canadian Armament Research and Development Establishment for the measurement of infrared solar spectra at Canadian latitudes and at 40,000 ft for sun altitudes, in the main, between $+10°$ and $-2°$. The Sunseeker instrument is mounted in the port wing-tip pod of a CF–100 Mk IV–B aircraft.

De Havilland was assigned the task of designing and developing the equipment necessary to direct the solar radiation from a lens, mounted on the outside skin of the pod, to the slit of a spectrometer mounted at a fixed location within the pod. Within this general frame of reference, the following specifications formed the basis of design for the Sunseeker:

1. The maximum variation in flux flooding the spectrometer shall not exceed ± 5 per cent for periods of time not less than 30 sec. This is equivalent to maintaining the direction of the solar radiation entering the slit to within $\pm 4'$ of arc relative to the spectrometer axis.
2. The Sunseeker shall be capable of so tracking the sun for all sun altitudes between $-2°$ and $+67°$.
3. The Sunseeker shall be capable of acquiring the sun for angles off the lens axis up to $\pm 5°$, and maintain lock-on for sun angles off the lens axis up to $\pm 7{\cdot}5°$.
4. The Sunseeker shall provide suitable steering and lock-on signals to the pilot and navigator to assist in orienting the aircraft for tracking, and for remote operation of the system.

The Sunseeker system which resulted from the above specification is illustrated in Fig. 1. The lens mounted on the skin of the pod directs the solar radiation to a gimballed control

mirror located immediately behind the lens. This mirror reflects the sun's rays along the axis of the pod to two mirrors located near the spectrometer. These mirrors direct the solar flux onto the spectrometer slit and to a detector array. This array is located and so oriented that the solar image formed thereon bears a one-to-one correspondence in position to the image at the slit. When the solar image is not on the slit, the detecting system produces error signals relative to a two-dimensional rectangular co-ordinate system, whose axes correspond to the two-axis motion of the reflected beam from the gimballed control mirror. Servo amplifiers convert the error signals to power levels which, when applied to the servo drives on each axis, move the control mirror in a direction so as to minimize the error signals from the detector, thereby closing the loop and maintaining the solar image on the spectrometer slit.

Since the pilot is given steering information, and thereby attempts to fly the aircraft in the most optimum fashion, the servo system is required only to remove the residual motions of the incident beam relative to the spectrometer axis.

GENERAL DESIGN CONSIDERATIONS

Since the direction of the radiation from the sun relative to the aircraft moves very slowly with respect to inertial space (about 15°/hr for low aircraft speeds), the obvious initial approach would be to mount the spectrometer and external optics on a gyro-stabilized

Vol. 1 1961

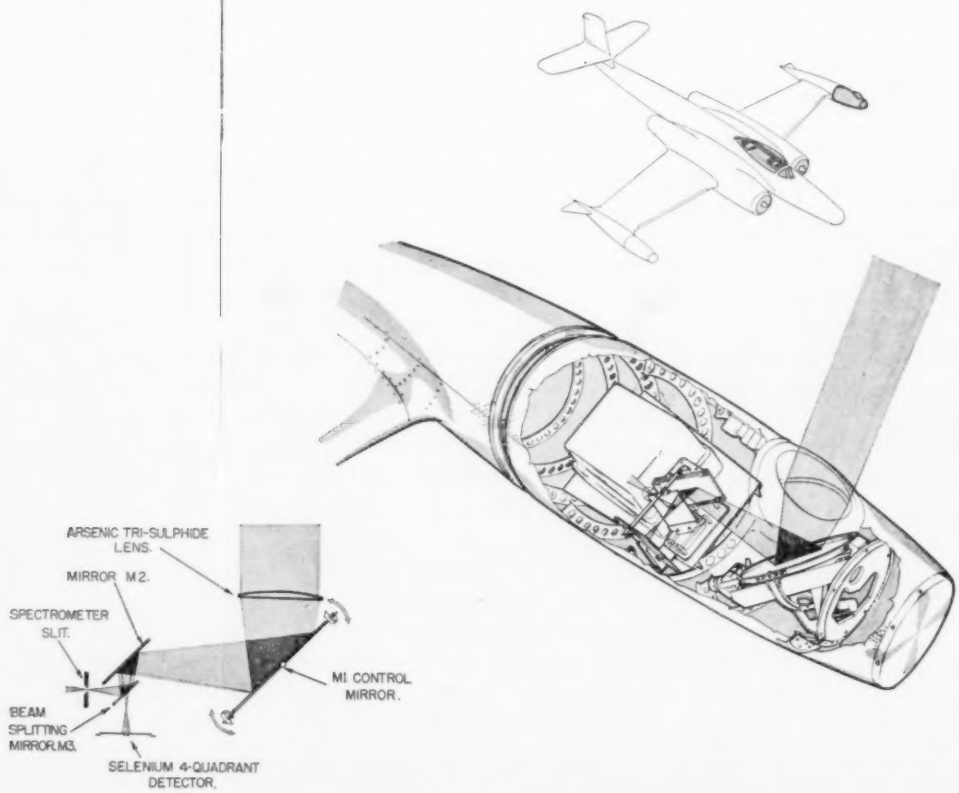

FIG. 1. Sunseeker system.

platform. However, due to space and weight limitations as well as the large amount of auxiliary equipment necessary for the spectrometer, a mount fixed to the pod structure had been specified. The angular motion of the entrance beam therefore had to be converted to aircraft motion relative to inertial space, so that a gyro-stabilized platform was not required.

Due to space limitations within the pod, the spectrometer axis was specified as parallel to, but displaced from, the pod axis by a few inches. The Sunseeker system had to cater for a 10 in. diameter lens on the pod's skin, and this required a control mirror which consumed practically all of the available cross-sectional area of the pod at the lens station. This immediately placed a requirement for the second and third mirrors shown in Fig. 1 in order to displace the entrance beam from the pod axis to the spectrometer axis.

Although a skin-mounted lens was specified, an alternative scheme was investigated where the lens was replaced by a plane window. In this case, a focussing system is required between the control mirror and the spectrometer slit. Since a lens adds an extra absorbing medium to the system, a Cassegrainian mirror system was considered. The advantage of this scheme over the skin-mounted lens system is the absence of condenser cone shift as the direction of the incident sunlight moves away from the normal to the plane window (sun angle-off). This results from operating the control mirror in parallel light. However, the additional complexity of mounting and aligning the primary and secondary mirrors of the Cassegrainian telescope, and the necessity of acquiring a plane window when the lens was already available made the system described earlier more attractive.

The question of the location and form of the error detecting system involved careful consideration. The most logical position to mount the detecting system would have been at the spectrometer slit, where rigidity and alignment problems are minimized. However, this has a disadvantage arising from difficulties due to the mechanical geometry of the slit, which involve major mechanical alterations to the spectrometer. In addition, the acquisition region for such a detector location would have been limited to a sun angle-off of only about $\pm 3°$, whereas the original specification called for acquisition up to $\pm 5°$. This is due to size limitations of the second and third mirrors in Fig. 1. These arguments resulted in locating the detectors behind the third mirror, which was designed to transmit about 5 per cent of the incident flux. Since this mirror is located quite close to the spectrometer slit, a rigid mounting did not present a major problem.

Selenium cells were selected for the detectors due to the high illuminance level available, their characteristic short respose time and their availability and relative cheapness. They are also easily mounted and do not occupy a large volume for the detecting area covered.

A considerable effort was directed toward setting the dynamic specifications for the servo loop response. To this end, an instrumented flight was scheduled to assess the residual roll, pitch and yaw oscillations of the aircraft when the pilot was attempting to fly straight and level at altitude. Sample recordings covered several 30 sec intervals, in order to obtain the maximum excursions to be expected during the specified tracking interval. Maximum excursions of roll and pitch amplitude were about $\pm 2{\cdot}2°$, yaw was $\pm 0{\cdot}6°$; roll and pitch rates were about $4{\cdot}0°$/sec maximum and the yaw rate was $1{\cdot}7°$/sec maximum. The principle roll and pitch periods were approximately 60, 6 and 2 sec; the principle yaw period was 3·3 sec.

Further disturbing inputs arise from flexure of the tip tank, vibration of the tank structure, sun's motion in the sky and internally generated noise within the servo loop. The results of the studies indicated that the servos should have bandwidths in the order of 10 c/s minimum, with a transient overshoot not exceeding 100 per cent. The maximum slewing rate of the control mirror was specified as 10°/sec to cope with any velocity demand arising from the

disturbing inputs, and to provide a reasonable lock-on time when the sun is captured at angles-off approaching $\pm 5°$.

Due to the high accuracy required in positioning the solar image, considerable attention was devoted to the selection of a suitable drive for the control mirror. Two alternatives were tested—a magnetic hysteresis clutch system and a conventional two phase gear-head servo motor. The hysteresis clutch was attractive because mechanical back-lash could be eliminated by mounting two direct-drive clutches back-to-back. However, because of insufficient accelerating torque, the clutch system was abandoned in favour of the conventional servo drive. Careful design and assembly of the gear resulted in a mechanical back-lash of less than $\pm 0{\cdot}5'$.

The above general design considerations led to the selection of the overall configuration and major components. In what is to follow, a brief summary is given of the salient design features of the sub-systems, followed by a description of the operation of the Sunseeker and the measured performance of the system when in operational use.

OPTICAL SYSTEM

The optical system, shown in Fig. 1, consists of an 8-in. diameter arsenic trisulphide lens of 36 in. focal length, a control mirror, and two diagonal mirrors to offset the optical axis onto the spectrometer axis. This was necessary due to mechanical limitations in the positioning of the PE Model 108 rapid-scan spectrometer.

It was originally intended that a 10-in. diameter arsenic trisulphide lens be used in the instrument, however early flights with the instrument cracked this lens and it was necessary to use an 8-in. diameter lens thereafter. This lens has a 36 in. focal length for $4{\cdot}3\,\mu$ radiation, and approximately a 32·5 in. focal length for $0{\cdot}65\,\mu$ radiation. This chromatic aberration gives an out-of-focus visual image of the sun at the i.r. focus (where the detector array must be located) of approximately one inch diameter.

The control mirror dimensions are such that for a 10-in. diameter lens all flux from the lens is reflected to diagonal mirror M2 for all positions of the control mirror. For the 8-in. diameter lens, this mirror is more than adequate in size. The control mirror is capable of moving $\pm 5°$ about the inner gimbal axis and $\pm 7{\cdot}5°$ about the outer gimbal axis, such that for all sun angles-off up to $\pm 7{\cdot}5°$, the sun can be imaged at the slit of the spectrometer with no loss of flux. The operation of the control mirror in convergent light from the lens results in non-coincidence between the 36-in. condenser cone axis and the spectrometer axis when the incident sunlight makes an angle with the lens axis. The system is so designed that for the maximum condenser cone shift corresponding to $\pm 7{\cdot}5°$ sun angle-off, the spectrometer collimator mirror is still completely filled. Also, due to this condenser cone shift, it is necessary to place the detector array at the same distance from the control mirror as the spectrometer slit, that is at the i.r. focus.

Diagonal mirrors M2 and M3 of Fig. 1 are of such size that all flux is reflected into the spectrometer slit for a 10-in. diameter lens. The diagonal mirror M3 has a 5 per cent visual-transmitting front surface aluminized mirror. The effect of sensing through this mirror was found to have negligible effect on the detector zero position, aside from the fixed displacement of the on-axis beam in passing through the 0·125 in.-thick parallel plate. Adjustments were provided at the detector array to compensate for this lateral shift. All mirrors have front surface evaporated aluminum coatings with an over-coat of silicon monoxide. The control mirror and diagonal mirror M2 are 0·25-in. thick and since surface quality need not be of optical standard, polished plate quality was specified.

Vol. 1 1961

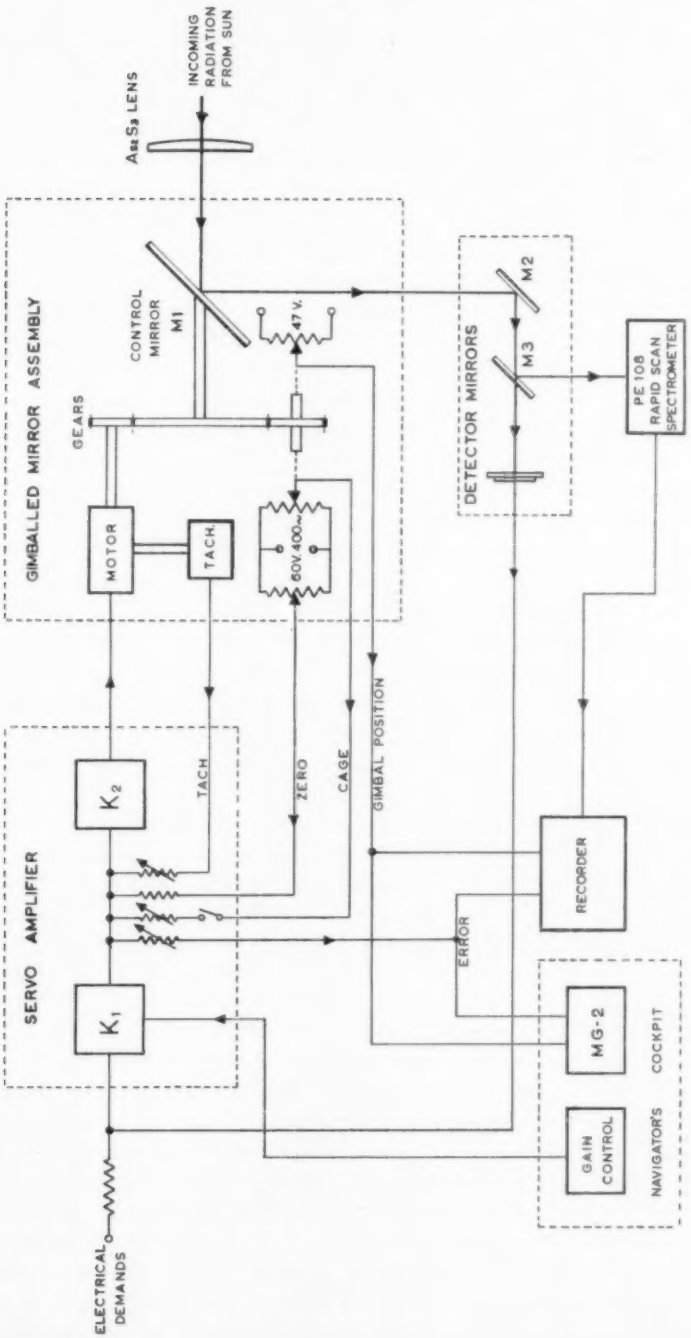

FIG. 2. Sunseeker block diagram.

SERVO SYSTEM

Figure 2 is a block diagram of the Sunseeker system. Radiation enters through the arsenic trisulphide lens on the right and is reflected from mirrors M1 and M2 onto mirror M3. This latter mirror transmits about 5 per cent of the incident radiation through to the detector, and reflects the remaining radiation into the spectrometer slit. The detector produces error signals, corresponding to the two drive axes of the control mirror which are applied to the inner and outer gimbal servo amplifiers, one of which is shown in Fig. 2.

The servo amplifier consists of a diode modulator and a miniaturized power amplifier which drives a size eighteen servomotor on the gimballed mirror assembly. A high precision gear train connects the servomotor to the control mirror, whose position determines the location of the solar image relative to the detector array and slit. This is the basic servo loop.

Since the detector array is within the basic servo loop, the loop gain and hence stability is directly dependent on the intensity of the solar image on the detector. As a result, the loop gain of the system varies with sun altitude. In order to compensate for this, the servo amplifier is divided into a variable gain portion (K_1) and a fixed gain portion (K_2). The variable gain K_1 is set by a subsidiary low-power servo system controlled from the navigator's cockpit. The navigator is thereby used to control the loop gain by a criterion to be described in a later section in order to maintain uniform servo response for various sun altitudes.

The servo system contains two secondary feedback loops. An adjustable tachometer feedback is incorporated to provide damping, which allows larger loop gains thereby improving the static and dynamic accuracy of the system. In addition, caging signals derived from potentiometers on the control mirror gimbals can be switched in as feedback signals in the error channels. These are required when the system is not tracking the sun, in order to maintain the mirror at its zero position while the aircraft is taking-off and flying to and from altitude. The navigator can then uncage the Sunseeker when tracking commences. Finally, in Fig. 2 electrical demands appearing on the left can be applied to the system for testing purposes.

The servo system for the Sunseeker is completely transistorized, and operates stably over the range -55 °C to $+71$ °C. The static deadband of the system is less than $\pm 0{\cdot}5'$, and the velocity constant of the servo is $6{\cdot}4'$ per r.p.m. input. The bandwidth of the servo system is about 12 c/s, and the system responds to a $20'$ step demand in 130 msec to within 5 per cent of steady state with a 90 per cent overshoot.

DETECTOR ARRAY

Figure 3 is a photograph of the diagonal mirror and detector assembly mounted in the tank. The detector array can be seen on the right, and consists of four International Rectifier Type B–30 selenium cells, each $3\frac{1}{4}$ in. square. The four cells are mounted in quadrants on a metallic backing which serves as a common electrode. The other electrode consists of deposited metallic strips in the form of a cross connected to a continuous strip around the edge of each cell. The edge strips are omitted at the center of the array to provide maximum sensitivity and linearity in this region where the solar image is located during normal operation. The outer dimensions of the array were selected to enable solar acquisition for sun angles-off of $\pm 5°$, when the control mirror is in the zero position (re-directing the lens axis along the pod axis). Diagonally opposite pairs of cells are connected back-to-back so as to provide error signals when the solar image is displaced from the center of the array. The array is so oriented that the solar image moves along lines parallel to the diagonals when the gimbals of the control mirror are moved independently. As mentioned previously,

Vol. 1 1961

the array is located such that there is a one-to-one correspondence in position to the spectrometer slit relative to the control mirror. This is necessary due to the shift in the condenser cone axis as the incident sunlight moves away from the lens axis.

The output current from a B–30 pair depends on the load across the pair. The choice of load was found to be governed by the following factors:

(1) maximum power transfer
(2) minimum noise at the null position from the modulator
(3) desirability to introduce A.G.C. at the detector to maintain servo gain margin in the presence of variations in the sun's illumination level at the selenium cells
(4) linearity in differential current output from the selenium cell pair for a range greater than $\pm 15'$.

It was found that using a 5 per cent transmitting mirror for M3, and for ground level sun illumination, maximum power transfer occurred for a load of approximately 300 Ω. However, due to other matching requirements, it was found that the modulator noise was high when the effective load for the pair was set so low. Consequently, the load was increased to 1000 Ω to reduce the noise in the system. The higher load does have the advantage of introducing A.G.C. into the system. It was found that for a 1000 Ω load, a 5:1 decrease in sun's illumination level only changed the detector gain by 2:1. It was also believed that maximum power transfer would be approached for a 1000 Ω load when very low sun altitude measurements were taken.

Under normal Sunseeker operation the cells of the detector array will be subjected to a wide range of temperature, humidity, and pressure conditions. Aside from withstanding high humidity the detector gain should not vary appreciably with temperature and, most important, no unbalance should occur in the null position at different temperatures. The variation in gain is not critical, since there are provisions for altering the amplifier gain during Sunseeker operation. Environmental chamber tests of the array indicated negligible change in the balance condition over the range +25 °C to −60 °C. Detector gain was found to increase by only 13 per cent from room temperature (20 °C) to −60 °C and decrease 25 per cent from 20 °C to +75 °C.

It has been specified that the Sunseeker system must operate for sun altitudes varying between +67° and −2°. The latter corresponds to the condition encountered when flying at 40,000 ft and looking tangentially to approximately 25,000 ft. In order to specify the correct maximum servo amplifier gain some measure of the sun's illumination level was necessary for the −2° case. The authors were not aware of any data in the literature that would provide this information. Theoretical considerations were made, but it was concluded that any calculations would be open to some doubt due to the absorption bands present in the 0·68 to 0·8 μ band. However, theory did indicate that the equivalent ground absorption path would exist for an apparent sun altitude of 0·8°. Simple measurements indicated that for the selenium–arsenic trisulphide combination, a sun illumination range of 20 : 1 existed between maximum sun altitude and −2° for a clear day. To cope with the uncertainties in these measurements and the possibility of more adverse atmospheric conditions, the system was designed for a 70 : 1 intensity ratio. With the A.G.C. inherent in the detector array, this reduced the amplifier gain variation to a factor of 12 : 1.

MECHANICAL DESIGN

Figure 1 illustrates the general arrangement of the component parts that make up the Sunseeker system. The forward section of the tip tank housing the spectrometer and

Sunseeker is capable of continuous rotation about the axis of the tank. In this fashion, the forward section can be indexed to correspond to the mean sun altitude for level flight, over the duration of the measuring period. This is accomplished by using a V-type "Marmon" clamp fastened to the tank by radial bolts, which can be rapidly tightened at the correct index position immediately prior to any flight.

The arsenic trisulphide lens is mounted in a heavy aluminum frame directly onto the skin of the tip tank. The control mirror assembly is mounted on a plate fastened to a stiffened former of the tip tank. The diagonal mirror and detector assembly is mounted on the same platform that holds the spectrometer to ensure that the detector and slit remain rigidly fixed with respect to each other.

Figure 3 is a photograph of the Sunseeker with spectrometer removed, as viewed from the break in the tank structure forward. The diagonal mirror and detector assembly can be seen in the background. Each mirror is clamped at its lower edge, and a top support is included to reduce mirror flexure due to vibration. Adjustments are provided for translational and rotational movement of the detector array relative to the spectrometer slit to allow for system alignment. In Fig. 3, the baffles behind the diagonal mirror assembly cover the control mirror assembly further forward.

Figure 4 is a photograph similar to Fig. 3, but with the baffles, the diagonal mirror and detector assembly removed. The Sunseeker electronics can be seen mounted to the skin of the tank out of the field of view. The control mirror assembly is shown in position. It is mounted in a conventional inner–outer gimbal system whose axes lie in the plane of the mirror at the zero position. The inner gimbal consists of a square aluminum frame to which the mirror is fastened by means of screws with teflon bushes passing through four holes in the mirror. In Fig. 4, the inner gimbal gear-head servo motor can be seen attached to the outer gimbal. Adjacent to this motor is the outer gimbal index dial. The lens hole in the skin is reflected by the mirror. All metal parts within the tank are painted matte black to reduce unwanted reflections, and baffles are provided about the detector assembly to eliminate spurious images and stray light which otherwise directly affect the apparent zero position of the solar image on the detector.

Vol. 1 1961

SUNSEEKER OPERATION

Prior to each flight, the front end of the pod is indexed so that the lens axis is aligned with the mean sun altitude to be studied. The time over which each flight must be carried out is then established to be compatible with the $\pm 7{\cdot}5°$ total lock-on field of view of the Sunseeker. In flight, the sun is acquired by altering the heading of the aircraft. When the solar image impinges on the detector during this "search" phase, the pilot's radar scope display is activated which consists of a steering dot whose displacement from the center position is a measure of the gimbal position relative to the zero position of the control mirror. The pilot then attempts to steer the aircraft so that the dot is within a circle on the radar scope, corresponding to the acceptable sun angles-off of $\pm 7{\cdot}5°$. With the control mirror in the central position, the solar image will impinge on the edge of the detector array for sun angles-off of about $\pm 5°$, and this has not been found to be too stringent for pilots with some experience.

The pilot's display also appears on the navigator's scope. The navigator uncages the system upon acquisition. Since displacements of the steering dot correspond to angular displacements of the control mirror, the stability of the servos can be observed directly on

Vol.
1
1961

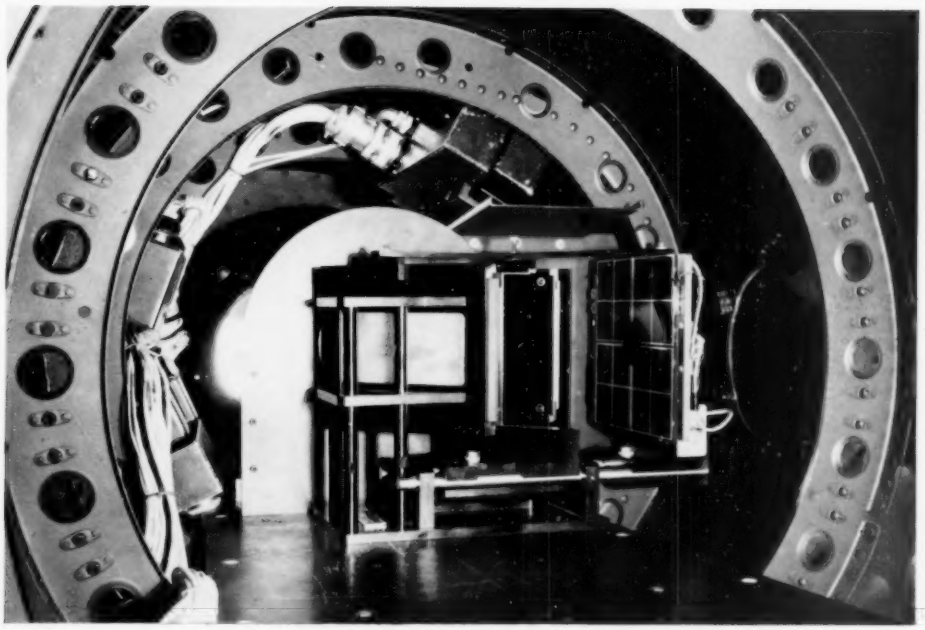

FIG. 3. Mirror-detector assembly in tank.

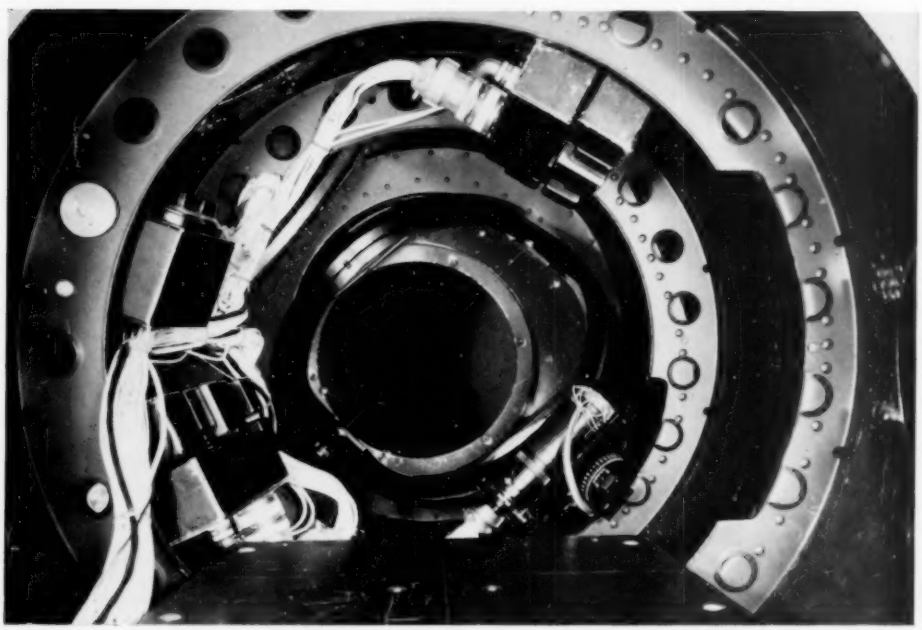

FIG. 4. Control mirror assembly in tank.

Facing Page 56

Vol.
1
196

the radar scope. The navigator then operates the subsidiary gain servos to maintain adequate gain margin for the sun illumination level being studied.

Changes in heading do not compensate for changes in sun altitude, so that without introducing roll to the aircraft a limited time is available for recording during each flight. During operation the following signals are recorded on an oscillograph recorder:

1. Gimbal positions
2. Servo error signals
3. Spectrometer output
4. Time
5. Atmospheric pressure
6. Outside air temperature
7. Air temperature within pod
8. Pitch and roll rates.

The gimbal position is a measure of the angle between the condenser cone axis and the spectrometer collimator axis. The error signal is a measure of the displacement of the solar image from the spectrometer slit, and is necessary in ruling out abnormal effects resulting from any Sunseeker malfunction.

SYSTEM PERFORMANCE

Numerous successful flights have been made with this equipment at 40,000 ft for the sun at low altitudes. A sample record of a flight is shown in Fig. 5. The error channel traces of this sample record show that the solar radiation is entering the spectrometer slit to within the $\pm 4'$ specified relative to the spectrometer axis.

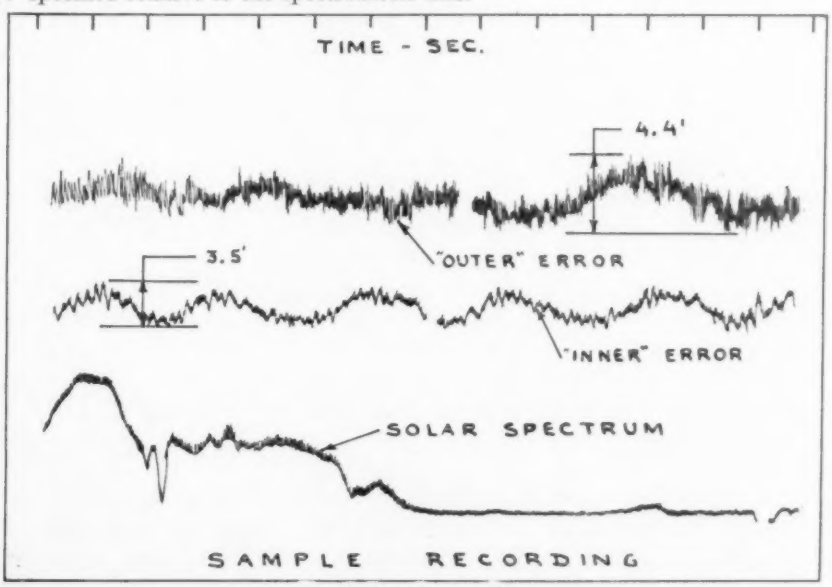

FIG. 5. Sample recording.

Acknowledgements—The authors would like to acknowledge the contributions of members of the Special Products Division, de Havilland Aircraft of Canada, Limited. In particular, Messrs. R. Penrose, A. Foulds, and D. S. L. Durie should be mentioned.

REFERENCES

1. CUMMINGS, C., and E. J. FJARLIE, C.A.R.D.E. TM 246/59.

Infrared Physics, 1961, Vol. 1, pp. 58–66. Pergamon Press Ltd., Printed in Great Britain.

INFRARED PHOTOGRAPHY USING PERSISTENT INTERNAL POLARIZATION IN PHOSPHOR PLATES

H. KALLMANN, J. RENNERT* and M. SIDRAN†‡

*Physics Department, New York University, Washington Square, New York
and
†Grumman Aircraft Eng. Corp., Research Dept., Bethpage, L.I., N.Y., U.S.A.

Vol. 1 1961

INTRODUCTION

THE application of the persistent internal polarization effect§ in phosphors to photography with visible light has been described elsewhere.[1] In the present investigation, the same method was used to form visible images on zinc cadmium sulfide (ZnCdS) phosphor plates using middle infrared light up to 2·5 μ as the depicting radiation instead of visible light. The polarization effects produced in the plates by both near and middle infrared radiation were also determined by measurements.

In p.i.p. photography with infrared as well as with visible light, the latent image consists of a pattern of polarization charge in the plate, corresponding to the energy distribution in the radiation to be depicted. There are two methods of making the latent image visible. First, it may be converted into a visible picture on a cathode-ray screen as in other infrared imaging devices,[2] by scanning the plate with a measuring probe or a moving light beam.[1] Secondly, it may be made visible by sprinkling dyed charged resin particles on the plate to form a print. Either a negative or positive copy of the object may be obtained. The print may be stabilized on the plate by fusing the resin to the plate by heat, or it may be transferred to a sheet of paper by known methods and then fused. The resin development of an infrared picture offers an advantage over other infrared imaging systems which form a transient image on a fluorescent screen, since the latter image can only be permanently recorded by means of conventional silver halide photography.[2, 3]

At present the speed of the infrared p.i.p. photographic process is considerably poorer than that observed in silver halide photography with visible light. Silver halide photography is, of course, completely insensitive in the middle infrared. To improve the speed of infrared p.i.p. photography, one should investigate the sensitivity of phosphors to polarization by infrared, in order to determine their regions of maximum sensitivity, and their long wavelength limits of response.

ELECTRONIC PROCESSES IN INFRARED P.I.P. PHOTOGRAPHY

Three methods are available for forming the latent image in infrared p.i.p. photography. These are designated as the de-exciting method, the polarizing method and the depolarizing method, respectively. The fundamental electronic processes pertinent to these three methods are described briefly below. The photographic procedures are discussed in a subsequent section.

When a phosphor is exposed to exciting radiation, electrons are raised to the conduction

‡ Formerly at New York University
§ Designated as the p.i.p. effect.

band from the valence band, or from the activator levels. Positive holes created in the valence band by the removal of electrons are captured by activator centers. The excited electrons may then either recombine with the positively charged activators, or fall into meta-stable levels (traps) below the conduction band. After excitation has ceased, the electrons in traps slowly escape to the conduction band by thermal stimulation. Most of them fall back into traps; the retrapping probability is much greater than the probability of recombination with positive centers. A quasi-equilibrium is established between trapped and mobile electrons, so that the conductivity decays very slowly.

Infrared radiation incident on an excited phosphor promotes the fast release of trapped electrons and holes, thus increasing the recombination rate. During infrared exposure, the conductivity of the phosphor may be either enhanced or quenched, depending on the type of recombination mechanism.[4] However, the ultimate decay of conductivity is accelerated by the infrared exposure. The depopulation of traps during infrared exposure, and the consequent changes in luminescent intensity provide the basis of two other infrared photographic processes developed earlier in this laboratory.[3]

When a d.c. field is applied across a photoconductor with a high concentration of free carriers, electrons and positive charges are separated by the field, and trapped inhomogeneously. A negative charge is concentrated near the positive electrode, and vice versa. This phenomenon is called persistent internal polarization (p.i.p.). The separation of trapped charges persists for months, unless it is destroyed by an exposure to visible or infrared light. Such an exposure releases the bound charges, so that the internal polarization field can then promote their recombination.

METHODS OF INFRARED P.I.P. PHOTOGRAPHY

In the de-exciting method and the polarizing methods of photography, the latent image is produced by altering the conductivity in different area elements of the phosphor plate, according to the energy distribution in the infrared radiation to be depicted. Thus, when the polarizing voltage is applied, each area element is polarized according to its conductivity.

In the de-exciting method, the infrared exposure is made before the polarizing field is applied. This method has no exact counterpart in visible-light p.i.p. photography.[1] It is illustrated schematically in Fig. 1. The plate is first sensitized by a uniform exposure to visible light, which creates a high concentration of both trapped and mobile carriers. Next, during the depicting infrared exposure, the concentration of these charges is quenched in the exposed areas. The polarizing voltage is then applied across the layer in the dark. Those areas which were not exposed to infrared retain their mobile carriers, and are therefore polarized by the applied field, while the areas de-excited by the infrared remain unpolarized. Thus a latent p.i.p. image is formed. When dyed charged resin particles are applied to the plate, they adhere to the unexposed areas to form a positive copy of the object.

In the polarizing method the infrared exposure is made during the application of the polarizing field. A similar sequence of operations is followed in the polarizing method with visible-light photography.[1] After the plate has been polarized by means of an electric field and infrared light, the application of dyed charged resin particles may produce either a positive or negative print, depending on whether the infrared quenches or stimulates the conductivity in the exposed areas. In the phosphor employed in this work, the conductivity was stimulated by the infrared. This case is illustrated schematically in Fig. 2. In this procedure the plate may or may not be presensitized by uniform excitation with visible light.

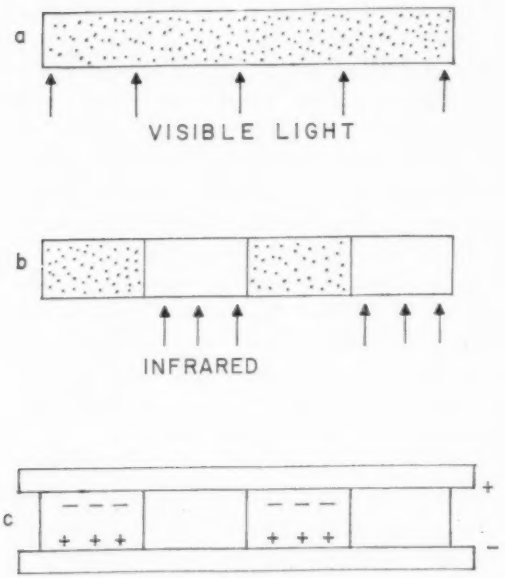

FIG. 1. De-exciting method (schematic).
(a) The layer is uniformly excited by exposure to visible light.
(b) An imagewise infrared exposure quenches excitation in exposed areas.
(c) A voltage applied in the dark polarizes areas previously shielded from infrared. Thus a latent "p.i.p." image is formed. A positive print is produced on resin development.

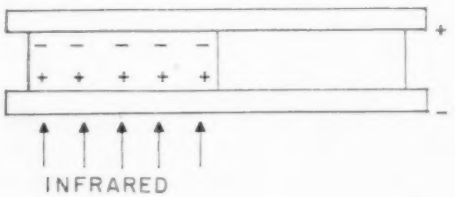

FIG. 2. Polarizing method (schematic).
An imagewise exposure to infrared during the application of the polarizing voltage increases the conductivity in exposed areas, which are therefore polarized. Thus a latent "p.i.p." image is formed. A negative print is produced during resin development.

In the third, or depolarizing, method the infrared exposure is made after the plate has been uniformly polarized using visible light and a polarizing voltage. This method is identical with the depolarizing method in visible-light photography,[1] except that the depicting radiation lies in a different spectral region. It is illustrated schematically in Fig. 3. The latent image is produced by discharging the polarization in the infrared-exposed areas. A positive print is obtained when resin is applied.

EXPERIMENTAL ARRANGEMENT

The photoconductor used in this work was a commercial ZnCdS phosphor designated as *K* powder.[1] It was chosen because of its large persistent internal polarization effect with

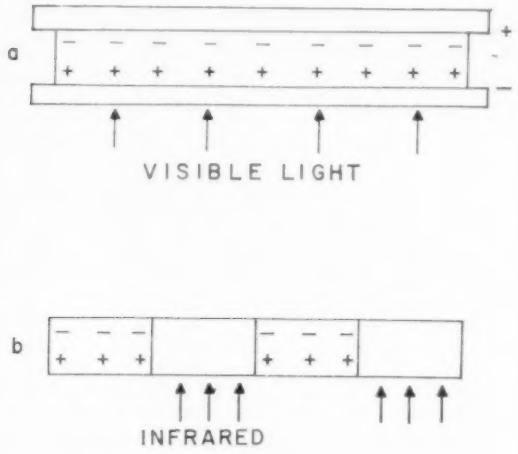

FIG. 3. Depolarizing method (schematic).
(a) The plate is uniformly polarized using light and a d.c. voltage.
(b) The polarizing light and voltage are removed. An imagewise exposure to infrared discharges the polarization in exposed areas. Thus a latent "p.i.p." image is formed. This gives a positive print during resin development.

visible light. The procedures for preparing phosphor plates and for producing the latent p.i.p. images were the same as those previously described.[1] The apparatus consisted of a light-protected dessicated chamber in which a phosphor plate could be polarized.[1] An aluminum foil electrode was placed in contact with the bare surface of the phosphor layer during polarization. This could be lifted away at the appropriate time. The infrared exposure was made through the conductive glass electrode.

The infrared source was a commercial heating lamp used in conjunction with several Corning color filters to select appropriate ranges of the infrared spectrum. Two spectral bands were used. One of these bands, transmitted by the Corning 7–56 filter, extended from 0·75 μ in the near infrared to 4·5 μ in the middle infrared. In this band, a total intensity of 250 mW/cm² was incident on the phosphor. The second band, transmitted by Corning filters 7–56 and 5–58 in combination, extended from 2·0 μ to 4·25 μ with a maximum intensity at 2·5 μ, and a total intensity of 3·8 mW/cm² incident on the phosphor. The low intensity in this band was due to the low output of the light source and the low transparency of the conductive glass in this spectral region. Due to this low intensity, long exposure times were required to produce observable contrast between exposed and unexposed areas.

The relatively large intensity transmitted in the first band, and the greater effectiveness of this band in photography indicate that most of its energy lies in a region of shorter wavelengths than those transmitted in the second band. The first band is therefore designated as the short-wavelength band, and the second as the long-wavelength band.

Measurements of the effects of near and middle infrared on the production and release of polarization in a phosphor layer were made using the standard circuit for measuring polarization charges.[5] The technique of radiation release was used in these measurements.[5] Measuring procedures are described in a subsequent section.

RESIN DEVELOPMENT OF INFRARED P.I.P. PHOTOGRAPHS

Resin prints were produced on phosphor plates by the de-exciting and depolarizing methods of infrared photography. Phosphor plates with conductive dots deposited on the surface were employed. The preparation and use of such phosphor plates has been described elsewhere.[1] The values of visible light exposures and polarizing voltages used in preparing the latent images were the same as those used for the quantitative experiments described later.

The depicting exposures were made by illuminating the plate with infrared in the long-wavelength band through a transparency showing an opaque letter "H". After the latent polarization image was formed, the plate was removed from the dry chamber, and the charged dyed resin powder was sprinkled on the surface to form the print.

In the de-exciting method, a 1 hr infrared image exposure was used. The positive print formed by resin development of the latent polarization image was faint, but sharp, with a very light background of resin adhering to exposed areas. The unexposed areas were slightly darker. In the depolarizing method, an infrared image exposure of 3 hr yielded a faint but definite positive print after resin development. There was no background.

No attempt was made to produce resin prints by the polarizing method.

In previous work, the density of resin adhering to the plate was studied as a function of polarization density.[1] The present experiments show that with middle infrared radiation of low intensity, resin prints can be produced on plates prepared from *K* phosphor.

Vol. 1 196

MEASUREMENTS OF POLARIZATION DENSITIES

Measurements were made of the polarization densities which are produced in exposed and unexposed areas of a phosphor plate by the three methods of photography described above.

Instead of comparing adjacent exposed and unexposed locations on the same plate, the polarization density was measured for the entire plate after uniform exposure to infrared in the two wavelength bands. This polarization density represented the infrared-exposed areas of the latent image. The polarization density in unexposed areas was determined by a separate control experiment, in which the infrared exposure was omitted, and a dark period of equivalent length substituted for it. These experiments are described below. All exposures to visible light were made using an intensity of 370 mW/cm² incident on the plate for the specified period.

In the control experiment for the de-exciting method, the plate was excited by a 2 min uniform exposure to visible light. After a 5 min dark period, a polarizing potential of 450 V was applied in the dark for 2 min. The polarization was then completely discharged by a 15 min exposure to visible light, and the released charge was measured by standard techniques.[5] A value of $6{\cdot}5 \times 10^{-9}$ C/cm² was obtained for the released polarization charge density.

In each experiment with infrared, the procedure of the control experiment was modified to include a 5 min uniform exposure to infrared, instead of the 5 min dark period preceding polarization. The polarization densities measured in the test experiments thus represent the background polarization in exposed areas of the latent image formed by the de-exciting method. As a result of such a test experiment with the short-wavelength band of infrared, the polarization density was reduced to $1{\cdot}7 \times 10^{-9}$ C/cm². This represents a reduction of 84 per cent, or a background polarization of 26 per cent.

The polarization density measured after the experiment with the long-wavelength band of infrared was exactly the same as that of the control experiment. Thus, no contrast could

be obtained by exposing the plate to depicting radiation in the long-wavelength band for only 5 min. Accordingly, the exposure time for the long-wavelength band was extended to 1 hr. For comparison, a new control experiment was run, with a 1 hr dark period between excitation and polarization. The measured polarization densities were $5{\cdot}7 \times 10^{-9}$ C/cm² for the control experiment, and $5{\cdot}0 \times 10^{-9}$ C/cm² for the experiment with infrared exposure. Thus the infrared reduced the polarization by 14 per cent. This represents a background polarization of 86 per cent in areas of a photograph receiving this infrared exposure.

In the experiments to test the polarizing method, the phosphor plate was first strongly de-excited using heat and infrared in the short-wavelength band for 10 min. The infrared intensity used for de-excitation was about twice that used in making test exposures.

In the control experiment for this method, the plate was kept in the dark while a polarizing potential of 450 V was applied for 3 hr. The polarization was then discharged by visible light. A measured value of $1{\cdot}7 \times 10^{-9}$ C/cm² was obtained for the polarization density. In this method, the control represents the background polarization in unexposed areas.

When the plate was exposed to the short-wavelength band during application of the polarizing potential, the polarization density was increased to $7{\cdot}4 \times 10^{-9}$ C/cm², or 4·4 times that of the control. This indicates that a background polarization of 23 per cent would be obtained in latent images formed with this wavelength band.

Exposure to the long-wavelength band during application of the potential yielded a polarization density of $3{\cdot}4 \times 10^{-9}$ C/cm², or twice that of the control. Thus a background polarization of 50 per cent would be found in latent images formed with this wavelength band. A measurable contrast can therefore be obtained using either wavelength band in the polarizing method.

The use of infrared in the depolarizing method was also evaluated. The plate was polarized using visible light and a 300 V potential applied for 2 min. In the control experiment, the polarization was allowed to decay in the dark for 1 hr. Then the remaining polarization was released by exposure to visible light. The polarization densities discharged during dark decay and radiation release are listed in Table 1.

TABLE 1. POLARIZATION CHARGE RELEASED IN THE DEPOLARIZING METHOD OF INFRARED PHOTOGRAPHY

(Plate polarized by 300 V for 2 min, concomitant with uniform visible light exposure)

No infrared exposure		Short-wavelength band exposure		Long-wavelength band exposure	
Operation	Charge ($\times 10^{-9}$ C/cm²)	Operation	Charge ($\times 10^{-9}$ C/cm²)	Operation	Charge ($\times 10^{-9}$ C/cm²)
5 min dark decay	3·4	5 min dark decay	3·1	5 min dark decay	2·9
Remaining 55 min dark decay	0·2	30 min i.r. exposure	6·5	1 hr i.r. exposure	1·9
Visible-light release	10·0	Visible-light release	2·3	Visible-light release	7·4
Total polarization density	13·6	Total polarization density	11·9	Total polarization density	12·2
% Quenching by infrared	0%	% Quenching by infrared	74%	% Quenching by infrared	20%
% Background	—	% Background	26%	% Background	80%

In the first experiment the dark decay period was 5 min, and then the plate was exposed to infrared in the short-wavelength band for 30 min. The remaining polarization was released by an exposure to visible light. The polarization densities discharged during dark decay, infrared exposure, and visible-light exposure are also listed in Table 1. These data show that about 74 per cent of the polarization persisting after dark decay is quenched by the exposure to short-wavelength infrared. This leaves a background polarization of 26 per cent. Thus the contrast is about the same as that obtained with this wavelength band in the de-exciting method.

During this exposure to the short-wavelength band, the polarization release was measured as a function of time under infrared. The data, corrected for the small amount of dark decay in the control during the same periods of time, are plotted in Fig. 4. The polari-

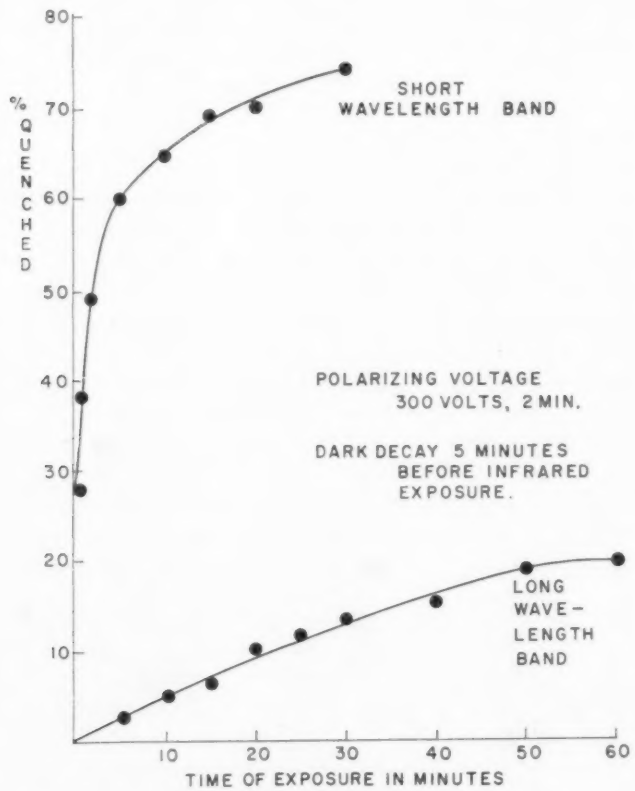

FIG. 4. Depolarization by infrared as a function of time of exposure.

zation density released by infrared is expressed as a percentage of that present at the beginning of exposure. The curve shows that most of the polarization is released during the first 5 min of infrared exposure. After that, the rate of release levels off, so that an increase in exposure time beyond 30 min would not be advantageous.

In the test experiment using the long-wavelength infrared band, the procedure was the

same as above, except that the infrared exposure time was 1 hr. The data, listed in Table 1, show that 20 per cent of the polarization remaining after dark decay was discharged by the infrared, leaving a background polarization of 80 per cent. The rate of discharge by infrared is shown in Fig. 4. Toward the end of the 1 hr exposure period, the rate had definitely levelled off.

Thus it has been shown that both near and middle infrared radiation can be used to produce a latent image by each of the three photographic methods. The long-wavelength band was about one-tenth as effective in producing contrast as the short-wavelength band. Since the intensity in the former band was only one-seventieth that in the latter, the long-wavelength band was actually quite effective.

Although the contrast obtained in these preliminary experiments was relatively poor for a photographic application, it was sufficient to demonstrate feasibility. The use of a stronger source of long-wavelength band radiation would probably produce a substantial improvement in contrast. Additional improvement could be effected by using a phosphor with more sensitivity to infrared, and by cooling the plates.

Vol. 1 1961

SUMMARY

The application of the persistent internal polarization effect to photography [1] has been extended to include the near and middle infrared regions of the spectrum up to about 2·5 μ. Latent polarization images were formed in thin layers of a ZnCdS phosphor (*K* powder), deposited on conductive glass plates. (In some applications, phosphor plates with conductive dots on the surface were used. [1]) The latent images consisted of polarization charge patterns corresponding to the object to be depicted. In forming the latent polarization image, the infrared image exposure may be made before the application of the polarizing voltage (de-exciting method), during voltage application (polarizing method), or after the application of voltage (depolarizing method).

The latent image may be developed by sprinkling charged dyed resin on the surface. The resin is fused to the surface by heat to form a permanent print. Either positive or negative resin photocopies may be obtained. As an alternative to resin development, the image may be viewed on a cathode ray screen.

For each method of infrared p.i.p. photography, the polarization charge density in exposed and unexposed areas of the latent polarization image was measured to determine the contrast obtained with different spectral bands. The background polarization was found to be about 25 per cent using radiation in the near infrared, and about 50–80 per cent for radiation in the middle infrared. The incident intensity in the latter region was extremely low. A substantial improvement in contrast and speed could probably be achieved by using a stronger source of middle infrared radiation. Other improvements could be made by (a) using a photoconductor with greater infrared sensitivity, (b) using a better infrared window material as the transparent electrode, and by (c) cooling the plates. It is suggested that some of the recently developed semiconductors which are sensitive to long-wavelength infrared radiation should be tested for this application.

Acknowledgements—The investigations were performed at New York University Physics Department, Washington Square, New York 3, N.Y. with the support of the National Carbon Company Research Laboratories (Contract 8–8546–706). This support is gratefully acknowledged.

REFERENCES

1. KALLMANN, H., J. RENNERT, and M. SIDRAN, A photographic process using persistent internal polarization in phosphors. To be published in *Photogr. Sci. Engng.*
2. MORTON, G. A., and S. V. FORGUE, *Proc. Inst. Radio Engrs., N.Y.* **47**, 1607 (1959).
3. KALLMANN, H., and J. RENNERT, *J. Opt. Soc. Amer.* **48**, 812 (1958).
4. KALLMANN, H., B. KRAMER, and A. PERLMUTTER, *Phys. Rev.* **99**, 391 (1955).
5. KALLMANN, H., and B. ROSENBERG, *Phys. Rev.* **97**, 1596 (1955).

Vol.
1
1961

Infrared Physics, 1961, Vol. 1, pp. 67–93. Pergamon Press Ltd., Printed in Great Britain.

THE THEORY OF THERMAL IMAGING, AND ITS APPLICATION TO THE ABSORPTION-EDGE IMAGE-TUBE

C. HILSUM and W. R. HARDING

Services Electronics Research Laboratory, Baldock, Herts.

Abstract—The detection of thermal radiation has received much attention in the past, but little has been done on the production of a visible picture of a thermal pattern.

We can distinguish three independent processes in the operation of a thermal image-converter. First, the focused thermal radiation falling locally on the sensitive layer disturbs the thermal balance between this region and its surroundings, and a new radiation balance is set up; as a result the local temperature changes. Secondly, the temperature pattern consequent on the new equilibrium results in a variation over the layer area of some physical property. Finally the changes in this property are communicated to the eye.

The efficiency of each of these processes is analysed, and it is shown that a converter is not most sensitive when the layer has an overall high absorption. The ideal layer has high absorption over the angle subtended by the optics, and zero absorption elsewhere. Calculations are made of the properties of a composite metal–dielectric film, and it is shown that this combination approximates to the ideal layer.

A simple converter, the absorption-edge image tube, is used to test these ideas. Measurements are made of the shape of the absorption edge of amorphous selenium, and the shift of the edge with temperature. Other materials are also examined. The sensitivity of a tube using selenium is calculated, and then measured by photographic photometry. Good agreement is obtained between theory and experiment.

The design principles which have resulted from this analysis are applied to obtain the highest sensitivity, and it is shown that bodies less than 10 °C above ambient temperature can be imaged with good resolution.

INTRODUCTION

CONSIDERABLE progress has been made since the war on the development of infrared detectors. The fundamental detection limits have been studied thoroughly, the sensitivity of old detectors improved, and new detectors invented for giving a wider spectral coverage. In contrast, little has been done towards providing picture-forming devices which convert the thermal radiation emitted from objects in the field of view into a picture that the eye can see. The photoemissive converters developed during the war were sensitive only to 1·2 μ, and could detect a target passively only if it were hotter than 300 °C. Infrared photographic plates and infrared phosphors are available, but these, too, are sensitive to only near infrared radiation.

If we want to image bodies a few degrees above ambient temperature we must use instruments which respond to longer wavelengths. Mechanical scanning viewing systems which rely on sequential operation of one or more infrared detectors have been described recently, but they are usually complex equipments, and they require a fairly long time to produce a picture. A selective image-tube analogous to the photoconductive cell, with a long-wavelength limit between 4 and 6 μ, could be made, but to work well it would need to be cooled at least to liquid air temperature. A form analogous to the non-selective detectors, such as

the bolometer and thermopile, is also possible, and this type of viewing device, which operates on the temperature changes induced by the image of a hot body, is called a "thermal image-converter". Previous work has been reported on evaporographs,[1, 2] phosphor imaging tubes,[3] liquid-film tubes,[4] and electron scanning tubes[5, 6, 7] (thermicons). The evaporograph is the most sensitive, but this is not continuous in operation. Published data on the other instruments indicates threshold sensitivities of at best 30 °C above ambient.

A simple converter was invented by Northrop[8] in 1953. The thermo-sensitive element is a thin self-supporting film of amorphous selenium, metallized to absorb the thermal radiation, and supported in a vacuum so that it can be observed by transmission of light from a sodium lamp (Fig. 1). Amorphous selenium is almost opaque at wavelengths less

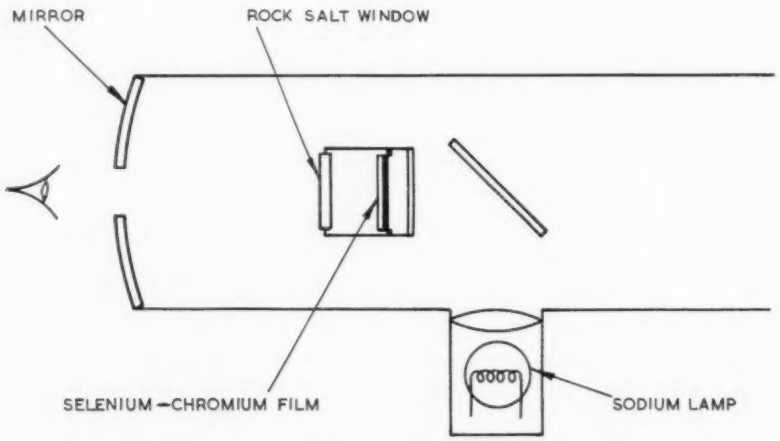

FIG. 1. An absorption edge image converter.

than 0·55 μ and quite transparent to wavelengths longer than 0·62 μ. The transmission–wavelength graph shows near 0·58 μ a rapid rise in transmission which is known as the absorption-edge. The position of the absorption-edge is temperature dependent, the edge moving bodily to longer wavelengths as the temperature increases (Fig. 2). As a result, if a

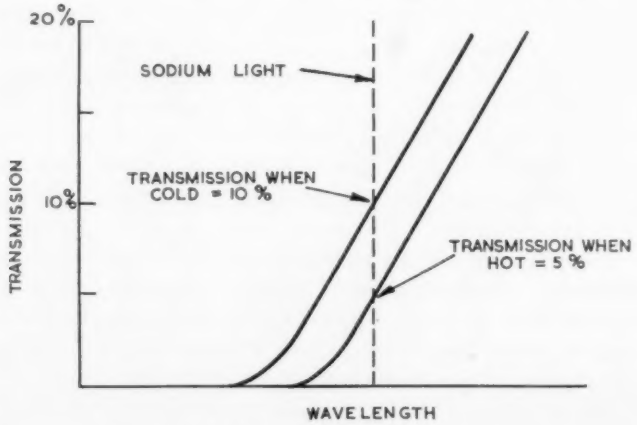

FIG. 2. Shift of absorption edge with temperature.

Vol. 1 1961

selenium film has a thermal image focused on it, the hot parts will look darker than the cold parts. The original tubes could image objects 30 °C above ambient temperature.

In this paper we analyse the thermal imaging process, and determine which factors are important for a successful converter. The theory is then applied to the absorption-edge image-tube (A.E.I.T.), and the limiting sensitivity deduced. Finally experiments to check the theory are described, and suggestions made for obtaining improved performance.

THE IMAGING PROCESS

We can distinguish three quite distinct processes in the operation of a thermal image-converter. In the first place the focused thermal radiation falling locally on the thermally sensitive layer disturbs the thermal balance between this region and its surroundings, and a new radiation balance is set up. As a result the local temperature changes to a new value. Secondly the temperature pattern consequent on the new equilibrium results in a variation over the layer area of some physical property. Finally the changes in this property are detected and communicated to the eye. The efficiency of each of these processes can be determined.

It is important that the temperature changes caused in the layer should reflect the pattern in the observed scene. The two main causes of degradation are (a) defects in the optics, (b) lateral heat spread in the thermally sensitive layer. It will be seen later that to obtain high sensitivity it is necessary to employ optics of large aperture ratio. Such systems give poor resolution except in the centre of the field, and unless some component, such as a Schmidt plate, can be included to correct for the aberration, the sensitivity for objects which are not on the optic axis will be lower than we shall predict here. The loss due to heat spread can be even more serious. In all practical converters thin films with a low lateral thermal conductivity are used. Edmond and King[5] point out that though they had a 1 μ film of glass, a material normally considered of low thermal conductivity, their resolution was very poor. As a rough guide we can say that the largest heat spread which can be tolerated is one-tenth of that of Edmond and King's, and we are free to achieve this by a reduction in film thickness, a reduction in thermal conductivity, or by using a mosaic layer with poor thermal contact between neighbouring elements.

Let us now consider in turn the three processes involved in imaging.

1. *Theory of Radiation Balance*

(*a*) *General.* To obtain an efficient transfer of energy from the object to the film it is not sufficient to use a film of high absorption. It is also important to isolate the film thermally, so that it can rise freely in temperature above its surroundings. Enclosing it in a vacuum is the first step towards this, but it is necessary to minimize radiation losses as well. If other loss processes are insignificant the radiation can be reduced only by lowering the emissivity, but this appears incompatible with the necessity for high absorption.

Consider an opaque object of area A_1, temperature T_1, emissivity ϵ_1 which is at a large distance D from a lens or mirror system of focal length p, radius r and numerical aperture N (Fig. 3). The optical system focuses the object on to a thin film, the emissivity of the side of the film facing the radiation being ϵ_2 and that of the other side being ϵ_3. The area of the image is A_2, and the temperature within the image area is T_2. The temperature of the object surroundings is T_0, and of the film surroundings is T_3.

We assume that the only heat loss from the image area is due to radiation, the film being in a sufficiently good vacuum, and having negligible lateral heat conductivity. It is also

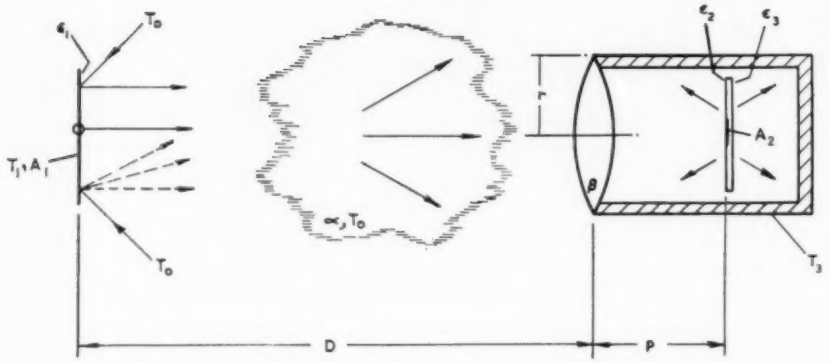

FIG. 3. Radiation balance of a thin film.

assumed that the film surroundings are black, so that we do not need to consider radiation passing through the film and being reflected back. In the practical tubes which have so far been constructed this effect is small, but theoretically it is possible in some cases to achieve a small sensitivity gain by utilizing the transmitted radiation, employing special constructions so that there is no appreciable loss in resolution.

If a shutter at temperature T_3 covers the lens, the film itself stabilizes at temperature T_3. When the shutter is removed the object is imaged on a part of the film, which rises in temperature to T_2. The *increase* in radiation incident and absorbed is balanced by the *increase* in radiation loss.

Increase in radiation loss $= A_2\, o(\epsilon_2 + \epsilon_3)\,(T_2^4 - T_3^4)$ where σ is Stefan's constant.

To calculate the radiation incident, we assume that the transmission of the atmosphere is α. The radiation arriving which originates at the object is $\sigma A_1\, \alpha\epsilon_1 T_1^4 \pi r^2/\pi D^2$. The radiation which is reflected, specularly or diffusely, from the object and reaches the film is $\sigma A_1\, \alpha(1 - \epsilon_1) T_0^4 \pi r^2/\pi D^2$. It is obviously assumed here that there is no contribution from hot or cold objects in such a position that their radiation is reflected from the target on to the film. A third factor is radiation from the atmosphere, which we have assumed is absorbing, and must therefore be emitting radiation. The amount reaching the film due to this is $\sigma A_1\,(1 - \alpha) T_0^4 \pi r^2/\pi D^2$. We subtract from these three terms the radiation which fell on the film from the shutter, which is approximately $\sigma A_2 T_3^4 \pi r^2/\pi p^2$. The increase in radiation incident is thus

$$A_2\,(r^2/p^2)\beta[\alpha\epsilon_1 T_1^4 + \alpha(1 - \epsilon_1) T_0^4 + (1 - \alpha) T_0^4 - T_3^4]$$

since $A_1/D^2 = A_2/p^2$ and where β is the fractional transmission of the optical system. Only a fraction of this will be absorbed, and we assume that the absorption of this side of the film is related to the emissivity ϵ_2 used above in deriving the increase in radiation loss. We denote it by ϵ_2'.

In equilibrium the two expressions are equal, so that

$$A_2\sigma\,(T_2^4 - T_3^4)(\epsilon_2 + \epsilon_3) = A_2\sigma \frac{r^2}{p^2} \beta\epsilon_2'[\alpha\epsilon_1 T_1^4 + \alpha(1 - \epsilon_1) T_0^4 + (1 - \alpha) T_0^4 - T_3^4]$$

Vol. 1 1961

which simplifies to

$$T_2^4 - T_3^4 = \frac{\epsilon_2'\beta}{4N^2(\epsilon_2 + \epsilon_3)} [\alpha\epsilon_1(T_1^4 - T_0^4) + T_0^4 - T_3^4] \tag{1}$$

This is the fundamental equation we require.

(*b*) *System at room temperature.* We now consider the simple case with the system at the same temperature as the object surroundings, so that $T_3 = T_0$. We have then

$$T_2^4 - T_0^4 = \frac{\epsilon_2'\epsilon_1\alpha\beta}{4N^2(\epsilon_2 + \epsilon_3)} (T_1^4 - T_0^4) \equiv \frac{1}{F}(T_1^4 - T_0^4) \tag{2}$$

If the temperatures involved are close to ambient, an approximation can be made.

$$\theta_2 = \theta_1/F \tag{3}$$

with

$$\theta_2 = T_2 - T_0, \qquad \theta_1 = T_1 - T_0$$

An expression similar to (3) has been obtained previously by Edmond and King, using a rather different treatment. Unfortunately the converters at present available are not sensitive enough to allow us to use the approximation without introducing large errors For an object 20 °C above ambient an error of 10 per cent is caused, and this increases rapidly with the object temperature. A more useful approximation is, with $T_0 \doteqdot 300$ °K,

$$\theta_2 = \frac{\theta_1(1 + \theta_1/200)}{F} \tag{4}$$

We can show that when F is between eight and twenty this relation is accurate to better than 2 per cent if θ_1 is less than 70 °C The relative accuracy of the two approximations is illustrated in Fig. 4, which gives the dependence of θ_2 on θ_1 according to the three relations (2), (3) and (4).

The factor determining the efficiency of the heat transfer from object to image we have denoted by F, where

$$F = \frac{4N^2(\epsilon_2 + \epsilon_3)}{\alpha\beta\epsilon_2'\epsilon_1} \tag{5}$$

To achieve high sensitivity in the image-converter we must minimize F. If the sensitive film is symmetrical and the emissivity is also independent of the angle of incidence, the three emissivities ϵ_2, ϵ_3, and ϵ_2' are equal, and the ratio $(\epsilon_2 + \epsilon_3)/\epsilon_2'$ is always two. The performance of the system is then independent of the absorbing properties of the film. However, if the absorption becomes very small other loss processes become more important than the radiation loss, so that for such low absorption values the relations are no longer valid. Nevertheless, provided we do not extrapolate to such extremes we can assume that for symmetrical films there is no first order dependence of sensitivity on absorption.

In fact it would be difficult to make a film with $\epsilon_2' = \epsilon_2$. The incoming radiation in our system is contained in a definite solid angle making only a small angle with the normal. The value to be taken for the absorption ϵ_2' will usually be near to the absorption measured at normal incidence. On the other hand, the emission takes place into the full hemisphere

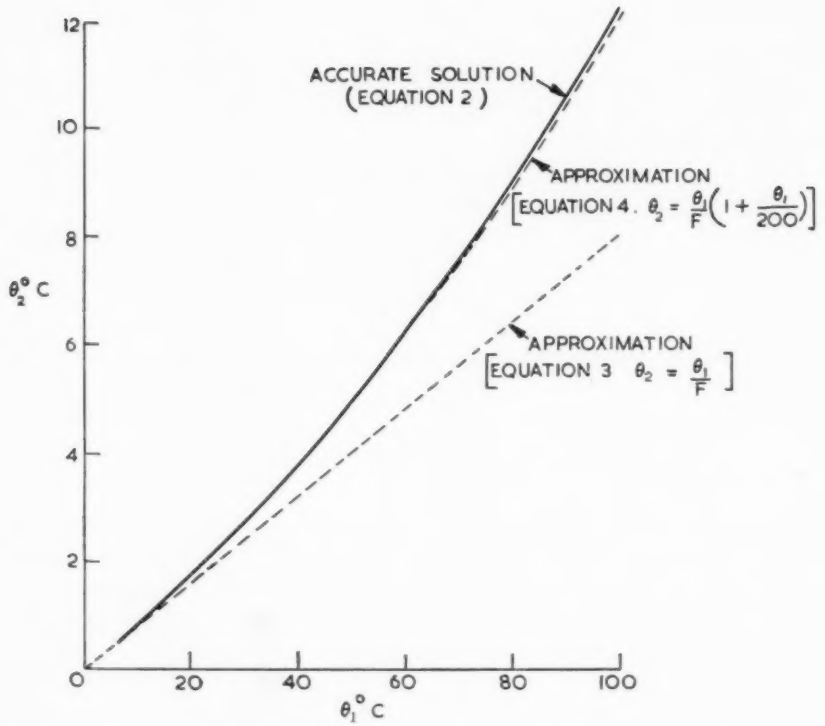

FIG. 4. Comparison of two approximations with accurate solution for radiation transfer (Tube at room temp. 300 °K, $F = 12{\cdot}5$).

and the value taken for ϵ_2 is integrated over *all* angles of emission from 0° to 90°. As the emission often falls at lower angles of incidence the integrated emission is usually lower than the "normal" absorption.

(*c*) *Properties of asymmetric combinations.* To obtain the highest sensitivities it is necessary to use asymmetrical systems, with ϵ_2 and ϵ_3 small and ϵ_2' large. We require a film with emissivity low except in the solid angle of the optical system aperture, i.e. the side facing the radiation should have high emissivity at angles near normal incidence and low emissivity at larger angles, and the other side should have low emissivity at all angles of incidence. These properties are given by a two-component film, with a metal layer deposited on a dielectric of high refractive index n.[9]

The absorption of the film depends on the thickness of both the dielectric and the metal, and with the thickness d of the dielectric chosen so that $\sin 2\pi nd/\lambda$ is unity, the absorption for radiation falling on the dielectric side is always n^2 times the absorption for radiation incident on the metallized side. This result is true for all metal thicknesses, and is illustrated in Fig. 5. If the dielectric thickness is such that $\sin 2\pi nd/\lambda$ is zero, the properties of the combination reduce to those of the unsupported metal film, and we have a symmetrical system. The dependence of absorption on the angle of incidence (ϕ) is shown in Fig. 6.[10] The high absorption is found only at angles of incidence less than 45°, precisely what we require for this application.

Vol. 1 1961

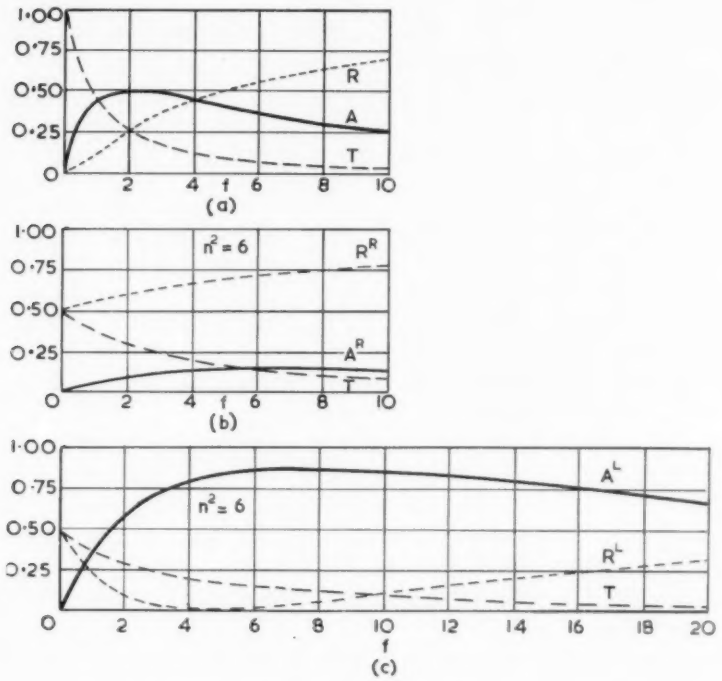

FIG. 5. Reflection transmission and absorption for a metal film.

(a) Unsupported.

(b) On a dielectric ($n^2 = 6$) with sin $2\pi nd/\lambda = 1$, radiation meeting metal first.

(c) On a dielectric ($n^2 = 6$) with sin $2\pi nd/\lambda = 1$, radiation meeting dielectric first.

f is a measure of the metal thickness, being the ratio of free space impedance to the resistance per square of the film.

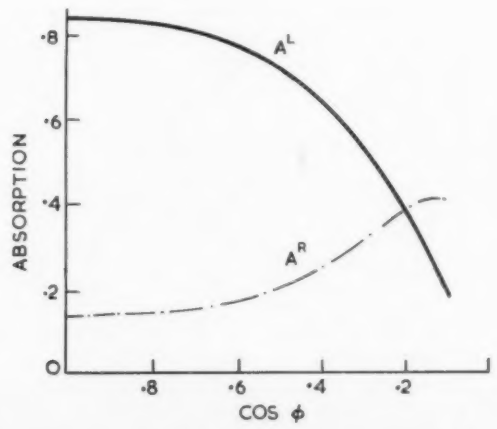

FIG. 6. Absorption of unpolarized light in composite film: $n = 2{\cdot}45$, $d = \lambda/4n$, $f = 5$.

2. *The Calculation of Radiation Balance*

Let us now calculate F for a metal dielectric combination, the dielectric refractive index being taken as 2·45, the value for selenium.

We have in equation (5)

$$F = \frac{4N^2(\epsilon_2 + \epsilon_3)}{\alpha\beta\epsilon_1\epsilon_2'}$$

Since the absorption of the metal–dielectric combination varies little with the angle of incidence for angles up to 45°, even for large aperture optical systems it is permissible to use for ϵ_2' the value calculated at normal incidence; to deduce ϵ_2 and ϵ_3 a numerical integration over the hemisphere must be made. The results obtained are dependent on the ratio of the dielectric thickness to the wavelength of the radiation, and we cannot restrict our analysis to monochromatic radiation. We must therefore make further numerical integrations over the wavelengths relevant to our problems.

(*a*) *Wavelength range*. The radiation emitted by the film, assumed to be uncooled, is given by the product of the emissivity and the black-body curve for an object at room temperature. By integrating from 4 μ to 100 μ we include over 99 per cent of the radiation involved.

The absorption need not be integrated over so large a range. If we assume that the target is also near room temperature, the same black-body curve is involved, but not all of this radiation arrives at the film, some being absorbed in the atmosphere, and some in the optical system. It is interesting to note that radiation beyond 15 μ cannot be ignored in this case, since we are dealing with such cool targets; over 40 per cent of the energy lies there. We must therefore consider the transmission of the atmosphere at these wavelengths.

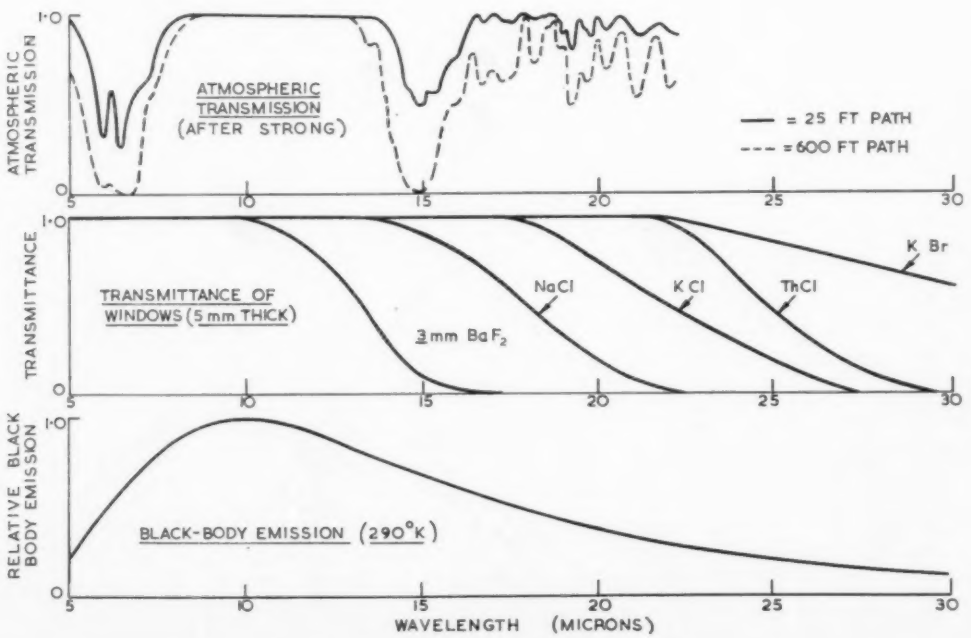

FIG. 7. Wavelength dependence of α, β, H.

Vol. 1 1961

Little has been published on the transmission of horizontal optical paths, but Adel[11] has shown that solar radiation, which is strongly absorbed at 15 μ, passes to some degree through the atmosphere at wavelengths out to 24 μ. Strong[12] has given some preliminary experimental results, but these should be accurate enough for our purpose; Strong quotes values for two path lengths, 25 ft, and 600 ft*. We consider the shorter path length, since this is a more generalized case, involving integration over a longer wavelength range.

The transmission curves are shown in Fig. 7. On the same diagram is given the black-body curve, and the transmittance† of some optical materials used in infrared devices. The wavelength range we need consider is determined to some extent by the material we use for our window.

(*b*) *Optical materials.* The conventional windows used for thermal detectors and converters are rock-salt, potassium bromide, caesium bromide, KRS5 and silver chloride. All have disadvantages. The first three are hygroscopic and their optical finish deteriorates in use unless great care is taken. Silver chloride loses its transmission gradually if it is exposed to daylight, and it is generally protected with a coating of silver sulphide. It is then not transparent in the visible and would not be suitable for our form of tube. Edmond and King used it fairly successfully, and developed techniques for sealing it to glass. KRS5 is also not very transparent in the visible.

Two windows which are mechanically quite good might prove useful in future image tubes. KRS6 was developed during the war in Germany but has not been made in quantity since, possibly because it is more difficult to make than KRS5. It is transparent in the visible. A more recently developed window material is barium fluoride. This has the good mechanical properties of lithium and calcium fluoride, but a transmission limit at about 13 μ.

A simple calculation indicates that if we substitute a 3 mm thick BaF_2 window for one of rock-salt we should lose 19 per cent of our sensitivity. This is not a high price to pay for the increased utility. In our experiments we shall use rock-salt windows since we are working under laboratory conditions and can ensure that they do not deteriorate. Our integration must then cover the range from 4 to 22 μ.

(*c*) *Emissivity of a composite film.* In reference 10 it was shown that the emissivities of the two sides of the film are given by

$$\epsilon_2 = \frac{2f'}{(f'+2)^2C^2 + n'^2S^2\left(\frac{f'+1}{n'^2}+1\right)^2} + \frac{2f''}{(f''+2)^2C^2 + n''^2S^2\left(\frac{f''+1}{n''^2}+1\right)^2}$$

$$\epsilon_3 = \frac{2f'(C^2+S^2/n'^2)}{(f'+2)^2C^2 + n'^2S^2\left(\frac{f'+1}{n'^2}+1\right)^2} + \frac{2f''(C^2+S^2/n''^2)}{(f''+2)^2C^2 + n''^2S^2\left(\frac{f''+1}{n''^2}+1\right)^2}$$

where

$$f' = f/\cos\phi, \qquad f'' = f\cos\phi,$$
$$n'^2 = (n^2 - \sin^2\phi)/\cos^2\phi, \qquad n''^2 = n^4/n'^2,$$

* Dr. H. Yates (N.R.L.) has indicated in a private communication that these results give too high a transmission at wavelengths longer than 15 μ. Use of the latest data would change our calculations by up to 3 per cent.

† Only the spectral dependence of transmission need be included. The reflection loss is not considered, since this may be brought in after the integration.

$$\begin{matrix} C \\ S \end{matrix} = \begin{matrix} \cos \\ \sin \end{matrix} \left\{ 2\pi d\sqrt{(n^2 - \sin^2 \phi)}/\lambda \right\}$$

n is the refractive index and d the thickness of the dielectric, and f is a measure of the thickness of the metal, being the ratio of free space impedance to the resistance per square of the film.

These expressions have been computed for $n^2 = 6$, $f = 1, 2, 3, 4, 5, 7, 10$ and 20, $S^2 = 0$ and 1, at values of $\cos \phi$ from 0·1 to 1·0 at intervals of 0·1. A numerical integration over $\cos \phi$ gives approximate values of the effective emissivity of these films. The results are given in Table 1.

TABLE 1. EMISSIVITIES OF COMPOSITE METAL–SELENIUM FILM

ϵ	f / S^2	1	2	3	4	5	7	10	20
ϵ_2'	1	0·375	0·593	0·720	0·793	0·833	0·858	0·830	0·658
ϵ_2	1	0·259	0·415	0·513	0·572	0·609	0·652	0·640	0·542
ϵ_3	1	0·105	0·163	0·197	0·217	0·227	0·228	0·227	0·180
ϵ_2'	0	0·444	0·500	0·480	0·444	0·408	0·343	0·278	0·165
ϵ_2	0	0·351	0·383	0·375	0·358	0·338	0·301	0·260	0·178
ϵ_3	0	0·347	0·387	0·380	0·365	0·348	0·312	0·275	0·194

The data is of course valid only for that particular wavelength at which $S = 1$ or 0. Later we shall be concerned with intermediate values of S, but for the moment we shall deal with these extreme values.

It can be seen from the data of Table 1 that the ratio $\epsilon_2'/(\epsilon_2 + \epsilon_3)$ does not vary markedly with f; the general trends are therefore illustrated by taking $f = 7$ from now on.

It is necessary to find how ϵ_2', ϵ_2 and ϵ_3 vary with S^2, so further computations are made with $n^2 = 6$, $f = 7$ at several intermediate values of S^2. From these results numerical integrations give the effective emissivities shown in Table 2.

TABLE 2. EMISSIVITIES OF COMPOSITE METAL–SELENIUM FILM ($f = 7$)

S^2	0	0·16	0·36	0·64	0·81	1·00
ϵ_2'	0·343	0·383	0·440	0·559	0·670	0·858
$\epsilon_2 + \epsilon_3$	0·613	0·633	0·656	0·709	0·761	0·880

We are now in a position to integrate over a wavelength range, interpolating between these values of S^2 when necessary.

(*d*) *Integration over the wavelength range.* The sensitivity is obtained from

$$\int_0^\infty H_\lambda(\alpha\beta\epsilon_2')_\lambda d\lambda \Big/ \int_0^\infty H_\lambda(\epsilon_2 + \epsilon_3)_\lambda d\lambda$$

where H_λ is the spectral distribution of black-body radiation at room temperature. The numerical integration is made at intervals of 1 μ from 4 to 30 μ, 10 μ from 30 to 50 μ, and 50 μ from 50 to 100 μ.

The procedure is first to calculate, at each wavelength, the relevant value of S^2 for the particular selenium thickness required. These values are then converted into values for ϵ_2' and $\epsilon_2 + \epsilon_3$ using a graph drawn from Table 2. Values of H_λ are obtained from a Blackbody Slide Rule, and α, β from Fig. 7. Quadruple multiplication gives the terms that make up the numerator, and simple multiplication the terms of the denominator. The numerator and denominator are then summed separately, and finally divided.

The summation has been carried out for the selenium thicknesses 0·5, 1·0 . . . 4·0 μ. The results are illustrated in Fig. 8.

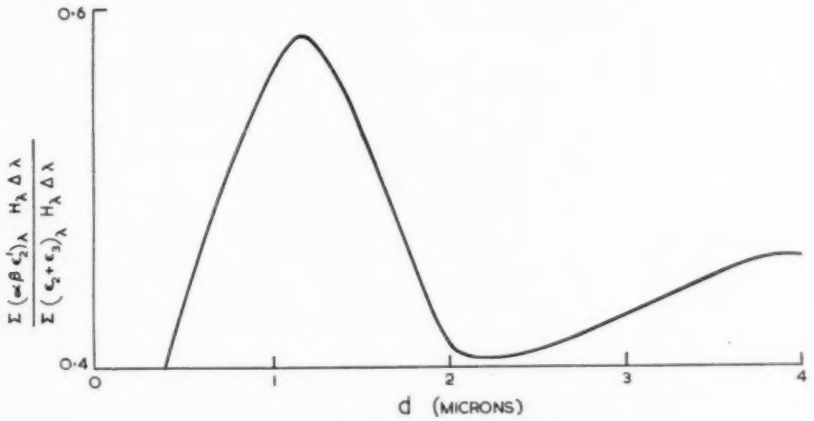

FIG. 8. Variation of sensitivity factor with selenium thickness.

(*e*) *Discussion.* A separate integration gives an effective value for $\alpha\beta$ of 0·59. Using this, we may deduce effective values of $\epsilon_2'/(\epsilon_2 + \epsilon_3)$ and these are shown in Table 3.

TABLE 3. RATIO EFFECTIVE ABSORPTION TO EMISSION

d (μ)	0·5	1·0	1·5	2·0	2·5	3·0	3·5	4·0
$\epsilon_2'/(\epsilon_2 + \epsilon_3)$	0·74 (0·62)	0·97 (0·77)	0·90 (0·71)	0·70 (0·63)	0·70 (0·63)	0·72 (0·63)	0·77 (0·66)	0·79 (0·66)

The bracketed numbers are the values which would have been obtained if the variation of ϵ with ϕ had been ignored. The sensitivity would have been under-estimated by about 20 per cent.

The more accurate procedure indicates that the sensitivity given for a 1 μ film is nearly twice that predicted for a symmetrical film. The most efficient use of the incident radiation is made by using a film 1·2 μ thick. This is 40 per cent more effective than a 2 μ film.

THE SENSITIVITY OF A SELENIUM A.E.I.T.

1. *Dependence of Sensitivity on Selenium Thickness*

The three processes which constitute thermal imaging have been described earlier. We are now able to express their effect numerically and deduce the resultant sensitivity of an A.E.I.T. In particular, we wish to learn if there is an optimum thickness for the selenium film.

(*a*) *Radiation balance.* A favourable radiation balance is obtained when the ratio $\epsilon_2'/(\epsilon_2+\epsilon_3)$ is high.

We have shown that this ratio is not markedly dependent on the thickness of the metal, and the variation with the selenium thickness was given in Table 3. It should be noted that the radiation balance is independent of the nature of the metal, provided that the infrared approximation is valid for the particular metal used ($\eta^2 = \kappa^2 = \sigma/2\omega\epsilon_0$).

(*b*) *Variation with temperature of the transmission of sodium light.* The transmission of the selenium film is given by

$$t = t_0 \exp(-\gamma d) \tag{6}$$

where t_0 is a constant, γ the absorption coefficient and d the film thickness.

Therefore

$$\frac{dt}{d\theta} = -td\frac{d\gamma}{d\theta} \equiv -td\delta \tag{7}$$

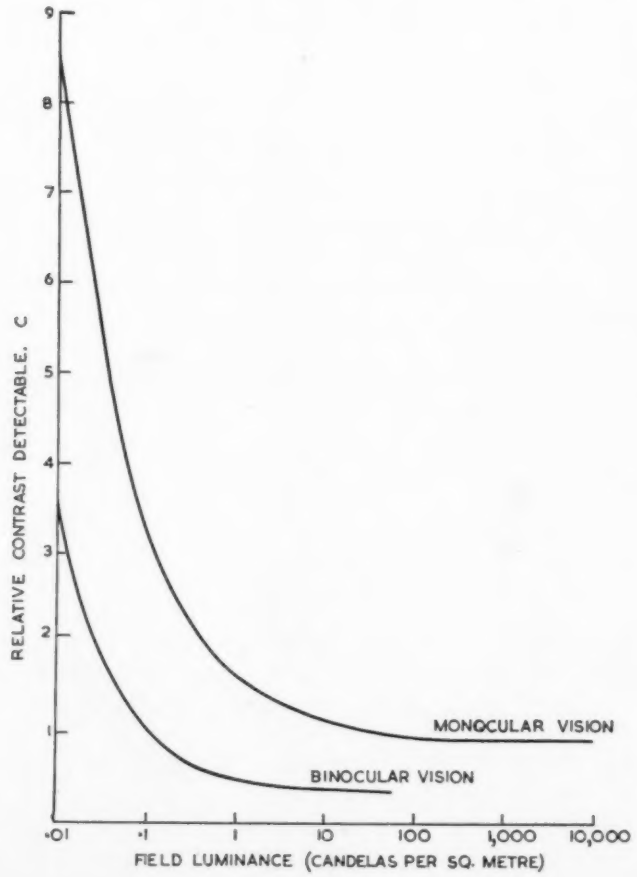

FIG. 9. Variation of relative contrast detectable with illumination (after ref. 13).

The fractional change in transmission is directly proportional to the thickness. Other factors apart, it is therefore preferable to use thick films.

(*c*) *Efficiency of detecting contrast.* Experiment has shown that the ability of the eye to detect contrast variations in the field of view is dependent on the illumination level. Using one eye it is possible, under good lighting conditions, to detect a change of 2 per cent. Such small contrasts are not detectable under poor lighting conditions, as shown in Fig. 9, deduced from curves in ref. 13. The contrast detectable is taken as 0·02C, and the variation of C with illumination level is shown. If we assume that this curve applies to the viewing conditions in the A.E.I.T. we may calculate how C varies with the film thickness.

Under typical conditions the illumination level before interposing the film is 2000 cd/m². We assume that the metal backing transmits 10 per cent of the sodium light, and deduce Table 4.

TABLE 4. DEPENDENCE OF DETECTABLE CONTRAST ON FILM THICKNESS

d (μ)	0·5	1·0	1·5	2·0	2·5	3·0	3·5	4·0
C	1·05	1·12	1·20	1·32	1·52	1·9	2·6	3·7

(*d*) *The resultant sensitivity.* We have from (7)

$$\Delta t/t = -\, d\delta\Delta\theta \tag{7a}$$

Then if $\Delta t/t$ is the minimum contrast detectable, it is equal to 0·02C, and the minimum temperature change on the film which can be observed is 0·02 C/$d\delta$.

The minimum temperature difference in the field of view which is detectable with the A.E.I.T. is given by

$$\theta_{\min} = \frac{0{\cdot}02\mathrm{C}}{\delta d} \cdot \frac{4N^2}{\alpha\beta} \cdot \frac{\epsilon_2 + \epsilon_3}{\epsilon_2'} \tag{8}$$

where we have ignored $\theta_{\min}/200$ compared with unity. Integration in the previous section gave $\alpha\beta = 0{\cdot}59$, and we should include a 10 per cent allowance for reflection loss in the rock-salt window. Previous measurements on selenium [14] have given $\delta = 0{\cdot}0190/\mu/°\mathrm{C}$, and the mirror we use has an effective aperture N of 0·91.

When these values are inserted in equation (8), it reduces to

$$\theta_{\min} = 6{\cdot}6\,\frac{\mathrm{C}}{d}\,\frac{\epsilon_2 + \epsilon_3}{\epsilon_2'} \tag{9}$$

The variation of $\mathrm{C}(\epsilon_2 + \epsilon_3)/\epsilon_2' d$ with d, deduced from Tables 3 and 4, is given in Table 5.

TABLE 5. DEPENDENCE OF SENSITIVITY FACTOR ON FILM THICKNESS

d (μ)	0·5	1·0	1·5	2·0	2·5	3·0	3·5	4·0
$\frac{\mathrm{C}(\epsilon_2 + \epsilon_3)}{d\epsilon_2'}$	2·83	1·15	0·89	0·94	0·87	0·88	0·96	1·16

In Fig. 10, the minimum temperature detectable is plotted against selenium thickness. It will be seen from the graph that in the present system the various factors involved have

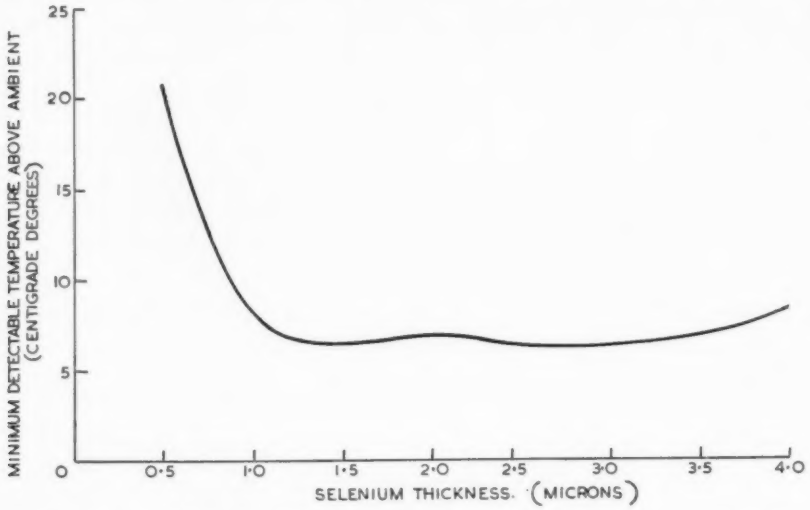

FIG. 10. Variation of minimum temperature detectable with thickness of selenium film.

such a relative importance that the sensitivity is almost constant for selenium thicknesses between 1·2 and 3·6 μ. At a thickness of 2·5 μ a *temperature of 5·7 °C above ambient* is theoretically detectable.

2. *Refinements in the Theory*

(*a*) *Heating effect of sodium light*. It is implicit in using the transmitted sodium light for detection that a large proportion of it must be absorbed in the film. It acts here in two ways. The overall absorption raises the temperature of the film above its surroundings, and thus reduces the sensitivity. But since the absorption is higher in the hot parts of the film, there is also an amplifying effect with a gain in sensitivity. It can be shown that both these effects are small in our present arrangement. If we assume that R mW of sodium radiation are incident on a square centimetre of film, there is a net sensitivity loss of 1·7 R per cent, i.e. about 2 per cent here, where $R = 1{\cdot}3$. In general the effect can be ignored unless $R > 10$ mW/cm^2.

(*b*) *Effect of sodium red line*. Sodium light is not monochromatic. The yellow doublet at 0·5890–0·5896 μ is far more intense than any other line, but for thick selenium films the transmission of the yellow lines is so small that lines at longer wavelength can have a measurable effect. In particular, the red line at 0·616 μ, which is about two orders of magnitude less intense than the yellow lines, appears to be of about equal intensity when viewed through a selenium film 3·5 μ thick. Since the red light is not modulated by movement of the absorption edge as much as the yellow light is, for the thicker films we cannot expect to get as high a sensitivity as the simple analysis indicates. We can calculate the necessary correction.

Consider the resultant transmission of a film when light at two wavelengths λ_1 and λ_2 is incident. We have

Vol. 1 1961

$$t = \frac{A \exp(-ad) + B \exp(-bd)}{A + B} \tag{10}$$

where a, b represent the two absorption coefficients, and A, B the relative intensities, ignoring the reflection loss.

By differentiation we obtain

$$\frac{1}{t}\frac{dt}{d\theta} = d\frac{da}{d\theta}\left\{1 - \frac{1 - l}{1 + (A/B)\exp[-d(a-b)]}\right\} \tag{11}$$

where l is $db/d\theta$ divided by $da/d\theta$. If λ_2 is a longer wavelength than λ_1 so that $a > b$ and $l < 1$, the quantity in square brackets must be less than unity. It can be seen, by comparison with (7), that the modulation is reduced.

An estimate of the effect can be made, with $\lambda_1 = 0{\cdot}589\,\mu$ and $\lambda_2 = 0{\cdot}616\,\mu$. Then $a = 1{\cdot}83/\mu$ and $b = 0{\cdot}56/\mu$. We assume that l is equal to b/a as we have no measured value for $db/d\theta$. The ratio of A to B can be measured, and is about 160.

Then for $d = 1\,\mu$ the term in square brackets is 0·99, and it decreases to 0·95 at $d = 2\,\mu$ and to 0·85 at $d = 3\,\mu$.

(*c*) *Interference effects.* The transmission curve of the selenium films does not show a monotonic increase with wavelength. It reveals a small number of subsidiary maxima and minima due to interference effects. For a given thickness d the transmission will not be exactly that given by

$$t = t_0 \exp(-\gamma d)$$

but will be a complicated expression involving the refractive index and the absorption coefficient. When the transmission is low, the effects of interference are small, but there may well be a measurable effect on the modulation.

It is possible to calculate the transmission of a composite metal–selenium film in terms of the two thicknesses, refractive indices and absorption coefficients, but the result should be treated with caution since the optical properties of the metal would not be known accurately. These constants can normally be determined only for clean films evaporated under carefully controlled conditions, and in our experiment the films must be subjected to certain treatments which can hardly be expected to give reproducible optical properties. The method for calculating the transmission has been given in ref. 9. Here we cannot use the infrared approximation for the metal, and the relations do not simplify, but it is not difficult to work them out numerically for a few chosen cases. It can be shown that the simple relation for sensitivity given in (8) should be modified by a factor $1/[1 + M\exp(-\gamma d)]$ where M is determined by the thickness and optical constants of the metal and the selenium. It may be either positive or negative, and it varies rapidly with the selenium thickness, the same values repeating at thickness intervals of about $0{\cdot}1\,\mu$. The extreme values of M define the limits of the possible swing in sensitivity due to interference, and this may be expressed as a percentage modulation. Some representative values are given in Table 6, with the selenium thickness taken as $0{\cdot}5\,\mu$.

For thicker metal films there would be a larger swing, but we could never be concerned with these because of their low visual transmission.

TABLE 6. INTERFERENCE EFFECTS AS A FUNCTION OF METAL THICKNESS

Metal thickness (Å)	0	50	100	200
Sensitivity swing	± 21%	± 8%	± 14%	± 22%

The swing will decrease for thicker selenium films, since $\exp(-\gamma d)$ decreases from 0·4 at $d = 0{\cdot}5\,\mu$ to 0·05 at $d = 2\,\mu$. For zero metal thickness the resultant swing decreases from the ± 21 per cent given in Table 6 for a $0{\cdot}5\,\mu$ selenium film to ± 10 per cent for a $1\,\mu$ film and to ± 3 per cent for a $2\,\mu$ film.

Most of our work will be done with selenium thicknesses greater than $1\,\mu$, and metal thicknesses around 100 Å. Our simplified analysis shows that within these limits the effect of interference will be a sensitivity swing of less than ± 7 per cent.

EXPERIMENTS TO VERIFY THE THEORY

1. *Principle of the Experiments*

We could check the theory of the A.E.I.T. by noting the minimum object temperature detectable by an observer, and observing how the sensitivity depended on parameters such as selenium thickness and metal thickness. In the first experiments with a tube it was seen that the performance which could be obtained depended to some extent on the skill of the observer. This is probably because the viewing conditions are rather unusual. The eye is accustomed to seeing objects by diffusely reflected light; when it is required to study a transparent film by transmitted light, there is a strong tendency to focus on the light source. Various optical systems with a small depth of focus were tried, and diffusing screens were interposed between the lamp and the mirror, but though some improvement was obtained, at least an hour's training was necessary before novices could detect contrasts of less than 10 per cent. Trained observers needed only a few minutes to reach their optimum performance, but the reproducibility they showed was not thought adequate to give a searching test of the theory. For this reason, and because it was thought preferable to have a permanent record of the results, the performance of the tube was measured photographically.

If Δt is the change in the transmission t caused by imaging a target θ °C above ambient temperature on the composite film we have from (4) and (7a)

$$\frac{\Delta t}{t} = -\frac{d\delta\theta(1 + \theta/200)}{F} \tag{12}$$

There are no adjustable parameters in this equation, and we may immediately calculate the values of $\Delta t/t$ we expect for a specific experimental arrangement. The purpose of the experiments now described was to measure $\Delta t/t$ for a series of composite metal–selenium films, studying the dependence on both selenium and metal thickness.

2. *Experimental Methods*

The apparatus used for the measurements is shown in Fig. 11. The general principle was to photograph the composite film in an absorption-edge tube, and measure the transmission first with and then without a hot target in the field of view.

The film enclosure was demountable, with rubber O-ring seals at the flanges and the two windows, one of which was glass and the other rock-salt. A vacuum of about 10^{-5} mm could be obtained, using a two-stage rotary pump, an oil diffusion pump and a liquid air trap.

Vol. 1 1961

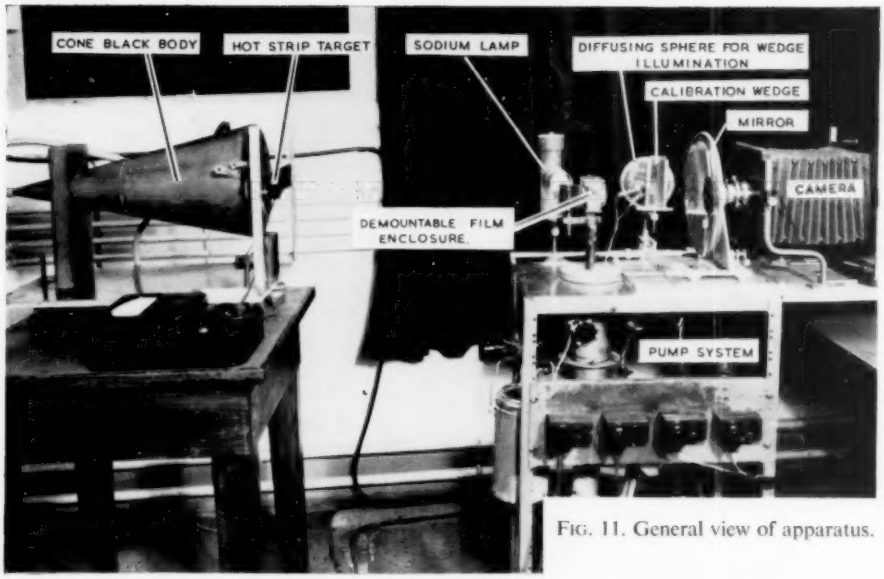

FIG. 11. General view of apparatus.

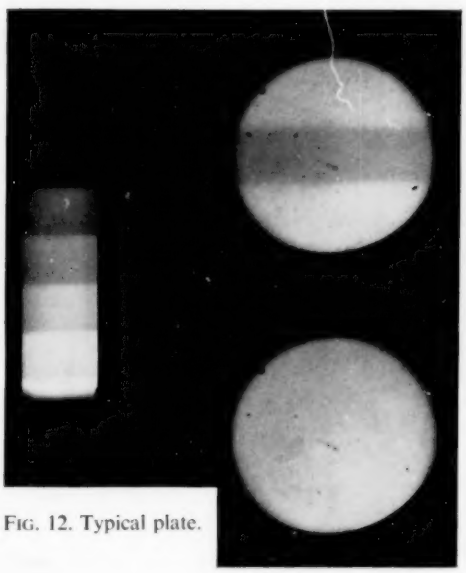

FIG. 12. Typical plate.

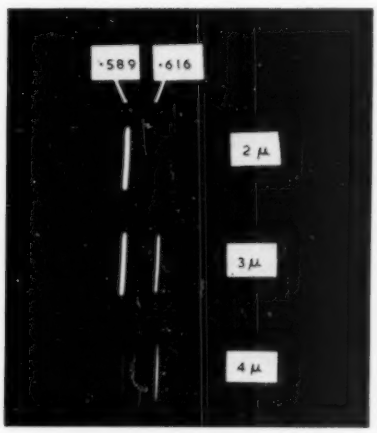

FIG. 14. Spectra of sodium source through 2, 3 and 4 μ films.

Facing Page 82

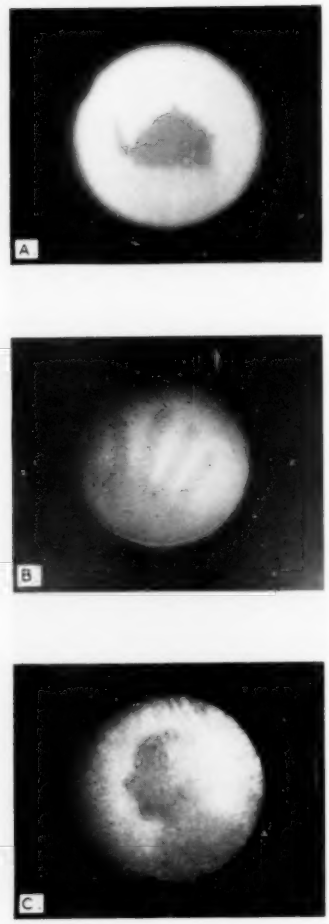

FIG. 19. Images of warm objects.
(a) Kettle at 80 °C. (b) Human hand. (c) Head.
In (b) and (c) contrast has been doubled by a photographic technique.

Vol.
1
196

For focusing the thermal radiation, a spherical mirror was used, with focal length 8·625 in., diameter 10·5 in., and a central hole 2 in. in diameter for observing the film. The illumination was provided by a 20 W Osram sodium lamp.

The thermal target which was focused on the film was a hollow copper strip, 2 in. wide and 9 in. long, placed horizontally in front of a cone black body, 9 in. diameter and 20 in. long, both being blackened with camphor soot. The cone was double-walled, and cold water was passed through to hold its temperature constant. The strip was heated by circulating hot water through it. In the experiments, a temperature difference of 32·5 °C was maintained between the strip and the cone, this being measured by means of chromel–alumel thermocouples.

The films which were tested ranged in selenium thickness from 0·8 to 3·5 μ. The metal layers were classified by means of their infrared transmission, and this varied from 23 per cent to 65 per cent in the films used, with a standard transmission of 23 per cent adopted when the dependence on selenium thickness was being investigated. The method of manufacturing and measuring the composite films is given in Appendix 2.

The films were photographed through the observation hole in the centre of the mirror, using Ilford Rapid Process Pan plates; these gave the best combination of speed $\times$ contrast of the several emulsions tested. Half of a completed plate is shown in Fig. 12. One photograph of the film was made with no hot target present, and then one with the strip focused on the centre of the film. For calibration, a transmission wedge of known characteristics was then photographed. The three exposures were duplicated on the other half of the plate to help in assessing the reproducibility of the measurements.

A recommended procedure [15] for developing, washing and drying the plates was adopted after test to ensure that consistent calibration curves were obtained from wedge photographs at different positions on the plate.

The plates were examined on a Hilger recording microphotometer. The gamma of each plate was found using the wedge images. The film images were then scanned along a line perpendicular to the strip edges, and the recordings superposed to find the change in density caused by the thermal image; measurements were made at six points away from the edge of each image, and the mean of the twelve values found. Using the gamma previously measured, $\Delta t/t$ could be deduced.

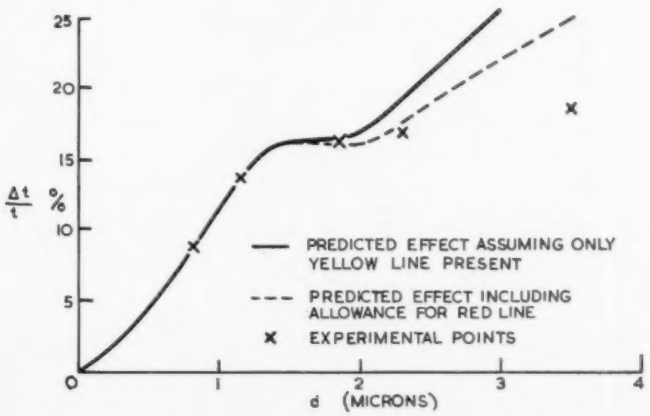

FIG. 13. Variation of sensitivity with selenium thickness.

3. *Results*

The predicted variation of sensitivity with selenium thickness is shown as a full curve in Fig. 13. The experimental results are given on the same graph, and it can be seen that the agreement is very good for thicknesses below 2 μ. Departure from this curve is to be expected for greater thicknesses, since the red sodium line, which had been ignored in our first analysis, then becomes important. An illustration of this effect is shown in Fig. 14, which is a series of spectrographs of the radiation from a sodium lamp after passing through selenium films of various thicknesses. When the film is 2 μ thick, the red line is of negligible intensity,

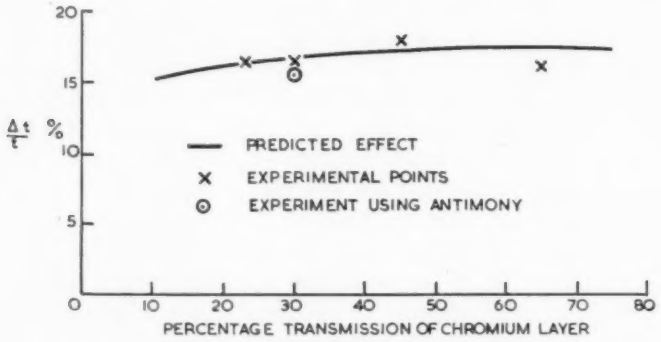

FIG. 15. Dependence of sensitivity on chromium thickness.

but it rapidly increases in importance until with 4 μ films it is the dominating line. The effect was discussed earlier, and a more accurate expression for sensitivity given in (11). A correction to $\Delta t/t$ may be deduced from this, and the corrected sensitivity is shown as the dotted line in Fig. 13. There still remains an apparent loss of sensitivity for the thickest film, but this may be an experimental error, due to the long exposures used in this test. The transmission of such thick films is so low that an exposure of 1 hr was necessary.

The variation of sensitivity with metal thickness is shown in Fig. 15. The layers are classified by their transmissions at 2 μ, and all were deposited on selenium films 1·8 μ thick.

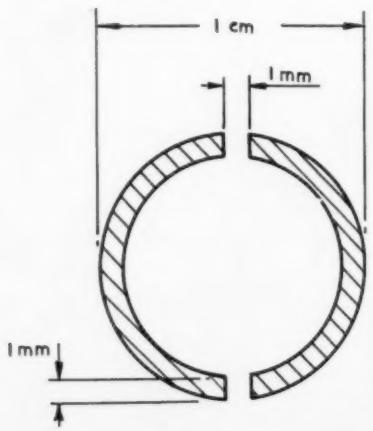

FIG. 16. Form and dimensions of evaporated Landolt circle.

Vol. 1 1961

Again the agreement with theory is good. In general, chromium was used for the metallizing, but as the sensitivity should not be dependent on the particular metal employed, on one occasion an antimony layer was tried. Within the experimental error, equivalent sensitivity was achieved. Attempts were made to use layers of aluminium, gold, and silver, but generally non-uniform films were obtained and the results were inconsistent.

4. *Contrast Detectable*

Though it has been said that the eye can detect contrasts of 2 per cent, the usual experiments from which results are obtained are carried out under very favourable conditions. We should not assume that such low contrasts would be observable in the A.E.I.T. without some experimental evidence. A limited number of tests were therefore made.

A series of Landolt broken circles (Fig. 16) were made by evaporating chromium through a metal mask on to glass discs. At the same time as each circle was made a monitor layer was prepared and its transmission was later measured on a spectrometer, set at 0·589 μ, and on a Baldwin transmission photometer. The transmission of uncoated glass discs was also measured, and the contrasts of the gaps in the broken circles deduced. The series ranged in contrast from 40 per cent to 1 per cent.

To simulate the viewing conditions of an actual A.E.I.T., some of the apparatus shown in Fig. 11 was used. The camera and the self-supporting selenium–chromium film were removed, and a glass disc with a 10 per cent transmitting chromium layer evaporated on was substituted for the clear glass window of the demountable film enclosure. Observations could be made through the hole in the centre of the mirror, and the luminance due to the transmitted sodium light was measured with a Holophane lumeter. The luminance of the window with chromium was 200 cd/m². A series of glass discs coated with different thicknesses of selenium had been prepared for experiments on the optical properties of selenium. If one of these was placed in the demountable film enclosure, the viewing conditions were similar to those in an A.E.I.T. with a composite selenium–chromium layer (Fig. 17). The

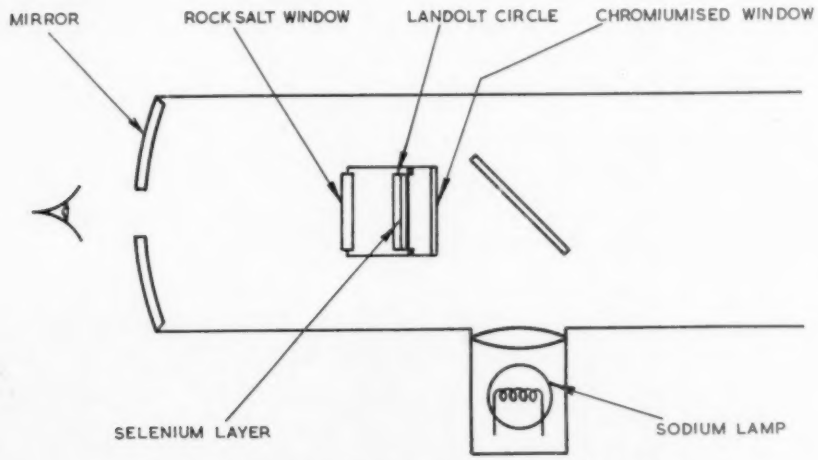

FIG. 17. Viewing system for measuring contrast detectable.

disc with the Landolt circle could now be placed in close contact with the selenium and turned round, the observer being asked to detect the poisition of the gap. It would have been

possible to do this experiment using self-supporting films, but there was a constant risk of fracturing the films during the rotation of the circle, or the substitution of a new ring or film.

The procedure adopted was to start with a thick selenium layer and a circle with large contrast. Circles of smaller contrast were substituted in turn until the observer could no longer see the gap. A thinner selenium layer was then used, and the observations repeated. The effective luminances of the layers could be calculated as the transmissions had been measured. The lowest luminance was 0·4 cd/m² and the highest 40 cd/m². The contrasts which should have been detectable can be read off from Fig. 9. The data for one trained observer (W.R.H.) were consistently almost twice as great as the calculated values. A second trained observer (C.H.) showed a greater spread in his results, detecting contrasts ranging from 1·5 to 3 times the calculated ones, with poor reproducibility. Since this observer wore spectacles and therefore could not put his eye close to the hole in the mirror, his results are given less weight.

5. *Performance of the Complete Tube*

We could conclude that since the transmission changes of the thermo-sensitive layer are close to those predicted, the minimum target temperature detectable by the eye will be just twice that shown in Fig. 10. But this would be only an average figure. An untrained observer, or a trained one working under less favourable conditions, could not do as well as this. On the other hand, a trained observer looking at a large target would do better. The dimensions of the Landolt rings were chosen to be near those of the smallest images which the tube can resolve. Trained observers are reported[16, 17] to have detected Landolt rings of these dimensions at contrasts between 1·8 and 6 per cent; when the test object was four times as large it could be detected at contrasts between 1·2 and 3·4 per cent.

If the image occupied over one-third of the area of the thermo-sensitive layer we should therefore expect a trained observer to detect a contrast of between 2 and 3 per cent, and the sensitivity would be given by Fig. 10. The sensitivity would be less for smaller objects by a factor of up to two, until the image size was about 1 mm square. Then the poorer eye performance and the lower definition, due to both heat spread and optical aberrations, would combine to give a much lower sensitivity.

METHODS OF INCREASING THE SENSITIVITY

We now consider possible ways of improving the performance of the A.E.I.T., dealing first with modifications and additions to the tube, and then with modes of operation which involve more complex thermo-sensitive layers.

1. *Increase of Aperture*

In the system described, the ratio of focal length to diameter for the mirror was 0·91. Since the sensitivity is inversely proportional to the square of this ratio, it would seem profitable to try optical systems of still larger aperture. However, a simple spherical mirror with an F number much less than unity has a poor optical performance off-axis, and it is probable that any gain due to increased aperture would be nullified by a loss in resolution. The sensitivity can be increased in this way only if the optics are corrected for spherical aberration.

We were able to work for a short time with a corrected Schmidt system, made from a spherical mirror and an 8 in. diameter potassium bromide aspheric corrector plate. The

Vol. 1 1961

complete system had an effective F number of 0·71 but the corrector plate had to be coated with a protective layer to ensure its surfaces did not deteriorate, and this introduced an extra 10 per cent loss in transmittance. These optics should theoretically give us 30 per cent higher sensitivity than the original simple mirror.

Visual observations indicated a sensitivity improvement near this figure, but the more striking effect was the improvement in resolution.

The additional weight and expense make this refinement less attractive than some of the other possibilities.

2. *Binocular Vision*

It has been found by experiment that the contrast detectable using both eyes is smaller than the figure of 2 per cent given for one eye. Both Stiles[18] and Lowry[19] show that under good lighting conditions a contrast of 0·6 per cent can be seen. Their results can be seen in Fig. 9.

It is doubtful if we can apply these results, obtained under carefully controlled conditions, to our own circumstances, where the eye is viewing a scene under rather unnatural conditions. Nevertheless on general grounds we might expect some gain if we change the system so that both eyes are used for the observations.

Our experiments showed this was not so. Different observing systems and different observers were tried, but in no case was higher sensitivity obtained by the use of two eyes. It should be remembered that the system used was designed for monocular viewing, and without radical changes it was not possible to make from it an ideal binocular system. As a result we could not conclude that there is no gain to be obtained by binocular viewing, but it is very doubtful if the sensitivity could increase by anything approaching the predicted factor of three.

3. *Change in the Observation Wavelength*

The considerations of radiation balance were quite independent of the method of detecting the temperature changes. They showed that the most efficient use of the incoming radiation is made by a layer 1·2 μ thick. It would therefore pay us to use illumination of a wavelength appropriate to this thickness. With sodium light the ratio d/C is a maximum at 2·5 μ, and this is why the sensitivity of the tube is almost independent of thickness over quite a large range of thicknesses. If the method of detecting the temperature changes was also most efficient for a thickness of 1·2 μ, we could expect that the sensitivity would be markedly thickness-dependent and the maximum would be higher than in the present tube. We should therefore use an observation wavelength which results in a maximum for d/C at 1·2 μ; the appropriate wavelength is that where γ, the absorption coefficient, is twice that at 0·589 μ. The optical constants are not known well enough to give this wavelength accurately, but it would lie near 0·58 μ. The mercury yellow doublet, symmetrical about 0·578 μ, might be suitable provided the intensity available were comparable to that of a sodium lamp. If we assume that the fractional change of absorption coefficient with temperature increase is not wavelength dependent, the resultant sensitivity can be calculated, and is given in Table 7. The sensitivity should be almost 50 per cent better than when using sodium light.

Experiments do not confirm these predictions, a tube using mercury yellow light being rather less sensitive than one using sodium light. Tests of the temperature modulation of transmission using some of the evaporated selenium layers showed that δ/γ was less at 0·578 μ than at 0·589 μ. A layer which should have changed in fractional transmission by 4·6 per cent actually changed only 2·6 per cent.

TABLE 7. PREDICTED SENSITIVITY FOR MERCURY YELLOW LIGHT

d (μ)	0·5	1·0	1·25	1·5	2·0
C	1·12	1·32	1·52	1·9	3·7
$(\epsilon_2 + \epsilon_3)/\epsilon_2'$	1·35	1·03	1·01	1·11	1·43
θ_{min} °C	10	4·5	4·1	4·7	8·7

If the absorption edge could be represented as a straight line in the graph of log γ against quantum energy, and the whole edge moved bodily along the energy scale as the temperature changed, the assumption that δ/γ was wavelength-independent would be justified. In fact, Cheeseman [20] shows that we might expect, on theoretical grounds, the edge to change in slope as the temperature changed, and this would be in agreement with our observations.

4. *Alternatives to Selenium*

There are several properties we need to find in an alternative material for the image-tube, apart from the obvious ones of a steep edge in the visible and a large temperature shift. They are

(1) availability as a uniform thin film

(2) low thermal conductivity

(3) stability of optical properties with time.

It is convenient if the material can be prepared as a self-supporting film in thicknesses down to a micron.

Selenium is satisfactory on all counts except stability. The amorphous modification tends to transform into metallic selenium at 40 °C, and if an image of a very hot body is focused on an amorphous selenium film, the film may well disintegrate.

It is not absolutely necessary to make the thermo-sensitive material as a self-supporting film, if it can be deposited on a substrate. In a subsidiary investigation, [21] thin self-supporting films of aluminium oxide have been made in thicknesses down to 1000 Å and sizes up to 2 in. diameter. The method used was a combination of the techniques of Hass [22] and Strohmaier [23], involving anodic oxidation of aluminium foil in an electrolyte of tartaric acid, and is not discussed here since the films were not in the event necessary. A check of their thermal conductivity was made by evaporating selenium and chromium on to some of them, and observing the thermal image in an A.E.I.T. Some degradation occurred, but the resolution was still satisfactory.

We confined our attention to materials which could be deposited by evaporation. There are other techniques of producing uniform thin films, but they are normally more restricted in their application. Organic dyes, sulphur, mixtures of sulphur and selenium, and several semiconducting compounds including germanium sulphide, stannous sulphide, antimony trisulphide, and phosphorus pentaselenide were tried, but the only promising alternative which was discovered was a mixture of arsenic pentasulphide and pentaselenide. It was found that an A.E.I.T. using a film made from 40% As_2S_5–60% As_2Se_5 would have a sensitivity comparable with that of the selenium tube.

No material was discovered which gave a better performance than this.

Vol. 1 1961

5. *Cooling*

The sensitivity is increased by cooling the image-converter. If the tube is cooled to CO_2 temperature the sensitivity is doubled, and there is a further gain of two on cooling to liquid-air temperature. However, the problem of obtaining uniformity in mean temperature across the film would be greatly increased.

6. *Contrast Expansion*

Some electronic imaging systems have inherent in them a small expansion of contrast. For many purposes this property is not required, and, indeed, special circuits are designed to correct for it. In our application contrast expansion would give a sensitivity gain but the complexity of the tube would be so increased that the modification could be justified only in very special circumstances.

7. *New Modes of Operation*

Our percentage modulation of transmission is small because a large amount of light reaches the eye when no heat image is present. There is a simple way of compensating for this. If we viewed the film by reflected light, we could obtain interference between the light reflected at the front and back surfaces respectively. If these two beams were of equal intensity and opposite phase the field would appear dark. The second beam passes through the selenium film twice, and it would therefore be modulated by the temperature changes. In principle we could obtain a depth of modulation many times higher than with the normal transmission mode of operation.

But unfortunately selenium has such a high refractive index that almost 20 per cent of the light would be reflected from the front surface. The beam reflected from the back surface would be much less intense unless the selenium were very thin, and the intrinsic modulation of a thin film is always small. We would prefer to work with an effective thickness of around $1\,\mu$, i.e. a film $0{\cdot}5\,\mu$ thick, and the intensity in the back-surface reflected beam could be only a few per cent at most. It would therefore be necessary to bloom the front surface of the film to reduce the reflection from this face to an equal intensity. Since a blooming layer about 1000 Å thick with a refractive index near 1·7 would be suitable, we may consider using aluminium oxide for this layer and building up our thermo-sensitive film on an aluminium oxide backing.

The complete film, a self-supporting reflection interference filter, would thus consist of a quarter wavelength film of aluminium oxide, of refractive index 1·62, a selenium layer of thickness an integral number of quarter wavelengths (refractive index ≈ 3), and a metal layer to give heat absorption. A metal layer is used rather than a metal black since the asymmetrical system with a dielectric $0{\cdot}5\,\mu$ thick gives a better radiation balance than a symmetrical film. There may, however, be a phase change at the selenium–metal surface, and the selenium thickness needed for optimum operation would not be an integral number of quarter wavelengths. Dr. O. S. Heavens[24] has suggested two other systems which might be equally suitable. The first is a transmission interference filter consisting of $\lambda/4$ selenium, $\lambda/4$ aluminium oxide, $m\lambda/2$ selenium and a metal film. The second selenium layer acts as a spacer, and needs to be an integral number of half-wavelengths thick, and the metal acts in the double role of a reflector of the visible radiation and an absorber of the infrared. Heavens' second suggestion is a simplification of the reflection interference filter. No blooming layer is used, and the front surface reflection is reduced by using polarized light and viewing at an angle near the Brewster angle. Heavens made a simplified calculation to

show that a modulation of 4·4 per cent could be obtained with a 0·5 μ film, compared with a value of less than 2 per cent for the simple 1 μ film.

A programme for the calculation of the modulation for the reflection interference filter and the transmission interference filter was prepared by Heavens, and the computations were made at the U.S. Army Engineer Research Development Laboratories, Fort Belvoir, Virginia. For the reflection filter the range of parameters covered was—selenium thicknesses between 0·49 and 0·74 μ, metal thicknesses between 100 Å and 400 Å and metal optical constants $\eta = 3$, 1 and 0·5, $\kappa = 5$. For the transmission filter the same metal constants and thicknesses were catered for, but the selenium thickness was varied from 0·49 to 1·57 μ.

The results showed that the transmission filter was little more efficient than the system normally used, but a reflection filter could give higher sensitivity. Figure 18 shows how the

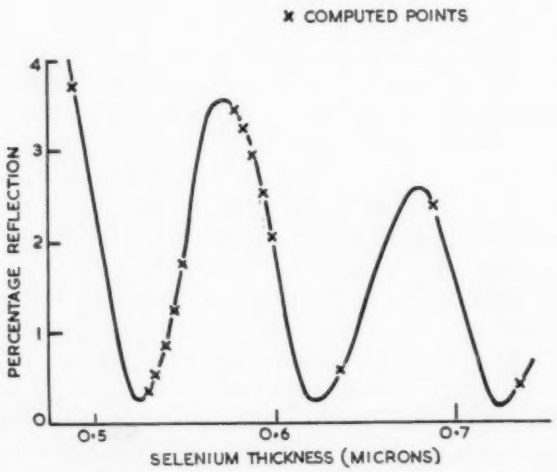

FIG. 18. Reflection of Al_2O_3–Se–Cr film as a function of selenium thickness.

reflection changes with selenium thickness. At a thickness of 0·53 μ a reflection of 0·4 per cent is obtained with a percentage modulation of this of 5 per cent/°C. The computed point was not actually at a reflection minimum, and it is probable that higher modulations would be found if computations were made at more points.

To take advantage of this prospective sensitivity gain, new preparation techniques would need to be developed. The methods used in the manufacture of interference filters could be adopted for this purpose. It is likely that a tube twice as sensitive as the simple absorption-edge image-converter could then be made.

CONCLUSION

It is clear from our analysis that the physics of even a simple thermal image-converter is quite complex. In previous work, it has often been assumed that the highest sensitivity would be obtained by using thermo-sensitive layers with the highest possible absorption. By breaking down the imaging operation into three independent phases, and analysing the first phase, the transfer of temperature from the target to the layer, we have shown that this

Vol. 1 1961

assumption is incorrect. The concept of radiation balance, which led us to the use of asymmetric layers, has been employed here to calculate the performance of a particular instrument, but the results have a broader significance. It appears that the radiation balance of composite metal–dielectric films can be accurately predicted, and therefore certain general principles may be formulated for the design of infrared detectors and thermal converters using such films.

(1) The radiation should be incident on the dielectric side of the film; if this is not possible the use of a metal–dielectric–metal sandwich should be considered.
(2) The best radiation balance is achieved with the dielectric of such thickness that the product of refractive index and thickness (in μ) is approximately three.
(3) The metal thickness is, within limits, immaterial to the question of sensitivity; in general, a thin layer will contribute less to thermal spread and a thick one, giving both high emissivity and absorption, will result in a shorter time constant. It is these points which should be borne in mind when deciding a thickness appropriate to a particular design.

Application of these principles to the absorption-edge image-tube has led to a sensitivity three or four times better than that of the original tubes. The improved A.E.I.T. is the most sensitive continuously operating converter yet reported. It is capable of imaging objects less than 10 °C above ambient temperature, with a time constant of less than 0·5 sec, and a resolution of 2 line-pairs/mm. Typical photographs taken with it are shown in Fig. 19.

Acknowledgements—We are grateful to Mr. I. M. Ross and Dr. O. Simpson for their encouragement and assistance throughout this work, and to Dr. O. S. Heavens and Dr. D. C. Northrop for valuable discussions. The arrangements for the computations carried out at Fort Belvoir were made by Dr. W. Weihe, and his kindness is appreciated. Permission to publish this paper has been given by the Admiralty.

APPENDIX I. THE EFFECT OF COOLING

We can express (1) in the form

$$T_2^4 - T_3^4 = \frac{1}{F}\left[T_1^4 - T_0^4 + \frac{1}{a\epsilon_1}(T_0^4 - T_3^4)\right] \tag{A.1}$$

It should be noted that any part of the film which receives radiation via the optical system stabilizes at a temperature higher than T_3, the temperature to which the tube is cooled. We may consider the film as made up of two parts; on one of these the target (at T_1) is focused, and the other receives radiation from the surroundings, at a temperature T_0. The temperature of the first part we have denoted by T_2, and the temperature of the second will be T_2'.

The sensitivity of the tube is dependent on the difference between T_2 and T_2^1, since this determines the contrast ratio observed between the part of the film on which the target is focused and the rest of the film.

We have, from A.1

$$T_2'^4 - T_3^4 = \frac{1}{Fa\epsilon_1}[T_0^4 - T_3^4] \tag{A.2}$$

and therefore

$$T_2^4 - T_2'^4 = \frac{1}{F}[T^4 - T_0^4] \tag{A.3}$$

Putting $\theta_2 = T_2 - T_3$, $\theta_2' = T_2' - T_3$ and, as before $\theta_1 = T_1 - T_0$ we obtain the approximation

$$\theta_2 - \theta_2' = \frac{\theta_1}{F}[1 + 3\theta_1/2T_0]\, T_0^3/T_2'^3 \tag{A.4}$$

If we compare this with (4) we see that there is a gain in sensitivity on cooling equal to $(T_0/T_2')^3$. From (A.4) it can be seen that T_2' decreases fairly rapidly at first as T_3 is brought below room temperature, but cooling below 150 °K has only a small effect on T_2'. In Fig. 20 is plotted the dependence of T_2' on T_3, taking

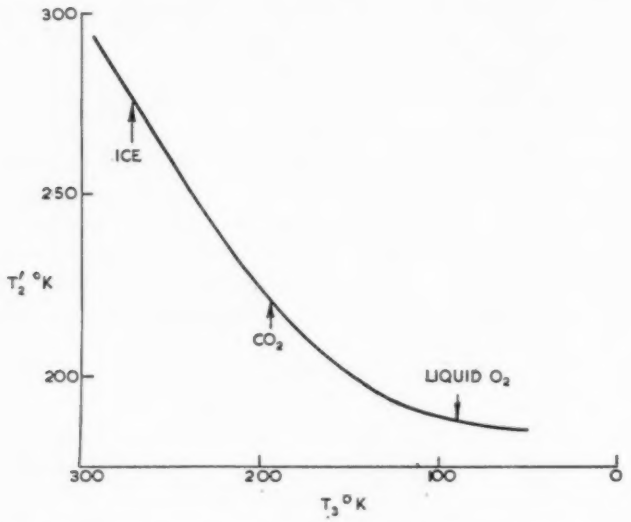

FIG. 20. Effect of cooling on temperature at which film stabilizes. ($F = 12{\cdot}5$, $T_0 = 293$ °K.)

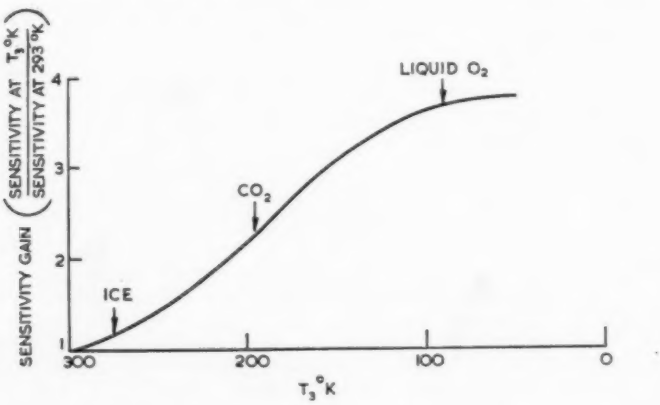

FIG. 21. Increase of sensitivity due to cooling.

F as 12·5, α as 0·5 and ϵ_1 as 1. As one cools from 250 °K to 150 °K, T_2' drops 60°. Further cooling to 50°K causes a change of only 14°. This effect is reflected in the gain in sensitivity obtained. In Fig. 21 this gain is plotted against T_3. A 20 per cent gain is obtained by cooling to ice temperature, a factor of over two at the temperature of solid CO_2, and nearly four at liquid-air temperature.

APPENDIX 2. THE PREPARATION OF SELENIUM METAL-COMPOSITE FILMS

The composite films are prepared in a standard vacuum system by evaporating 99·9 per cent pure selenium shot from a tantalum boat on to a 2 in. diameter glass substrate, which has previously been lightly polished with a Teepol-impregnated cloth. The metal coating is then evaporated on to the selenium, and the glass disc removed and placed on a frame in a water tank, held at an angle of 45° to the vertical.

Distilled water is slowly siphoned in, and as the water level rises, the Teepol dissolves, and the film is

Vol. 1 1961

separated from the substrate. When the level reaches the top of the disc, the film floats freely on the water surface, and it can then be picked up on a glass annulus, and left to dry.

During the selenium evaporation, a thickness monitor is made on a similar glass disc, and this is examined by the Tolansky multiple beam fringes method to determine the film thickness.

The metal layers are classified by their infrared transmission. As for the selenium, a monitor is made during the evaporation of metal, and the transmission measured at a wavelength of 2 μ on a Beckmann infrared spectrometer.

REFERENCES

1. Czerny, M., *Z. Phys.* **53**, 1 (1929).
2. Robinson, D. Z., Unpublished work at Baird Associates, Inc.
3. Urbach, F., N. Nail, and D. Pearlman, *J. Opt. Soc. Amer.* **39**, 1011 (1949).
4. Heintz, E., *J. Phys. Radium.* **7**, 293 and 336 (1946).
5. Edmond, J., and P. G. R. King, S.E.R.L. Q/R 17, January 1950.
6. Frank, K., and R. L. Stow, English Electric Valve Co. Final Report on Contract 13145/53.
7. Goff, G., Cathodeon Co. reports on Contract 15588/53, 1953–1956.
8. Northrop, D. C., S.E.R.L. Q/R 31, July 1953.
9. Hilsum, C., *J. Opt. Soc. Amer.* **44**, 188 (1954).
10. Hilsum, C., *J. Opt. Soc. Amer.* **45**, 135 (1955).
11. Adel, A., *J. Opt. Soc. Amer.* **37**, 769 (1947).
12. Strong, J., *The Infra-Red Atmospheric Transmission Problem*, Office of Naval Research, Washington (1948).
13. Walsh, J., *Photometry* p. 60. Constable, London (1953).
14. Hilsum, C., *Proc. Phys. Soc., Lond.* B **69**, 506 (1956).
15. Dobson, G., S. Griffith, and H. Harrison, *Photographic Photometry*, Clarendon Press, Oxford (1926).
16. Blackwell, H. R., *J. Opt. Soc. Amer.* **36**, 624 (1946).
17. Vos, J., A. Lazet, and M. Boumon, *J. Opt. Soc. Amer.* **46**, 1065 (1956).
18. Stiles, W., Illum. Res. Tech. Pap. No. 8, H.M.S.O. (1929).
19. Lowry, E., *J. Opt. Soc. Amer.* **18**, 29 (1929).
20. Cheeseman, I. C., *Proc. Phys. Soc., Lond.* A **65**, 25 (1952).
21. Hilsum, C., and M. Burr, S.E.R.L. Tech. Memo. 77, September 1953.
22. Hass, G., *J. Opt. Soc. Amer.* **39**, 532 (1949).
23. Strohmaier, K., *Z. Naturf.* **6**, 508 (1951).
24. Heavens, O. S., Vacation Consultant Report, S.E.R.L. July 1956.

/ol.
1
961

Infrared Physics, 1961, Vol. 1, pp. 94–103. Pergamon Press Ltd., Printed in Great Britain.

A HIGH-PRESSURE SCANNING FABRY–PEROT INTERFEROMETER FOR THE INFRARED

R. BEER and J. RING

The Physical Laboratories, The University, Manchester, 13, England
First submitted, 11 May 1960 and in final form, 1 September 1960

Abstract—The design and construction of a high-pressure scanning Fabry–Perot interferometer for use in the range 1–8 μ (1250–10,000 cm^{-1}) is discussed. Some defects in the apparatus are described and results are shown at a resolving power of at least 240,000. The flux gain of the interferometer over the grating spectrometer used as a premonochromator is shown to be about 50.

INTRODUCTION

JACQUINOT [1] has shown that axially symmetric interferometers used as spectrometers can have many times the luminosity of grating spectrometers operating at the same resolving power. A Fabry–Perot interferometer (FPI) used on-axis in a parallel beam of light has such symmetry and therefore can operate as a high-luminosity spectrometer. [2]

The FPI has multiple pass-bands according to the equation

$$n\lambda = 2\mu t \quad \text{on axis,}$$

where n = order of interference, λ = wavelength, μ = refractive index of the spacer medium and t = thickness of the spacer.

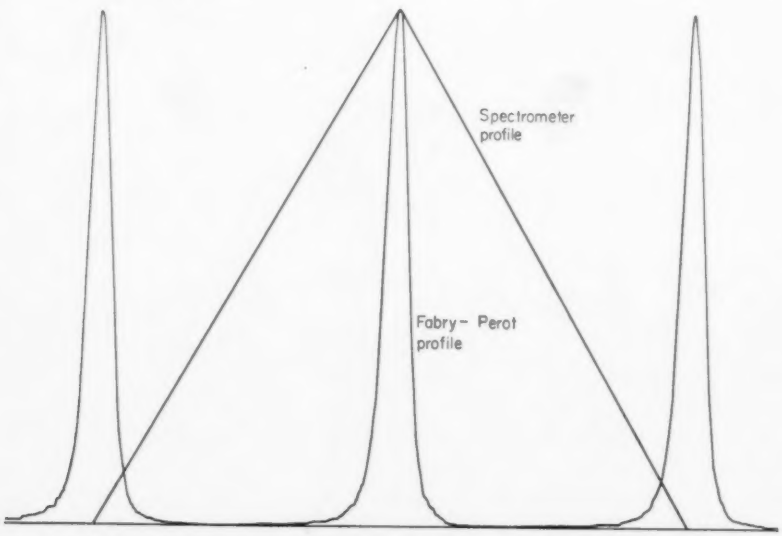

FIG. 1. Spectral profile of a Fabry–Perot interferometer and a slit spectrometer.

Vol. 1 1961

In order for the FPI to act as a spectrometer, one of these pass-bands must be isolated. In general, the isolator (premonochromator) employed is a grating spectrometer, although other FPI's or filters can be used for this purpose in particular circumstances.[3]

The grating spectrometer need only reject adjacent orders of the interferometer and the ideal combination of spectral profiles is that shown in Fig. 1, where it is assumed that the grating spectrometer has the theoretical triangular profile. However, should the spectrum be in emission, it is possible that no lines coincide with the adjacent orders of the FPI. In this case, the spectrometer profile can include more than one interferometer order and hence wider slits can be used.

In any case, the resolution attained for a given spectrometer profile width and a given interferometer spacer is only dependent on the ratio of the FPI inter-order distance to the half-width of one fringe. This ratio is known as the "finesse" and is a constant for a given interferometer in proper adjustment. It can be shown that the finesse is numerically equal to the effective number of interfering beams[4] and that it is principally a function of the reflectivity of the interferometer coatings and the roughness of the optical flats employed.[5] The finesse recorded (N_e, the effective finesse) is compounded from these quantities as

$$N_e^{-2} = N_r^{-2} + N_l^{-2}$$

where N_r, the reflecting finesse $= \pi\sqrt{R}/(1-R)$ (R is the reflectivity of the coatings) and N_l, the limiting finesse, $= P/2$ if the flats are rough or misaligned to λ/P, λ being the wavelength of operation.

The limiting finesse is so named because even if the reflecting finesse approaches infinity ($R \to 1$), the effective finesse never exceeds N_l. In this limiting case, the transmission τ of the FPI approaches zero, even with non-absorbing coatings, since

$$\tau = \frac{N_e}{N_r}$$

Therefore, there is an optimum value for N_r, and Chabbal[6] shows that this condition is attained if $N_r = N_l$, although 80 per cent of the optimum performance is achieved if $N_l/2 < N_r < 2N_l$. If the coatings absorb, the peak transmission is further reduced by a factor

$$\tau_a = \left(\frac{T}{T+A}\right)^2$$

where T is the geometric mean transmission of the coatings and A is the absorption. Since one would prefer the highest effective finesse and transmission possible, it is necessary to achieve high values of N_l. Values up to at least 100 could be matched without difficulty using conventional multilayers[7] but this would demand flats good to $\lambda/200$. In the visible, it is unlikely that glass or quartz could be polished to this accuracy, but any pair of flats accurate to $\lambda/20$ at $\lambda 5461$ Å would be $\lambda/200$ at $\lambda 5{\cdot}46\,\mu$ in the infrared. Unfortunately, at this wavelength, neither glass or quartz is transparent and an alternative material must be sought. The authors chose Calcium Fluoride (CaF_2) as offering the most advantages and a pair of optical flats in this material are being polished to $\lambda/20$ at $\lambda 5461$ Å. The rest of the optical train of the FPI was also made in CaF_2.

THE DESIGN OF THE INTERFEROMETER

The FPI must be able to scan in wavelength in order to act as a spectrometer. The merits of various methods of performing this scanning have been discussed.[8] The authors decided to employ pressure scanning in view of its elegance and the fact that a number of successful pressure scanning systems have previously been constructed in this laboratory.[9]

The range of scan provided by this method can be determined as follows:

Differentiation of the interferometer equation $n\lambda = 2\mu t$ gives

$$\Delta\lambda = \lambda \,.\, \Delta\mu/\mu$$

Now it is well-known that the refractivity $(\mu - 1)$ of a gas is proportional to the gas density and hence, provided that the gas obeys Boyle's law, to the pressure, i.e.,

$$(\mu - 1) \propto P$$

or

$$(\mu - 1) = KP$$

where P is the pressure, and K is a constant. If $\mu = \mu_1$ when $P = 1$ standard atmosphere, then $K = (\mu_1 - 1)$. Therefore $(\mu - 1) = (\mu_1 - 1)P$ if P is in atmospheres or, differentiating, $\Delta\mu = (\mu_1 - 1) \,.\, \Delta P$ whence

$$\frac{\Delta\lambda}{\lambda} = \frac{(\mu_1 - 1)}{\mu} \,.\, \Delta P$$

From an examination of the above equation, it is obvious that in order to obtain a large wavelength range of scan a gas with a high refractivity is required. Such gases do exist (e.g. Propane: $(\mu_1 - 1) = 0{\cdot}0011$) but, in general, they also exhibit strong infrared absorption bands. Homopolar molecules such as O_2 and N_2 have no absorption, but they also have low refractivities.

A representative selection of such refractivities is given in Table 1.

TABLE 1.

Gas	Refractivity
H_2	0·00014
O_2	0·00027
Cl_2	0·00078
N_2	0·00030

Chlorine has by far the highest value but is unusable owing to its most objectionable chemical properties. Of the three remaining gases, nitrogen presents itself both optically and physically, being much less dangerous under pressure than either hydrogen or oxygen.

One of the design criteria was a range of scan of 1 per cent of the mean wavelength of operation. With nitrogen this demands a pressure range of 40 atm (600 lb/in²). Upon investigation it was decided that such a pressure was tolerable and the instrument was designed accordingly.

Vol 1 196

The pressure rise (or fall) must proceed in a controlled manner at fairly low rates (~10 lb/in²/min). For small pressure ranges (<100 lb/in²) the Edwards VPCI standard pressure controller has been successfully used [9] but no suitable alternative has been found for higher pressures. It was therefore decided to employ the supersonic leak method of Rank *et al.* [10] It is shown in textbooks of aerodynamics [11] that provided the ratio of the pressures on both sides of a nozzle is greater than

$$\left(\frac{2}{\gamma+1}\right)^{\gamma/\gamma-1}$$

where γ is the ratio of the principal specific heats, then a pressure discontinuity occurs near the aperture and the rate of mass flow of gas is independent of the lower pressure. For nitrogen, this ratio is 0·528. Therefore, assuming that source of nitrogen at 80 atmospheres or more pressure is available, it is possible to cause the pressure within a chamber to rise linearly from 0 to 40 atm. However, the rate of flow is not independent of the higher pressure and this should therefore be kept constant.

Vol. 1 1961

THE CONSTRUCTION OF THE FPI

Figure 2 shows a longitudinal cross section of the pressure chamber used. It was turned

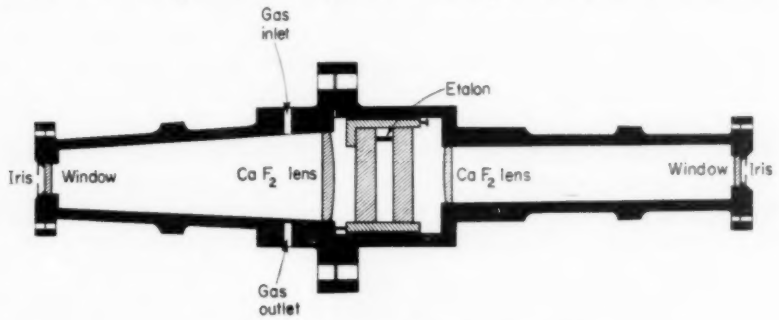

FIG. 2. Cross section of the pressure chamber.

from a single piece of mild steel shafting for strength and dimensional stability. Normal pressure chambers for FPI's contain only the etalon, but this implies windows of the same aperture as the flats. In view of the high pressure and the costliness of CaF_2 it was decided to enclose the collimator and condenser lenses within the chamber. The pressure windows were put near the entrance and exit pinholes where the beam diameter is small and quite small windows could be used. The flats could have a maximum diameter of 3 in. but since the reflecting films used may be opaque to visible radiation (e.g. multilayers containing Germanium or Tellurium) only the central 2 in. are coated leaving a clear annulus for alignment purposes. To this end, one of the lenses was made 3-in. diameter whilst the other is of 2 in. clear aperture. Both are plano-convex singlets of CaF_2, the focal length being 9·6 in. Doublets, corrected for spherical aberration would undoubtedly be preferable, but the cost would be excessive.

The etalon is mounted on push-pull screws and is located by three vee-grooves in the chamber body. Since the gas must be allowed free transport throughout the chamber, ports are cut round the lenses and in the etalon wall.

The pressure windows are mounted within the focal points in order that the iris diaphragms at either end should be readily accessible. The small aperture for the supersonic leak is provided by a needle-valve, of which a cross section is shown in Fig. 3. The needle is a

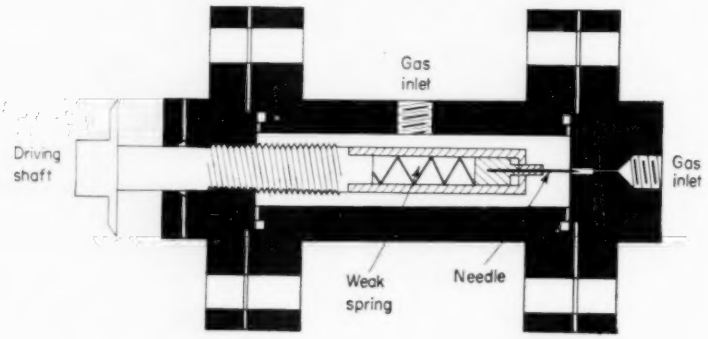

FIG. 3. Cross section of the needle-valve.

Vol. 1 1961

conventional sewing needle of shaft diameter 18/1000 in., and the size of hole into which it fits is that of the smallest standard drill—13/1000 in. The needle is force-fitted into a block which can slide backwards against a weak spring to prevent damage to the needle should it be driven in too far. The drive for the needle is provided directly by a large-diameter 48 thread/in. screw.

The gas is obtained from a commercial cylinder at 1800 lb/in², and is fed directly to the needle valve which in turn connects to the pressure chamber. Gas release is effected by a magnetic valve whose operation can either be manual or automatic. The safety device is a bursting disc assembly in the pressure chamber which blows off at 750 lb/in².

PERFORMANCE

Dr. L. Bovey of A.E.R.E., Harwell, invited the authors to collaborate with him in an experiment to observe some emission lines of Uranium, Neptunium, Plutonium and Americium at high resolution in the 1·6 to 2·1 μ region. It was decided that this would provide an excellent test of the FPI even though at such a short wavelength the limiting finesse would be reduced (see above). Since the CaF_2 flats were not yet available, a pair of fused silica flats were coated with seven alternate $\lambda/4$ layers of Zinc Sulphide and Cryolite having a maximum reflectivity of about 0·91 at 1·9 μ, the useful range being 1·6–2·3 μ.

The aperture of the flats was 1 in., this being the aperture needed to match the grating. As can be seen from Fig. 4, the effective finesse attained was thirty-five at 1·9 μ with a transmission of about 50 per cent. This was determined by illuminating the etalon normally with a parallel beam of white light from a Tungsten lamp and scanning the resultant Edser–Butler fringes with a spectrometer. The interferometer spacing was 50 μ and there are about four resolved elements in each fringe shown.

Since the lines to be studied were, in the main, unidentified with specific transitions, the choice of resolution was somewhat arbitrary. Resolving powers of 150,000 and 300,000 were chosen and invar spacers 4 mm and 8 mm thick were therefore prepared and used, even though the instrument was originally designed to achieve resolving powers up to

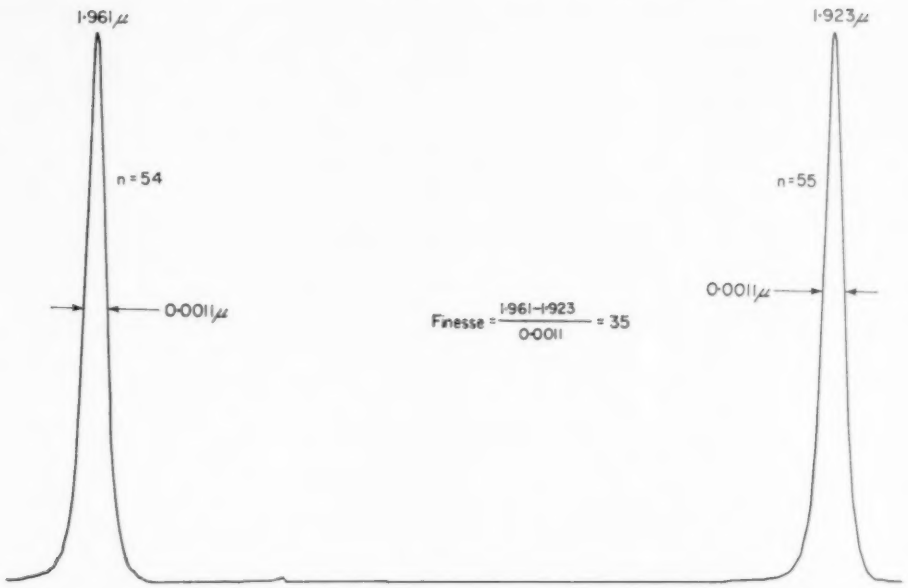

FIG. 4. White-light scan of the interferometer fringes.

20,000 only. For some purposes the resolutions attained were too high, in that the inter-order distances were too small, and a 2 mm spacer would have been useful. With the spacers employed and the peak finesse of thirty-five, maximum resolving powers of 130,000 and 270,000 were attained. These allowed the use of limiting apertures of 1·7 mm and 1·2 mm dia. respectively, assuming the criterion [12]

$$1/R = \theta^2/2$$

where θ is the maximum allowable off-axis angle for a resolving power R to be attained.

The FPI was used in conjunction with the 1 metre Ebert Spectrometer of A.E.R.E., Harwell; [13] the optical layout of the system is shown in Fig. 5. The spectra studied con-

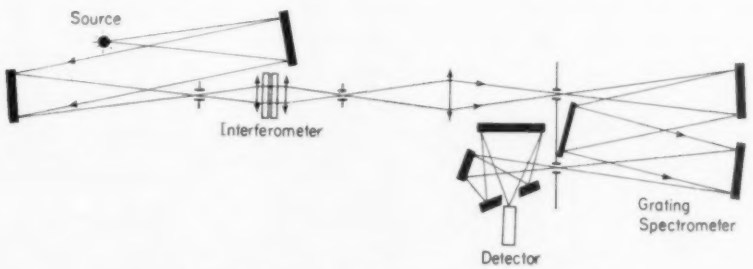

FIG. 5. Optical layout of the interference spectrometer.

sisted of a limited number of well-separated, strong, atomic emission lines with a rather larger number of weaker ones. It was therefore decided, as a first experiment, to ignore the weaker lines and merely to isolate the stronger ones with the spectrometer. As a result, the

slits were employed at their maximum width of 1·8 mm (≡ 25 cm^{-1} spectral width) which allowed all the light from the FPI (operating at F/10) to be accepted by the spectrometer (also operating at F/10). Furthermore, in view of the fact that the scan range was about 1 cm^{-1}, it was not necessary to scan the spectrometer and it was kept stationary at each line chosen. The intensity error introduced by this practice was about 1 per cent. It might be pointed out that no difficulty was experienced with this crude filtering: out of some twenty-five strong lines studied, only one had to be rejected because of the weaker lines.

The high pressure for the supersonic leak scanning was provided by a commercial cylinder of nitrogen at 1800 lb/in^2. Since no form of high pressure regulation was employed, the scan rate was necessarily non-linear. However, as Fig. 6 shows, the scan rate was more non-linear than expected and, furthermore, was not completely reproducible.

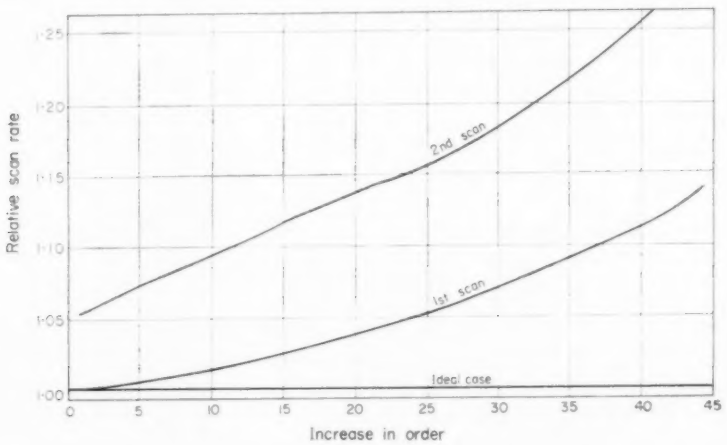

FIG. 6. Scan rate vs. increase in order of interference.

The two experimental curves shown were taken consecutively by scanning the 2·06 μ He line with the FPI (using a 4 mm spacer in the etalon) through forty-four orders (0–600 lb/in^2 in pressure) each time. The cause of the large non-linearity and non-reproducibility is not yet entirely understood. The effect on the accuracy of the results was small, since wavenumber measurements were never extrapolated beyond one order and the resultant error was about 0·002 cm^{-1}, less than the random errors.

However, the variation in scanning rate due to the changing cylinder pressure does imply that this scanning method is unsuitable for cases where it is necessary to scan the interferometer in synchronism with the spectrometer, e.g. for the study of absorption spectra. With this in mind, the authors intend to investigate other means of high-pressure control that do not suffer from this defect.

A further difficulty experienced was that the focal lengths of the lenses altered by about 1 per cent, since they were immersed in a medium of varying refractive index. The effect of this on intensity determinations was made small by defocusing the exit aperture of the interferometer in the opposite sense to the expected movement and by opening the entrance aperture somewhat. The defocusing caused the image in the exit plane to pass through the point of best focus at about 300 lb/in^2 pressure. Opening the entrance aperture a little prevented any of the useful incident light from being obstructed as the focus moved whilst

Vol. 1 1961

still rejecting stray light. However, since the focal length changed, the acceptable area of source also changed as the scan progressed. The artifice is therefore unsuitable for use with inhomogeneous sources.

RESULTS

Figure 7 (a, b) shows two sets of scans.
(a) The isotope shifts from the 5254 cm^{-1} line of U^{238} taken at a resolution of 0·040 cm^{-1}.
(b) The hyperfine structure of some Am^{241} lines taken at a resolution of 0·020 cm^{-1}.

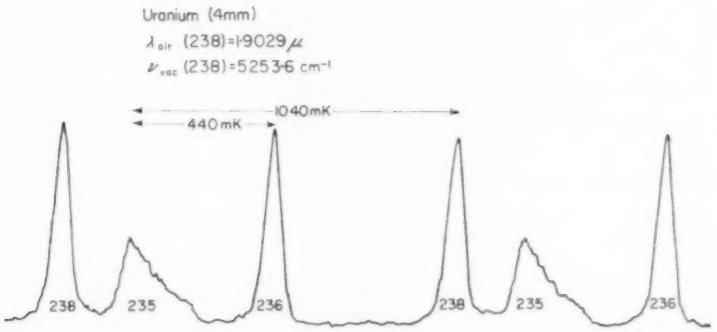

FIG. 7(a). Isotope shifts from the 5254 cm^{-1} line of U^{238} (4 mm spacer).

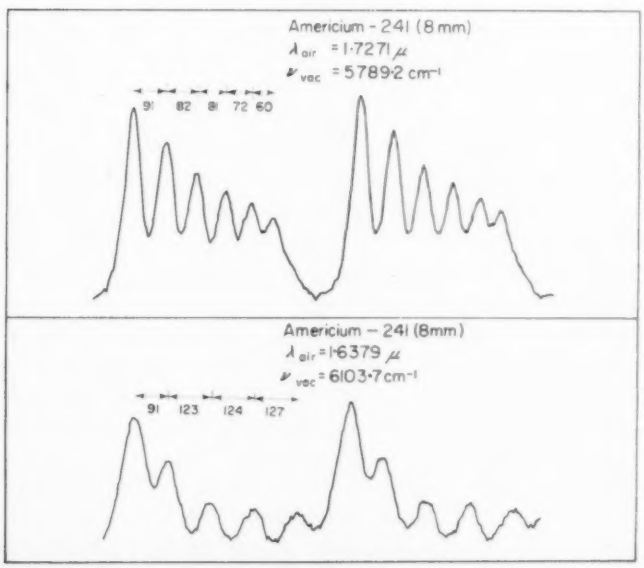

FIG. 7(b). Hyperfine structure in some Am^{241} lines (8 mm spacer).

It has been ascertained that the resolution was source limited, since line widths did not decrease when the resolving power was doubled. Furthermore, it is known that the vapour pressure within the sources (microwave excited electrodeless discharge tubes) was of the order of half an atmosphere, which could explain the line widths of 0·04–0·06 cm^{-1} recorded.

As a result, the hyperfine structure of U^{235} was not resolved, although, as can be seen from the figure, strong asymmetries were apparent.

The results and their preliminary analysis are published elsewhere.[14]

COMPARISON WITH THE GRATING SPECTROMETER

According to Jacquinot,[15] the resolution–luminosity product RL for a grating monochromator used in a Littrow manner is given by

$$RL = B\tau\beta A \sin\theta$$

where B = source brightness, τ = transmission factor, β = angular slit height (10/1020 in. in this case), A = grating area (73·5 cm^2) and θ angle of grating from normal ($\sin\theta = 0{\cdot}3$ at $2\,\mu$).

The correction factor to be applied if the grating is used in an Ebert arrangement is very small.

In this case,

$$RL = 0{\cdot}23B\tau \text{ for the grating alone.}$$

On the other hand, for a FPI,

$$RL = 3{\cdot}4B\tau A$$

whence

$$RL = 16{\cdot}7B\tau$$

since A = 4·9 cm^2.

Therefore, assuming equality of B and τ in both cases, the FPI has, in theory, eighty times the luminosity of the grating spectrometer at the same resolving power.

An experiment was performed to ascertain what the gain was in practice. The 5366 cm^{-1} line of U^{238} was first scanned with the spectrometer alone using 50 μ slits. The interferometer was then added as quickly as possible (to guard against fluctuations in source brightness) and the line scanned again, using the 8 mm spacer.

With the interferometer, the spectrometer slit widths employed were larger than the image of the FPI exit aperture at the slit plane, and therefore this image formed the entrance pupil of the spectrometer. The area employed was then 1·13 mm^2, whereas previously, without the FPI, the slits were 50 μ × 10 mm = 0·50 mm^2. Hence, neglecting for the moment transmission losses in the interferometer, the light level should have increased by a factor 2·2 on adding the FPI, the solid angle contained by the light being unaltered. At the same time, the resolving power increased from 6000 (spectrometer alone) to 240,000 (estimated for the FPI)—a factor 40. The product of these two factors, eighty-eight, is the increase in RL obtainable by the use of the interferometer. It compares well with the eighty obtained from Jacquinot's direct argument.

The determination of the actual gain was complicated by the fact that with the spectrometer alone the line was totally unresolved whereas with the addition of the FPI, the line was completely resolved. It was therefore necessary to determine what the light level would have been had the line still been unresolved. This was estimated by dividing the resolved pattern into resolved elements (twelve in all) and the average signal in each added. The

Vol. 1 1961

result was that at the high resolution there was slightly more light than with the spectrometer alone, the overall gain being about fifty. This figure is less than the possible eighty as a result of the transmission loss in the interferometer system.

CONCLUSION

In the opinion of the authors this instrument has clearly demonstrated the power of interferometric techniques in laboratory infrared spectroscopy and shows that a gain of at least fifty is possible in the infrared region. It must be emphasized that this gain may be entirely used to increase the resolving power without loss of luminosity to values far in excess of the theoretical resolution of even the best gratings available for these wavelengths. It is also apparent that the gain achieved was entirely limited by the quality of the optical flats used and that further tests are required to discover by how much the gain increases at longer wavelengths. To this end, the experiments on emission spectra are to continue, and, in addition, it is the authors' intention to employ the interferometer in absorption spectroscopy further out in the infrared as soon as suitable CaF_2 flats become available and the defects in the pressure scanning system are rectified.

Acknowledgements—The authors are indebted to Dr. L. Bovey of A.E.R.E., Harwell, for the use of his spectrometer and many helpful discussions.

REFERENCES

1. Jacquinot, P., *J. Opt. Soc. Amer.* **44**, 764 (1954).
2. Jacquinot, P., *J. Phys. Radium* **19**, 223 (1958).
3. Chabbal, R., Ph.D. Thesis, Paris (1958).
   Davies, L. B., and J. Ring. In preparation.
4. Bright, R. J., D. A. Jackson, and H. Kuhn, *Proc. Phys. Soc., Lond.* A **62**, 225 (1949).
5. Chabbal, R., *J. Phys. Radium* **19**, 295 (1958).
6. Chabbal, R., *J. Phys. Radium*, **19**, 297 (1958).
7. Ring, J., Ph.D. Thesis, Manchester (1957).
8. Jaffe, J. H., *J. Phys. Radium* **19**, 273 (1958); R. Chabbal, and M. Soulet, *Ibid.* **19**, 274 (1958); J. Gobert, *Ibid.* **19**, 278 (1958); J. Roig, *Ibid.* **19**, 284 (1958); R. Dupeyrat, *Ibid.* **19**, 290 (1958); J. Blaise, *Ibid.* **19**, 335 (1958); J. Ring and N. J. Woolf, *Ibid.* **19**, 354 (1958).
9. Geake, J., J. Ring, and N. J. Woolf, *Mon. Not. R. Astr. Soc.* **119**, 616 (1959).
10. Rank, D. H., and J. N. Shearer, *J. Opt. Soc. Amer.* **46**, 463 (1956).
11. Liepmann, H. W., and A. E. Puckett, *Introduction to the Aerodynamics of a Compressible Fluid.* Chapman & Hall (1947).
12. Jacquinot, P., *J. Opt. Soc. Amer.* **44**, 764 (1954).
13. Bovey, L., and E. B. M. Steers, A.E.R.E. Report R2827 (1959).
14. Beer, R., and L. Bovey. *Proc. Phys. Soc. Lond.* **76**, 569 (1960).
15. Jacquinot, P., *J. Opt. Soc. Amer.* **44**, 764 (1954).

Infrared Physics, 1961, Vol. 1, p. 104. Pergamon Press Ltd., Printed in Great Britain.

RESEARCH NOTE

Infrared Optical Properties of Lead Halides

CRYSTALS of PbF_2, $PbCl_2$ and $PbBr_2$ have been grown and their optical transmission measured.

The crystals were grown from the melt in a Stockbarger type vacuum furnace, as developed by Jones[1] and his co-workers. The material was given a prolonged heating and degassing treatment before growing the crystal, the whole process (including subsequent annealing) taking 3–4 days for each material.

Specimens were cut, ground and polished, and transmission measurements carried out using a Leiss double monochromator fitted with NaCl, KBr, or CsI prisms. The results obtained, corrected for surface losses, are shown in the attached diagram. The long wavelength absorption edge found for the PbF_2 seems to be at a somewhat longer wavelength than that found by Jones *et al*[1] for the same absorption coefficient. The chloride and bromide show good transparency up to 16 μ and 24 μ respectively.

The refractive index of $PbBr_2$ was determined with white light from the ratio of real to apparent thickness. The value obtained was $n = 2{\cdot}53$, which is consistent with the transmission of 64 per cent obtained throughout the 2 μ to 20 μ region. For comparison, the published indices for PbF_2 and $PbCl_2$ are $n = 1{\cdot}76$[1] and $n = 2{\cdot}2$[2] respectively for yellow light.

As the solubilities are fairly low ($PbCl_2$ and $PbBr_2$ are ~40 times, and PbF_2 ~500 times, less soluble than NaCl or KBr) these materials may be useful alternatives to the alkali halides.

T. S. MOSS*
A. G. PEACOCK†

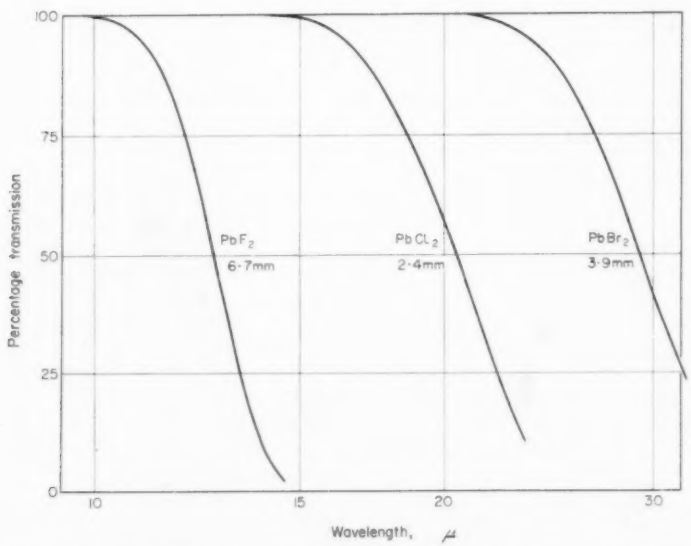

FIG. 1. Infrared transmission of lead halide crystals of thicknesses shown. (Corrected for surface losses.)

Acknowledgements—We wish to thank T. D. H. Hawkins for assistance with the transmission measurements.

REFERENCES

1. JONES, D. A., R. V. JONES, and R. W. H. STEVENSON, *Proc. Phys. Soc., Lond.* B **65**, 906 (1952).
2. *Handbook of Chemistry and Physics*. Chemical Rubber Publishing Co., Ohio.

* *Royal Aircraft Establishment, Farnborough, Hants.*
† *Mervyn Instruments, Woking, Surrey.*

Vol. 1 1961

Infrared Physics, 1961, Vol. 1, pp. 105–110. Pergamon Press Ltd. Printed in Great Britain

INFRARED SPECTRAL EMISSIVITIES OF CO_2 IN THE 2·7 MICRON REGION*

R. H. TOURIN

The Warner & Swasey Company, Control Instrument Division,
32–16 Downing Street, Flushing 54, N.Y., U.S.A.

(*Accepted* 31 *October* 1960)

Abstract—Spectral emissivities of hot CO_2 in the 2·7 μ region were measured. Obscuration by H_2O emission, which occurs in flame spectra, was eliminated by use of CO_2 samples heated in a closed gas cell. These measurements of emissivity can be used to calculate radiant power of hot CO_2 over a given spectral region, by means of an approximate integration technique. The CO_2 absorption near 2·7 μ was found to be independent of pressure at 1273 °K, from 50 mm to 700 mm Hg. This contrasts with the case of CO_2 absorption at room temperature. It results from overlapping of vibration-rotation transitions of the types $v_1 v_2^l v_3 - (v_1 + 1)\, v_2^l\, (v_3 + 1)$ and $v_1 v_2^l v_3 - v_1 (v_2 + 2)^l\, (v_3 + 1)$, originating from excited states as well as from the ground state. This overlapping produces "temperature-smearing" of the spectrum, analogous to pressure broadening.

INTRODUCTION

FLAMES and combustion gases exhibit strong infrared emission in the spectral region near 2·7 μ. This emission is contributed by infrared vibration-rotation bands of carbon dioxide and water vapor. The 2·7 μ carbon dioxide bands in a flame spectrum are obscured by the strong emission of the water vapor fundamental bands in the same spectral region. For this reason no detailed studies of these CO_2 bands in hot gases have been reported previously.

The present paper describes measurements of the 2·7 μ infrared absorption bands of carbon dioxide at high temperatures. The measurements were made primarily to determine spectral emissivities of CO_2 as a function of temperature and molecular concentration. The measurements were made with samples of pure, dry CO_2 heated in a special gas cell. Spectra were measured with a Perkin–Elmer Model 12C infrared spectrometer. The experimental methods and some of the results of measurements in the 4·3 μ region have been reported previously.[1, 2]

MEASUREMENTS

Figure 1 shows the spectral emissivity of CO_2 in the 2·7 μ bands for temperatures from 394 °K to 1300 °K, measured with an optical depth *ps* of 2·67 cm atm, at 700 mm Hg total pressure. The path length was 12·7 cm, and dry nitrogen was used to adjust the pressure. Most prominent in Fig. 1 are the CO_2 combination bands (00^00)–(02^01) and (00^00)–(10^01), centered at frequencies 3613 cm^{-1} and 3715 cm^{-1} respectively. Near 3560 cm^{-1}, there is an extra peak, suggesting additional bands. This peak is probably mainly due to the transition (01^10)–(03^11), for which ν_0 equals 3579 cm^{-1}.

* Supported in part by the U.S. Air Force, through the Geophysics Research Directorate, Bedford, Mass.

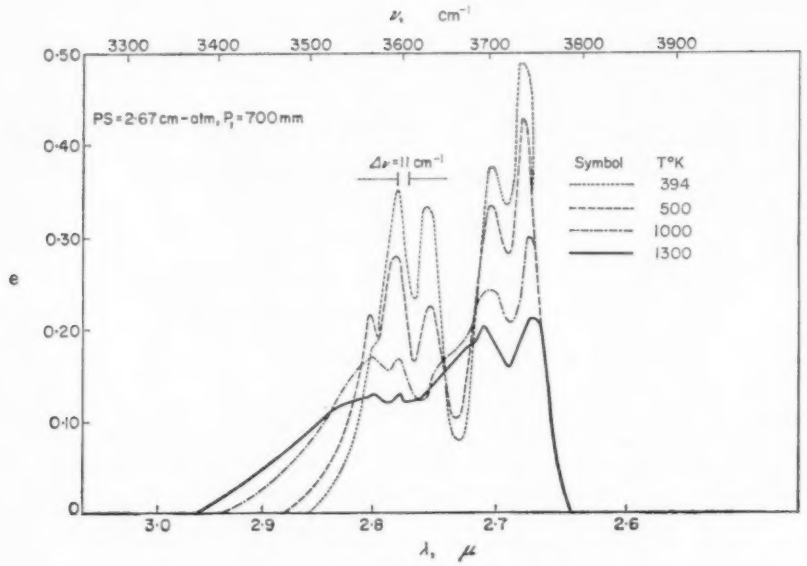

FIG. 1. Temperature variation of the spectral emissivity of CO_2 in the 2·7 μ region.

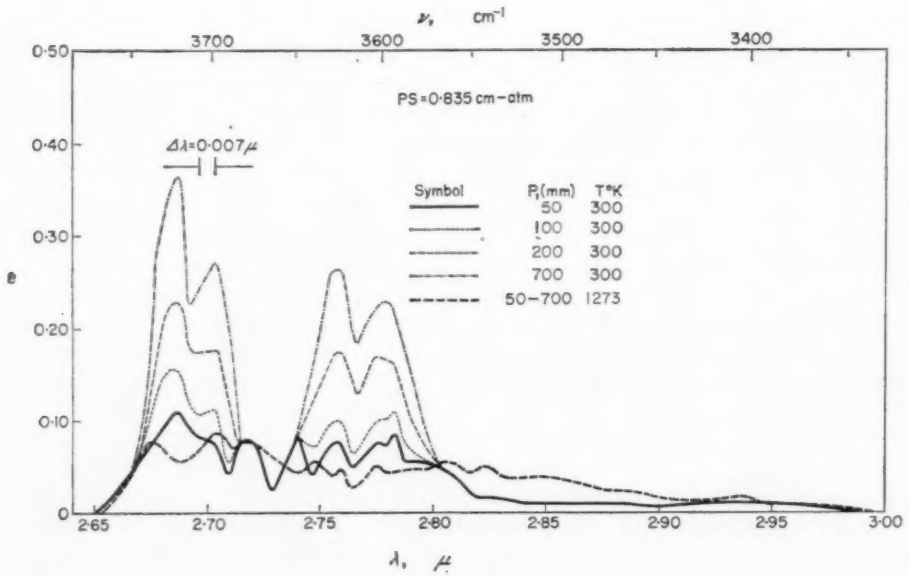

FIG. 2. Spectral emissivity of CO_2. Comparison of temperature and pressure effects in the 2·7 μ region.

The high-temperature spectrum is insensitive to pressure variation. Fig. 2 summarizes measurements at several pressures, at 300 °K and 1273 °K, for $ps = 0{\cdot}84$ cm atm. The effect of pressure on the emissivity at room temperature is apparent, while at 1273 °K there

Vol. 1 1961

is no observable pressure effect, as can be seen from the fact that the curves for 50 mm and 700 mm total pressure coincide.

Although independent of pressure, the high-temperature spectrum is quite sensitive to absorber concentration, as indicated by Fig. 3. The lower curve of Fig. 3 reproduces the lower curve of Fig. 2. The upper curve in Fig. 3 corresponds to a much higher concentration, at the same temperature and pressure.

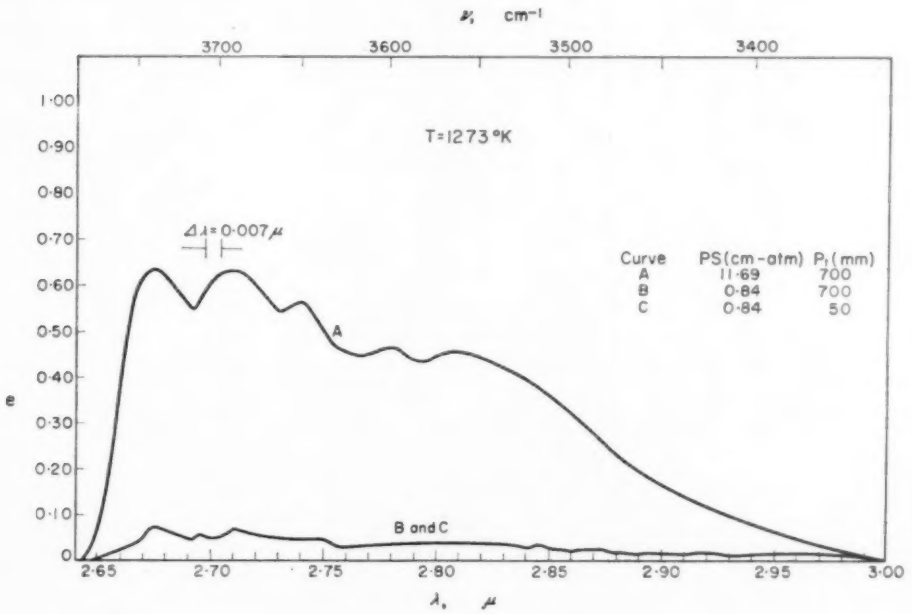

FIG. 3. Spectral emissivity of CO_2 at 1273 °K; the 2·7 μ region. Increasing the absorber concentration changes the emissivity by a comparable amount, while changing pressure by more than a factor of ten has no effect.

Absolute spectral radiance may be calculated from the spectral emissivity plots shown in Figs. 1, 2 and 3, by multiplying the emissivities point-by-point by the appropriate values of the Planck function. Fig. 4 shows the spectral radiance of carbon dioxide at 1273 °K calculated by this method. The power radiated in any spectral interval may be calculated from Fig. 4 by integrating over the interval. To simplify this calculation the approximation

$$P_{\Delta\lambda}(T) = \int_{\Delta\lambda} e(\lambda, T)J(\lambda, T)d\lambda \approx \bar{J}_{\lambda}(T) \int_{\Delta\lambda} e(\lambda, T)d\lambda,$$

may be used, where $P_{\Delta\lambda}(T)$ is the spectral radiant power of the hot gas in the interval $\Delta\lambda$, $e(\lambda, T)$ is the spectral emissivity at wavelength λ and temperature T, $J(\lambda, T)$ is the Planck function, and $\bar{J}_{\lambda}(T)$ is the average value of $J(\lambda, T)$ over $\Delta\lambda$. Table 1 compares integrated radiances calculated in this way to radiances obtained by multiplying the emissivities point-by-point by the Planck radiation function and integrating. The agreement between the approximate and exact calculations is very good.

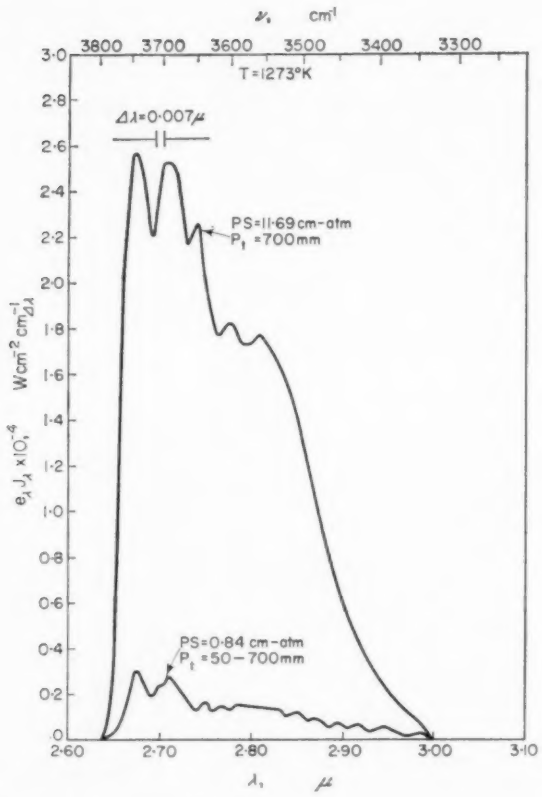

FIG. 4. Spectral radiance of CO_2 at 1273 °K, calculated from emissivity measurements; 2·7 μ region.

TABLE 1. CO_2 EMISSIVITY AND RADIANCE INTEGRALS IN THE 2·7 μ REGION

T °K	Band ($\Delta\lambda$)	P(atm)	PS(cm atm)	P_t (atm)	$\int e d\lambda$	$\int J e d\lambda$(W/cm²)	$\bar{J}$: $\int e d\lambda$(W/cm²)	Difference %
1273	2·635–3·000	0·07	0·8	0·07	0·0109	$0·42 \times 10^{-1}$	$0·42 \times 10^{-1}$	0
1273	2·635–3·000	0·07	0·8	0·92	0·0109	$0·42 \times 10^{-1}$	$0·42 \times 10^{-1}$	0
1273	2·635–3·000	0·92	11·7	0·92	0·1182	0·48	0·46	− 4·2
305	2·656–2·820	0·07	0·8	0·07	0·00991	$0·81 \times 10^{-7}$	$0·86 \times 10^{-7}$	+ 6·2
305	2·656–2·856	0·07	0·8	0·92	0·02387	$0·20 \times 10^{-6}$	$0·23 \times 10^{-6}$	+15·0
305	2·656–2·865	0·92	11·7	0·92	0·1035	$0·90 \times 10^{-6}$	$1·01 \times 10^{-6}$	+12·2
1273	2·660–2·920	0·07	0·8	0·07	0·00960	$0·38 \times 10^{-1}$	$0·38 \times 10^{-1}$	0
1273	2·660–2·920	0·07	0·8	0·92	0·00960	$0·38 \times 10^{-1}$	$0·38 \times 10^{-1}$	0
1273	2·660–2·920	0·92	11·7	0·92	0·1116	0·45	0·44	− 2·2
305	2·670–2·800	0·07	0·8	0·07	0·00913	$0·76 \times 10^{-7}$	$0·79 \times 10^{-7}$	+ 3·9
305	2·670–2·800	0·07	0·8	0·92	0·0221	$0·19 \times 10^{-6}$	$0·19 \times 10^{-6}$	0
305	2·670–2·800	0·92	11·7	0·92	0·0896	$0·75 \times 10^{-6}$	$0·77 \times 10^{-6}$	+ 2·7

Vol. 1 1961

DISCUSSION

The radiation from CO_2 in the 2·7 μ region is contributed by two sets of vibration-rotation transitions: those for which $\Delta v_1 = 0$, $\Delta v_2 = 2$, $\Delta v_3 = 1$, $\Delta l = 0$, with band centers at frequencies of 3613 cm^{-1} and lower; and bands corresponding to transitions where $\Delta v_1 = 1$, $\Delta v_2 = 0$, $\Delta v_3 = 1$, $\Delta l = 0$, which occur at frequencies below 3715 cm^{-1}. Table 2 shows four transitions of each type, listed in order of relative population of the lower state. For each

TABLE 2. VIBRATIONAL POPULATION FACTORS AND TRANSITION PROBABILITIES FOR CO_2 BANDS IN THE 2·7 μ REGION

Lower state	Upper state	ν_0	Transition probability	Population of lower vibrational state at 300 °K	at 1273 °K
$(v_1 v_2^l v_3)$	$(v_1 v_2^l v_3)$				
(a) $\Delta v_1 = 0$, $\Delta v_2 = 2$, $\Delta v_3 = 1$, $\Delta l = 0$					
(00^00)	(02^01)	3613 cm^{-1}	2	0·920	0·211
(01^10)	(03^11)	3579	6	0·074	0·199
(02^00)	(04^01)	3565	12	0·002	0·049
(10^00)	(12^01)	3593	2	0·001	0·044
(b) $\Delta v_1 = 1$, $\Delta v_2 = 0$, $\Delta v_3 = 1$, $\Delta l = 0$					
(00^00)	(10^01)	3715	1	0·920	0·211
(01^10)	(11^11)	3722	1	0·074	0·199
(02^00)	(12^01)	3696	1	0·002	0·049
(10^00)	(20^01)	3716	2	0·001	0·044

transition in Table 2, the vibrational population factor for the lower state is shown at 300 °K and at 1273 °K. The calculation of these factors is described in a report by Tourin and Henry.[3] The transition probabilities shown in Table 2 were calculated from a formula given by W. S. Benedict.[4]

The intensities of the overlapping CO_2 bands occurring in the 2·7 μ spectral region are proportional to the product of transition probability and initial state population. It can be seen from Table 2 that at high temperatures there may be many overlapping bands of approximately equal intensity.

The absorption coefficients in this region are not extremely high, as shown by Fig. 3. Nevertheless, the large pressure effect observed in the room temperature spectrum vanishes at high temperatures, as shown by Fig. 2. Evidently the spectrum is not fully pressure broadened at 700 mm. Another effect occurs instead, which has the same effect as pressure broadening in smearing out the rotational structure. Each of the overlapping bands has a *P* and an *R* branch; hence there are many rotational lines of slightly different frequency for each value of rotational quantum number *J*. As a result of the manifold vibrational and rotational overlapping, the high-temperature spectrum is virtually continuous.

REFERENCES

1. TOURIN, R. H., *J. Chem. Phys.* **20**, 1651 (1952). See also *Nat. Bur. Stands. Circ.* #523, 87 (1954).
2. TOURIN, R. H., *J. Opt. Soc. Amer.* **51**, 175 (1961).
3. TOURIN, R. H., and P. M. HENRY, AFCRC TN–59–262, Geophysics Research Directorate, Bedford, Mass., December 1958.
4. BENEDICT, W. S., *Rep. Nat. Bur. Stand.* 1123, 49 (1951).

Vol.
1
1961

Infrared Physics, 1961, Vol. 1, pp. 111–115. Pergamon Press Ltd. Printed in Great Britain

INFRARED ABSORPTION IN GALLIUM ARSENIDE

T. S. Moss and T. D. F. Hawkins

Royal Aircraft Establishment, Farnborough, Hants., England

(*Received* 14 *December* 1960)

Abstract—Measurements of absorption constant covering the range 1 cm^{-1} to 10^4 cm^{-1} have been made on single crystal gallium arsenide. The absorption edge is very steep up to ~4000 cm^{-1}, where there is a knee beyond which the absorption increases relatively slowly with photon energy. The energy bands have been calculated using Kane's theory. From these we have obtained a theoretical absorption curve which shows very good agreement with the experimental data.

INTRODUCTION

Gallium arsenide is a semiconductor with many interesting properties and it has been studied quite extensively since the III–V compounds were first described by Welker. [1]

In recent months it has become of great technological interest for use in devices such as transistors, Esaki and parametric diodes. It is also a very promising solar battery material, [2] and for use in this field in particular it is necessary to have detailed optical data up to high absorption levels.

Original measurements of absorption, near the edge, were made by Oswald and Schade. [3] These results (which reached an absorption level of only 100 cm^{-1}) have not been extended to any shorter wavelengths, although papers on long wavelength properties such as free carrier absorption[4] and Reststrahlen,[5] have been published recently.

EXPERIMENTAL DETAILS AND RESULTS

The measurements were made on very pure single crystal material (3×10^{16} electrons cm^{-3}) kindly provided by the Plessey Co. A tungsten lamp and Leiss double monochromator (fitted with flint glass prisms) provided the radiation. The resolution was 5×10^{-3} eV and great care was taken to ensure spectral purity. The detector was an infrared photomultiplier. Satisfactory measurements could be made with specimen insertion losses up to $10^3 : 1$ in the region of rapidly varying absorption and up to $10^4 : 1$ on the flat part of the absorption curve.

The material was cut, ground, and polished with diamond paste. Specimens 7 μ to 1 cm in thickness were used; those over 50 μ were self supporting and their thickness was measured by direct gauging, those below 50 μ were glued to glass backing plates and were measured interferometrically using wavelengths in the 5–15 μ region.

The results obtained for the absorption coefficient (K) are shown in Fig. 1. It will be seen that the absorption edge is very steep, K rising rapidly from 4 cm^{-1} to 4000 cm^{-1}. The main part of the absorption edge is exponential, as has now been observed for many other solids. [6] The slope is 100 eV^{-1}—i.e. three times steeper than would result from a simple $1/kT$ Boltzman factor, and about ten times steeper than for silicon. [2]

At higher levels the absorption increases only slowly with energy. At long wavelengths there is a "tail" on the absorption curve and K does not fall below $\sim$1 cm^{-1} within the range of measurement, although the computed free carrier absorption [6] is only 0·04 cm^{-1} at 1 μ.

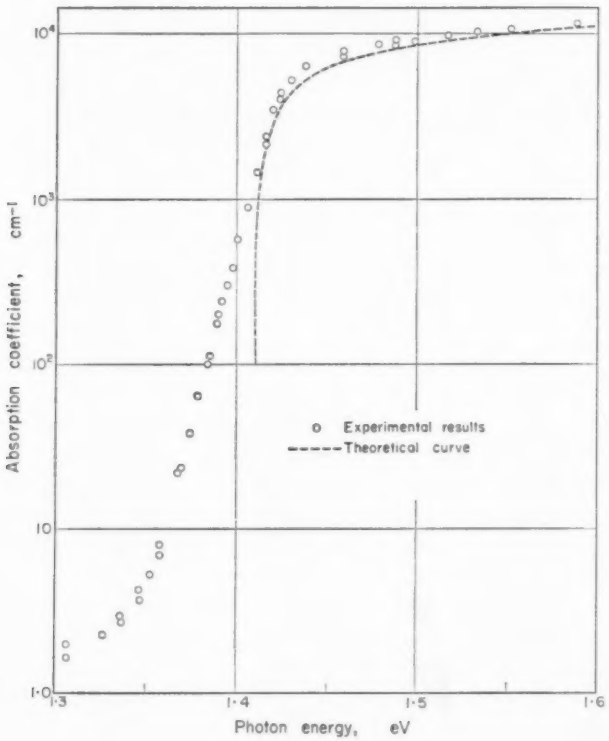

FIG. 1. Absorption in gallium arsenide.

CALCULATION OF ENERGY BANDS AND ABSORPTION COEFFICIENT

The energy bands have been computed following Kane. [7] The E–k curves are given by:

$$k^2P^2 = E_i(E_i - E_g)(E_i + \Delta)/(E_i + 2\Delta/3) \tag{1}$$

where E_g is the energy gap, Δ is the spin orbit splitting and

$$P^2 = E_g(E_g + \Delta)/(E_g + 2\Delta/3)\, 2m_c^* \qquad \text{atomic units}\dagger \tag{2}$$

where m_c^* is the electron mass at the bottom of the conduction band.

The parameters used are:

$$m_c^* = 0{\cdot}072\, m_0 \,[8]$$
$$\Delta = 0{\cdot}33 \text{ eV} \,[9]$$

† In atomic units, $m = e = h/2\pi = 1$. The unit of length is the first Bohr orbit radius, 0·53 Å.

and $E_g = 1{\cdot}4$ eV (estimated room temperature value)
giving $P^2 = 0{\cdot}38$ atomic units.

Equation (1) gives results for the conduction band (E_c) the light hole band (E_2) and the split-off valence band (E_3). They are plotted against k^2 in Fig. 2. Also shown is the heavy hole band (E_1), drawn simply to correspond to a mass $m_1 = 0{\cdot}68\ m_0$.[10] It will be seen that

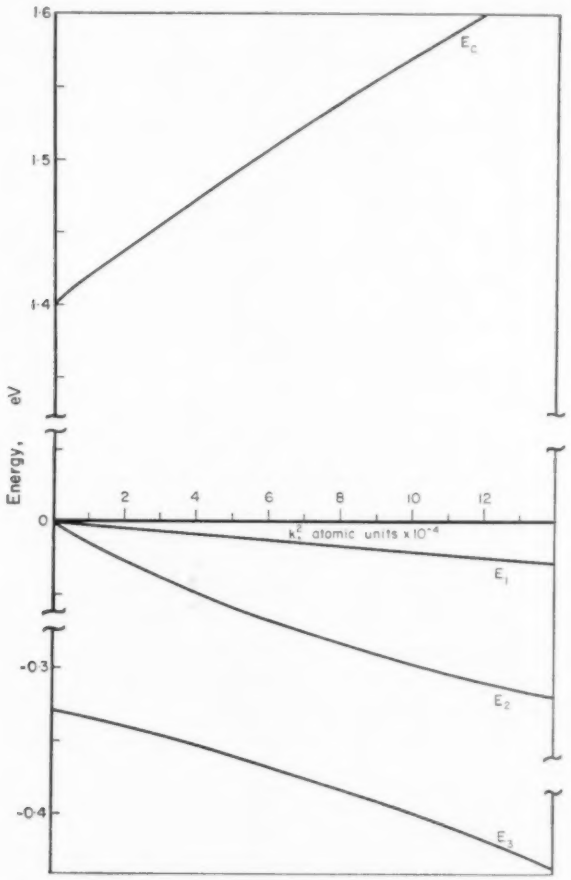

FIG. 2. E–k curves for gallium arsenide.

there is little curvature of the conduction band (in the plot against k^2), but the light hole band is quite non-parabolic. The masses of the light hole and split-off bands can be found from the slopes of the curves as $k \to 0$. They are:

$$m_2 = 0{\cdot}085\ m_0$$
$$m_3 = 0{\cdot}25\ m_0$$

The absorption coefficient, assuming direct, vertical, transitions is given by:[7]

$$K = \frac{4\pi^2}{cnE_p} \sum_j M_j^2 \rho_j \text{ atomic units} \tag{3}$$

where n is the refractive index, E_p the photon energy and the summation is over the three valance bands ($j = 1, 2, 3$).

The optical matrix element is:

$$M_j^2 = (2P^2/3)\ \{(A_cC_j + C_cA_j)^2 + (A_cB_j - B_cA_j)^2\} \tag{4}$$

where the bracketed term—which is always near unity—is computed for each k value from the coefficients:

$$A_i = kP(E_i + 2\Delta/3)/N$$
$$B_i = 2^{\frac{1}{2}}(E_i - E_g)\,\Delta/3N$$
$$C_i = (E_i - E_g)\,(E + 2\Delta/3)/N$$

where the suffix i refers to bands E_c, E_2 and E_3 and N is a normalizing factor such that

$$A^2 + B^2 + C^2 = 1$$

For the parabolic E_1 band, $A_1 = 0$, $B_1 = 1$ and $C_1 = 0$.
The density of states ρ_j is given in terms of the slopes of the E–k curves by

$$\rho_j = k^2/2\pi^2\,(dE_c/dk - dE_j/dk) \tag{5}$$

The absorption coefficient plotted from equation (3) is shown in Fig. 1. The agreement with the experimental data is seen to be very good, particularly at short wavelengths where the calculated curve does not depend on the use of any arbitrary constants or adjustable parameters. In the neighbourhood of the absorption edge the fit has been improved by sliding the curve slightly sideways. This process gives a value for the energy gap at 292 °K of $E_g = 1{\cdot}41$ eV, which is considered to be rather more accurate than the value of 1·4 eV assumed in the analysis.

The above absorption theory is essentially that for a perfect Ga–As lattice—with no perturbations due to thermal vibrations or crystalline irregularities.[11] The presence of these could well explain the slope of the edge observed under the experimental conditions.

The steepness of the edge and the good agreement between the magnitudes of the theoretical and experimental absorption coefficients confirm that the assumptions of vertical transitions and band extrema at k000 are correct.

Acknowledgements—Thanks are due to Dr. D. H. Roberts of the Plessey Co. for providing the gallium arsenide and to Miss D. Webber for assistance with the band theory computations.

REFERENCES

1. Welker, H., *Z. Naturf.* **7a**, 744 (1952) and **8a**, 248 (1953).
2. Moss, T. S., *Solid State Electron.* **2**, 222 (1961).
3. Oswald Von F., and R. Schade, *Z. Naturf.* **9a**, 611 (1954).

Vol 1 196

4. SPITZER, W. G., and J. M. WHELAN, *Phys. Rev.* **114**, 59 (1959).
5. FRAY, S. J., F. A. JOHNSON, and J. E. QUARRINGTON, *Proc. Phys. Soc.* **77**, 215 (1961).
6. MOSS, T. S., *Optical Properties of Semiconductors*, pp. 30, 39. Butterworths, London; Academic Press, New York (1959/1961).
7. KANE, E. O., *J. Phys. Chem. Solids* **1**, 249 (1957).
8. MOSS, T. S., and A. K. WALTON, *Proc. Phys. Soc.* **74**, 131 (1959).
9. BRAUNSTEIN, R., *J. Phys. Chem. Solids* **8**, 280 (1959).
10. EHRENREICH, H., *Phys. Rev.* (in press).
11. PARMENTER, R. H., *Phys. Rev.* **97**, 587 (1955).

Vol.
1
1961

Infrared Physics, 1961, Vol. 1, pp. 116–132. Pergamon Press Ltd. Printed in Great Britain

SPECTROSCOPIC OBSERVATIONS OF THE VERTICAL DISTRIBUTION OF SOME MINOR CONSTITUENTS OF THE ATMOSPHERE

J. S. SEELEY* and J. T. HOUGHTON†

Royal Aircraft Establishment, Farnborough, England

(*Accepted* 30 *December* 1960)

Abstract—Observations have been made from an aircraft of absorption bands due to CH_4, CO and N_2O in the infrared solar spectrum. From studies of these bands the total quantity of the gases above various levels in the atmosphere has been deduced. Their mixing-ratio is substantially constant with height within the altitude range studied. The 5·3 μ region has been examined for lines of NO. No evidence of them has been found.

Vol. 1 1961

INTRODUCTION

OBSERVATIONS of the infrared solar spectrum from ground level are hampered by intense absorption due to the water vapour and carbon dioxide present in the lower atmosphere. At higher altitudes substantial parts of the spectral region 1–6 μ which are completely obscured at the ground become available for study; comparatively weak absorption bands due to the rarer atmospheric constituents, carbon monoxide, nitrous oxide and methane are revealed in much greater detail than from the ground. Observations of absorption lines in these bands have been made from an aircraft flying at different altitudes, and their rate of growth with increasing atmospheric path has been studied. Subsequent comparison with

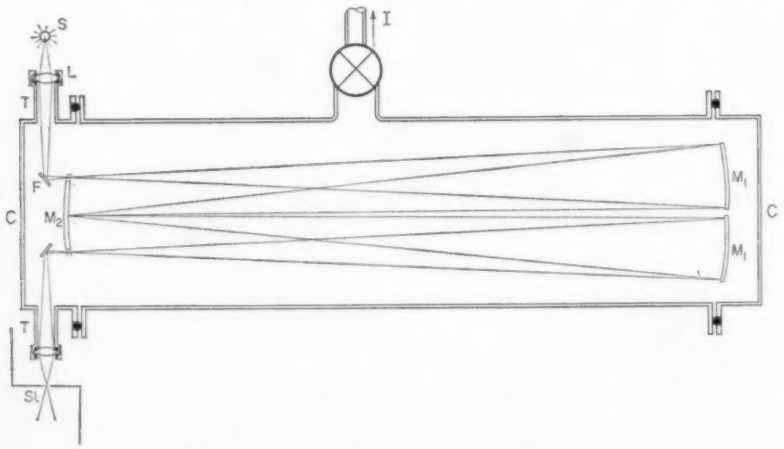

FIG. 1. Optical arrangement of Absorption Chamber (not to scale).
S, Source; L, Arsenic Trisulphide lenses (5 cm focal length); F, small flat mirrors; M_1, M_2, spherical mirrors 125 cm focal length; Sl, spectrometer entrance slit; C, removable end covers; T, German-silver tubes providing thermal isolation for the lenses; I, gas inlet, to pump.

* Now at Queen Mary College, University of London.
† Now at Clarendon Laboratory, Oxford.

laboratory measurements of the same lines, made at varying pressures and path lengths, have enabled estimates to be made of the concentration of these gases at different altitudes.

The infrared spectrometer and heliostat installed in a Canberra aircraft has been described by Houghton, Moss and Chamberlain.[1] The spectra have been presented in systematic form by Seeley, Houghton, Moss and Hughes,[2] and the results of a study of selected lines in the 2·7 μ band of water-vapour spectra have been described by Houghton and Seeley.[3]

LABORATORY AND AIRCRAFT MEASUREMENTS

The rates of growth of selected absorption lines have been measured in the laboratory with the same spectrometer as was used in the aircraft and the absorption chamber illustrated in Fig. 1. This is a multiple traversal cell following the general optical design described by White.[4] Path-lengths involving more than 48 traversals are possible with suitable adjustment, but short paths of only 2 or 4 traversals were found to be sufficient for the work described here. The end covers of the chamber may be removed to align the spherical mirrors, the number of traversals being controlled by simultaneous adjustment of the two mirrors M_1. The arsenic trisulphide lenses match the numerical aperture of the optical system of the absorption cell (f : 20) to that of the spectrometer (f : 6). The joints between the end covers and the central tube are sealed with hard rubber gaskets so that the cell can be evacuated completely before filling with measured quantities of absorbing gas or mixture of gases. Air admitted to the cell for use as a pressure broadening agent can be thoroughly dried. The external optical arrangement leaves paths of only 2 cm of laboratory air between lens and spectrometer entrance slit or between lens and source; absorption by water vapour is therefore substantially eliminated by filling the spectrometer itself with dry air.[3]

At first a carbon arc was used as a source. However, sufficiently steady burning of the arc proved difficult to maintain and a globar heated to about 1300 °C proved to be a more satisfactory source of radiation. The same photoconductive detectors were fitted in the spectrometer as for the measurements made in the aircraft, a PbSe detector with a bloomed silicon window or a PbTe detector, both cooled with liquid oxygen. The spectrometer slits were required to be slightly wider in the laboratory for an acceptable signal : noise ratio than the settings used to obtain the atmospheric spectra.

Typical laboratory and atmospheric spectra are compared in Figs. 2, 3 and 4, the slit widths being shown in each case. These illustrations are reproductions from originals recorded at high speed on photographic paper, 60 mm wide.[2] All the spectral regions shown in the Figures took less than 1 minute to record. In the case of the spectra recorded in the aircraft additional information is provided by the signal from a selenium photo-cell monitoring the total light entering the spectrometer. Noise signals from the detecting system recorded with no sunlight entering the spectrometer are indicated by short traces with most records.

Variations in the signal from the monitor photo-cell are present for two reasons; the sun's image may not have been held steady on the input slit of the spectrometer due to imperfect functioning of the heliostat, or movements of the aircraft may have affected the degree of obscuration of the gauze covering the hole through which the light entered the aircraft. Such variations do not necessarily affect the light incident on the monitor photo-cell and detector in the same proportion, since the spectrometer is interposed between the two. Thus, although variations in the monitor signal are faithfully reflected by variations in the background corresponding to 100 per cent transmission which may be imagined to

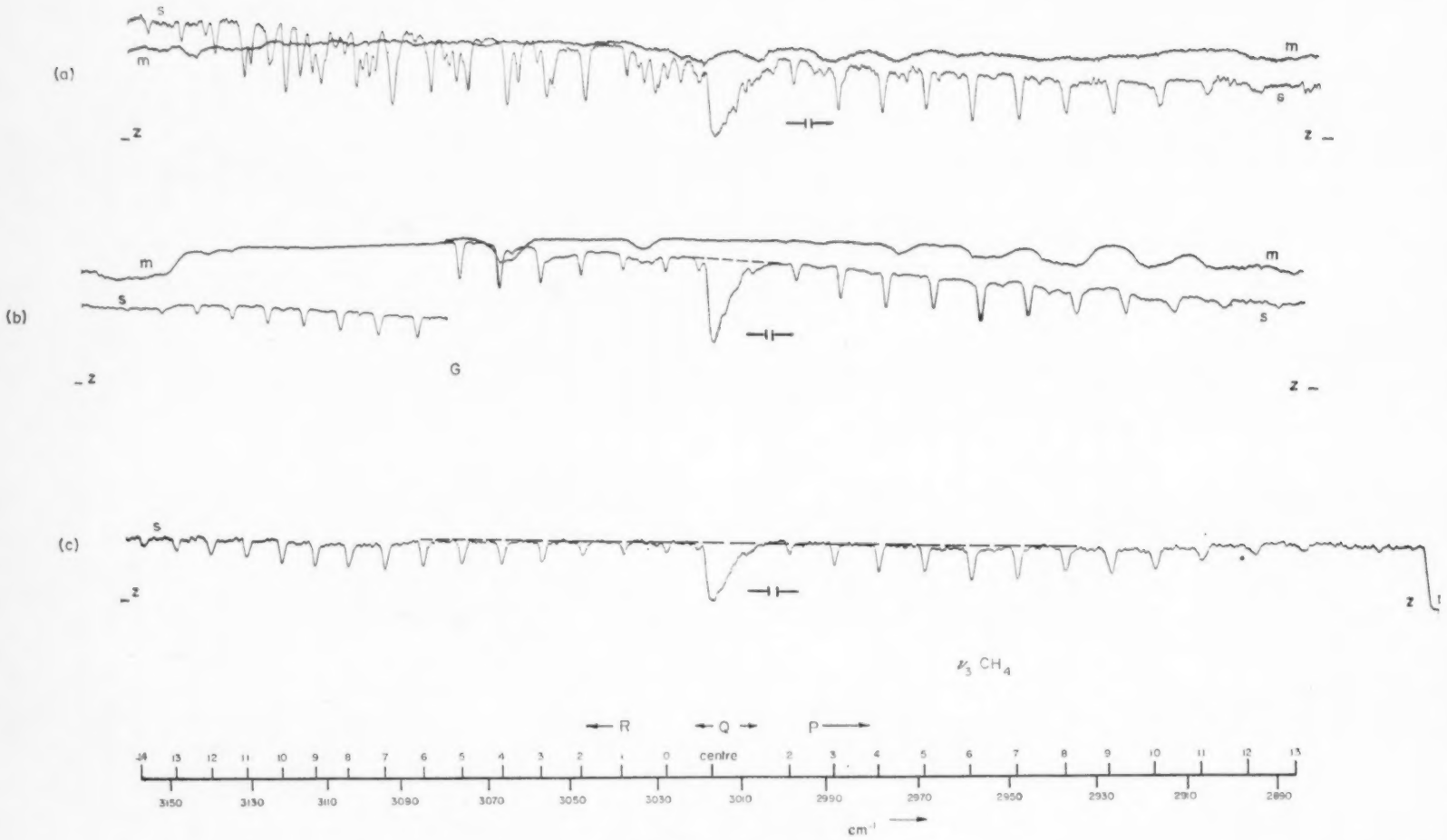

FIG. 2. Spectra of ν_3 band of CH_4.

(a) Solar spectrum observed on 29 July 1958, at 11.00 G.M.T. at an altitude of 20,000 ft, solar elevation 53·5°. Absorption lines due to $2\nu_2$ of H_2O are still prominent between 3030 and 3100 cm^{-1}. (b) Solar spectrum observed on 29 July 1958, at 14.15 G.M.T. at an altitude of 40,000 ft, solar elevation 48°. (c) Spectrum observed in the laboratory using the absorption chamber illustrated in Fig. 1, total pressure 294 mb, 0·382 atm cm of CH_4. The air in the absorption chamber and spectrometer contained negligible amounts of H_2O vapour.

G, gain change in detecting amplifier; S, signal from detector; m, signal from monitor photo-cell; z, noise signal from detector; — — — background line (see text).

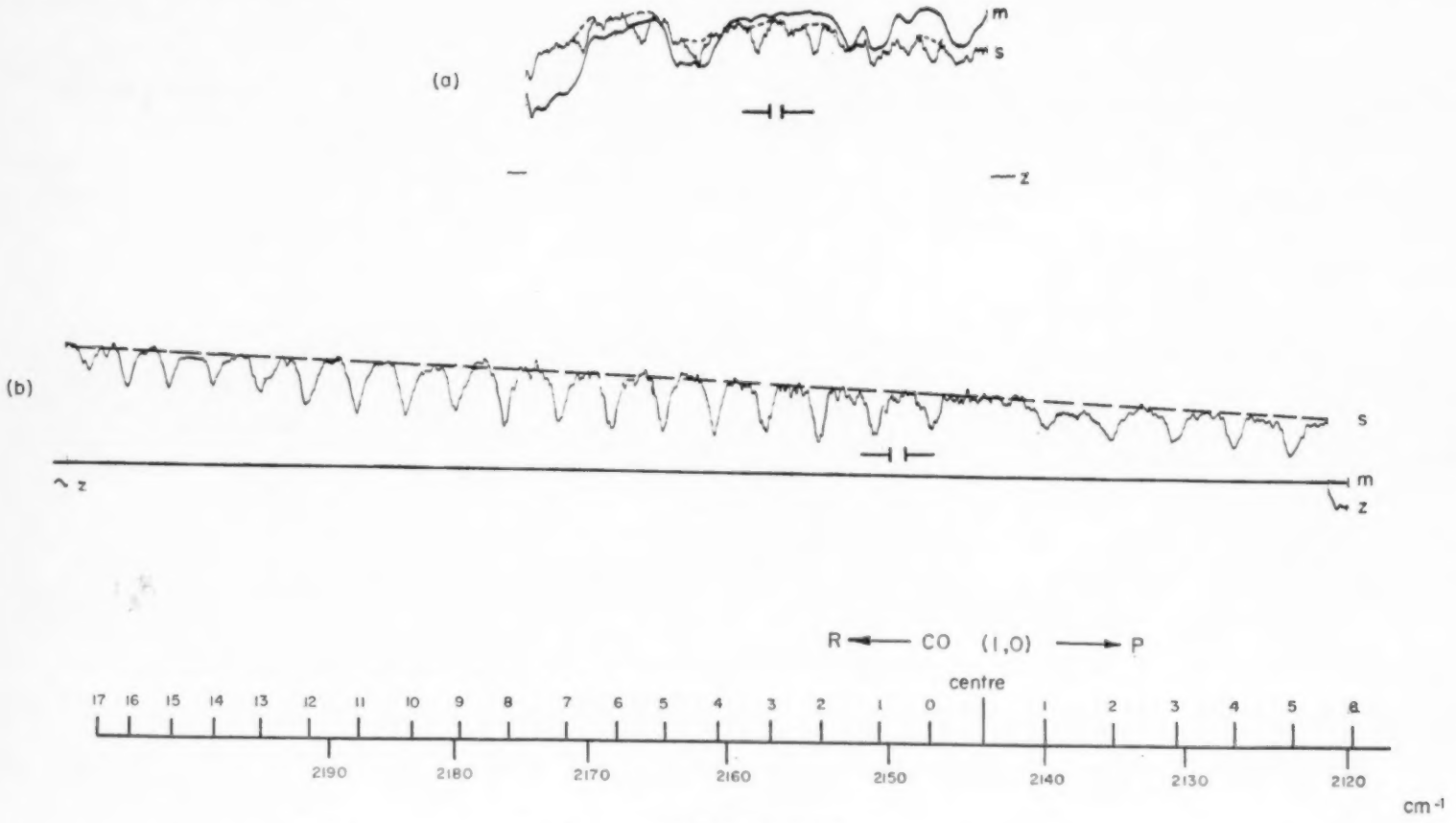

FIG. 3. Spectra of (1–0) band of CO.
(a) Solar spectrum observed on 15 August 1958, at 11.15 G.M.T. at an altitude of 25,000 ft, solar elevation 50·5°. (b) Spectrum observed in the laboratory. 0·390 atm cm of CO, total pressure 300 mb.

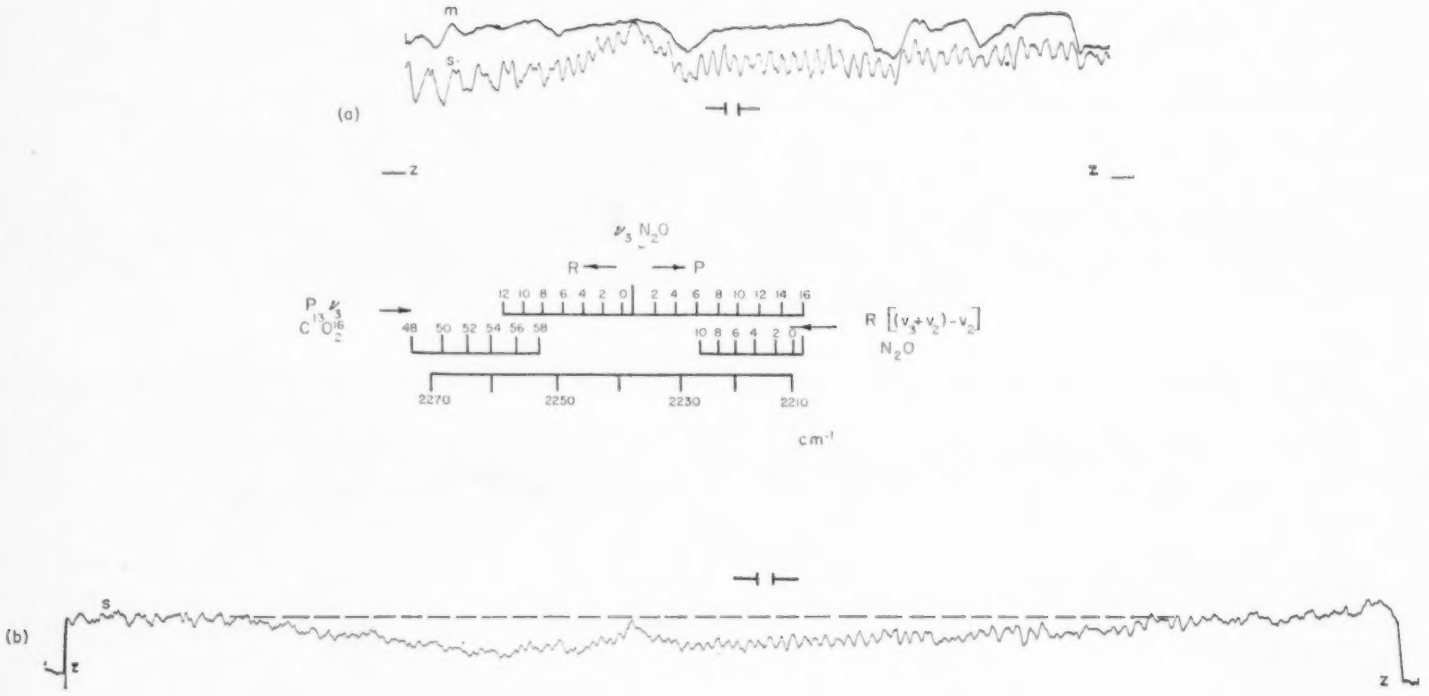

FIG. 4. Spectra of ν_3 band of N_2O.
(a) Solar spectrum observed on 15 August 1958, at 14.50 G.M.T. at an altitude of 40,000 ft, solar elevation 40°. (b) Spectrum observed in the laboratory. 0·195 atm cm of N_2O, total pressure 58·9 mb.

lie above absorption lines in the spectrum, the relation between the two is neither linear nor constant. An approximate background line for a short spectral region is easily constructed by careful inspection of both signals, as shown by dotted lines in Figs. 2(b) and 3(a). The background curve to the laboratory spectra is drawn as a straight line over short regions. Integrated absorptions are evaluated as $(\int y \,.\, d\nu)/\bar{y}$ for either single lines or groups of lines, $\int y \,.\, d\nu$ being the area under the background curve and $\bar{y}$ being the mean level of the background curve.

GROWTH OF SPECTRAL LINES

The integrated absorption or equivalent width in frequency units of a single spectral line of Lorentz shape is given by the expression due to Ladenburg and Reiche:[5]

$$\int_0^\infty A.\, d\nu = W = 2\pi\gamma x e^{-x}\,[J_0(ix) + iJ_1(ix)] \tag{1}$$

where $x \dfrac{Sw}{2\pi\gamma}$

A is the fractional absorption at frequency ν
w is the path-length of absorber
S is the line strength
γ is the half-width of the line
J_0 and J_1 are Bessel functions of zeroth and first orders respectively.

For large x ($x > 10$) the expression reduces to

$$W = 2(S\gamma w)^{1/2} \tag{2}$$

According to simple kinetic theory, the half-width γ varies with pressure p and temperature T according to the expression:

$$\gamma(p, T) = \gamma_0 \frac{p}{p_0} \left(\frac{T_0}{T}\right)^{1/2} \tag{3}$$

where γ_0 is the half-width at p_0 and T_0.

The line strengths also vary with temperature due to changes in the distribution of the molecules between the different energy levels.

The population n_J and hence the strength of the level having rotational quantum number J varies approximately according to the Boltzmann expression

$$n_J \propto \frac{1}{b(T)} \exp\left(-\frac{Bhc\,J(J+1)}{kT}\right) \tag{4}$$

where $Bhc\,J(J+1)$ is the energy corresponding to the level J, $b(T)$ is the rotational partition function and is approximately proportional to T for a diatomic molecule such as CO or a linear molecule such as N_2O and to $T^{3/2}$ for a spherical top molecule such as CH_4.[6]

Using expression (3) we may write equation (2)

$$W = A(T) \left(\frac{pw}{p_0}\right)^{1/2} \tag{5}$$

where $A(T) = 2(S\gamma_0)^{1/2}\left(\frac{T_0}{T}\right)^{\frac{1}{2}}$

In the atmospheric observations of integrated absorption which have been made, the path is that between the observer and the top of the atmosphere. If a constant volume mixing-ratio, r, of absorber is assumed for this path, then (5) may be written

$$W = A(T)\left(\frac{rH \operatorname{cosec}\theta}{2}\right)^{1/2}\frac{p}{p_0} \tag{6}$$

where p is now the pressure at the level from which observations are being made, H is the scale height of the atmosphere considered at 0 °C and θ is the solar elevation.

It will be seen from the above that, if the approximate equation (2) can be used, the interpretation of absorption spectra of the atmosphere is very much simplified. According to Plass,[7] the error made will be approximately e per cent where

$$e = 12{\cdot}5/x.$$

Now for a line which is observed in the atmosphere due to the absorption of a gas of mixing-ratio r, x can be written

$$x = \frac{SrH \operatorname{cosec}\theta}{\pi\gamma_0}$$

and is thus constant with height. The values of γ_0 for individual lines are not known with great accuracy, but estimates of its value for the lines of some band of the gases studied can be found in the literature. It is unlikely to be widely different for different bands of the same gas. For CH_4, γ_0 is about 0·05 cm^{-1},[8] for CO, 0·08 cm^{-1},[9] and for N_2O, 0·16 cm^{-1}.[10] For the lines studied and for atmospheric concentrations of these gases, x lies between one and ten, so that at worst, the approximation of equation (2) will introduce an error of about 10 per cent. That it is justified to use this approximation is also demonstrated experimentally by the fact that the laboratory results presented in the following sections give straight line graphs when W is plotted against $(pw/p_0)^{1/2}$.

Using spectra observed in the laboratory, graphs of $(\int y \,.\, d\nu)/\bar{y}$ against $(pw/p_0)^{1/2}$ have been plotted, so that for any given line or group of lines $A(T)$ can be found. If a mean temperature for an atmospheric path is assumed, an adjustment may be made to the value of $A(T)$ using equations (3) and (4). The adjusted value may then be used to interpret the spectra obtained from the aircraft, and thus to determine the mean quantity of absorber present at different altitudes. The observations for the different gases are described separately.

METHANE

The line R(1) of the ν_3 band at 3·3 μ of methane has been chosen for study. It is not possible to use any of the lines corresponding to transitions to states of higher J because these lines are not single but split into a number of components due to a Coriolis interaction. This splitting has been studied by Boyd, Thomson and Williams;[11] it is proportional to $J(J+1)$ and is larger in the P branch than in the R branch. Because of these overlapping

TABLE 1. LABORATORY MEASUREMENTS OF RATE OF GROWTH OF R(1) OF ν_3, CH_4

Pressure (mb)	w(atm cm)	Integrated absorption $\left(\frac{\int y \, . \, d\nu}{\bar{y}}\right)$ cm^{-1}
216	0·096	0·10
291	0·096	0·14
195	0·193	0·146
291	0·193	0·171
196	0·382	0·177
294	0·382	0·210
34	0·573	0·134
103	0·573	0·164
186	0·573	0·227
285	0·573	0·271
426	0·573	0·328

components the curves of growth of these lines do not follow a simple law but will be a complex function of path-length and pressure. This is illustrated by the curve of growth obtained in the laboratory for line P(6) shown in Fig. 5. Figure 5 also includes the curve

TABLE 2. ATMOSPHERIC MEASUREMENTS OF R(1) OF ν_3, CH_4

Date	Time (G.M.T.)	Solar elevation (θ)	Altitude (ft)	$\left(\frac{\int y \, . \, d\nu}{\bar{y} \, . \, \sqrt{\text{cosec}\theta}}\right)$ cm^{-1}
29 July 1958	11.00	53·5°	20,000 (465 mbs)	0·30
29 July 1958	14.00	50·5°	25,000 (376 mbs)	0·17
	14·15	48°	40,000 (187 mbs)	0·10
15 Aug. 1958	11.30	50°	25,000	0·18
20 Oct. 1958	16.00	10°	40,000	0·16
		8°	45,000 (147 mbs)	0·09
21 Oct. 1958	12.30	27·5°	30,000 (301 mbs)	0·20
		25·5°	40,000	0·12
		23·5°	46,000 (140 mbs)	0·10
21 Nov. 1958	12.00	18°	20,000	0·19
			40,000	0·12
Migeotte *et al.*		42°	11,000 (670 mbs) (on Jungfraujoch)	0·34

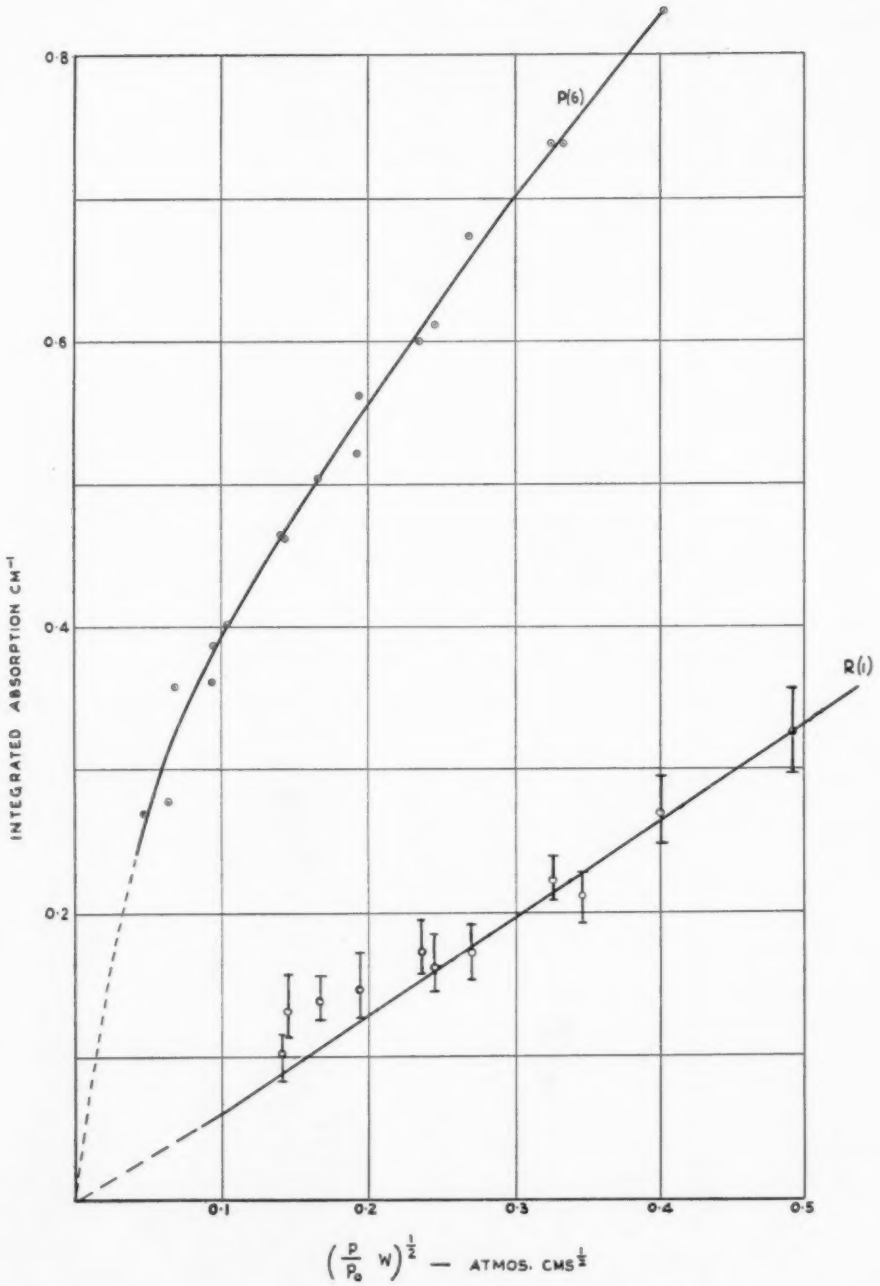

FIG. 5. Growth of integrated absorption as a function of $(pw/p_0)^{1/2}$ for two lines of ν_3, CH_4. $T = 290$ °K. (a) for line P(6), (b) for line R(1). Data presented in Table 1.

Vol. 1 1961

of growth for line R(1), for which the splitting is much smaller. This is a straight line when plotted against $(pw/p_0)^{1/2}$, and so can be used with confidence for quantitative interpretation. The equivalent widths of this line obtained from the airborne spectra are presented in Table 2 and Fig. 6.

Comparison has been made between the laboratory and airborne measurements on line R(1) presented in Figs. 5 and 6. A correction has been made using equations (3) and (4)

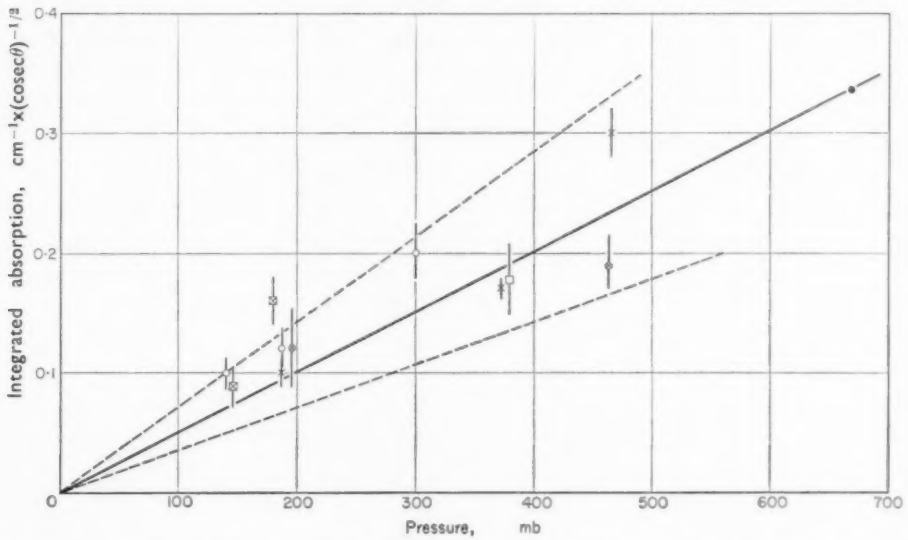

FIG. 6. Integrated absorption ÷ (cosec θ)$^{1/2}$ as a function of pressure for R(1) of ν_3, CH_4 in the solar spectrum. Data presented in Table 2.
× 29 July 1958. □ 15 August 1958. ⊠ 20 October 1958. ○ 21 October 1958. ⊗ 21 November 1958.
● Migeotte *et al.* (1956) on Jungfraujoch.
Full line corresponds to constant mixing-ratio r; dotted lines correspond to constant mixing ratios $2r$ and $r/2$.
Probable error is indicated by vertical lines through each point.

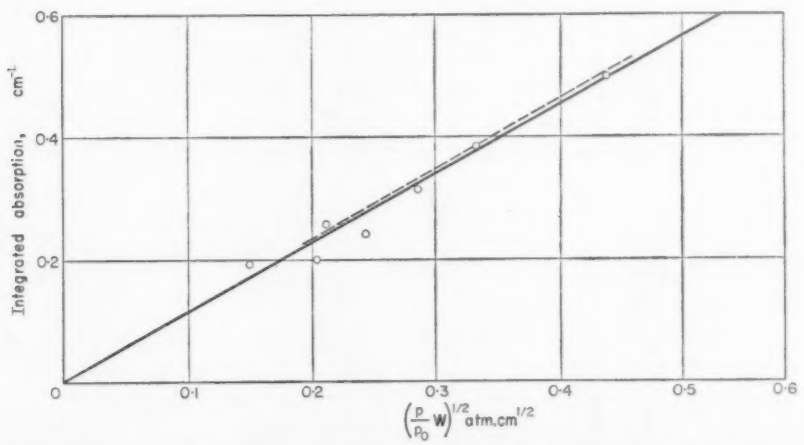

FIG. 7. Growth of integrated absorption as a function of $(pw/p_0)^{1/2}$ for R(3) of (1–0) CO. T = 290 °K.
Data presented in Table 3. — — — as found by Shaw (1958).

to make the laboratory measurements carried out at 290 °K apply to the airborne measurements for which a mean temperature of 240 °K has been assumed. The mean volume mixing-ratio of CH_4 as given by the measurements is $1{\cdot}05 \times 10^{-6}$. This corresponds to a total quantity in a vertical column of the whole atmosphere of 0·84 atm cm.

CARBON MONOXIDE

Curves of growth have been measured in the laboratory for the lines R(1) to R(5) and P(4), of which R(3) is presented as an example in Fig. 7 and Table 3. The atmospheric data is presented in Table 4 and Fig. 8. A temperature correction has been made to each of the airborne measurements of integrated absorptions using equations (3) and (4). This correction is different for each line and has been applied before the values of integrated absorption

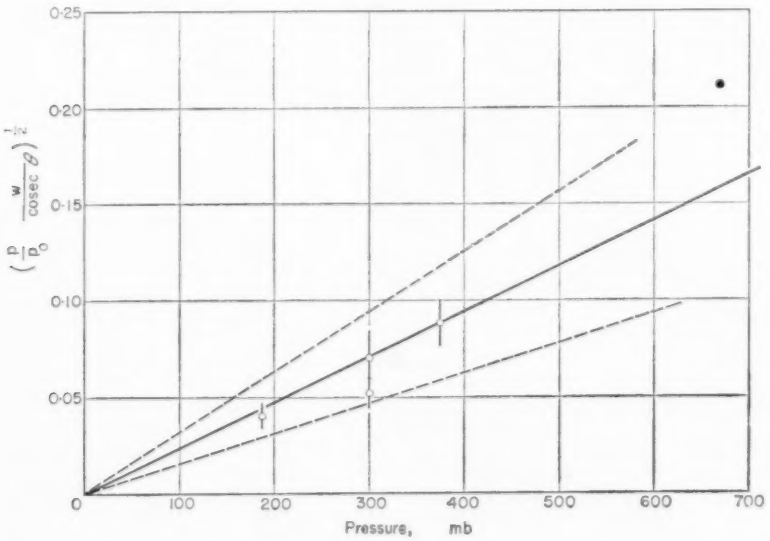

FIG. 8. $(pw/p_0 \operatorname{cosec}\theta)^{1/2}$ as a function of pressure for lines in (1–0) band of CO in the solar spectrum.
Data presented in Table 4. ● Migeotte *et al.* (1956) on Jungfraujoch.
Full line corresponds to constant mixing-ratio r; dotted lines correspond to constant mixing-ratios $2r$ and $r/2$.
Probable error is indicated by vertical lines through each point.

TABLE 3. LABORATORY MEASUREMENTS OF RATE OF GROWTH OF R(3) OF (1–0), CO

Pressure (mb)	w (atm cm)	Integrated absorption $\left(\frac{\int y \, . \, d\nu}{\bar{y}}\right)$ cm^{-1}
307	0·20	0·240
215	0·20	0·210
117	0·20	0·194
495	0·39	0·500
300	0·39	0·385
214	0·39	0·294
117	0·39	0·255

Vol. 1 1961

TABLE 4. ATMOSPHERIC MEASUREMENTS OF (1–0), CO

Date	Time (G.M.T.)	Solar elevation (θ)	Altitude (ft)	Line	Integrated absorption corrected to 290 °K (cm^{-1})	Mean $\left(\frac{pw}{p_0 \operatorname{cosec} \theta}\right)^{1/2}$ from graphs such as Fig. 7
15 Aug. 1958	11.15	50·5°	25,000 (376 mbs)	R(5)	0·157	
				R(4)	0·138	
				R(3)	0·102	0·088
				R(1)	0·127	
				P(4)	0·130	
15 Aug. 1958	14.30	41°	30,000 (301 mbs)	R(3)	0·077	0·052
	14.50	40°	40,000 (187 mbs)	R(3)	0·060	
				R(4)	0·035	0·040
				R(5)	0·044	
21 July 1959	14.10	50°	30,000 (301 mbs)	P(4)	0·087	0·070

have been plotted in the table. The calculations of mean volume mixing-ratio has been carried out as for CH_4, giving $0{\cdot}12 \times 10^{-6}$. The corresponding total quantity in the atmosphere is 0·10 atm cm.

TABLE 5. LABORATORY MEASUREMENTS OF RATE OF GROWTH FOR REGION 2223·8–2218·2 cm^{-1}, COVERING P(1)–(6) OF ν_3, N_2O

Pressure (mb)	w (atm cm)	Integrated absorption $\left(\frac{\int y \, . \, dv}{\bar{y}} \text{ cm}^{-1}\right)$
39	0·010	0·66
96	0·010	0·76
225	0·010	1·07
24	0·011	0·28
60	0·097	1·25
116	0·097	1·67
193	0·097	2·25
282	0·097	2·74
403	0·097	3·32
743	0·097	3·56
59	0·195	2·39
131	0·195	2·60
211	0·195	3·13
286	0·195	3·63

NITROUS OXIDE

The absorption due to this gas near 2220 cm^{-1} is shown in Fig. 4. Difficulty is experienced in using this spectrum for a quantitative analysis because neither a single line nor the entire ν_3 band can be isolated accurately. The small separation of the lines, less than 1 cm^{-1},

TABLE 6. ATMOSPHERIC MEASUREMENTS OF P:(1)–(6) OF ν_3, N_2O

Date	Time (G.M.T.)	Solar elevation (θ)	Altitude (ft)	$\left(\frac{\int y \, . \, d\nu}{\bar{y} \, . \, \sqrt{\text{cosec}\,\theta}}\right)$ cm^{-1}
15 Aug. 1958	11.15	50·5°	25,000 (376 mbs)	1·50
15 Aug. 1958	14.30	41°	30,000 (301 mbs)	0·98
	14.50	40°	40,000 (187 mbs)	0·80
	15.20	38°	45,000 (147 mbs)	0·66
Migeotte *et al.*		42°	11,000 (670 mbs)	2·73

means that resolution of the individual lines has not been possible. At ground level most of the band is obscured by the P branch of $C^{13}O_2^{16}$ or by lines of CO and CO_2. At the heights at which aircraft observations have been made, the R branch above R(6) is overlapped by lines of $C^{13}O_2^{16}$ and above P(9) overlapping still occurs with lines of CO and CO_2. A weak band $(\nu_2 + \nu_3) - \nu_2$ of N_2O, centred at 2210 cm^{-1}, also makes a contribution to the absorption in this region.

Examination of records obtained in the laboratory both with and without N_2O in the absorption tube shows that at the centre of the band at 2220 cm^{-1}, there is 100 per cent transmission (see Fig. 4). Since the records obtained from the aircraft using the sun as a

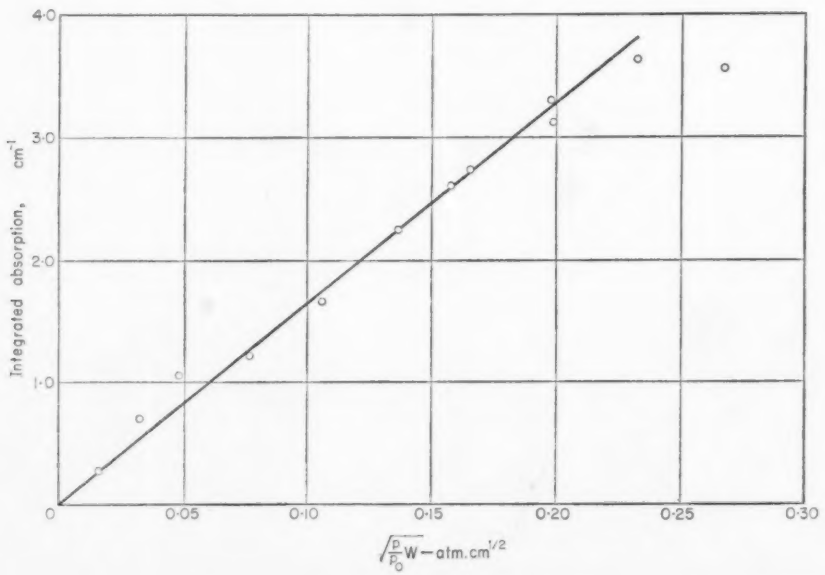

FIG. 9. Growth of integrated absorption as a function of $(pw/p_0)^{1/2}$ for the region 2223·8 to 2218·2 cm^{-1} covering lines P(1) to (6) of ν_3, N_2O. Data presented in Table 5.

Vol. 1 1961

source were obtained with narrower slit widths and higher resolution, there must be complete transmission at 2220 cm^{-1} in these cases also. For quantitative analysis of the spectrum, the section from 2223·8 cm^{-1} to 2218·2 cm^{-1}, comprising lines P(1) to P(6) has been used. The integrated absorption has been measured between these frequency limits. For the laboratory measurements, this integrated absorption is plotted in Fig. 9. Despite this somewhat arbitrary method of analysis, the integrated absorption over these lines is quite satisfactorily proportional to $(pw/p_0)^{1/2}$, at least for integrated absorptions up to 3 cm^{-1}. Above this value the curvature of the line of best fit may reasonably be attributed to overlapping of the lines. Measurements of the integrated absorption on the aircraft records is more difficult, because of some uncertainty about the background line corresponding to 100 per cent transmission. In drawing this, the monitor signal has been followed; a typical record is shown in Fig. 4(a). The aircraft measurements are presented in Table 6 and Fig. 10. The temperature correction has been made according to equations (3) and (4) and

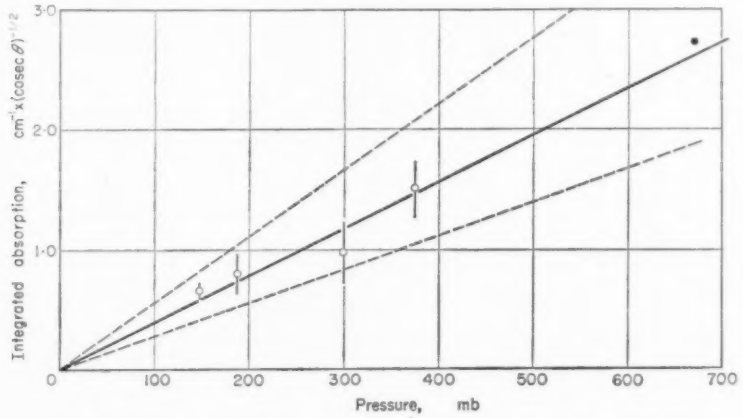

FIG. 10. Integrated absorption ÷ (cosec θ)$^{1/2}$ as a function of pressure for lines P(1) to (6) of ν_3, N_2O, in the solar spectrum. Data presented in Table 6. ● Migeotte *et al.* (1956) on Jungfraujoch.
Full line corresponds to constant mixing-ratio r; dotted lines correspond to constant mixing-ratios $2r$ and $r/2$
Probable error is indicated by vertical lines through each point.

calculations carried out as for CH_4. There is some uncertainty about the magnitude of the temperature correction in this case because of the contribution from lines of $(\nu_2 + \nu_3) - \nu_2$. The mean volume mixing-ratio of N_2O in the atmosphere is found to be $0{\cdot}12 \times 10^{-6}$. This corresponds to a total amount in the atmosphere of 0·10 atm cm.

Observations of the $2\nu_1$ band at 3·9 μ from the ground[2] have been compared with the record given by Migeotte *et al.*[12] of the same band, indicating that the mixing ratio of N_2O is constant in the troposphere between 0 and 11,000 ft altitude. This band has not been studied in the laboratory.

NITRIC OXIDE

In previous work (for instance Nielsen and Shaw[13]) the region near 1870 cm^{-1} has received close scrutiny for lines in the band of NO, because of the probable importance of this gas in photochemical reactions in the ionosphere. The region is overlapped by strong lines in the ν_2 band of H_2O at 6·26 μ and weaker lines of $3\nu_2'$ of CO_2 at ground level. Fig. 11 shows a spectrum recorded at an altitude of 45,000 ft, and laboratory spectra for similar

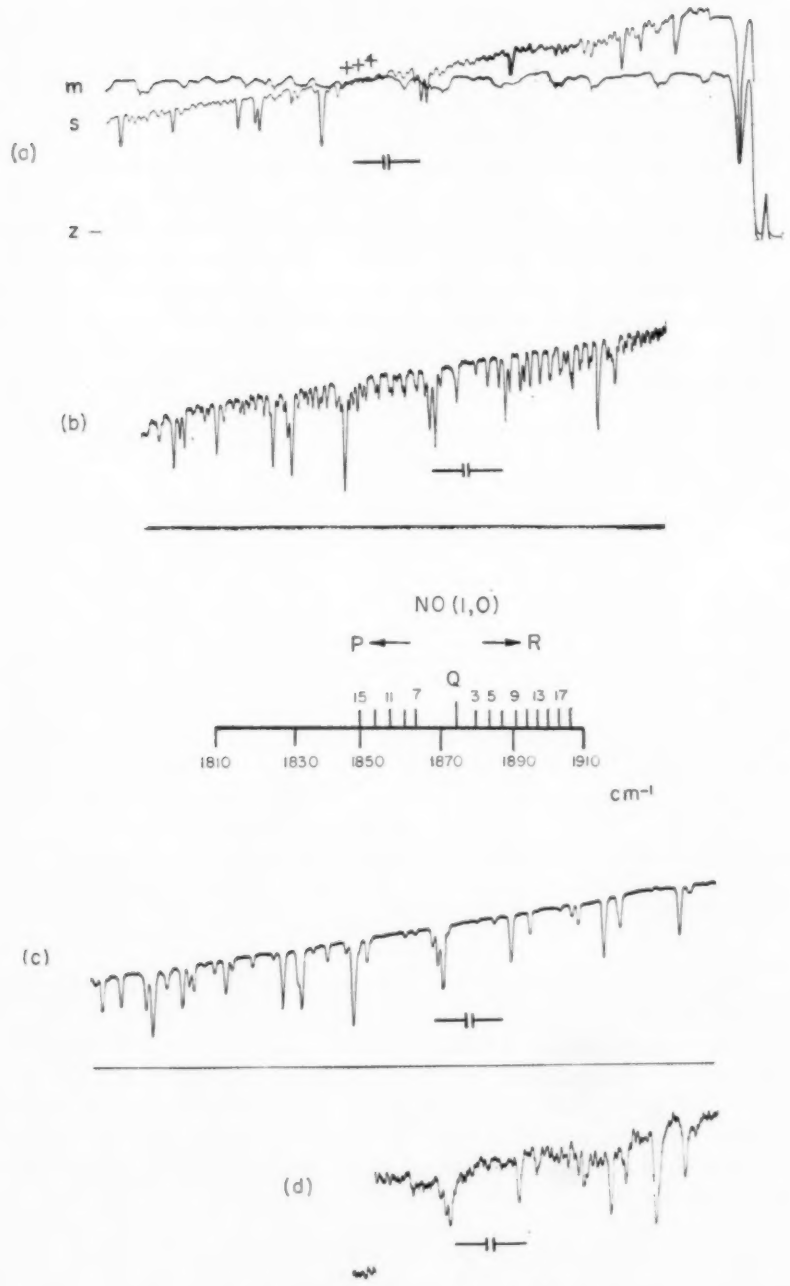

FIG. 11. Spectra near 1870 cm^{-1}.
(a) Solar spectrum observed on 16 September 1959, at 11.10 G.M.T. at an altitude of 45,000 ft, solar elevation 40°. (b) Laboratory spectrum of air column at 130 mb pressure containing 0·07 atm cm of NO and approximately 10^{-3} precipitable cm of H_2O vapour. (c) Laboratory spectrum of H_2O vapour, as in (b), alone. (d) Laboratory spectrum of 490 atm cm of CO_2 at atmos. pressure, with H_2O vapour present.

Vol. 1 1961

amounts of CO_2, and also H_2O vapour with and without nitric oxide present; also shown are the theoretical locations of the NO lines. The lines in Fig. 11(a) can all be identified with lines of $3\nu_2'$ CO_2 or ν_2 H_2O except a possible identification of the lines shown with an asterisk as the doublets P(9, 11, 13) of NO. There is, however, no evidence of the Q branch of NO being present at 1876 cm^{-1}. Spectra recorded at other altitudes and with different slit widths and scanning speeds have also revealed the absence of any lines corresponding to the Q branch of NO. It has not been possible to record spectra at really low solar elevations, however, and so we cannot reduce the value of 0·02 atm cm given by Migeotte and Neven [14] as an upper limit for the content of this gas in a vertical column of the atmosphere.

DISCUSSION

The presence of the gases methane, carbon monoxide and nitrous oxide in the atmosphere has been discussed by a number of workers. In particular, Bates and Witherspoon [15] have reviewed the evidence for sources at the earth's surface and also for the part played by these gases in photochemical reactions in the upper atmosphere. Since the levels at which significant photochemical manufacture or destruction could occur are above 50 km and thus well above the highest level of our observations, and since there is considerable mixing throughout the troposphere and lower stratosphere, it is not surprising that our results indicate that these gases are present in substantially constant mixing-ratio up to altitudes of 15 km. Inspection of Figs. 6, 8 and 10 shows that the variations found for all the gases are no more than a factor of two greater or less than the appropriate mean mixing-ratio. Because of the influence of pressure on infrared absorption, such spectroscopic observations as have been made are not sufficiently sensitive to detect larger changes in mixing-ratio which may be present at levels above about 25 km.

Good agreement has been found with the observations of Migeotte, Neven and Swensson [12] at the Jungfraujoch, and the values of mixing-ratio for the three gases which have been deduced do not differ greatly from those quoted by other workers who have made observations mainly from ground level. For methane, Goldberg [16] has observed the absorption in the 1·67 μ band from Mount Wilson. He deduced a mixing-ratio of $1{\cdot}6 \times 10^{-6}$, and his observations on the curves of growth of lines at very low solar elevations were consistent with a mixing-ratio constant with height. For carbon monoxide, Shaw [9] has made an extensive study of the 4·7 μ band as observed from Columbus, Ohio. He has found very considerable variability in the amount present in the whole atmosphere, between the limits of 0·04 and 0·13 atm cm. Our measurements lie well within this range. For nitrous oxide, Goody [17] making observations in the 7·8 μ band from an aircraft up to an altitude of 25,000 ft found a mixing-ratio of $0{\cdot}27 \times 10^{-6}$ which is about twice the value we have deduced from our observations at 4·5 μ. Birkeland and Shaw [18] have observed the 4·5 μ band from the ground and also found a mixing-ratio of $0{\cdot}27 \times 10^{-6}$ which did not vary significantly with time. McMath *et al.*, [19] from observations near 2·2 μ quote a total quantity in the atmosphere of about 0·4 atm cm which corresponds to a mixing-ratio of $0{\cdot}5 \times 10^{-6}$. Goldberg and Müller [20] also using the 2·2 μ bands have obtained curves of growth at very low solar elevations which are consistent with a mixing-ratio constant with height. As has been mentioned above, comparison of our spectra recorded at the ground and at altitude with those of Migeotte *et al.* [12] also indicate a mixing-ratio constant with height, although the value we have deduced is significantly less than that quoted by other workers. Some of this discrepancy may well be due to the difficulty of interpretation of the spectroscopic data, as discussed earlier.

Acknowledgements—The atmospheric data presented in this paper is based on a comprehensive series of airborne measurements undertaken from the Royal Aircraft Establishment, Farnborough. The successful conclusion to the flying programme is due to the unfailing co-operation of the air crew, groundstaff and all associated services of Radio Flight, Royal Aircraft Establishment.

Miss Shirley Wallis and Mr. I. D. F. Birch were of great assistance during the laboratory measurements and Mr. T. D. F. Hawkins acted as observer to obtain the atmospheric spectra on several of the flights.

REFERENCES

1. HOUGHTON, J. T., T. S. MOSS, and J. P. CHAMBERLAIN, *J. Sci. Instrum.* **35**, 329 (1958).
2. SEELEY, J. S., J. T. HOUGHTON, T. S. MOSS, and N. D. P. HUGHES (1961), *Phil. Trans. Roy. Soc.* In press.
3. HOUGHTON, J. T., and J. S. SEELEY, *Quart. J. R. Met. Soc.* **86**, 358 (1960).
4. WHITE, J. U., *J. Opt. Soc. Amer.* **32**, 285 (1942).
5. LADENBURG, R., and F. REICHE, *Beibl. Ann. Phys.* **42**, 181 (1913).
6. HERZBERG, G., *Infrared and Raman Spectra*, p. 505. Van-Nostrand (1945).
7. PLASS, G. N., *J. Met.* **11**, 163 (1954).
8. GOLDBERG, L., O. C. MOHLER, and R. E. DONOVAN, *J. Opt. Soc. Amer.* **42**, 1 (1952).
9. SHAW, J. H., *Astrophys. J.* **128**, 428 (1958).
10. GOODY, R. M., and T. W. WORMELL, *Proc. Roy. Soc.* A **209**, 178 (1951).
11. BOYD, D. R. J., H. W. THOMSON, and R. L. WILLIAMS, *Proc. Roy. Soc.* A **213**, 42 (1952).
12. MIGEOTTE, M., L. NEVEN, and J. SWENSSON, *Mem. Soc. Sci. Liège* (special issue) (1956).
13. NIELSEN, H., and J. H. SHAW, Progress Report, Ohio State University (1954).
14. MIGEOTTE, M., and L. NEVEN, *Mem. Soc. Sci. Liege, 4th Ser.* **12**, 165 (1952).
15. BATES, D. R., and A. E. WITHERSPOON, *Mon. Not. R. Astr. Soc.* **112**, 101 (1952).
16. GOLDBERG, L., *Astrophys. J.* **113**, 567 (1951).
17. GOODY, R. M., *The Physics of the Stratosphere*, p. 79. Cambridge University Press (1954).
18. BIRKELAND, J. W., and J. H. SHAW, *J. Opt. Soc. Amer.* **49**, 637 (1959).
19. MCMATH, R. R., A. K. PIERCE, O. C. MOHLER, L. GOLDBERG, and R. A. DONOVAN, *Phys. Rev.* **78**, 65 (1950).
20. GOLDBERG, L., and E. A. MÜLLER, *J. Opt. Soc. Amer.* **43**, 1033 (1953).

Vol.
1
1961

Infrared Physics, 1961, Vol. 1, pp. 133–145. Pergamon Press Ltd. Printed in Great Britain

INFERENCE OF TWO-DIMENSIONAL WIENER SPECTRA FROM ONE-DIMENSIONAL MEASUREMENTS

J. A. JAMIESON

The Aeronutronic Division, The Ford Motor Company, Newport Beach, California, U.S.A.

(*Received* 9 *January* 1961)

Abstract—It is proposed to summarize present measurements and understanding about infrared background variance density spectra in one spectrum referred to the center of the earth. An important part of the non-stationarity of the apparent background process is accounted for by this transformation.

An example is given of the use of this concept to extrapolate one-dimensional background measurements for calculation of discrimination for a scanning system.

I. INTRODUCTION AND SUMMARY

THIS paper is concerned with background noise and background discrimination in infrared systems. The term background noise describes spatial fluctuations in radiance of an effective object surface of the optical part of the system due to scattering, reflection, and emission of radiation by bodies other than targets sought by the system. In a scanning or chopping system these irregularities in radiance cause fluctuating voltages at the detector which contain unwanted information and may confuse the system. The term background discrimination describes measures taken by the system designer to minimize the effect of background noise. These measures are an important part of design because background noise is often the limiting influence on the sensitivity of real systems.

The theory of background noise has been developed by Jones[1] and others[2, 3, 4] by analogy to the theory of Gaussian noise occurring in electronic systems due to other causes. The principal description of the noise proposed by this theory is a variance density spectrum called a Wiener spectrum. This function is often defined as the Fourier transform of the autocorrelation function of the radiance pattern on the effective object surface. Since the radiance pattern is defined on a surface it has two dimensions, so also do the autocorrelation function and the Wiener spectrum.

It is frequently assumed that the autocorrelation function depends only on scalar separations of the points whose radiance is correlated. The random process is then called isotropic and can be described by a one-dimensional autocorrelation function and Wiener spectrum.

Measurements based on this assumption have been reported.[5, 6]

It will be assumed, as a model, that there exists a background random process which is responsible for background noise and that this process would be isotropic if it were seen from the center of the earth. The sample functions of random processes observed by real infrared systems looking up at the sky or down at the sky and earth are mappings of sample functions of the true process distorted by the particular viewing geometry and by the differential absorption and emission of the atmosphere. For the purposes of this paper relief characteristics of true backgrounds will be neglected as will the position of the sun

and little will be said about the effect of path length. It is hoped that these vitally important influences on real backgrounds can be considered in later work.

The arrangement of the paper is first the analysis of the geometry of the situation, secondly the application of the geometrical results to mapping the spectrum. Some comments about the form of spectrum will then be offered. Finally, an example will be worked in which data are taken from an actual measurement and used to predict the performance of a hypothetical system.

II. GEOMETRY

The geometry involved in this problem is illustrated in Figs. 1 and 2. The background process is referred to a large spherical object surface. A system above or below this surface

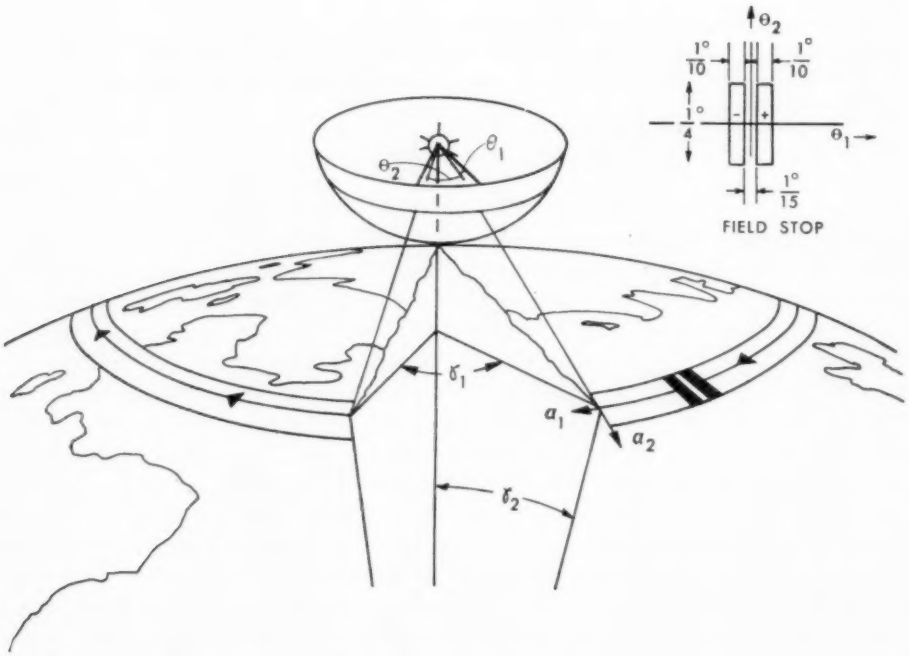

FIG. 1. Hypothetical system.

sees the surface in terms of its own set of spherical coordinates. Most systems are arranged to scan in azimuth and elevation coordinates. Some systems, however, scan directly above or below them. In this case two elevation coordinates must be used since the azimuth circle shrinks to zero. The purpose of this section is to relate system angular coordinates to angular coordinates based on the center of the earth. For the meanings of symbols in the following analysis please see attached list of symbols, pages 144–145.

Azimuth Angles

The azimuth angle θ_3 seen by the system is always the same as the azimuth angle α_3 seen at the center of the earth. It will be convenient, however, to use the variable θ_1 to denote the

quantity $\theta_1 = (h \sin \theta_2)\theta_3/h$ where h is the height of the system above or below the effective background object surface. The variable α_1 is defined similarly as

$$\alpha_1 = \alpha_3 \sin \alpha_2$$

Thus

$$\alpha_1 = \theta_1 \frac{\sin \alpha_2}{\sin \theta_2} \tag{1}$$

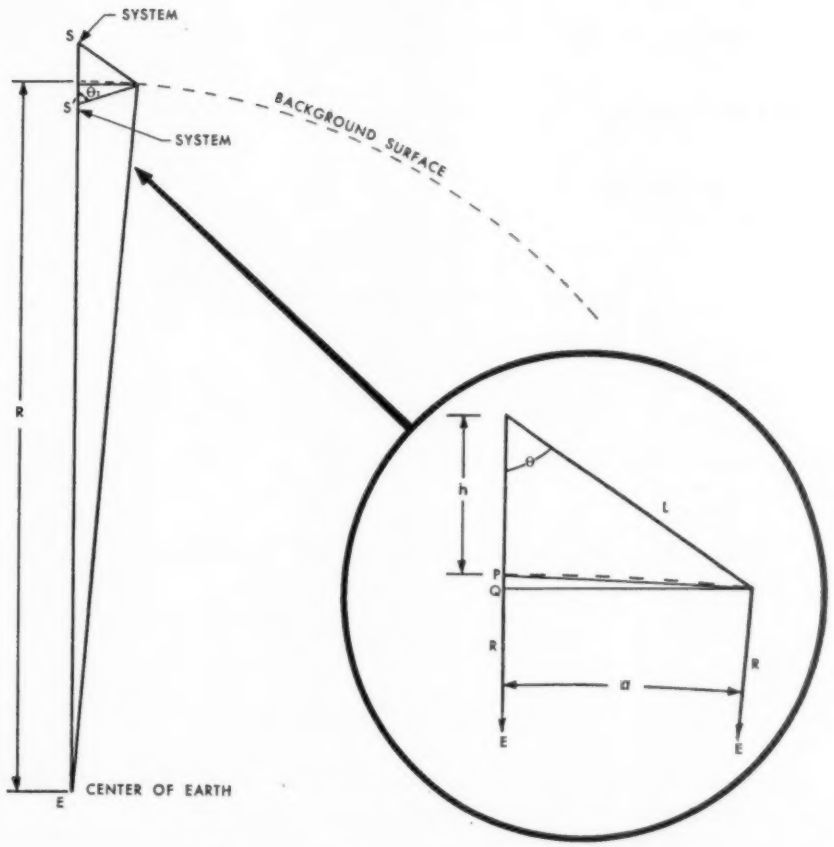

FIG. 2. Geometry of system coordinates and earth coordinates.

Elevation Angles

Figure 2 shows a background surface in relation to the center of the earth below the surface and observing systems above and below the surface. An enlarged sketch shows the geometry of the system above the surface more clearly. Examining the length of the line QR

$$L \sin \theta_2 = R \sin \alpha_2 \tag{2}$$

and the triangle SPR

$$4R^2 \sin^2 \frac{\alpha_2}{2} = h^2 + L^2 - 2hL \cos \theta_2 \tag{3}$$

It is clear that these two equations hold whether S is above or below the background surface. Now from the trigonometry of half angles:

$$2\sin^2(\alpha/2) = \frac{\sin^2\alpha}{2} + \frac{\sin^4\alpha}{8} + \frac{\sin^6\alpha}{16} + \dots$$

Multiplying by $2R^2$ and substituting from (1)

$$4R^2\sin^2(\alpha/2) = L^2\sin^2\theta + \left\{\frac{L^4}{4R^2}\sin^4\theta + \frac{L^6}{8R^4}\sin^6\theta + \dots\right\}$$

Substituting from (3) in (2)

$$L^2\cos^2\theta - 2hL\cos\theta + h^2 = \left\{\frac{L^4}{4R^2}\sin^4\theta + \frac{L^6}{8R^4}\sin^6\theta + \dots\right\}$$

so that if

$$\tfrac{1}{2}\left(\frac{L}{R}\right)^2\sin^2\theta = \tfrac{1}{2}\sin^2\alpha \ll 1$$

$$L\cos\theta - h \simeq \pm\frac{L^2}{2R^2}\sin^2\theta \tag{4}$$

Evidently the positive sign holds for a system above the background surface, the negative sign for a system below,
Then:

$$L = \{2R\cos\theta_2 \pm \sqrt{(4R^2\cos^2\theta_2 \pm 4hR\sin^2\theta_2)}\}/(\pm 2\sin^2\theta_2)$$

$$\sin\alpha_2 = \cot\theta_2\left\{1 - \sqrt{\left(1 - \frac{2h}{R}\tan^2\theta_2\right)}\right\} \tag{5}$$

or

$$\cot\theta_2\left\{\sqrt{\left(1 + \frac{2h}{R}\tan^2\theta_2\right)} - 1\right\} \tag{6}$$

It may easily be verified that (5) holds for the system above the surface, (6) for the system below. If α_2 is small enough that $\alpha_2^2/6 \ll 1$ then $\sin\alpha_2 \simeq \alpha_2$ in (5) and (6).
By straightforward differentiation we find for the four possible cases, the results listed in Table 1.

In all cases the approximations implicit in the formulae hold if $\sin^2\alpha_2/2 \ll 1$ and $\alpha^2/6 \ll 1$. The second condition will be taken to imply the first.

In addition,

$$\alpha_i(\theta_1, \theta_2) = \alpha_i(\theta_{10}, \theta_{20}) + (\theta_i - \theta_{i0})\,\alpha_i'(\theta_{10}, \theta_{20}) + \frac{(\theta_i - \theta_{i0})^2}{2}\,\alpha_i''(\theta_{10}, \theta_{20}) + \dots$$

$$\simeq \alpha_i(\theta_{10}, \theta_{20}) + (\theta_i - \theta_{i0})\,\alpha_i'(\theta_{10}, \theta_{20})$$

provided that

$$\frac{(\theta_i - \theta_{i0})\,\alpha_i''}{2\alpha_i'} \ll 1$$

Vol. 1 1961

TABLE 1(A). COORDINATE TRANSFORMATION AZIMUTH–ELEVATION

Azimuth–elevation system above the background surface	Azimuth–elevation system below the background surface
(7) $a_1 = \dfrac{\cot\theta_2}{\sin\theta_2}\left\{1 - \sqrt{\left(1 - \dfrac{2h}{R}\tan^2\theta_2\right)}\right\}\theta_1$	$a_1 = \dfrac{\cot\theta_2}{\sin\theta_2}\left\{\sqrt{\left(1 + \dfrac{2h}{R}\tan^2\theta_2\right)} - 1\right\}\theta_1$ (8)
(5) $a_2 = \cot\theta_2\left\{1 - \sqrt{\left(1 - \dfrac{2h}{R}\tan^2\theta_2\right)}\right\}$	$a_2 = \cot\theta_2\left\{\sqrt{\left(1 + \dfrac{2h}{R}\tan^2\theta_2\right)} - 1\right\}$ (6)
(9) $a_1^1 = \dfrac{\cot\theta_2}{\sin\theta_2}\left\{1 - \sqrt{\left(1 - \dfrac{2h}{R}\tan^2\theta_2\right)}\right\}$	$a_1^1 = \dfrac{\cot\theta_2}{\sin\theta_2}\left\{\sqrt{\left(1 + \dfrac{2h}{R}\tan^2\theta_2\right)} - 1\right\}$ (10)
(11) $a_2^1 = \dfrac{\left[1 - \dfrac{2h}{R}\tan^2\theta_2\right]^{-1/2} - 1}{\sin^2\theta_2}$	$a_2^1 = \dfrac{1 - \left[1 + \dfrac{2h}{R}\tan^2\theta_2\right]^{-1/2}}{\sin^2\theta_2}$ (12)
$a_1'' = 0$	$a_1'' = 0$

$$a_2'' = \frac{\dfrac{2h}{R}\dfrac{\tan\theta_2}{\cos^2\theta_2}\dfrac{1}{\left(1 - \dfrac{2h}{R}\tan^2\theta_2\right)} - 2\cot\theta_2\left\{1 - \sqrt{\left(1 - \dfrac{2h}{R}\tan^2\theta_2\right)}\right\}}{\sin^2\theta_2\sqrt{\left(1 - \dfrac{2h}{R}\tan^2\theta_2\right)}} \tag{13}$$

$$a_2'' = \frac{\dfrac{2h}{R}\dfrac{\tan\theta_2}{\cos^2\theta_2}\dfrac{1}{\left(1 + \dfrac{2h}{R}\tan^2\theta_2\right)} - 2\cot\theta_2\left\{\sqrt{\left(1 + \dfrac{2h}{R}\tan^2\theta_2\right)} - 1\right\}}{\sin^2\theta_2\sqrt{\left(1 + \dfrac{2h}{R}\tan^2\theta_2\right)}} \tag{14}$$

TABLE 1(B). COORDINATE TRANSFORMATION ELEVATION–ELEVATION

Elevation–elevation system above the background surface	Elevation–elevation system below the background surface
(5) $a_i = \cot\theta_i\left\{1 - \sqrt{\left(1 - \dfrac{2h}{R}\tan^2\theta_i\right)}\right\}$	$a_i = \cot\theta_i\left\{\sqrt{\left(1 + \dfrac{2h}{R}\tan^2\theta_i\right)} - 1\right\}$ (6)
(15) $a_i^1 = \dfrac{\left[1 - \dfrac{2h}{R}\tan^2\theta_i\right]^{-1/2} - 1}{\sin^2\theta_i}$	$a_i^1 = \dfrac{1 - \left[1 + \dfrac{2h}{R}\tan^2\theta_i\right]^{-1/2}}{\sin^2\theta_i}$ (16)

TABLE 1(B)—*cont.*

$$a_i'' = \frac{\dfrac{2h}{R}\dfrac{\tan\theta_i}{\cos^2\theta_i}\dfrac{1}{\left(1-\dfrac{2h}{R}\tan^2\theta_i\right)} - 2\cot\theta_i\left\{1-\sqrt{\left(1-\dfrac{2h}{R}\tan^2\theta_i\right)}\right\}}{\sin^2\theta_i\sqrt{\left(1-\dfrac{2h}{R}\tan^2\theta_i\right)}} \qquad (13)$$

$i = 1{\cdot}2$

$$a_i'' = \frac{\dfrac{2h}{R}\dfrac{\tan\theta_i}{\cos^2\theta_i}\dfrac{1}{\left(1+\dfrac{2h}{R}\tan^2\theta_i\right)} - 2\cot\theta_i\left\{\sqrt{\left(1+\dfrac{2h}{R}\tan^2\theta_i\right)}-1\right\}}{\sin^2\theta_i\sqrt{\left(1+\dfrac{2h}{R}\tan^2\theta_i\right)}} \qquad (14)$$

$i = 1{\cdot}2$

III. THE BASIC SPECTRUM AND OBSERVED SPECTRA

Suppose the Wiener spectrum for a background surface referred to the center of the earth is:

$$W_{aa}(k_1, k_2)$$

then it is associated with an autocorrelation function

$$R_{aa}(g_1, g_2) = < I(a_1, a_2)\, I(a_1 + g_1, a_2 + g_2) > \qquad (16)$$

$$= \int_{-\infty}^{\infty} dk_1 \int_{-\infty}^{\infty} dk_2 \quad W_{aa}(k_1, k_2)\, e^{j2\pi\,(k_1 g_1 + k_2 g_2)} \qquad (17)$$

In equation (16) it has been assumed that R_{aa} is stationary depending only on the differences g_1 and g_2 in coordinates. It seems reasonable that for all except very large or very special regions of the surface that R_{aa} should also be isotropic. That is unless the region in question contains, for example, both the South Pole and the Sahara Desert there does not seem to be any reason to expect the statistics to be oriented in any one direction rather than any other. Then:

$$R_{aa}(g_1, g_2) = R_{aa}\left[\sqrt{(g_1^2 + g_2^2)}\right] = R_{aa}(g) \qquad (18)$$

in this case

$$W_{aa}(k_1, k_2) = W_{aa}(k) \qquad (19)$$

But now correlations observed by a system are the same as those described by R_{aa} only to a different scale and perspective. Suppose that g_i is small enough that:

$$a_i + g_i \simeq a_i(\theta_0) + (\theta_i - \theta_{i0})\, a_i'(\theta_0) \qquad (13)$$

$$g_i \simeq (\theta_i - \theta_{i0})\, a_i'(\theta_0) = p_i\, a_i'(\theta_0)$$

Vol. 1 1961

then it is true that:

$$R_{\theta\theta}(\theta_{10}, \theta_{20}, p_1, p_2) = R_{aa}\left[\sqrt{\{[a_1'(\theta_0)\, p_1]^2 + [a_2'(\theta_0)\, p_2]^2\}}\right] \tag{20}$$

and

$$W_{\theta\theta}(\theta_{10}, \theta_{20}, m_1, m_2) = \int_{-\infty}^{\infty} dp_1 \int_{-\infty}^{\infty} dp_2\, R_{aa}\{\sqrt{[(a_1' p_1)^2 + (a_2' p_2)^2]}\}\, e^{-j2\pi (m_1 p_1 + m_2 p_2)}$$

$$= \int_{-\infty}^{\infty} \frac{dq_1}{a_1'} \int_{-\infty}^{\infty} \frac{dq_2}{a_1'} R_{aa}\{\sqrt{(q_1^2 + q_2^2)}\} \exp\{-j2\pi(m_1 q_1/a_1') + (m_2 q_2/a_2')\}$$

$$= W_{aa}\{\sqrt{[(m_1/a_1')^2 + (m_2/a_2')^2]}\}/a_1' a_2' \tag{21}$$

For example, suppose a spectrum is observed from above by an elevation–elevation system. At angles θ_{10} and θ_{20} both close enough to zero that $a_i''(0)\, \theta_i/2 \ll a_i'(0)$

Then

$$a_i'(0) = \lim_{\theta_i \to 0} \frac{L_{im}}{\sin^2 \theta_i} \frac{1 - \sqrt{\left(1 - \frac{2h}{R} \tan^2 \theta_i\right)}}{\sqrt{\left(1 - \frac{2h}{R} \tan^2 \theta_i\right)}} = \frac{h}{R}$$

So that

$$W_{\theta\theta}(0, 0, m_1, m_2) = \frac{R^2}{h^2} W_{aa}\left\{\sqrt{\left[\left(\frac{m_1 R}{h}\right)^2 + \left(\frac{m_2 R}{h}\right)^2\right]}\right\}$$

$$= \frac{R^2}{h^2} W_{aa}\left(\frac{mR}{h}\right)$$

which shows that the spectrum observed near the nadir (or the zenith) should also be isotropic as one would expect.

Measurements (mostly taken under conditions different from these) suggest that W_{aa} may be inversely proportional to k^t, $1{\cdot}5 \leqslant t \leqslant 3$. Taking $t = 2$ as an example:

$$W_{\theta\theta}(0, 0, m_1, m_2) = \frac{R^2}{h^2} \frac{\text{constant}\ h^2}{m^2 R^2} = \frac{\text{constant}}{m^2}$$

which is independent of h. It is interesting to note that this would not be true for other values of t. For example if $t = 2{\cdot}7$

$$W_{\theta\theta}(0, 0, m_1, m_2) = \frac{h^{0{\cdot}7}}{R^{0{\cdot}7}} \frac{\text{constant}}{m^{2{\cdot}7}}$$

so that background discrimination by a system above the background surface which has a constant field of view and angular resolution would improve with increasing altitude.

It is also clear from equation (21) that spectra observed at angles away from $(\theta_1, \theta_2 = 0, 0)$

are not isotropic. Their contours of equal variance density rather than being circles are ellipses of eccentricity $\alpha_1'(\theta_0)/\alpha_2'(\theta_0)$.

The most extreme case occurs on the horizon (or slightly below if the height of the observer and atmospheric refraction are accounted for) with:

$$\alpha_1'/\alpha_2' = \sqrt{(2R/h)} \tag{22}$$

IV. INFERENCE OF $W_{\alpha\alpha}(k)$

The measurements reported in the literature have been made by scanning an aperture in a certain pattern across sample functions of the process and using the variance spectrum of the detection voltage to estimate some form of observed one-dimensional spectrum.

To make the spectral estimate as accurate as possible the field stop of the instrument should be a thin slit as wide as possible perpendicular to the direction of scan and as narrow as possible in the direction of scan. Scans should be made as long as possible in many directions passing through (0, 0). All scans, however, should lie in the region where $\alpha_i''(0, 0)\, p_i \ll 2\alpha_i'(0, 0)$. Because the scan dimensions are finite and only a certain amount of data can be processed the estimate will be "smoothed" having only a finite resolution in wavenumber. The estimate will also extend over only a finite range of wavenumbers and will show some statistical fluctuation from the true spectrum.

The distortions may be described by:

$$W_{vv}(f) = \frac{R_0^2}{v}\int_{-\infty}^{\infty} dm_2 \int_{-\infty}^{\infty} dx_1 \int_{-\infty}^{\infty} dx_2\, W_{\theta\theta}(x_1, x_2)\, Q\left(x_1 + m_1, x_2 + \frac{f}{v}\right) \left|\left(Gm_1, \frac{f}{v}\right)\right|^2$$

$G[m_1, (f/v)]$ is the transfer function of the field stop and aberrations of the measuring equipment modified by the frequency response of the detectors. Typically, this function would be a two-dimensional low-pass filter restricting the maximum wavenumber observable in either dimension to the order of the reciprocal of the angular coverage of the detector in that direction. The exact details of this function depend on the detectivity contours of the detector, the shape of the optical blur pattern, and the amplifier frequency response.

$Q(x_1, x_2)$ is the transform of the scan pattern of the measurement. This quantity convolved into the spectrum $W_{\theta\theta}$ existing but not itself observable leads to the smoothing and the variability and the low wavenumber limit of the observed spectrum. Because the scan pattern is of finite length H_1 the resolution and low wavenumber limit of the spectrum of the order of $1/10H_1$ if the statistical perturbation of the estimate is to be held within reasonable limits for a reasonable number of measurements and data reduction.

R_0 and v take account of the detector responsivity, amplifier gain, etc., and the velocity of scan.

It must be pointed out that the spectrum $W_{\alpha\alpha}$ is defined on a closed interval $\alpha_i \leqslant 2\pi$ it is therefore a discrete spectrum (whether or not the stationarity hypothesis is valid) with a lowest possible wavenumber in either direction of $1/\pi$ c/rad. The ideally observable spectrum $W_{\theta\theta}(m_1, m_2)$ is similarly limited to wavenumbers above $1/\pi\, \alpha_i'(\theta_0)$ and since any sample function of the random process must return in one rotation of the surface to its original value this spectrum must also be discrete. Since this behavior is not explicitly observable from one point, however, it is often considered that the segment observed is a portion of an imaginary sample of infinite length and a continuous spectrum or a continuous envelope of

Vol. 1 1961

a discrete spectrum is estimated. Problems of integrability of a spectrum varying inversely with wavenumber are merely faults of the mathematical model. They have no significance for the real situation.

In principle, combining (21) and (23) and remembering (19) the basic spectrum $W\text{-}(k)$ can be estimated from well planned measurements made in a carefully recorded way from:

$$W_{vv}(f) = \frac{R_0^2}{v}\int_{-\infty}^{\infty} dm_2 \int_{-\infty}^{\infty} dx_1 \int_{-\infty}^{\infty} dx_2\, W_{aa}[\sqrt{(x_1^2 + x_2^2)}]\, Q\left(x_1 + \frac{m_1}{a_1'}, x_2 + \frac{f}{va_2'}\right) \left|G\left(\frac{m_1}{a_1'}, \frac{f}{va_2'}\right)\right|^2 \quad (24)$$

V. EXAMPLE

In reference 6 a series of four point estimates are given for one-dimensional spectra measured at night in the wavelength region $1\,\mu$ to $24\,\mu$. The geometry is:

$$-\pi/3{\cdot}6 \leqslant \theta_1 \leqslant \pi/3{\cdot}6; \quad \Delta\theta_1 = \pi/720; \quad \theta_2 = 179\pi/180; \quad \Delta\theta_2 = \pi/360$$

These measurements were very carefully made and their author is in a position to perform the calculation below in precise detail. The purpose of the approximate treatment given here is to outline a method rather than to arrive at numerical values.

To simplify the example, the experimental results will be represented (from Fig. 5 of the reference) by an apparent one-dimensional spectrum.

$$W(0, 179\pi/180, m_1) = 3 \times 10^{-12}/m_1^2 \ \text{[W/cm}^2\ \text{ster]}^2\text{/c/rad}$$

Assuming the average height h of the backgrounds to be about 10,000 feet the following values are obtained from the formulae in Section II:

$$\alpha_1(0) = 0 \qquad \alpha_2\left(\frac{179\pi}{180}\right) = 0{\cdot}0276$$

$$\alpha_1(0) = 0{\cdot}0276 \qquad \alpha_2'\left(\frac{179\pi}{180}\right) = 0{\cdot}876$$

$$\Delta\theta_1 = 2\pi \qquad \Delta\theta_2 = 0{\cdot}0035$$

$$\alpha_1^2/6 = 0 \qquad \alpha_2^2/6 = 0{\cdot}00013$$

($\Delta\theta$ is the range of θ over which the error in $\alpha(\theta) = \alpha(\theta_0) + \Delta\theta\,\alpha'(\theta_0)$ is less than 10 per cent).

The distortions due to Q and G in the dimension m_1 have been corrected by the author of reference 5 in reducing his data.

The next step is to find a function of $\sqrt{[(m_1/a_1')^2 + (m_2/a_2')^2]}$ which when integrated over m_2 from $-180/\pi$ to $180/\pi$ will yield a fit to $3 \times 10^{-12}/m_1^2$ over the range $14 \leqslant m_1 \leqslant 91$ (or since the previous discussion has been developed in two sided spectra, which fits $1{\cdot}5 \times 10^{-12}/m_1^2$ over the ranges $14 \leqslant |m_1| \leqslant 91$.

Trying the simplest possible function

$$\int_{-180/\pi}^{180/\pi} \frac{dm_2\, A}{(m_1/0{\cdot}0276)^2 + (m_2/0{\cdot}876)^2} = \frac{2 \times 0{\cdot}876 \times 0{\cdot}0276}{m_1} \tan^{-1}\left(\frac{180 \times 0{\cdot}0276}{0{\cdot}876 \times m_1}\right)$$

Since in the ranges

$$14 \leqslant |m_1| \leqslant 91 \text{ c/rad}$$

the argument of the tangent is

$$0{\cdot}02 \leqslant \frac{1{\cdot}81}{|m_1|} \leqslant 0{\cdot}129$$

Therefore:

$$\int \frac{dm_2\, A}{(m_1/\alpha_1')^2 + (m_2/\alpha_2')^2} \simeq \frac{114{\cdot}5\, A}{(m_1/0{\cdot}0276)^2}$$

and the value of A can be estimated as

$$A \simeq 1{\cdot}5 \times 10^{-12}/114{\cdot}5 \times (0{\cdot}0276)^2 = 1{\cdot}72 \times 10^{-11}$$

and hence the form of the basic spectrum is estimated from:

$$\frac{1}{\alpha_1'\alpha_2'} W_{aa} \Bigg\} \sqrt{\left[\left(\frac{m_1}{\alpha'}\right)^2 + \left(\frac{m_2}{\alpha_2'}\right)^2\right]} \Bigg\} = \frac{1{\cdot}72 \times 10^{-11} \times 0{\cdot}0276 \times 0{\cdot}876}{0{\cdot}0276 \times 0{\cdot}876 \left\{\left(\frac{m_1}{0{\cdot}0276}\right)^2 + \left(\frac{m_2}{0{\cdot}876}\right)^2\right\}^2}$$

so that

$$W_{aa}(k) = 4{\cdot}15 \times 10^{-13}/k^2$$

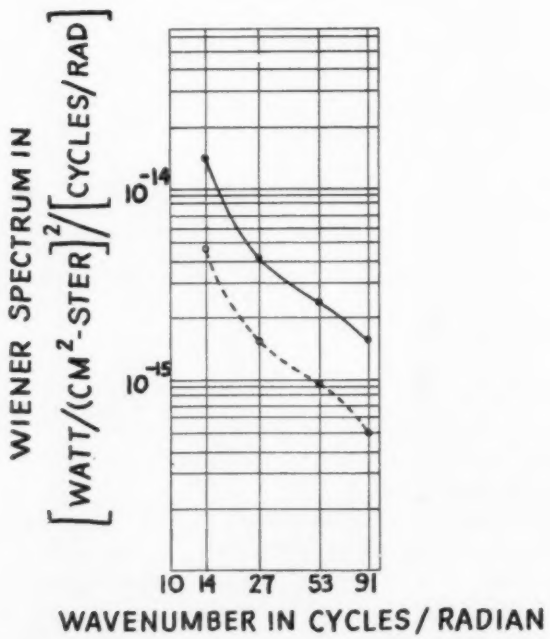

FIG. 3. Measured Wiener spectrum. The observed spectrum between 14 and 91 c/rad represented by

$$W_{\theta\theta}\left(0, -\frac{179\pi}{180}, m_1\right) = \frac{3 \times 10^{-12}}{m_1^2} \text{ [W/cm}^2 \text{ ster]}^2\text{/c/rad.}$$

Vol. 1 1961

Now suppose that this same basic spectrum describes "the other side" of the background surface in the same spectral region at night. Suppose that a system in a satellite looks down on this surface (Fig. 1) scanning a circle at 45° to the zenith and suppose the field stop consists of two 1/4° by 1/10° strips spaced at 1/15° and connected in opposition as shown in the figure. Suppose the responsivity of the detectors is uniform and the optical blur circle is small compared to the field stop.

The square of the transform of this field stop can easily be shown to have the form

$$\left|G(m_1, m_2)\right|^2 = \left|\frac{\sin\left(\frac{\pi^2 m_2}{720}\right)\left\{\cos\left(\frac{\pi^2 m_1}{675}\right) - \cos\left(\frac{\pi^2 m_1}{2700}\right)\right\}}{\pi^2 m_1 m_2}\right|^2$$

This function is plotted in Fig. 3.

At an altitude such that $2h/R = 0{\cdot}05$ the observed spectrum is

$$W_{\theta\theta}(0, \pi/4, m_1, m_2) = \frac{4{\cdot}15 \times 10^{-13}}{(0{\cdot}0354)(0{\cdot}0514)\{(m_1/0{\cdot}0354)^2 + (m_2/0{\cdot}0514)^2\}}$$

To find the effective r.m.s. background noise irradiance at the entrance aperture of the system it is necessary to evaluate the square root of the integral.

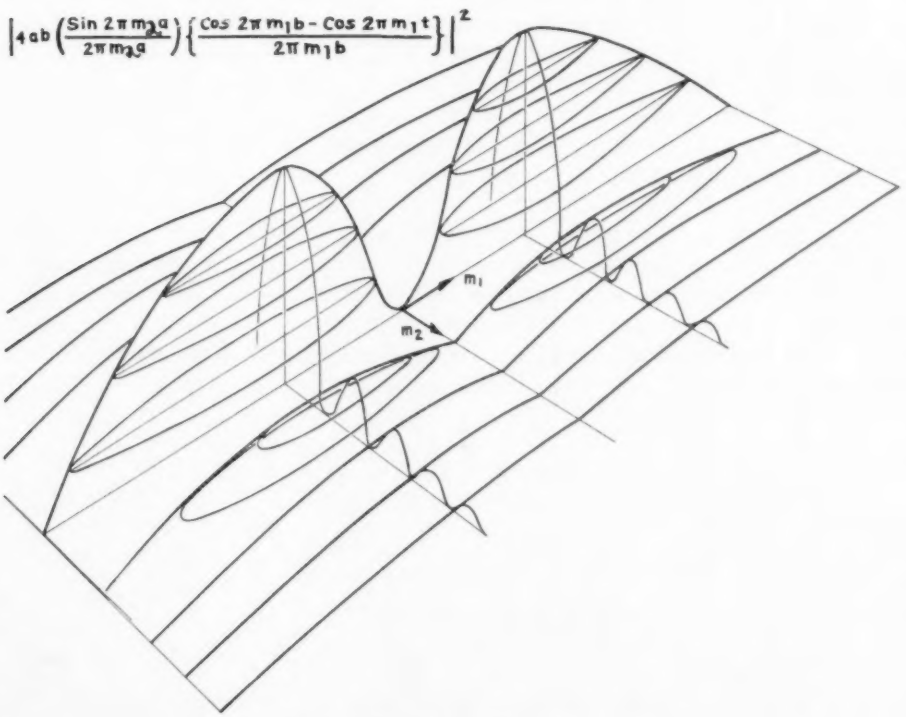

FIG. 4. System transfer function.

$$N^2 = \int_{\infty}^{\infty} dm_1 \int_{\infty}^{\infty} dm_2 \; W_{\theta\theta}(0, \pi/4, m_1, m_2) \; |G(m_1, m_2)|^2$$

It will be a sufficient estimate for the present purposes to multiply the value of the spectrum $W_{\theta\theta}$ at the peaks of the transfer function G by the peak value of G and the 6 *db* bandpasses.

These values are:

Peaks of $G = 1{\cdot}27 \times 10^{-5}$ steradian
Occur at $m_1 = \pm 148$ c/rad; $m_2 = 0$
Bandpasses $\Delta m_1 = 2 \times 172$ c/rad
$\Delta m_2 = 186$ c/rad
$W_{\theta\theta}(0, \pi/4, 148, 0) = 13{\cdot}1 \times 10^{-18}$ [W/cm^2 ster]^2/c/rad^2.
R.m.s. background $N \simeq 10^{-11}$ W/cm^2.

It might also be interesting to remark that approximately 77 per cent of the spectral emittance of a 300 °K blackbody lies below 21 μ, approximately 0·01 per cent below 3 μ.

CONCLUSIONS

It has been suggested, as a hypothesis, that the background space fluctuations observed in measurements and by background discriminating infrared systems are mappings of sample functions of a basic background process. This background process is supposed to be isotropic if expressed in coordinates originating at the center of the earth. This approach has been used to give a precise meaning to zonal stationarity of apparent background processes, to local isotropy near the zenith and nadir, and to elliptical foreshortening at other angles. The effect of gross changes in system altitude depends according to this hypothesis on the index of the Wiener spectrum. Misgivings about the integrability of the spectrum have been shown to be unfounded. An example has been given of a method for using the hypothesis to estimate the background discrimination capability of an hypothetical system.

The hypothesis rests on several assumptions, particularly the existence of a background process, and the validity of reference to a background surface. The assumption that the background surface has the same statistics from either side is only necessary until some valid measurements are made from above. The neglect of sun position, relief characteristics and the variation of atmospheric attenuation with path length are important omissions which conceivably could be corrected without a change in philosophy.

SYMBOLS AND NOTATION

A	Undetermined constant in basic Wiener spectrum.
f	Electrical frequency.
G	Transfer function of a space filter.
g_i	Lag in autocorrelation function of basic process.
H	Length of scan.
h	Height of infrared system above or below background surface.
I	Radiance function of background surface.
i	Coordinate index (1 or 2).
j	Imaginary operator.
k_i	Wavenumber in basic spectrum.
k	$\sqrt{(k_1^2 + k_2^2)}$
L	Path length from system to point of observation.

Vol. 1 1961

m_i Wavenumber in observed Wiener spectrum.
p_i Lag in observed autocorrelation function.
Q Transform of scan pattern.
q_i Normalized lag in observed autocorrelation function.
R Radius of background surface.
R_0 Responsivity and system gain.
$R_{\alpha\alpha}$ Basic autocorrelation function.
$R_{\theta\theta}$ Observed autocorrelation function.
t Index in Wiener spectrum.
v Scan speed.
$W_{\alpha\alpha}$ Basic Wiener spectrum.
$W_{\theta\theta}$ Observed Wiener spectrum.
W_{vv} Spectrum of detector voltage.
x_i Dummy variable of integration.
α_i Background surface coordinate referred to center of earth.
α_i' First derivative of α_1 with respect to θ_i.
α_i'' Second derivative of α_1 with respect to θ_i.
θ_i Background surface coordinate referred to system.

REFERENCES

1. Clark-Jones, R., *Sky Noise, Its Nature and Analysis*. Polaroid Corporation Research Department Rept. No. 480 (1953).
2. Elias, P., P. Grey, and D. Z. Robinson, *J. Opt. Soc. Amer.* **42**, 127 (1952).
3. Karr, P. R., *Mathematical Study of Background Noise*. Ramo Wooldridge Corporation, unpublished memorandum.
4. Robinson, D. Z., *Proc. Inst. Radio Engrs., N.Y.* **47**, 1554 (1959).
5. *Infrared Sky Background Investigation*. Ramo Wooldridge Corporation, Los Angeles, California. RW 16370, 84, 87 (1957).
6. Free, L. J., *J. Opt. Soc. Amer.* **49**, 1007 (1959).
7. Blackman, R. B., and J. W. Tukey, *The Measurement of Power Spectra*. Dover Publications, Inc., New York (1959).

Infrared Physics, 1961, Vol. 1, pp. 146–152. Pergamon Press Ltd. Printed in Great Britain

EFFECT OF COOLED APERTURES ON PbS DETECTORS

J. J. McARDLE

Infrared Industries, Inc., Waltham, Massachusetts, U.S.A.

(*Received* 2 *February* 1961)

Abstract—A comparison of the electrical behavior of lead sulfide (PbS) detectors, looking at a target through a cooled aperture which has a restricted field of view limiting the background radiation, with that of similar detectors without such an aperture.

EFFECT OF COOLED APERTURES ON PbS DETECTORS

Vol.
1
1961

DURING the latter part of 1959 and the early part of 1960, Infrared Industries, Inc. undertook, on behalf of the Boeing Airplane Company, to construct a series of cooled-aperture lead sulfide detector assemblies. The objective of this development program was to evaluate the expected over-all increase in detector sensitivity. During the course of the effort, however, several other interesting phenomena were observed:

1. With increased responsivity, signal-to-noise ratio increased as the signal response, while noise demonstrated no appreciable change from unshielded cell operation.
2. Detector long-wavelength response is extended.

The results of this investigation appear to be consonant with data obtained by R. M. Talley, T. H. Johnson, and D. E. Bode,[1] resulting from similar experimentation performed upon PbSe surfaces.

The results of our investigation confirm that by causing the detector to view its target through a cooled aperture, thus restricting background radiation, several important detector parameters can be significantly improved—as discussed hereunder.

In the experiment, pairs of detectors were fabricated and placed in demountable dewars (Fig. 1). The fabrication processes were closely monitored to ascertain that each pair of detectors was identical in its physical parameters. In addition, throughout the experiment close control was kept to maintain all pairs of detectors at the same level of sensitization.

Initially, the detectors were placed in demountable dewars of the type shown in Fig. 1; these were then evacuated. The detectors were tested at −78 °C and −196 °C and the data recorded. After testing, the detectors were remounted in permanent dewars. One detector of each pair went into a standard evaluation dewar (Fig. 2), which had neither a cooled cavity nor shielding. This detector assembly was used as a control unit in the experiment, to insure that any changes observed were due only to the cooled aperture. The second detector of each pair was placed in a cooled aperture dewar which is detailed in Fig. 3.

The refrigerant well of the cooled aperture dewar was coated with opaque paint to insure that the detector viewed a relatively cool background. The outer circumference of the coolant well was coated with platinum for both electrical and radiation shielding. The

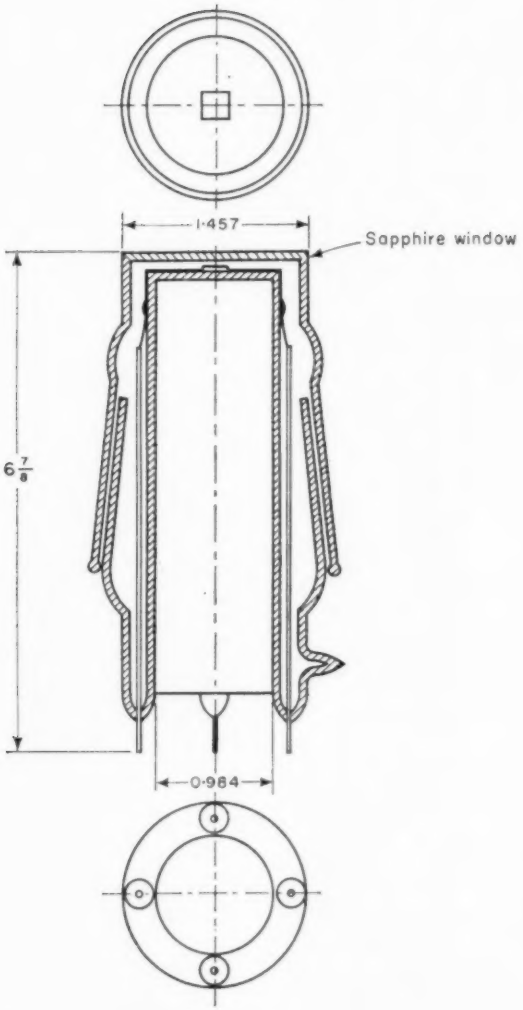

FIG. 1. Demountable dewar.

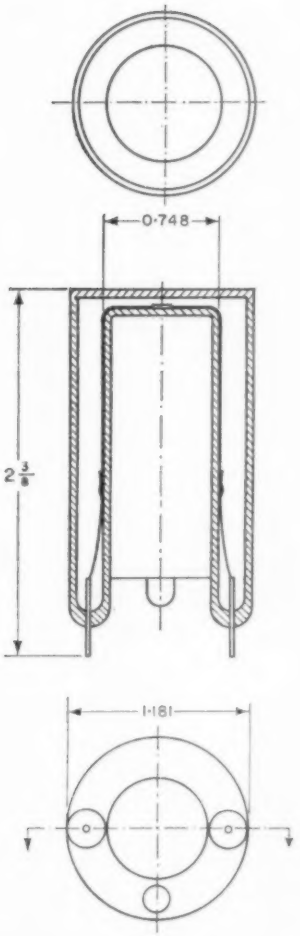

FIG. 2. Evaluation dewar.

detector was mounted at the bottom of the cavity. An aperture plate, 0·020 in. $^{+0.000}_{-0.001}$ thick with an 0·062 in. $\pm$ 0·001 aperture centered over the detector, was placed over the mouth of the cavity. This plate was also coated to block all radiation from the detector, except for that entering through the aperture. The dewar was sealed with a sapphire window.

The dewars were evacuated and the cells tested at −78 °C and −196 °C. The data, outlined in Table 1, can be summarized as follows:

1. Resistance—Increases at −78 °C ranged from a factor of 1·9 to a factor of 6·2; while increases at −196 °C ranged from a factor of 3·1 to 7·9 between non-shielded and shielded operation.

2. Signal Response—One of the two most significant changes was in the signal response;

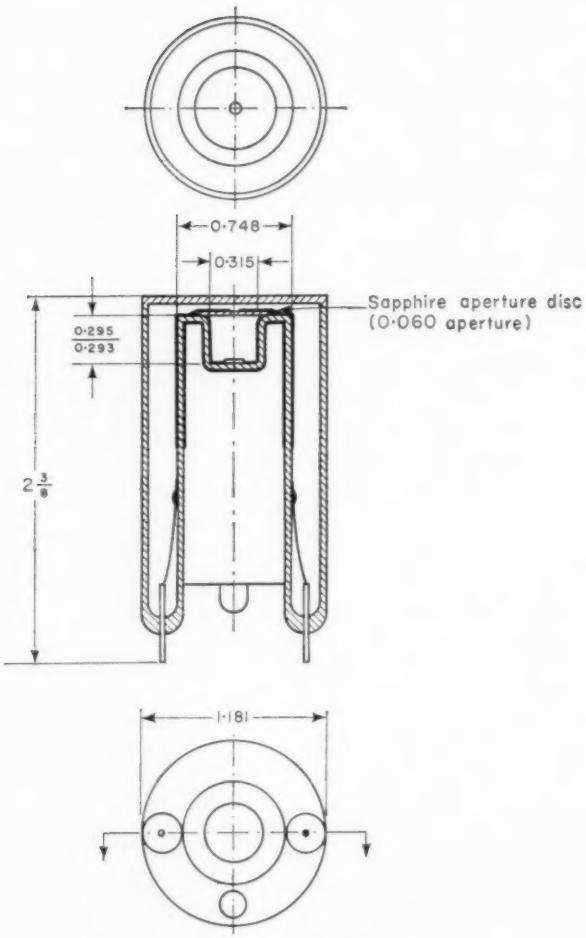

FIG. 3. Cooled aperture dewar.

it increased an average factor of 2·18 at −78 °C and 3·3 at −196 °C. This increase was much more uniform than that observed for resistance.

3. Signal-to-Noise Ratio—This increased approximately as the signal response, since the noise showed no significant change between shielded and non-shielded operation.

4. Time Constant—The data shows the time constant was shorter at −196 °C than at −78 °C when the detectors were operated unshielded. This effect was reversed when the detector was shielded. In all cases where the cell was shielded, the time constant lengthens with lowered temperature.

5. Spectral Response—This is the second really significant change. As shown in Figs. 4 and 5, the effective wavelength cut-off (30 per cent.) is increased by approximately 0·05 μ at −78 °C. However, the increase becomes 0·15 μ at −196 °C as seen in Figs. 6 and 7. This increase would be particularly important in the detection of 4·0 μ to 4·4 μ radiation.

6. Frequency Response—Figure 8 shows the signal response versus frequency. This curve

Vol. 1 1961

TABLE 1. COMPARATIVE DATA

			Test data				
Cell#	Temp. (°C)	R_{cell} (MeV)	Signal (dB/1 μV)	Noise (dB/1 μV)	S/N (dB)	μsec	Dewar
1	− 78	0·21	42	+20	22	1400	
2	− 78	1·3	47·5	+20	27·5	2500	Shielded
1	−196	0·48	59·5	+20	39·5	1000	
2	−196	3·8	71	+21	50	3000	Shielded
3	− 78	0·45	48	+25	23	1000	
4	− 78	2·5	54	+24	30	2100	Shielded
3	−196	1·0	64	+21	43	800	
4	−196	7·0	75	+22	53	2300	Shielded
5	− 78	0·13	51	+14	37	1000	
6	− 78	0·33	58	+14	44	2000	Shielded
5	−196	0·31	56	+13	43	800	
6	−196	1·3	66	+13	53	2400	Shielded
7	− 78	0·16	52	+16	36	1200	
8	− 78	0·41	60	+15	45	2400	Shielded
7	−196	0·40	58·5	+16	42·5	1000	
8	−196	2·1	69	+17	52	3000	Shielded
9	− 78	0·043	45	+ 6	39	1400	
10	− 78	0·082	52	+ 6	46	3000	Shielded
9	−196	0·16	50	+10	40	1200	
10	−196	0·50	59	+11	48	3500	Shielded
11	− 78	0·5	47	+ 5	42	1500	
12	− 78	1·5	54	+ 4	50	2800	Shielded
11	−196	1·3	52	+10	42	1000	
12	−196	5·9	62	+11	51	2300	Shielded

gives indication of the dual or multi-time constant effect that we have noted when detectors are unshielded. This disappears when the detectors are shielded.

The results of this experiment seem conclusive in that increased PbS detector performance can be obtained by using the cooled aperture and cooled cell technique. The two aspects of cell performance most affected are responsivity and spectral distribution of response.

Subsequent discussion with N. Anderson of Infrared Industries, Inc., brought forth the possibility that the unchanging noise figures might be attributed to 90 c/s being a crossover point for the noise spectra unapertured versus the noise spectra apertured. We are, therefore, in the process of compiling data on the variation of signal-to-noise ratio with frequency and temperature for shielded and non-shielded operation. In addition, we are investigating the results of operation with and without cooled filters. Current data shows an increasing slope of noise versus frequency as temperature is decreased. This ranges from approximately 2 dB/octave at room temperature to 6 dB/octave or more at very low temperatures.

Finally, the empirical data presented herein shows increased responsivity, extended spectral response and increased time constant, indicating that PbS is background limited at −78 °C and lower. Estimates are that very sensitive PbS cells can be background limited at temperatures as high as −20 °C.

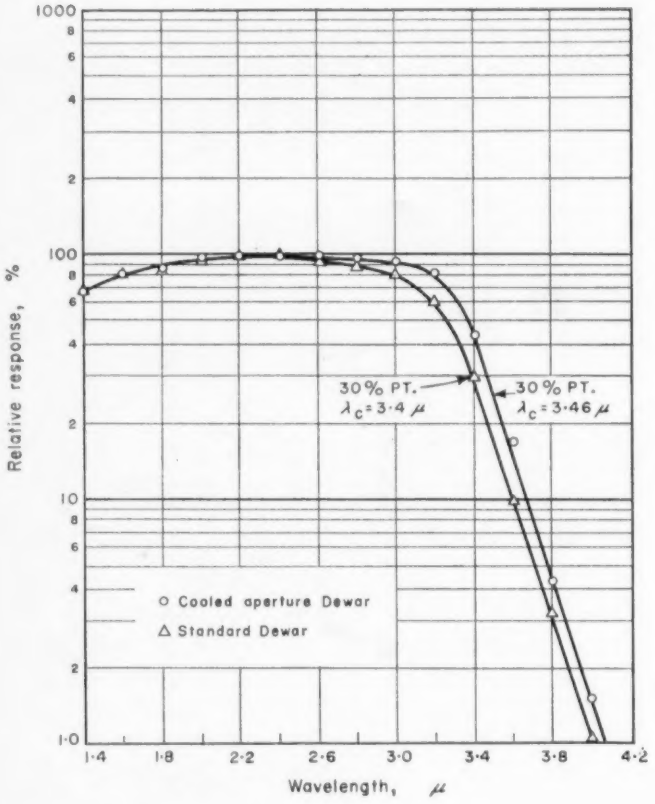

FIG. 4. Spectral distribution of response curves normalized at 2·4 μ temperature = −78 °C.

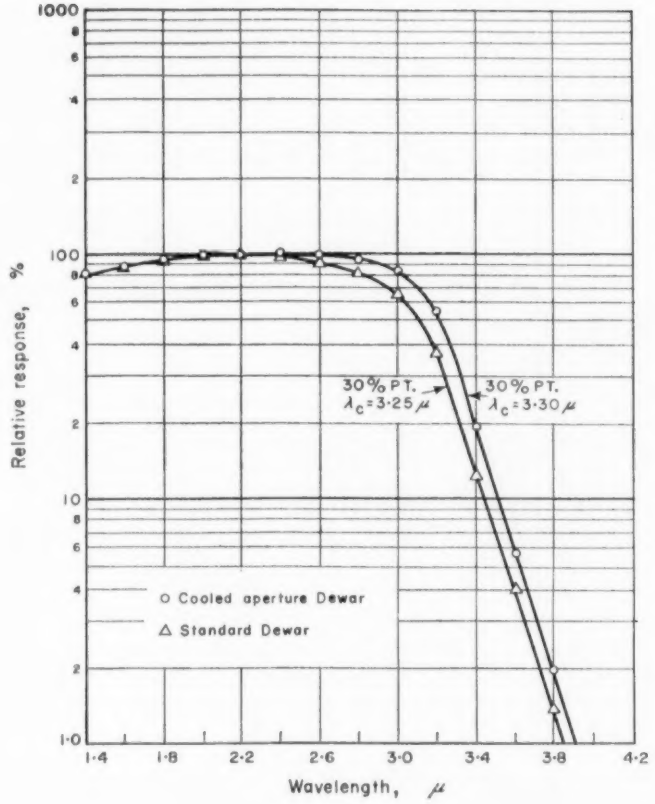

FIG. 5. Spectral distribution of response curves normalized at 2·3 μ temperature = −78 °C.

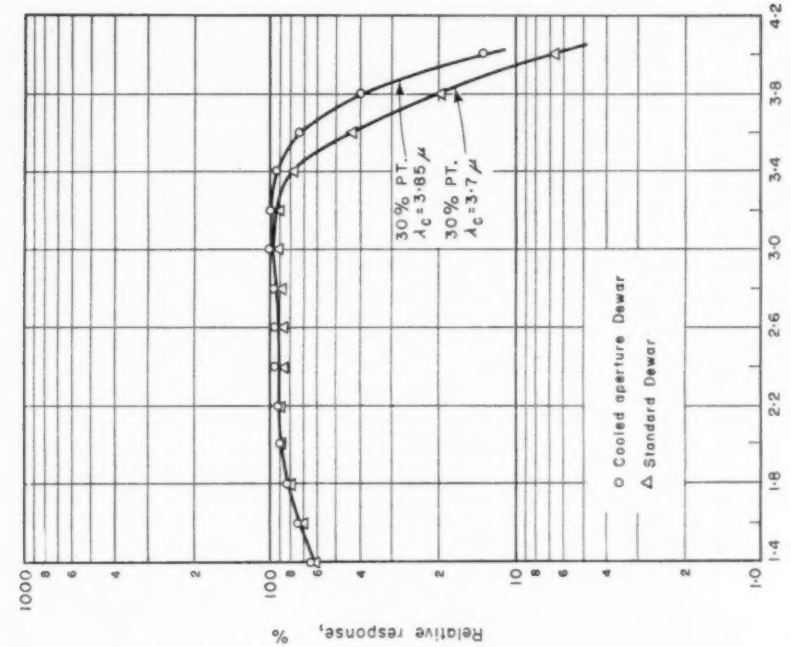

FIG. 7. Spectral distribution of response curves normalized at 3·0 μ temperature = −196 °C.

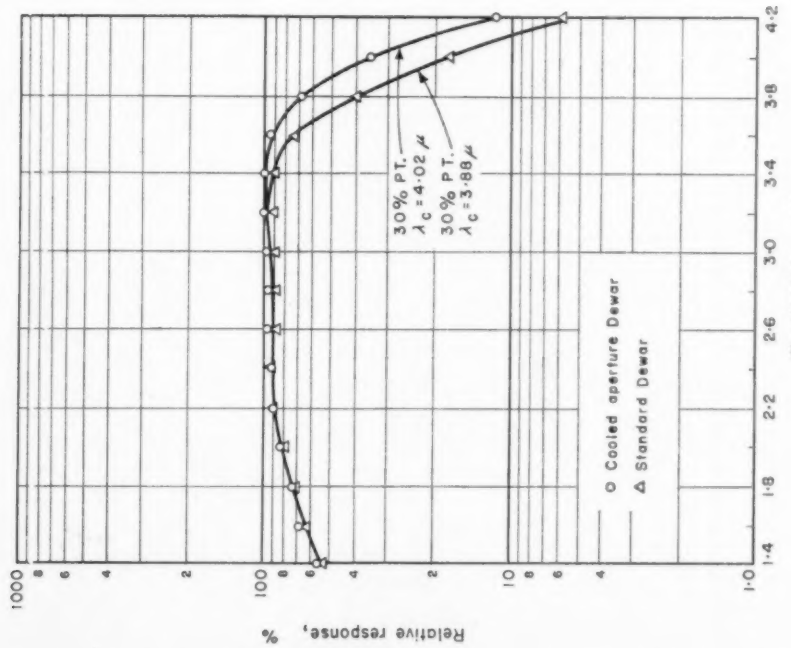

FIG. 6. Spectral distribution of response curves normalized at 3·2 μ temperature = −196 °C.

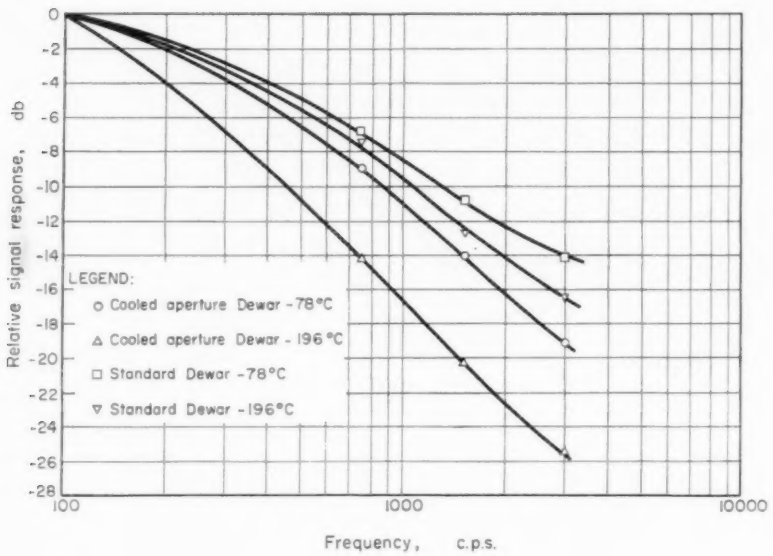

FIG. 8. Frequency response.

Test Conditions

Source: 500 °K blackbody such that the r.m.s. value of the total radiation incident on the detector equals 2·2 μW/cm².
Frequency: 90 c/s
Noise Effective Bandwidth (NEB): 5 c/s
Load: Matched load conditions
Total bias: 22·5 V
Note: Total bias is the voltage across the detector and load.

REFERENCE

1. TALLEY, R. M., T. N. JOHNSON, and D. E. BODE. Private communication.

Vol. 1 1961

Infrared Physics, 1961, Vol. 1, pp. 153–162. Pergamon Press Ltd. Printed in Great Britain

INFRARED DETECTION IN BRITISH AIR DEFENCE, 1935–38

R. V. JONES

Natural Philosophy Department, University of Aberdeen, Scotland.

(*Accepted* 27 *February* 1961)

Abstract—British work on the detection of aircraft by infrared means during 1935 to 1938 was primarily directed towards a compact airborne thermal equipment giving ranges against single-engined aircraft of the order of one mile, to fill in a possible gap between minimum radar range and maximum visual range at night.

The experimental equipment developed had a crude scanning system giving directional indications of a hot or cold source in a 30° field of view; the scanning mirror was 11 cm in diameter. Thermopiles and bolometers were tried, the former being preferred; the fastest had a time constant of 10 msec. Thermionic amplifiers were used, with vibration galvanometers as indicators. Sensitivity was rather better than 10^{-8} W for 1 cycle bandwidth. The possibility of detecting aircraft by radiation from aerodynamic heating was appreciated.

Other devices tried or suggested included optical radar, an infrared detector based on the increase of thermionic emission with temperature, an infrared memory cathode ray screen, and "Window", the resonant strips used as decoys for radar.

INTRODUCTION

THE work done in Germany and in America on infrared detection for military use in World War II has been published in some detail; it has recently been reviewed by Arnquist.[1] The purpose of the present account is to outline what was done in Britain between 1935 and 1938 on the application of infrared means to the detection of aircraft. The account is largely a personal one since, until I was joined in 1937 by Dr. G. L. Pickard (now Director of the Institute of Oceanography in the University of British Columbia), the total effort was solely mine. It has not been published previously; publication before the war would have been unwise, even though we had by then decided to concentrate instead upon radar. Afterwards, most of our results, some of which seem to have been ahead of contemporary work elsewhere, had been duplicated and improved upon; we therefore left them unpublished. However, in view of recent references (Blackett[2]), and for comparison with Arnquist's[1] account, it may now be of some interest to set our pre-war work in perspective. The details can be substantially verified from official documents.

Commander Paul MacNeil

In February 1935, I was developing thermopiles and bolometers in the Clarendon Laboratory at Oxford in order to investigate, with Professor H. H. Plaskett in the University Observatory, the infrared spectrum of the sun at high resolution. At this time I was approached by Commander Paul MacNeil, formerly of the U.S. Navy, who was trying to interest various governments in his infrared detector, which was based on a Moll thermopile with a mechanical circuit interrupter and an a.c. amplifier. His thermopile had broken down, and he needed a replacement urgently for a demonstration to the Royal Air Force at Farnborough. I made several thermopiles for him, using evaporated elements of bismuth and antimony on collodion film, but they broke fairly quickly and did not reach a very

high sensitivity, mainly owing to the poor electrical properties of the evaporated films. MacNeil's trial at Farnborough failed, but I subsequently saw him detect aircraft at some hundreds of yards on the ground at Croydon Airport.

The Tizard Committee

When I told the Head of the Laboratory, Professor Lindemann (afterwards Lord Cherwell) of my activities, he remarked that he had proposed infrared as a means of detecting aircraft in 1916, and that he would like to see me working on the technique officially for the British Government. General interest in scientific aids to air defence had already been aroused—both publicly and privately—by Mr. Winston Churchill, Sir Austen Chamberlain and Professor Lindemann; and two official committees (the Air Defence Research Committee, under the Committee of Imperial Defence, and the Committee for the Scientific Survey of Air Defence, under the Air Ministry) were coming into operation. The latter Committee had Mr. (later Sir) Henry Tizard as its Chairman; at its first meeting, in January 1935, it had listed infrared as a possible means of detection, but this was rapidly overshadowed by radar, following Mr. (later Sir) Robert Watson Watt's demonstration at Daventry in February 1935. As is well known, relations between Professor Lindemann and Mr. Tizard—once most cordial—had already become strained; and it may have gratified the former to have a detection technique being developed in his own laboratory which had been dismissed by the Tizard Committee, particularly since he might reasonably claim to have invented it. At that time, moreover, the possibilities of radar as an air-to-air system were not completely clear, and it was therefore prudent to consider seriously any alternative means.

Vol. 1 1961

TRIALS OF NOVEMBER 1935

The Tizard Committee doubted whether infrared techniques were worth developing, in view of the ease with which aircraft engines could be screened, but Lindemann (who had now joined the Committee) contended with reason that there must be much energy radiated from the hot exhaust gases, and he insisted that trials should be undertaken, although it was known that an investigation by Dr. A. B. Wood in 1926 had yielded negative results. The new trials, which were to have been made by Dr. J. S. Anderson of the National Physical Laboratory with myself as an independent observer, were in fact carried out with the personal roles reversed, because I at least had some infrared equipment whereas the N.P.L. had virtually none; we therefore used a copper constantan thermopile made by the method of Wilson and Epps (Jones[3]), and a galvanometer amplifier (Jones[4]). The trials, which began on 4 November 1935, bore out Wood's results: with the 500 h.p. piston engines and infrared detectors then current, there was insufficient infrared radiation from the exhaust gases, at least outside the atmospheric absorption bands, although there was considerable energy radiating from the hot surfaces of the engines.

TRIALS OF JUNE 1936

Despite this negative result, the Tizard Committee—rather surprisingly, in the strained circumstances—asked me to continue the work on a full-time basis, with the object of developing an airborne infrared detector. I had already (November 1935) outlined several schemes dependent on the use of fast thermoelements or bolometers. All the schemes involved the comparison of one element of the field of view with an adjacent element, so as to eliminate as far as possible the effects of the background, and to show up the presence of

point sources. The simplest scheme used a pair of adjacent thermoelements connected in opposition to the input transformer of an a.c. amplifier; an image of the target was to be oscillated at about 20 times/sec from one thermoelement to the other by rocking the concave collecting mirror. The most elaborate scheme used the same optical system, but the opposing thermoelements were to be replaced by an a.c. bolometer bridge operating at 500 c/s, with power fed into the bridge by making two of the arms secondary windings of a single transformer. The carrier frequency was to be amplified, and the low-frequency modulation due to any warm or cool source of small area in the field of view was to be detected after amplification. This bolometer was rather similar to the one used in 1941 by Zeiss in the Wärmepeilgerät 15.

In the first few months of 1936, I made both thermoelements and bolometers, but decided to concentrate in the first place on the former, owing to their greater simplicity, and to the need for rapid results; some bolometers made from platinum foil proved comparatively noisy, and there was no time to investigate the source of the noise. The system was tested

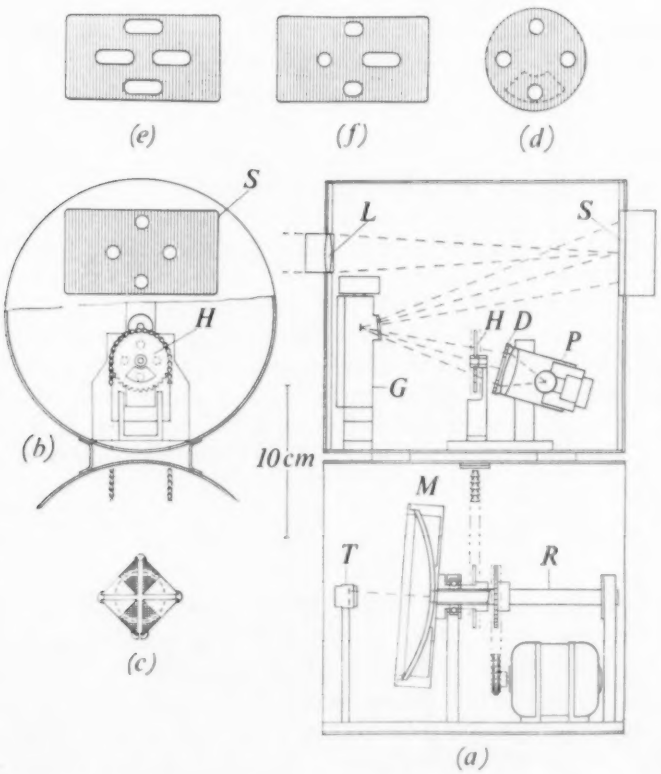

FIG. 1. (a) Section through infrared detector for airborne trials, showing general scheme of scanning system (lower compartment) and indicating system (upper compartment). (b) Axial view through upper compartment, showing form of rotating shutter H, and appearance of screen S in absence of a target. (c) Layout of 4 element thermopile, actual size about 10 mm × 10 mm; each element consists of constantan (unshaded)–manganin (shaded). Dotted line indicates track of image when target is dead ahead. (d) Frontal appearance of diaphragm D (enlarged); quadrantal sector of H shown dotted. (e) Appearance of screen when target is dead ahead. (f) Appearance of screen when target is in right sector of field.

on the ground at Farnborough in June 1936, using an 11 cm diameter collecting mirror, giving a $4° \times 1{\cdot}5°$ field of view; it was a rather simpler version of the equipment described in more detail below. The trials involved the measurement of the relative distribution of energy radiated by typical aircraft, and the detectability of aircraft in flight against clear sky and clouds; the speeds make odd reading now—one target aircraft, a Westland Wapiti, sometimes making runs at 70 m.p.h. Aircraft were satisfactorily detected in flight during daylight at ranges of about one mile; ground measurements showed that a range of two miles would be possible at night. Cloud edges in the field of view caused disturbances, but these were reduced by ten to fifty times by the interposition of a selenium powder filter in front of the thermoelements. The same filter was also used to eliminate the effect of reflected light from the aluminium-painted aircraft, since this was found to reach a magnitude comparable with that due to a hot engine. A fluorite filter was used to cut out radiation beyond 9 μ wavelength, to improve the differentiation against cloud.

It was decided that the trials were sufficiently encouraging to proceed to the next stage, which was to build an instrument to mount in an aircraft. The main improvements in this instrument were its larger field of view, a circle of about 30° diameter, and an indicating device for showing the direction of the target relative to the line of sight. The scheme is outlined in Fig. 1.

Vol. 1 1961

Scanning System

The collecting mirror M was 11 cm in diameter, and of 5 cm focal length, with the four-element thermopile T approximately in its principal focal plane. The mirror was mounted somewhat askew on a rotating shaft R, whose axis of rotation passed through the centre of T. Thus when the shaft rotated, the image of a distant point on the axis of rotation traversed a circular path on the surface of T, generating four equal thermoelectric pulses of alternate sign as the image fell on each element in turn. An object on the line of sight thus gave rise to a regular alternating output of twice the frequency of rotation of the shaft. An object in the field of view off the line of sight gave a signal for that part of the rotational period in which its image was made to fall on the thermopile, whose output thus contained phase information giving roughly the direction of the target relative to the axes (up/down and right/left) of sight.

Thermopile

The four elements of the thermopile (Fig. (1c)) were mounted to fill a square of 10 mm size. Each element was in the shape of a 45° set square, and was made of constantan–manganin foil; this foil was made by butt-welding a rod of constantan to one of manganin, and rolling the composite rod into foil, the rolling direction being in the plane of the weld. The ultimate thickness was about $0{\cdot}1\ \mu$, and the best time-constant achieved (in air) was about 10 msec; an averagely good time constant was 25 msec. The shape of the thermoelements was suitable both to the geometry of the scanning system and to thermal efficiency considerations. The four elements were connected in series to the primary of the input transformer of the amplifier, adjacent elements being connected in opposition. Various metallic blacks were tried, but the curious fact was found that—providing the thermopile was operated at normal atmospheric pressure, as it was in this apparatus—a carbon black from a camphor flame had little harmful effect on the time constant.

Windows

Various materials were investigated, the objective being an infrared transmitting material obtainable in sufficient strength and size to permit a 6 in. aperture in the fuselage. Mica of 30 μ thickness, reinforced by a grid of thin steel wire, was fairly successful; but it was decided to grow single crystals of silver chloride and bromide (thallous chloride, bromide, and iodide were also considered, but were not actually grown, because they were said to produce disconcerting physiological effects). Single crystals of silver chloride and bromide were grown in 1937 up to about 250 g in weight, and windows made from them. The surfaces were protected from actinic action by evaporated layers of selenium.

This work was the origin of the crystal-growing programme undertaken at Aberdeen after the war ended.

Amplifier

Several four-stage amplifiers were built, but a three-stage R–C coupled amplifier was sufficient for operating the indicating system. The thermopile (resistance about 10 Ω) was coupled to the amplifier by a mumetal-cored 1:300 transformer made by Ferranti Ltd. The transformer was screened by a double mumetal shield surrounded by a $\frac{1}{4}$ in. soft iron screening box, but there was still some trouble with inductive pick-up in the transformer, and with low-frequency microphonic effects.

Indicating System

In the 1936 trials, the indicator was a simple vibration galvanometer, tuned to the oscillation frequency of the mirror. More elaborate schemes involving phase-sensitive rectifiers of the commutator type were contemplated, but the urgency for a demonstration of the possibilities of infrared detection made the simplicity of the vibration galvanometer a key factor.

Similarly, for the 1937 trials, a direction indicating system involving a cathode-ray presentation was considered, but it was found that the vibration galvanometer could be adapted for the purpose. The galvanometer G was mounted in a brass tube on top of that containing the mirror and thermopile. A small projector system P was used to illuminate the galvanometer mirror, and an image of the diaphragm D (immediately in front of P) was focused on the screen S after reflexion in the galvanometer mirror. The diaphragm D had four circular holes in it, arranged at the corners of a square with one diagonal vertical (Fig. 1(d)); a rotating shutter H was mounted in front of D, with a quadrantal sector cut in it so that light from only one of the holes in D passed through H at any one time. The shutter H (made from a "Meccano" sprocket wheel) was coupled to a similar sprocket wheel on the axis of rotation of the main mirror M and the phasing of the sector arranged so that the sector "selected" the top illuminated spot on the screen S as the image of the target was at the highest point of its circular path on the surface of the thermopile T.

If a target was dead ahead, the path of its image crossed all four elements of the thermopile, and four kicks in turn were delivered to the galvanometer. This was rather less than critically damped with a natural frequency twice that of the mirror rotation frequency, and thus gave four kicks (two forwards and two backwards) for each revolution of the mirror. Each kick was indicated by the appropriate light spot on S, and the appearance was as indicated in Fig. 1(e); owing to the frequency of repetition of the kicks, each light spot appeared to be drawn out into a continuous band. The amplitude of the bands gave an indication of the strength of the target. If a target was to one side, the kicks during a cycle

of the mirror varied in magnitude, and caused the pattern on the screen to change, in such a way that a rough estimate could be made of the direction in which the apparatus had to be turned in order to look directly at the target (Fig. 1(f)).

A lens L was added to project a direct picture of the view ahead on to the screen S, so that both visual and infrared information was available on one screen.

The indicating system worked well, at the expense of the integration that was lost by damping the galvanometer, and operating it at a high frequency. The rotation frequency of the mirror was about 20 c/s, and the galvanometer was operating at twice this frequency; the thermopile elements had to respond substantially in about 1/80 sec.

Results

The noise limit of the thermopile and amplifier, when used with a vibration galvanometer giving an effective integration time of about 1 sec, was rather better than 10^{-8} W noise equivalent power; when used with the direction indicator, the performance was not as good. One "demonstration" with the instrument was to project the light spot from a hand torch on to a black screen about five metres distant, and to "scan" the screen with the infrared detector after the torch had been switched off. It could detect the region that had been warmed by the incident light one minute after the light had been switched off.

Vol. 1 1961

In the field, ground-to-air detection ranges of about two miles were achieved, using the 11 cm diameter mirror. In flight, the range fell to rather less than 800 m on single-engined aircraft owing to the increased noise level arising from microphonic disturbance. The flight test was on 27 April 1937, when a Vickers Vincent (Bristol Pegasus III air-cooled engine, 635 h.p.) was detected in the broadside-on position at about 500 m range. This may have been the first occasion on which one aircraft was detected in flight from another by infrared means.

Unusual observations in the evening of 30 August 1937 on an Armstrong-Whitworth Whitley aircraft with Armstrong-Siddeley Tiger engines suggested that radiation from the engines might not be the only means of infrared detection of aircraft in flight. This aircraft was on the ground and was being viewed from the top of a building; it was found that the galvanometer deflexion decreased as the engines were warmed up. It turned out that the aircraft had been standing under cover all day, and that its fuselage was therefore at a lower temperature than the ground beneath. It was therefore giving a large indication which was substantially reduced as the engines warmed up; this led to an investigation of the possibility of detecting aircraft by the temperature difference between fuselage and background. Calculations showed that with the 1937 apparatus an aircraft of frontal area 100 ft^2 travelling at 150 m.p.h. should have been detected from the front at about one mile against a clear night sky background, using aerodynamic heat alone. This possibility was therefore proposed as an alternative means of aircraft detection.

In the foregoing connection, we measured the effective black-body temperatures of the clear sky and of low cloud at night in Oxford, by the simple method of hanging a suitable black body from a gibbet, and viewing this against the background of cloud or sky with the infrared detector. When the black body was adjusted to the appropriate temperature, the signal from the detector vanished, since the detector measured any difference in radiation coming from different parts of the field of view. At ground level, the effective clear sky temperatures measured (in September 1937) were about -5 °C; cloud temperatures were about $+16$ °C.

THERMIONIC DETECTOR AND PICTURE DEVICE

An attempt was made to develop a thermal picture apparatus. The principle was to replace the normal cathode of a photoelectric image converter by a thin foil blackened on one side, and coated with a low-work-function thermionic emitter, such as caesium–silver oxide. The increased thermionic emission caused by heating due to the incidence of infrared radiation would cause a brightening of the appropriate region of the fluorescent screen of the image converter, which could thus be made to register a thermal picture. A Secret Patent was granted for this device: crude trials in 1937 with a tube made by E.M.I. Ltd. showed coarse images of hot sources. It was also proposed to develop a simple detector using thermionic emission, with chopped incident radiation, in place of a thermopile or bolometer, but the development ceased when a policy decision stopped infrared work in the Air Ministry in 1938.

PULSED SEARCHLIGHT AND OPTICAL RADAR

Another device which was outlined in some detail was the pulsed searchlight. This arose out of our attempts to eliminate the back-scattered glare from a visible searchlight, by using an infrared system, with an image converter. There was no improvement, because any reduction in back-scatter was offset by the comparative insensitivity of image converters, but the work stimulated the conception of a pulsed searchlight, with an image converter which was to operate as a shuttered detector by the appropriate pulsed application of its accelerating potentials. The device could be used as an optical radar, or as a picture device sensitive only after the back-scattered radiation from the nearer part of the searchlight beam was behind the receiving lens, thus eliminating the glare from the nearer part of the beam; it was also contemplated, alternatively, to sensitize the image-converter to light scattered back from the portion of the beam beyond the target, so that this might be seen in silhouette—rendering the system effective against black-painted aircraft. The original memorandum, dated 27 January 1938, reposed in an Air Ministry file until October 1939, when the Tizard Committee expressed interest, but it was then thought too long term a project to start.

INFRARED MEMORY TUBE

A further device which was of some subsequent interest was an infrared operated memory device. The research establishment at Bawdsey had asked for ideas to improve the signal–noise ratio for radar in the presence of jamming. One obvious way was to integrate many successive sweeps of the cathode ray tube, since the echo from an aircraft then showed up as a "nick" in the baseline, cutting into the illumination above the baseline caused by the noise.

The use of slow decay phosphors in the screen was suggested for this purpose, but it was found that these phosphors could not be stimulated effectively by electron bombardment. Sir Thomas Merton therefore suggested a two-component screen, consisting of a fluorescent component which was stimulated by the electron beam, and a phosphor component which was stimulated by the light from the fluorescent component. This device was very satisfactory, and is still in use. Another scheme, which originated with me in 1938, was to use the type of phosphor which is primed by ultraviolet light, and which emits the stored energy as visible light when triggered by an infrared photon. Trials showed that electron bombardment was effective in priming this type of phosphor, and that a "memory" tube could thus

be built which stored up many sweeps of the time base, which could all be shown up simultaneously by flooding the screen with infrared light. This device has since been successfully brought into use.

PHOTOCONDUCTIVE DETECTORS

While photoelectric detectors would have been much more convenient for aircraft detection, we thought that we should very probably have to cool them for successful operation. Our attempts in that direction were much inhibited, partly by the shortage of time, and partly by the advice of a Government Establishment, which had worked on infrared photoconductive cells for eighteen years and which stated that it had tried a very wide range of substances, and that none had been found to go much beyond the Case "Thalofide" surface. Despite, therefore, Lange's publication of the photoconductivity of lead sulphide out to about 3 μ wavelength, little was done in this field in Britain, most regrettably, before 1944; although I did construct an apparatus for evaporating and evaluating photoconductive surfaces at the Admiralty Research Laboratory for the late C. A. Luxford to use in 1939.

Vol. 1 1961

TERMINATION OF THE OXFORD INFRARED WORK

By September 1937 infrared was shown to be a feasible means of detecting one aircraft from another, but it had two important disadvantages. It would not work through cloud, and it gave no range information. Neither disadvantage was in itself fatal, but in March 1938 the system was abandoned on the recommendation of the Tizard Committee in favour of radar. The decision was substantially a correct one: I at least had all the time realized that radar was potentially a much more powerful technique, and had been rather surprised to be told, as I was in 1936, that it was not very promising for airborne use. It transpired that the doubt had arisen because at that time it was uncertain whether radio pulses of less than a few microseconds duration could be generated, and whether a receiver could recover sufficiently rapidly from the effects of the transmitter pulse to give a minimum range of less than a mile. Had these defects materialized, we might have had an awkward gap between the range at which radar became ineffective and that at which the pilot's eyes could take over. It was only in view of this that I had spent the effort in developing an infrared method.

At the time that we stopped, in March 1938, we were probably ahead, as may be judged from the records, of any other country, with the important exception of the photoconductivity work in Germany. We believed that the ultimate solution would probably lie in a fusion of the 1·5 m radar and infrared philosophies, leading to a system using a wavelength long enough to penetrate cloud, and short enough to be focused. On 4 November 1937 I had concluded that "salvation lies between 1 and 10 mm" in a report to the Director of Scientific Research at the Air Ministry. Unfortunately I could not see the ultimate way of generating and detecting radiation of these wavelengths; but the experience contributed to the general background that led to the initiation of the microwave programme of 1938/9.

It has recently been represented that radar and infrared were two rival methods of detection, backed respectively by Sir Henry Tizard and Lord Cherwell; and that, had the latter been able to dictate the prewar policy, Britain would have had no radar in 1940. This picture is false: Sir Robert Watson Watt has stated how valuable Lord Cherwell's support was to him in radar and, as for the notion that Sir Henry Tizard considered infrared

of no account, I may record that in October 1937 he asked me whether I would transfer from the Clarendon Laboratory to Imperial College, where he was Rector, and continue the infrared work there.

There never was, in fact, any serious rivalry between radar and infrared, nor could there have been. The former technique, obviously powerful, had a large research team (for those days) devoted to it; the latter, obviously slender, for much of the time had only myself. I had no doubts about the unrewarding prospects, but it was simply a matter of duty for someone with the appropriate experience to try to take infrared methods to their limits in case apparently better methods failed. This is a familiar type of decision where military matters are involved, although it is rarely the happiest of experiences to be the one to be selected to attempt the "forlorn hope". In retrospect, I should have been saved much personal effort had the work been stopped, as I expected that it would be, after the 1935 trials, but it might have been expecting too much to get a clear decision in the circumstances.

WINDOW

An example of Sir Henry Tizard's foresight was his recommendation in July 1937 that "The experiments now being conducted at Oxford on infrared radiation should continue in the hope that they will have an application to air defence other than the detection of aircraft from the air." In a curious way this speculation came to be justified by an unforeseen, but satisfactory, outcome; this was "Window", the resonant tin foil strip decoys designed to confuse radar.

The idea was such an obvious one that it may well have been invented by many people independently; but the first discussion of it known to me, and certainly the one that ultimately led to its use in World War II, occurred in 1937. At that time, infrared detection was being rightly criticized for being unable to work through cloud; but it struck me, in drawing a comparison between the weaknesses of the two methods, that radar, even on a clear night, might be almost as impotent as infrared would be in cloud, if the air space were cluttered up with resonant dipoles at a density of the order of a few per "resolution volume" of the radar system, and that this might be achieved with relatively small effort. The original idea, with the comparatively long wavelength then used by our radar stations, was to suspend wires of the appropriate length from small balloons, so that they would remain in the field of view for a considerable time. When Professor Lindemann told me in the autumn of 1937 that the Tizard Committee were contemplating the stopping of infrared work, I therefore pointed out this vulnerability of radar to him; as a result, I believe, Mr. Churchill raised the matter with the Air Defence Sub-Committee of the Committee of Imperial Defence. No notice appears to have been taken of the suggestion at that time; certainly no trials were made.

In the autumn of 1940, after Mr. Churchill had become Prime Minister, Professor Lindemann was able to insist that some trials be made. The results were so striking that there were many misgivings that we might harm ourselves by using it since it would show the Germans an easy way of neutralizing our radar defences; the argument went on for more than two years (and an almost parallel argument was going on in Germany). Ultimately the matter went to the Prime Minister for decision. He held a meeting in June 1943, in which it fell to me to present the final technical case for using the device. Having heard the arguments on both sides, he gave the decision: "Open the Window!".

CONCLUSION

In some ways, the infrared work of 1935–38 was a lost effort; it was essentially of a short-term nature since we believed, rightly, that we had very little time. It could not be published early enough to influence other infrared work, although it anticipated several developments elsewhere; and it diverted my effort from completing in 1937 what would probably have been the first superconducting bolometer. It may, however, have contributed something to the soundness of our general decisions in scientific aids to defence, and it brought me into contact with many defence problems (Jones[5, 6, 7]) in a way which was to prove unexpectedly helpful when the war occurred.

REFERENCES

1. ARNQUIST, W. N., *Proc. Inst. Radio Engrs., N.Y.* **47**, 1420 (1959).
2. BLACKETT, P. M. S., *Nature, Lond.* **185**, 647 (1960).
3. JONES, R. V., *J. Sci. Instrum.* **13**, 84 (1937).
4. JONES, R. V., *J. Sci. Instrum.* **11**, 302 (1934).
5. JONES, R. V., *Journal R.U.S.I.* **92**, 352 (1947).
6. JONES, R. V., *Research, Lond.* **9**, 347 (1957).
7. JONES, R. V., *A Physics Anthology*, (Edited by N. CLARKE), p. 121, Chapman & Hall, London (1960).

Vol. 1 1961

Infrared Physics, 1961, Vol. 1, pp. 163–166. Pergamon Press Ltd. Printed in Great Britain

COMPARATIVE PERFORMANCE OF COOLED INFRARED PHOTOCONDUCTORS

N. C. ANDERSON

Infrared Industries, Inc., Waltham 54, Massachusetts, U.S.A.

(*Received* 2 *February* 1961)

Abstract—Several cooled infrared sensitive photoconductors, i.e., PbS, PbSe, Ge, and InSb, are compared spectrally for a given set of test conditions. All cells are of best reported sensitivity. Using this basic data, relative S/N ratios are computed for various radiation sources for the following cases: (1) Use of a 3·0 μ cut-on filter to minimize high temperature background radiation, (2) assuming a 300°K background, and (3) transmission of the target radiation through the earth's atmosphere. For all cases, PbS gives superior performance because of its high spectral sensitivity in the 3·0–4·0 μ region. Also given are crossover wavelengths and crossover source temperatures for the various detectors.

INTRODUCTION

SINCE the detector is the heart of an infrared system, the infrared system designer continually strives to select the optimum detector for his particular application. This selection is often difficult to make, especially when cooled detectors are used, because of the large number of factors that must be considered. For this reason, a technique is presented in this paper to aid the system designer in the selection of an optimum detector.

The vital detector information required for consideration in a specific IR system is a noise equivalent power (NEP) versus wavelength curve for a set of test conditions that closely approximates the system requirements for the particular sensitive area and modulation frequency involved. The value of the bandwidth for noise determination is relatively unimportant since a simple computation can be made to convert NEP for different bandwidths.

Radiation source characteristics are important, i.e., blackbody radiator, plume emission or both, as is information concerning a detection requirement in the presence of one more of the following:

(1) Direct or reflected sunlight from earth or clouds.

(2) Night sky, night clouds, or night earth.

(3) The earth's atmosphere.

Workers in the infrared field generally agree that the 3·0 μ–5·0 μ spectral region, using cooled detectors, appears most promising for detection in the presence of the above backgrounds. This implies the use of a 3·0 μ cut-on filter to restrict the response of the detector below 3·0 μ.

Use will now be made of the NEP versus wavelength curves for cooled detectors together with the appropriate radiation source data to calculate relative S/N ratios for various sources using a 3·0 μ cut-on filter and assuming a 300 °K background radiation.

RELATIVE S/N RATIOS TO BLACKBODY SOURCE USING A 3·0μ CUT-ON FILTER

For this and subsequent calculations, the following representative conditions are established: (1) Modulation frequency of 1000 c/s, and (2) sensitive area of 1 mm $\times$ 1 mm. The bandwidth chosen for the calculations is 5 c/s.

The detectors to be compared are PbS, PbSe, Ge, InSb, all cooled to $-196°C$, as well as a PbS cell cooled to $-78°C$.

The source temperatures are 400°K, 500°K, 800°K, and 1500°K.

The NEP versus wavelength curves for the various detectors are shown in Fig. 1. Also shown are the crossover wavelengths and crossover source temperatures of the detectors compared to PbS. The crossover wavelength is defined as that point on the spectral plot at which the two detectors compared have the same NEP; below this wavelength point PbS is the better detector. Likewise, the crossover source temperature is that source temperature for which the two detectors compared have the same NEP; for higher source temperatures,

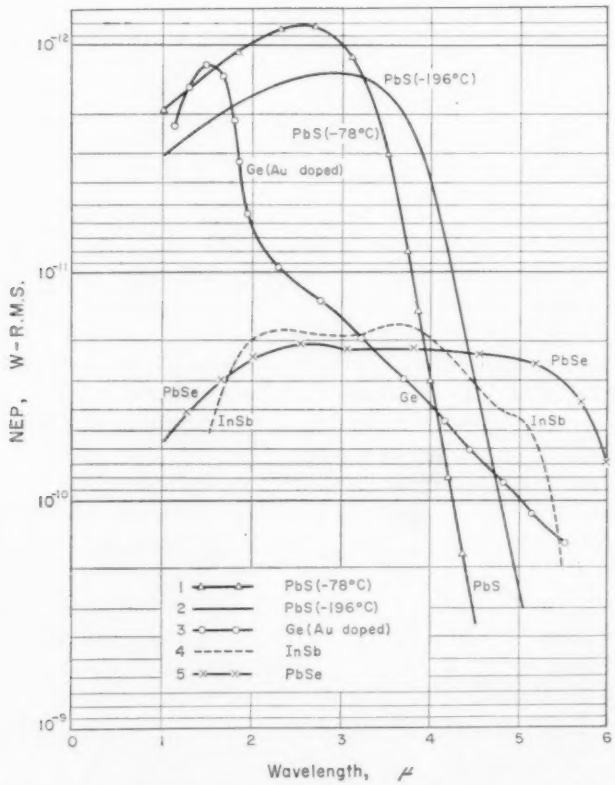

FIG. 1. Optimum NEP versus wavelength for various cooled detectors.

PbS is the better detector. The crossover wavelength is determined directly from the NEP plots. The crossover source temperatures are obtained by an integration process involving the NEP data of Fig. 1 and various blackbody spectral distributions. Then that blackbody temperature is found for which the two detectors being compared have the same NEP. A remarkable fact must be noted in reference to the crossover source data in Fig. 1; that is,

Vol. 1 1961

PbS at −196°C is a better detector of 300°K or higher sources than any other detector at −196°C, even though the peak energy of a 300°K source is at 9·7 μ and the wavelength cut-off of the PbS detector is only 4·0 μ compared to PbSe which extends out to 6·3 μ. This means, of course, that peak spectral sensitivity, which is high for PbS, is extremely important in considering the comparative advantages of two detectors.

The integration process discussed above is used to determine the relative S/N ratios of the cooled detectors to 300°K, 400°K, 500°K, 800°K, and 1500°K. These ratios are

TABLE 1

Det.	Temp. (°C)	λc	Relative S/N (3·0 μ cut-on filter) to various sources					Relative signal (3·0 μ cut-on) to 300 °K background radiation			
			300°K	400°K	500°K	800°K	1500°K	400°K	500°K	800°K	1500°K
Ge	−196	4·5 μ	1·0	1·0	1·0	1·0	1·0	1·6	2·8	3·9	5·0
InSb	−196	5·3 μ	2·7	2·0	1·4	1·1	1·0	1·2	1·4	1·6	1·9
PbSe	−196	6·3 μ	5·5	3·4	2·0	1·4	1·1	1·0	1·0	1·0	1·0
PbS	−196	4·0 μ	5·3	6·7	7·3	9·0	11·0	2·0	3·8	6·6	10·5
PbS	− 78	3·5 μ	2·4	4·3	5·3	9·0	12·0	2·9	6·1	14·4	25·0

Standard test conditions
(1) Cell area = 1 mm × 1 mm
(2) Mod. freq. = 1000 c/s
(3) Bandwidth = 5 c/s.

shown in Table 1 together with the signal to 300°K background ratios that should be obtained on these detectors for various source temperatures. All of the results shown in Table 1 are for a 3·0 μ cut-on filter. It should be noted that in all cases where 300°K background radiation is assumed unimportant, the best detector is a PbS cell at −196°C for

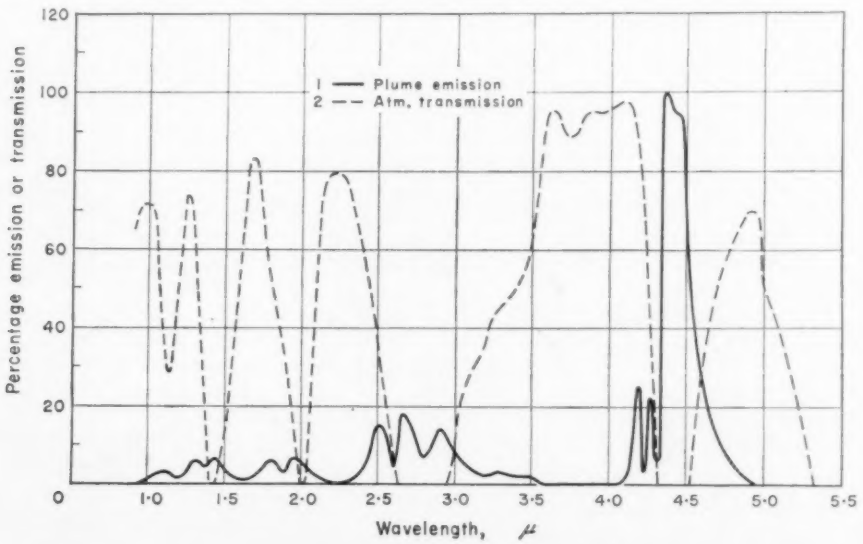

FIG. 2. Plume emission and atmospheric transmission.

source temperatures below 800°K and PbS at −78°C for sources above 800°K. For all sources where 300° K background may limit the detectivity of the detector, the PbS cell at −78 °C is superior.

RELATIVE S/N RATIOS TO PLUME RADIATION

Similar integration techniques can be used on plume type radiation. Fig. 2 shows a typical plume emission characteristic as represented by emission spectra of a bunsen flame taken by E. Plyler of the Bureau of Standards. The integration process was used for plume radiation, with and without the 3·0 μ cut-on filter; also for plume and 500°K source radiation as it passes through the earth's atmosphere. The resulting comparison data is shown in Table 2 for PbSe at −196°C, PbS at −196°C, and PbS at −78°C.

TABLE 2

Det.	Det. temp. (°C)	λc	Relative S/N			Relative S/N 3·0 μ cut-on		Relative S/N 3·0 μ cut-on atm. trans.	
			Plume	600°K	500°K	Plume	500°K	Plume	500°K
PbSe	−196	6·3 μ	1·0	1·0	1·0	1·0	1·0	1·0	1·0
PbS	−196	4·0 μ	5·9	6·0	4·0	5·0	3·7	5·6	5·0
PbS	− 78	3·5 μ	7·8	7·2	4·0	4·2	2·7	4·8	3·2

Standard test conditions
(1) Cell area = 1 mm × 1 mm
(2) Mod. freq. = 1000 c/s
(3) Bandwidth = 5 c/s.

Some of the interesting conclusions to be derived from analysis of the data in Table 2 are

(1) The equivalent blackbody temperature for plume radiation using detectors with wavelength cut-offs in the range of 3·5 μ to 6·3 μ is about 600°K.
(2) PbS at −78°C is the best detector for unfiltered plume radiation.
(3) PbS at −196°C is the best detector for plume radiation using a 3·0 μ cut-on filter.
(4) PbS at −196°C is the best detector for plume radiation using a 3·0 μ cut-on filter and assuming normal atmospheric transmission losses.
(5) PbS at −78°C is the best detector for plume radiation assuming the 3·0 μ cut-on, atmospheric transmission losses, and a 300°K background condition. The relative S/N ratios are
   (a) PbSe — 1·0
   (b) PbS (−196°C)— 5·9
   (c) PbS (− 78°C)—11·0

CONCLUSIONS

An integration process has been used to calculate comparative S/N ratios for stated source and background radiation conditions. The results show that high peak monochromatic sensitivity, such as exhibited by PbS, is more important than wavelength response, especially for detection in the presence of low temperature background. It is hoped that some of the ideas advanced here may be useful in determining an optimum detector for other source and background conditions.

Vol. 1 1961

Infrared Physics, 1961, Vol. 1, pp. 167–174. Pergamon Press Ltd., Printed in Great Britain.

INFRARED MEASUREMENT OF THE OPTICAL CONSTANTS OF THE LOW MELTING TEMPERATURE GLASS SYSTEM OF 30% ARSENIC – 34% SULFUR – 36% THALLIUM

P. S. McDermott, R. L. Powell and E. R. Stack*

International Business Machines Corporation, FSD Space Guidance Center,
Owego, New York

(*Received* 31 *May* 1961)

Abstract—The low melting temperature, heavy metal sulfide glass system of arsenic, sulfur, and thallium has proven to be optically clear from 1 to 23 μ in wavelength. The optical constants, consisting of absorption coefficient, reflection coefficient, extinction coefficient, and refractive index, have been determined from 2 to 23 μ in wavelength. The reflection coefficient was calculated from a plot of transmission measurements as a function of sample thickness, extrapolated to zero thickness. In turn, this data, through the application of the Kramers–Kronig relationship, has yielded both the real and imaginary portions of the refractive index.

As a result of the low working temperature of this composition glass, the possibility exists of manufacturing lenses and domes by molding between Teflon dies and other materials.

INTRODUCTION

The ternary and quaternary systems of arsenic, sulfur, selenium, and thallium, demonstrating glass properties, were first reported by Flaschen, Pearson, and Northover.[1] These glasses have been called low melting temperature glasses because of their relatively high fluidity between the temperatures of 125° and 350 °C.[1] This low working temperature permits the glasses to be shaped or molded between sheets or dies of Teflon[2, 3] or other materials. Further work with these glasses has shown them to be optically transmitting in the conventional sodium chloride region in the infrared region from 2 to 15 μ in wavelength.[2, 4] This material can be vacuum deposited and used as a lens coating, either optical or protective in nature.[2] Because of these favorable characteristics, an investigation of the specific optical properties of a single representative composition of these glasses was undertaken.

EXPERIMENTAL

All the optical measurements were made from a single composition of 30%As–34%S–36%Tl. This glass was purchased in "chunk" form from Baker and Adamson,† and was further worked by pressing, at an elevated temperature, into disc shapes for optical measurements. These discs were produced on a specially constructed jig shown in Fig. 1. The framework of the jig was made of aluminum with the pressing faces, as illustrated, being constructed of Pyrex glass.

Three copper–constantan thermocouples were used to monitor the temperature of the

* Hughes Research Laboratories, Malibu, California.

† General Chemical Division, Allied Chemical Co., 40 Rector Street, New York 6, New York.

pressing apparatus. As illustrated in Fig. 1, thermocouples Nos. 1 and 2 were in physical contact with the Pyrex glass pressing plates and thermocouple No. 3 was cemented to the back portion of the aluminum frame. All the thermocouples were fixed in position by Sauereisen cement. The temperature reading resulting from thermocouples Nos. 1 and 2

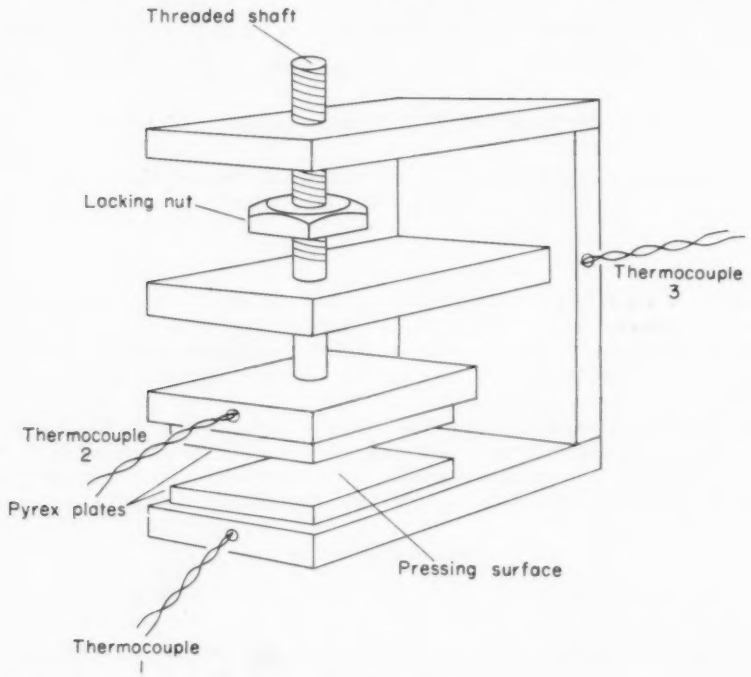

Fig. 1. Pressing jig.

were recorded continuously on a dual pen potentiometric recorder which was internally referenced. The temperature from thermocouple No. 3 was determined with a student-type potentiometer.

Discs were pressed for the optical measurements by placing the pressing jig on a hot plate in a hood and heating it to a temperature approaching the softening point of the low melting temperature glass. Then, two sheets of either Teflon or aluminum foil (cut just slightly larger in area than the Pyrex glass plates of the pressing jig) were placed between the glass plates of the jig. This was done because the low melting temperature glass was found not to readily wet these materials. Next, a piece of low melting temperature glass was placed between the foil, then the plunger was forced down with a pressure sufficient to make a disc of desired thickness. The plunger was then locked in place with a locking nut and the jig was removed from the hot plate and placed on an aluminum block which acted as a heat sink. The plunger, being locked in place, assured that the disc would remain flat during and after cooling. After cooling, the jig was opened and the Teflon, or aluminum, was then readily peeled off the glass disc. Aluminum was the final choice because the Teflon that was available produced a rough, non-finished surface on the pressed disc. Also, the aluminum assured a more uniform pressing temperature because of its better heat conducting

Vol. 1 1961

properties. The discs were held to an approximate diameter of 1·2 cm. The variation in the thickness was within ± 5 per cent of the total, as sampled along a diameter. The thickness measurements were made on an electronic micrometer with a tolerance of $\pm 0{\cdot}005$ mm.

Several of the discs were polished to determine the amount of optical scattering occurring at the shortest wavelengths. No appreciable difference was found between the polished and unpolished discs on transmission and reflection curves.

A Perkin–Elmer model 21 infrared spectrometer containing NaCl optics was used for the experimentally measured data from 2 to 15 μ in wavelength. A holder was designed and built to contain the discs during transmission runs such that each disc could be precisely and reproducibly placed in the beam. The spectrometer was also fitted with a reflectance attachment such that the per cent of the incident radiation reflected from a given disc could also be measured as a function of wavelength. For some of the data, the wavelength range of the spectrometer was extended by the use of a Cesium bromide prism interchange unit.

DISCUSSION

Gottlieb[5] and others[6, 7] have shown that the optical constants of refractive index n and extinction coefficient k can be determined from a knowledge of the reflection coefficient R as a function of wavelength. The reflection coefficient, however, can be determined experimentally from transmission data by measuring the transmission of samples of varying thickness as a function of wavelength. Then, by plotting transmission versus thickness at a given wavelength, an extrapolation of the curve is made to zero thickness. This extrapolated value at zero thickness, when applied to equation 1 of Fig. 2, will give the reflection coefficient for the case of a single reflection at each face of the disc, which holds in cases where either the absorption coefficient is very high or the sample is very thick. In the instance where there is a possibility of multiple reflections within the sample, the value of transmission at zero thickness is applied to equation 2 of Fig. 2. For the data presented in this paper, equation 1 was used for measured transmission values below 10 per cent. Equation 2 was applied to values of greater transmission. Thus, reflection coefficient R as a function of

1. $$\frac{I}{I_0} \equiv T(\lambda) = [1 - R(\lambda)]^2 \, e^{-\alpha t}$$

2. $$T(\lambda) = \frac{(1 - R)^2}{e^{\alpha t} - R^2 \, e^{-\alpha t}}$$

3. $$r = |r| e^{j\theta} = \frac{n - jk - 1}{n - jk + 1}$$

4. $$\theta(\omega_0) = \frac{2\omega_0}{\pi} \int_0^\infty \frac{\ln |r(\omega)|}{\omega^2 - \omega_0^2} d\omega$$

5. $$n = \frac{1 - r^2}{1 + r^2 - 2|r| \cos\theta}$$

$$k = \frac{1 - r^2}{1 + r^2 - 2|r| \cos\theta}$$

FIG. 2. Math relationship.

wavelength can be computed. Now, the complex square root of the reflection coefficient can be shown by equation 3 of Fig. 2. If $1n|r|$ (where $|r| = \sqrt{(R)}$) is known over the entire wavelength spectrum, θ at any single wavelength can be determined from the Kramers–Kronig relation (see equation 4, Fig. 2) between the real and imaginary parts of the complex function $1nr = 1n|r| + j\theta$. Once the dependence of θ upon frequency, or wavelength as the case may be, is known, n (the refractive index) and k (the extinction coefficient) follow from equations 5 and 6 of Fig. 2.

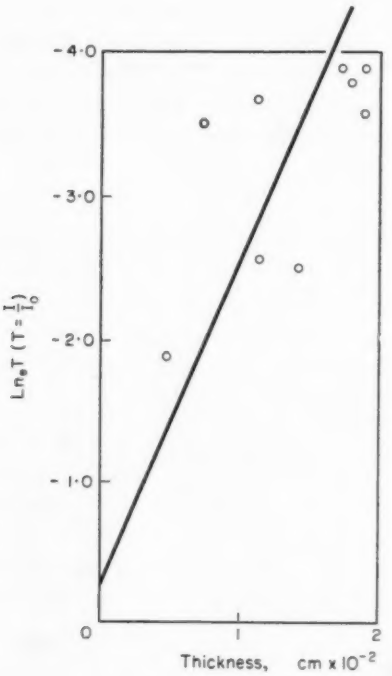

FIG. 3(a). Ln_e thickness (cm $\times$ 10^{-2}) at 5 μ in wavelength.

The transmission data taken from experimental runs had a considerable scatter when plotted against disc thickness at a given wavelength (Fig. 3). A reason for this scatter was found in the following manner: Because of the small probable error in the measured values of transmission and thickness, it was assumed that any variance of the data outside the normal experimental error was due to a changing absorption coefficient. A least-squares fit was applied to the data taken at 10 μ wavelength and the resulting line was extrapolated to zero thickness. A value of the reflection coefficient R was obtained from this plot. Assuming R to be correct, a line can be drawn from the extrapolated transmission value at zero thickness to each plotted point in Fig. 3(b). The slope of each of these lines would then be the absorption coefficient (a) for each disc. Now, for each of these points, a pressing temperature was also known and a plot of absorption coefficient versus pressing temperature was made. This plot is illustrated in Fig. 4. It is obvious from this curve that the pressing temperature, under the experimental conditions used, directly affects the value of the

Vol. 1 1961

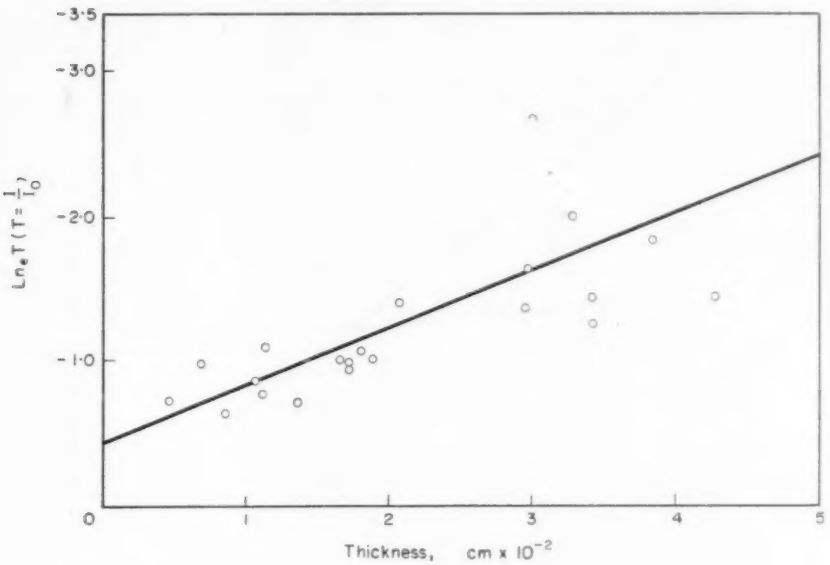

FIG. 3(b). Ln_e transmission vs. thickness (cm $\times$ 10^{-2}) at 10 μ in wavelength.

absorption coefficient. There is no explanation as to the cause of this phenomenon. A study of the transmission spectra beyond 23 μ in wavelength failed to show any differences in the absorption bands which would indicate structural changes, composition changes, or inhomogeneity from disc to disc.

The data taken from the same discs, when placed on the reflectance attachment of the spectrometer, can be handled similarly to the transmission data. Thus, an extrapolation to

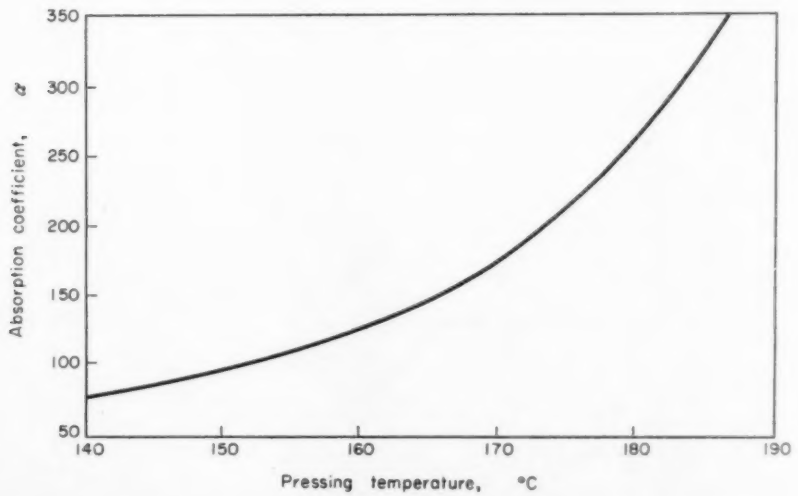

FIG. 4. Absorption coefficient (a) vs. pressing temperature (°C) at 10 μ in wavelength.

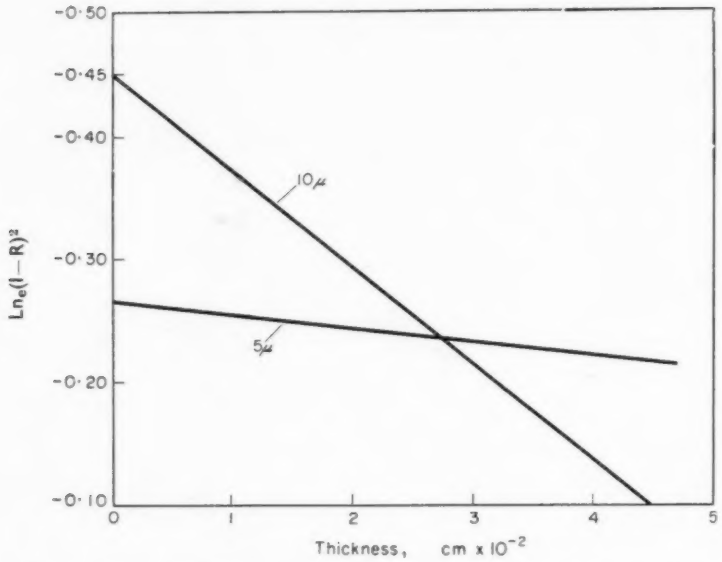

FIG. 5. $Ln_e\,(1 - R)^2$ vs. thickness (cm $\times$ 10^{-2}) at 5 μ and 10 μ in wavelength.

zero thickness of the reflectance values can lead to the computation of R, the reflection coefficient. In Fig. 5, this has been done for two particular wavelengths, 5 and 10 μ. The numerical value at which these extrapolated curves, of both transmission and reflectance, cross the ordinate axis for a particular wavelength should be equal, and this is found to be true within experimental error.

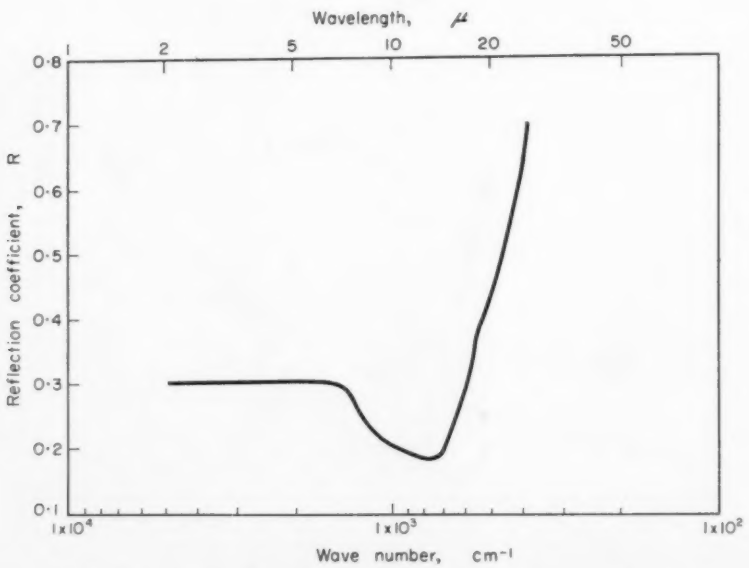

FIG. 6. Reflection coefficient (R) vs. wavelength (μ) wave number (cm^{-1}).

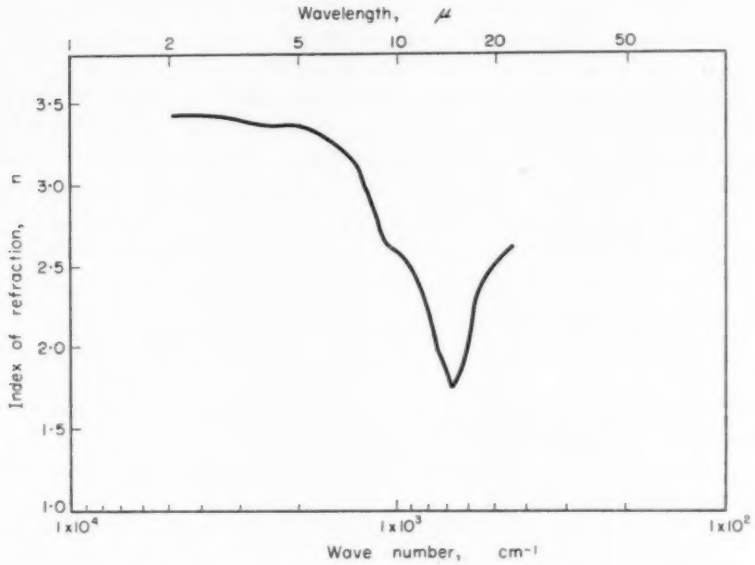

FIG. 7. Index of refraction (n) vs. wavelength (μ) wave number (cm^{-1}).

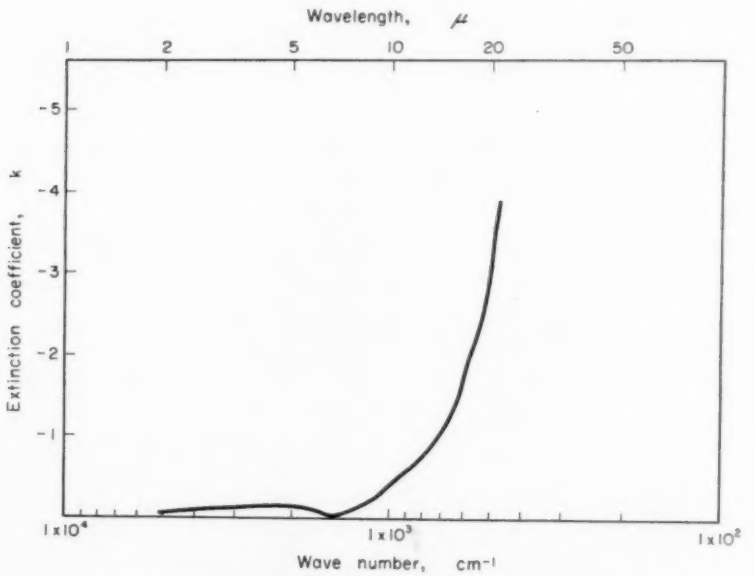

FIG. 8. Extinction coefficient (k) vs. wavelength (μ) wave number (cm^{-1}).

It is apparent from Figs. 3(a) and (b) that, as the shorter wavelengths are approached, the absorption coefficient changes much more rapidly than does the reflection coefficient.

For machine calculation of R, n, and k as a function of wavelength, transmission and reflectance values were measured at 1-micron intervals on the experimentally recorded

curves for all samples. These values were processed on an IBM 7090 computer for a least-squares treatment and extrapolation to zero thickness. The computer then generated the reflection coefficient (R) as a function of frequency for the 2–23 μ range.

In the computer solution of the Kramers–Kronig relation, the integration range was divided into three intervals, namely, (1) 2–23 μ, (2) above 23 μ, and (3) below 2 μ. It was assumed that, for region (2), R as a function of frequency was the same as the value of R at 23 μ, and that, for region (3), R as a function of frequency was the same as the value of R at 2 μ. It has been assumed that the integral is insensitive to contributions from R as a function of frequency (ω) for which $\omega - \omega_0$ is large. Neuringer[6] has indicated that this is the case. From $R(_\omega)$ and $\theta(_\omega)$, expressions were computed for $n(\omega)$, $k(\omega)$, $\alpha(\omega)$, $\epsilon_1(\omega)$, and $\epsilon_2(\omega)$. The results are illustrated in Figs. 6, 7, and 8.

CONCLUSIONS

The composition of 30% As–34% S–36% Tl can, under controlled temperature conditions, be pressed into desired forms for optical use.

The temperature at which the arsenic–sulfur–thallium glass is pressed has a decided effect on the absorption coefficient.

Knowledge of the optical constants of the arsenic–sulfur–thallium glass makes possible the useful production of lenses, domes, and coatings in the infrared region from 2–23 μ in wavelength.

Acknowledgement—The authors wish to thank D. P. Obrien for his assistance in obtaining the experimental data for this report.

REFERENCES

1. Flaschen, S. S., A. D. Pearson, and W. R. Northover, *J. Amer. Ceram. Soc.* **42**, 450 (1959).
2. McDermott, P. S., and E. R. Stack, *Studies on the Vacuum Deposition of the Low Melting Temperature Glass System of Arsenic, Sulfur, and Thallium*, 1960 Vacuum Symposium Transactions, Pergamon Press, London (1961).
3. Baker and Adamson, 40 Recter St., N.Y. 6, N.Y. Product Information Sheet, UN-1000-1.
4. Personal Communication, American Refining and Smelting Co., South Plainfield, New Jersey.
5. Gottlieb, M., *J. Opt. Soc. Amer.* **50**, 343.
6. Neuringer, L. J., *Infrared Fundamentals and Techniques*, Electrical Manufacturing Basic Science and Engineering Series, Article 15, C-M Technical Publications Corp. (1960).
7. Radiation Lab Report—M.I.T. No. 735, May 1945.

Vol. 1 1961

Infrared Physics, 1961, Vol. 1, pp. 175–186. Pergamon Press Ltd., Printed in Great Britain.

GERMANATE GLASSES: REMOVAL OF OH ABSORPTION BANDS

A. F. FRAY and S. NIELSEN

Royal Radar Establishment, Malvern, England
(*Received in amended form*, 7 *June* 1961)

Abstract—Further work on glasses containing germanium dioxide is reported. Particular attention is paid to the preparation of glasses with uniformly good transmission in the 1–5 μ region, and consequently to methods of removing the OH absorption bands.

INTRODUCTION

GERMANIUM dioxide, GeO_2, forms a glass with good transmission in the 1–5 μ region of the infrared. Unfortunately this glass is difficult to prepare and is also subject to chemical attack, being for example readily attacked by boiling water. However, addition of certain oxides and fluorides facilitates glass formation and in certain cases the glasses become more resistant to chemical attack. Previous work on this has been described [1] and further data is reported here.

Several impurities, e.g. H, Be, B, Si, N, Al, P, S, etc. give rise to absorption bands between 1 and 5 μ. Of these, H is the most common, this being present as dissolved or absorbed water, but mainly as O–H and hydrogen-bonded O–H groups in the glass network. This

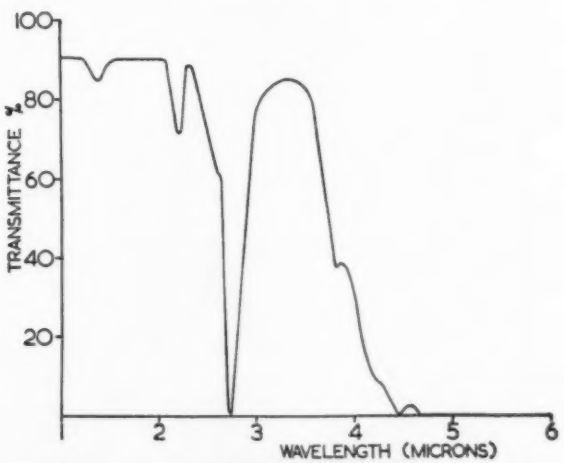

FIG. 1. Fused SiO_2 (after Adams and Douglas [2]).

has been discussed recently for silica and the silicate glasses by Adams and Douglas, [2] who assign the absorption bands at 2·73, *circa* 6·25, 1·38, 2·22 and 2·60 μ to O–H vibrations. The spectrum of fused silica is illustrated in Fig. 1. This shows bands also at 3·81 and 4·45 μ,

but these are attributed to combinations of the various Si–O vibrations. They also note that addition of modifiers to silica results in the formation of hydrogen-bonded O–H groups with a resulting shift of the absorption bands to slightly longer wavelengths. Earlier Scholze and Dietzel[3] had shown that the O–H content of silicate glasses could be conveniently estimated from the 2·85 μ absorption band. They estimated that the actual amount of water present varied from 0·04–0·08 per cent for glasses prepared from dry powders in a 10–12

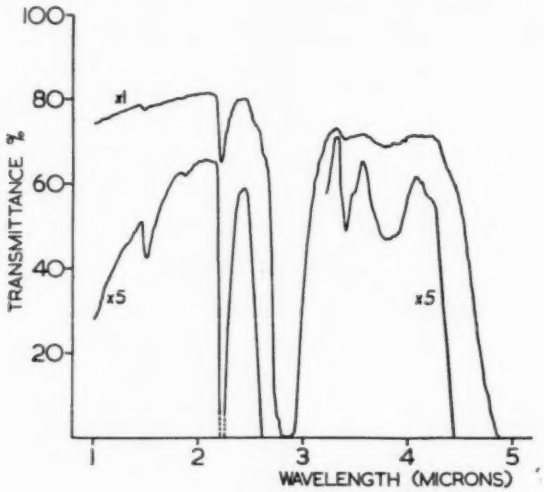

FIG. 2.
(a) Fused GeO_2 (1·5 cm thick). (×1)
(b) Expanded ordinate scale. (×5)

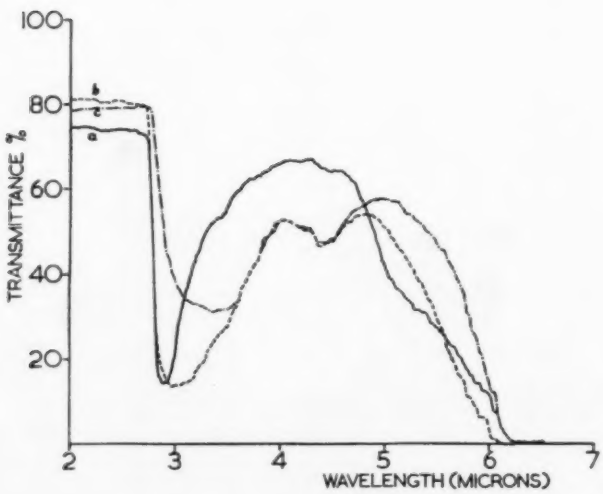

FIG. 3.
(a) GeO_2 90, PbO 10 mole per cent.
(b) GeO_2 70, PbO 30 mole per cent.
(c) GeO_2 46·3, PbO 46·4, NaF 7·3 mole per cent.

Vol. 1 1961

per cent humidity, to as high as 0·48 per cent for glasses prepared in 100 per cent humidity.

GeO_2 and glasses containing GeO_2, may be expected to behave in the same way. Figure 2(a) shows the spectrum of fused GeO_2, parts of which have been expanded (Fig. 2(b)) to define the absorption bands. Following Adams and Douglas the bands at 2·85, 2·2, 1·5 and 2·6 μ may be assigned to O–H, and bands at 3·8 and possibly 3·4 μ to Ge–O. The expected shift to longer wavelengths with increasing modifier is shown in Fig. 3. Figure 3 also shows a prominent absorption band at 4·4 μ. The intensity of this band varies as the intensity and width of the 2·85 μ band, suggesting that hydrogen-bonded O–H is responsible for this, although dissolved gases such as CO_2, perhaps associated with the O–H content may be responsible. There are indications also of a step some way before the absorption edge. Figure 4(a) shows this step beginning at 4·8 μ in a thin specimen of GeO_2. This may

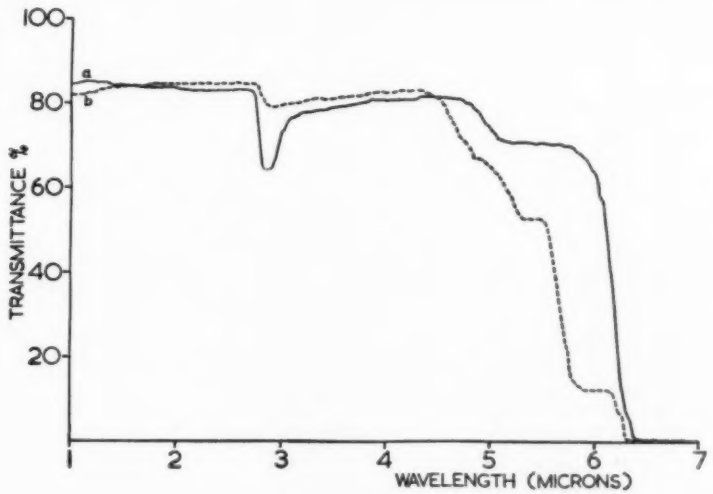

FIG. 4.
(a) Fused GeO_2 (0·5 mm thick).
(b) GeO_2 65, PbO 30, SiO_2 5 mole per cent (0·5 mm thick).

be due to an impurity in the GeO_2, and Fig. 4(b) shows that the impurity could be silica. For high transmittance in the 1–5 μ region therefore, particular impurities, especially H, must be reduced as much as possible.

Several methods may be used to remove the O–H absorption bands from glasses. These include melting in dry atmosphere, melting in vacuum, bubbling dry gases through the melt, addition of fluoride to the melt, preliminary drying of constituents, and diffusion from the solid glass. The last two methods are not usually practicable; preliminary drying of the constituents, especially GeO_2, is extremely difficult, and diffusion processes in the solid may take a prohibitively long time.[4] Harrison[5] was able to remove H from B_2O_3 glass by bubbling dry BCl_3 through the melt, and Florence *et al.*[6] showed that bubbling dry air through silicate and germanate melts gave glasses with much improved transmission. Previous work on other glass systems suggested that melting in vacuum[7] or addition of fluoride to the melt[8] were effective in moving H, and we report here on the use of these and other methods for the germanate glasses.

EXPERIMENTAL

The materials used in these experiments were of AnalaR grade, except the GeO_2 which was Johnson Matthey Spectrographically Standardised. Glasses were prepared in 5 g amounts in 0·005 in. platinum sheet bent into the form of a rectangular crucible and heated in an apparatus of the type described previously.[1] Glass specimens were obtained directly from the platinum crucible without intermediate pouring. After grinding and polishing, the transmission between 1 and 7 μ was measured on a Perkin Elmer Model 21. The curves shown here are not compensated for reflection losses and are—except where stated—for specimens 2 mm thick.

The range of glass forming compositions shown in Fig. 5 for the systems GeO_2–PbO–X_nO_m (where X_nO_m was ZnO, CdO, La_3O_3, CeO_2, Y_2O_3, BaO, Na_2O, K_2O, Li_2O) was obtained by increasing addition of X_nO_m to a GeO_2–PbO melt, until a glass no longer formed after normal cooling.

TABLE 1.

Composition (mole %)	"Softening point" (°C)	Wt lost in g/cm² area/h in H_2O at 100 °C
GeO_2 100	1050	0·1584
GeO_2 70, PbO 30	600	0·0000
GeO_2 32, PbO 48, AlF_3 20	680	0·0000
GeO_2 77·5, PbO 7·8, ZnO 12·7	680	0·0050
GeO_2 79, PbO 10, CdO 11	670	0·0019
GeO_2 84, PbO 11, La_2O_3 5	650	0·0167
GeO_2 80, PbO 18, Y_2O_3 2	600	0·0046
GeO_2 30, PbO 30, TeO_2 40	560	0·0178
GeO_2 32, PbO 48, TiO_2 20	550	0·0040
GeO_2 70, PbO 23, PbF_2 7	340	0·0070
GeO_2 63, PbO 27, Sb_2O_4 10	300	0·0010
GeO_2 80, Bi_2O_3 20	640	0·4480
GeO_2 60, Bi_2O_3 20, Sb_2O_4 20	550	0·0007
GeO_2 82·3, Na_2CO_3 10·2, $CaCO_3$ 7·5	640	0·0706
GeO_2 73, Na_2CO_3 10, TiO_2 17	620	0·0044
GeO_2 72, Na_2CO_3 9·8, ZnO 19·2	520	0·0615
GeO_2 5, TeO_2 47·5, ZnO 47·5	460	0·0459

Table 1 records a "softening point" and the resistance to boiling water of the various glasses. This "softening point" was obtained by suspending a weighted thread of the glass through a vertical furnace and recording the temperature at which the weight began to move. This procedure does not measure the true softening point but provides an indication of how the softening point may be expected to vary with composition. The resistance to boiling water was obtained by suspending glasses in boiling water for several hours, measuring the change in weight and recording the weight loss/cm² of surface/h.

Glasses were vacuum melted in platinum crucibles of the type described previously, a vacuum of 10^{-3} mm Hg being maintained by an oil rotary pump. In these experiments, the temperature of the glass was increased slowly as considerable frothing took place when melting was carried out under vacuum. When the main evolution of gas was complete (5–10 min) the temperature of the melt was increased such that the loss of material by evaporation was small, and—in general—melted under vacuum for about 30 min.

Vol. 1 1961

RESULTS

GeO_2 glasses

An indication of the glass forming regions in the ternary systems GeO_2–PbO–X_nO_m, expressed in mole per cent, is shown in Fig. 5. This illustrates, in conjunction with previous

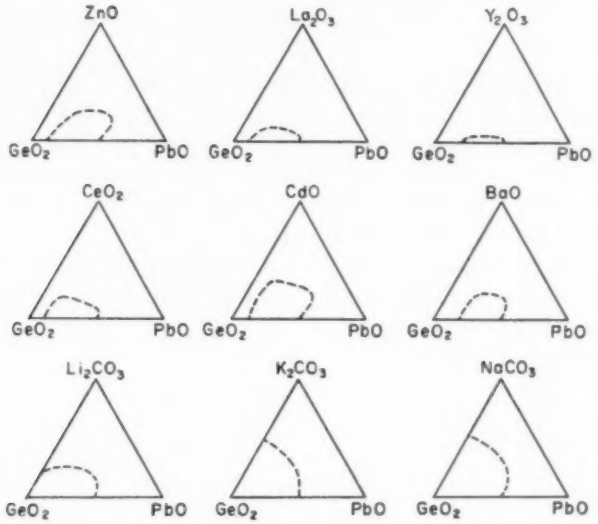

FIG. 5. Glass forming regions in ternary GeO_2–PbO–systems.

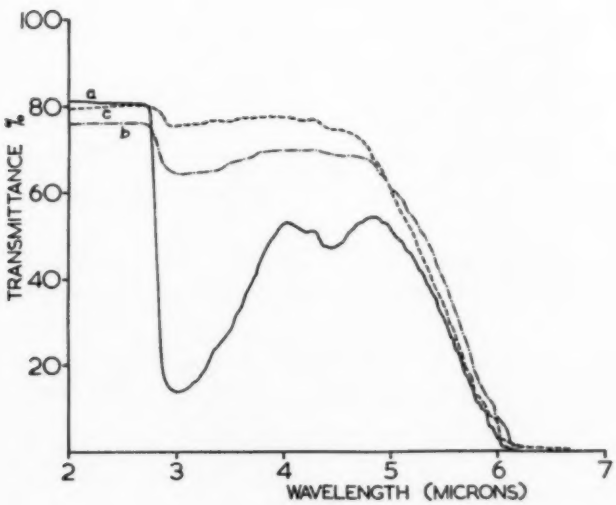

FIG. 6.
(a) GeO_2 70, PbO 30 mole per cent as prepared.
(b) GeO_2 70, PbO 30 mole per cent after melting *in vacuo* for 10 min.
(c) GeO_2 70, PbO 30 mole per cent after melting *in vacuo* for 1 h.

results,[1] that a considerable amount and variety of modifiers can be used with the GeO_2 glasses. This may be an advantage in that the cost of such glasses can be substantially reduced, and that the absorption bands due to impurities in the GeO_2, and due to Ge–O vibrations, can also be reduced. In addition, Table 1 shows that the softening points and resistance to boiling water may be altered by addition of modifiers, indicating, with previous results, that a range of properties can be obtained.

Vacuum Melting

Figure 6 shows transmission curves for a glass of composition GeO_2 70, PbO 30 mole per cent (a) as prepared, (b) after melting *in vacuo* until bubbling in the glass ceased (approximately 10 min) and (c) after melting *in vacuo* for 1 h. These and other results indicate that the rate of removal of H is initially very rapid but later becomes much slower, the final traces of H being difficult to remove. Between 2 and 4 per cent of the melt was lost by evaporation during 1 hour's melting under vacuum.

Glass compositions containing fluoride were also vacuum melted, the addition of fluoride improving the rate of removal of H. Figure 7, for example, shows the transmission curves

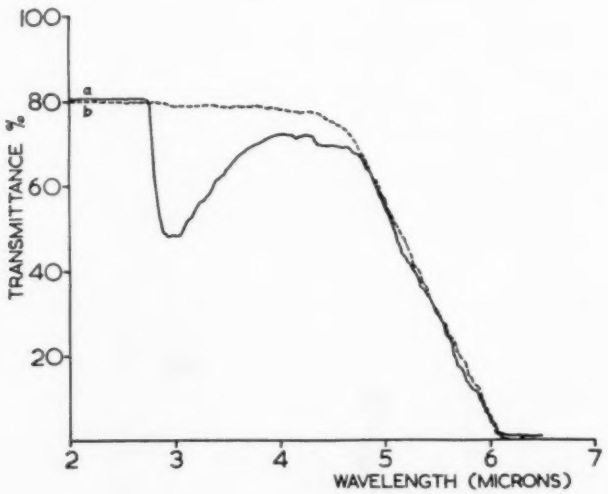

FIG. 7.
(a) GeO_2 60, PbO 20, AlF_3 20 mole per cent after $\frac{1}{2}$ h at 900 °C.
(b) GeO_2 60, PbO 20, AlF_3 20 mole per cent after $\frac{1}{2}$ h at 900 °C *in vacuo*.

for a glass of composition GeO_2 60, PbO 20, AlF_3 20 mole per cent (a) after melting for $\frac{1}{2}$ h at 900 °C and (b) after melting *in vacuo* for $\frac{1}{2}$ h at 900 °C. In this case loss of material by evaporation was about 10 per cent.

Addition of Bubbling Agents

Materials which decompose at temperatures between 700 and 1000 °C were added to glass melts to provide turbulence during melting. The materials chosen were $CaCO_3$ and Sb_2O_4. Figures 8 and 9 show that the addition of either reagent increases the rate of removal of H.

Vol. 1 1961

Bubbles in the melt were also conveniently produced by electrolysis, but this resulted in a reduction of PbO to Pb, resulting in inhomogeneous black glasses and no method of making up the oxygen deficiency was found.

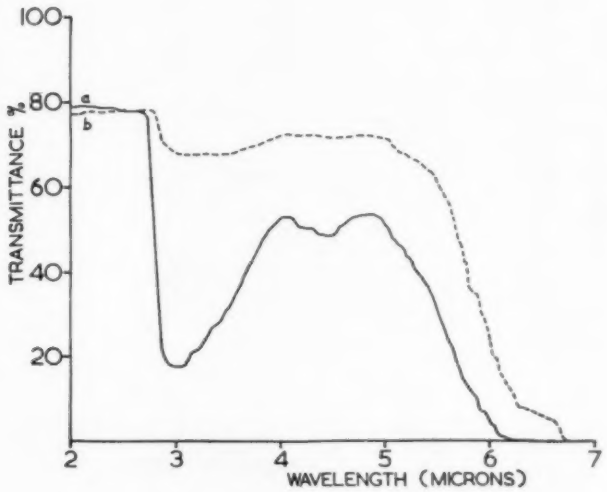

FIG. 8.
(a) GeO_2 70, PbO 30 mole per cent after 1 h at 1000 °C.
(b) GeO_2 63, PbO 27, $CaCO_3$ 10 mole per cent after 1 h at 1000 °C.

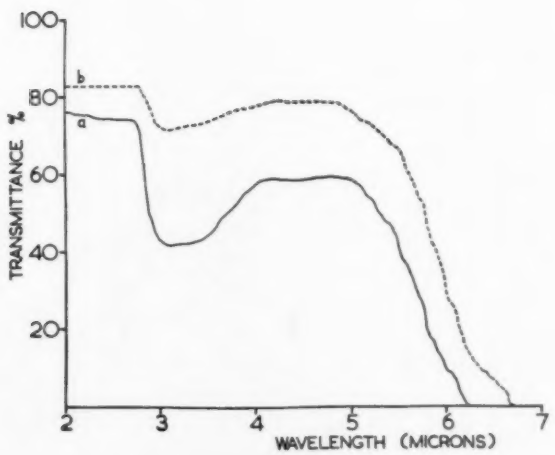

FIG. 9.
(a) GeO_2 70, PbO 30 mole per cent after 1 h at 1160 °C.
(b) GeO_2 63, PbO 27, Sb_2O_4 10 mole per cent after 1 h at 1250 °C.

Addition of Fluoride

Addition of fluoride to the melt resulted in all cases in an improved rate of removal of H. Typical results are shown in Figs. 10–12, and Fig. 13 indicates that complete removal of H

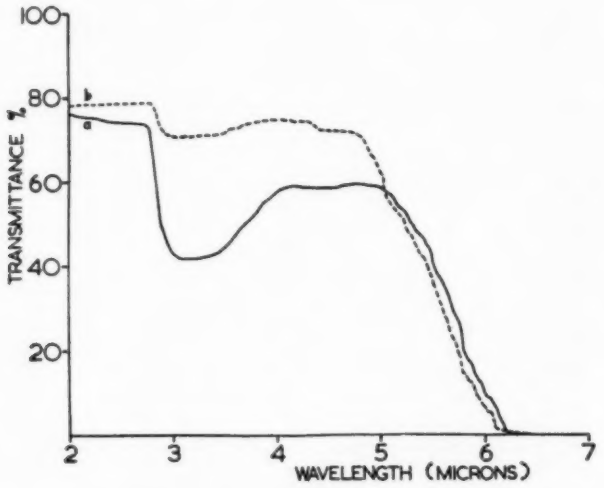

FIG. 10.
(a) GeO_2 70, PbO 30 mole per cent after 1 h at 1160 °C.
(b) GeO_2 70, PbO 24, PbF_2 6 mole per cent after 1 h at 1160 °C.

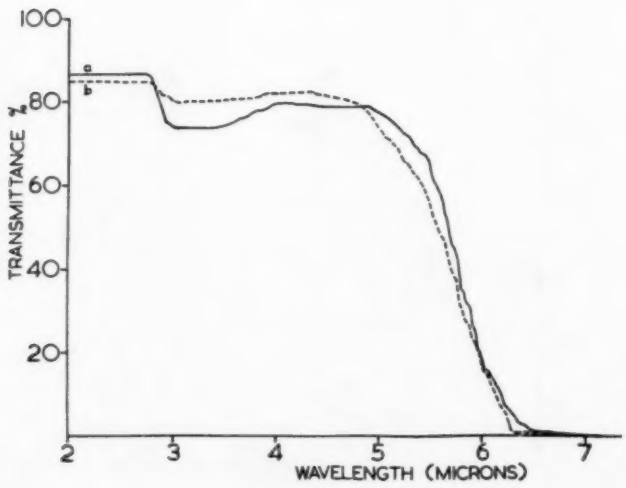

FIG. 11.
(a) GeO_2 63, PbO 27, $CaCO_3$ 10 mole per cent after 1 h at 1000 °C.
(b) GeO_2 63, PbO 17, CaCO 10, AlF_3 10 mole per cent after 1 h at 1000 °C.

Vol. 1 1961

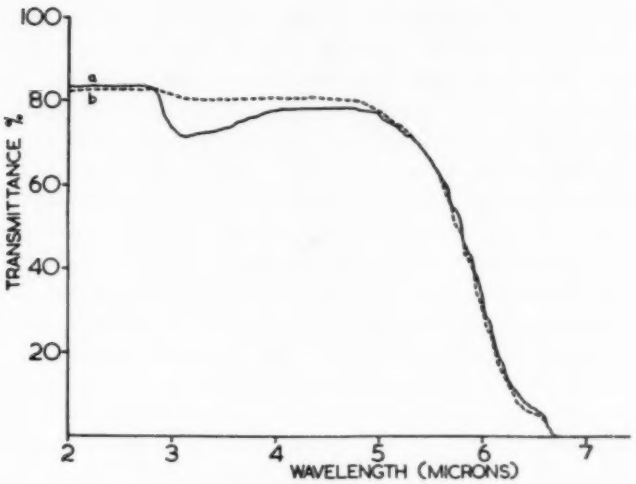

FIG. 12.
(a) GeO_2 63, PbO 27, Sb_2O_4 10 mole per cent after 1 h at 1250 °C.
(b) GeO_2 54, PbO 26, Sb_2O_4 10, PbF_2 10 mole per cent after 1 h at 1250 °C.

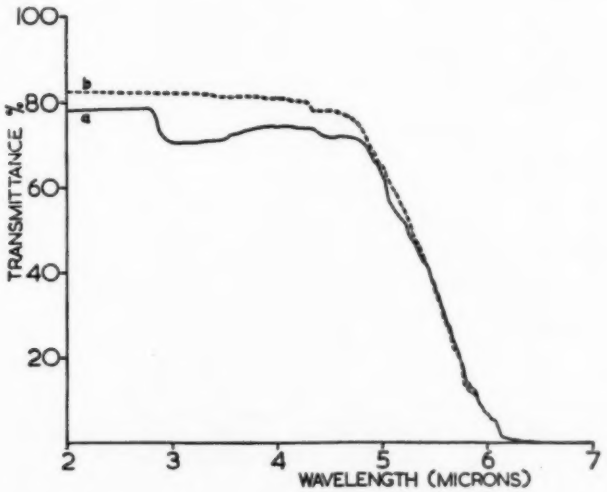

FIG. 13.
(a) GeO_2 70, PbO 24, PbF_2 6 mole per cent after 1 h at 1160 °C.
(b) GeO_2 70, PbO 24, PbF_2 6 mole per cent after 6 h at 1060 °C.

is possible with longer melting times. Some variation was obtained between runs in these experiments, and it was not possible to obtain quantitative data on variables such as fluoride content, temperature and time of melting.

DISCUSSION

It is reasonable to suppose that the removal of the O–H absorption bands from molten glasses involves (a) the diffusion of O–H or H ions to the surface and (b) the formation and

release of H_2O or volatile hydride at the surface. Diffusion processes should be encouraged by a reduced viscosity and by any turbulence or thermal stirring in the melt. Florence *et al.*[6] have shown that bubbling dry air through the melt removes H much more rapidly than passing air over the melt, suggesting that turbulence in the melt is a more important factor than viscosity. Our own results also suggest the importance of turbulence in the melt. Thus the addition of $CaCO_3$ or Sb_2O_4 (Figs. 8 and 9) resulted in very turbulent melts although, judging from the appearance, the viscosity of the melt was not altered appreciably. Figures 8 and 9 also indicate that an increase in temperature favours the removal of H, and this could be attributed to an increased thermal stirring.

Stirring, created by evolution of gas or vapour, or by convection currents, is probably an important factor in vacuum melting. The initial rapid removal of H may be associated with the initial rapid evolution of gas from the melt. Subsequently the melt becomes less turbulent and removal of H is less rapid. Turbulence, due to bubble formation, may be observed in the germanate melts even after melting for 3 h *in vacuo*. On the other hand, boric oxide melts *in vacuo*, bubble vigorously for some time and then become very quiet and free from bubbles. This may explain to some extent the difficulty experienced in removing H from boric oxide; Fig. 14(a) shows for example that the removal of H from boric oxide is far

Vol. 1 1961

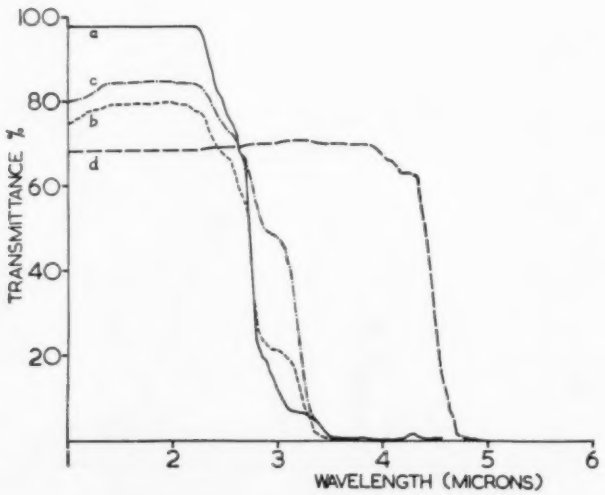

FIG. 14.
(a) B_2O_3 after melting *in vacuo* for 4 h.
(b) B_2O_3 90, NaF 10 mole per cent after melting *in vacuo* for 1 h.
(c) B_2O_3 90, NaF 10 mole per cent after melting *in vacuo* for $2\frac{1}{2}$ h.
(d) Microscope slide glass + Li_2CO_3, Na_2CO_3, PbO.

from complete after melting for 4 h *in vacuo*. By comparison, Fig. 14(d) shows a complete removal of H from a soft silicate glass after melting for only $\frac{1}{2}$ h *in vacuo*, this melt showing considerable turbulence. It is possible that a more rapid removal of H would be possible if the heating arrangements were deliberately designed to encourage thermal stirring in the melt.

The increased rate of removal of H from melts containing fluoride, illustrated in Figs. 7, 10, 11, 12 and 13 may to some extent be explained in the same way. However, it seems probable that in this case HF is being liberated from the surface, and that this reaction is more rapid than the liberation of H_2O. This is reasonable if one considers only that an H ion diffusing from the interior of the melt has a greater probability of meeting an F ion on the surface than an OH ion.

Results on other glass systems suggests that the rate at which H ions reach a surface and the probability of meeting OH or F ions, are not the only important factors. For example it is extremely difficult to remove H from boric oxide glasses even using fluoride additions and vacuum melting combined (Figs 14(b) and (c)). On the other hand H is very easily removed from tellurite glasses containing fluoride. Figure 15, for example, shows the

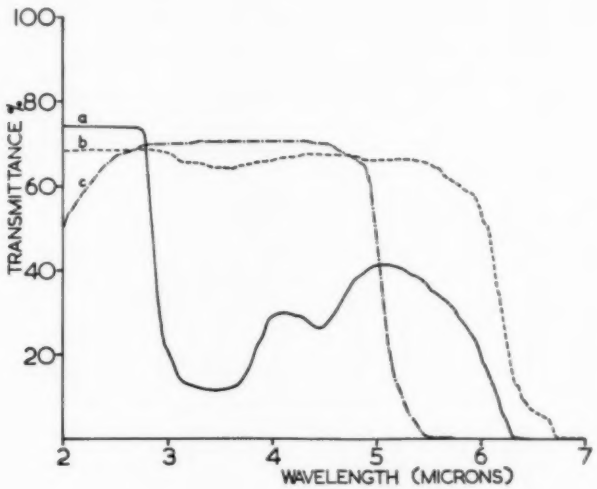

FIG. 15.
(a) TeO_2 25, PbO 50, GeO_2 25 mole per cent.
(b) TeO_2 60, PbO 10, ZnF_2 30 mole per cent after 10 min at 750 °C.
(c) TeO_2 20, PbO 20, AnF_2 20, V_2O_5 40 mole per cent after 10 min at 750 °C.

spectra of tellurite glasses of the type originally described by Stanworth,[8] indicating that complete removal of H is possible after melting at 750 °C for only 10 min. (These glasses were made in platinum crucibles and consequently contamination has reduced total transmission.) It seems reasonable, therefore, to assume that the nature of the glass determines the rate of reaction at the surface. In the cases cited, boron would be assumed to have a greater chemical affinity for OH than tellurium for OH, removal of H consequently being more difficult from boric oxide glasses than from tellurite glasses.

CONCLUSION

We conclude that a range of germanate glasses with uniformly good transmission between 1 and 5 μ can be prepared. Hydrogen, present in the glass network as O–H groups and hydrogen-bonded O–H groups, can be removed by vacuum melting or by addition of fluoride or by a combination of these processes. We suggest that the rate of removal of H is determined

(a) by the rate at which H can reach a surface and (b) by a chemical reaction at the surface to form a volatile hydride. The former process is encouraged by any turbulence in the melt, particularly bubble formation, and the latter by the presence of fluoride ions. The efficiency of removal of H from different glasses may also be determined by the chemical affinity of the cations in the melt for OH groups.

Acknowledgements—Acknowledgement is made to W. D. Lawson foı helpful discussions, to M. C. Hopper, D. J. Perrin and Miss J. Lancey for expert assistance, and to the Controller, Her Majesties Stationery Office for permission to publish this paper.

REFERENCES

1. NIELSEN, S., W. D. LAWSON, and A. F. FRAY, *Infrared Physics* **1**, 21 (1961).
2. ADAMS, R. V., and R. W. DOUGLAS, *Glastech. Ber.* **32**, 5 *te International Glaskongress* 7, 12 (1959).
3. SCHOLZE, H., and A. DIETZEL, *Naturwissenschaften* **42**, 342 (1955).
4. TODD, B. J., *J. Appl. Phys.* **26**, 1238 (1955).
5. HARRISON, A. J., *J. Amer. Ceram. Soc.* **30**, 362 (1947).
6. ALLSHOME, C. C., J. M. FLORENCE, F. W. GLAZE, and C. H. HAKNER, *J. Res. Nat. Bur. Stands.* **45**, 121 (1950).
   BLACK, M. H., F. W. GLAZE, and J. M. FLORENCE, *J. Res. Nat. Bur. Stands.* **50**, 187 (1953).
   GLAZE, F. W., *Bull. Amer. Ceram. Soc.* **34**, 291 (1955).
7. LAWSON, W. D., S. NIELSEN, and J. PLANT. Unpublished.
8. ADAMS, R. V., and R. W. DOUGLAS. Private communication.
9. STANWORTH, J. E., *J. Soc. Glass. Techn.* **36**, 3 (1952).

Vol.
1
1961

Infrared Physics, 1961, Vol. 1, pp. 187–196. Pergamon Press Ltd., Printed in Great Britain.

LONG-PATH INFRARED SPECTROSCOPY FOR AIR POLLUTION RESEARCH

E. R. STEPHENS*

Franklin Institute Laboratories, Philadelphia, Pennsylvania

(*Received* 30 *September* 1960)

Abstract—Two long-path absorption cells have been designed and built for the measurement of gaseous contaminants in the atmosphere and for the laboratory study of reactions occurring in such atmospheres. These instruments are based on the White multiple-reflection system, having two large mirrors of 3 m radius of curvature at one end of the cell and a smaller mirror of the same radius at the other end.

To avoid excessive losses of radiant energy, the image of the infrared source is magnified and demagnified to match the cell to the spectrometer. Optimum path for maximum absorption signal is reached when reflection losses reduce the energy to $1/e$ of its initial value. This corresponds to a path length of 120 m with the present cells although they have been successfully used at paths several times this length. It is possible to detect and identify many contaminants of importance in air pollution at concentrations of a few tenths of a part per million. The absorptions of water vapor and carbon dioxide make some regions of the spectrum opaque, but this interference is not serious over most of the spectrum.

The first of these cells was used for laboratory studies in Philadelphia and the second was mounted in a laboratory trailer and taken to southern California where it has been in use since 1956 for the study of the atmosphere and related problems.

ONE of the most serious problems encountered in air pollution research is that of obtaining adequate analytical methods. Often one must try to analyze a complex mixture whose composition can only be guessed and in which the components of interest are present in very minute amounts. Chemical methods applied to such a problem suffer from the shortcoming that serious interferences may be caused by components whose presence is not only unknown but unsuspected. An example of this is the potassium iodide method used to measure "oxidant" in the Los Angeles atmosphere. Although most of the so-called "oxidant" is believed to be ozone, the question of how much of it might be other oxidizing agents is still unresolved.

To meet the need for more specific analytical methods for the many substances of interest in air pollution, the Franklin Institute Laboratories have been developing the technique of long-path infrared absorption spectroscopy.

The primary interest in this work, which is sponsored by the Smoke and Fumes Committee of the American Petroleum Institute, has always been the chemistry of air pollution rather than optics, spectroscopy, or analytical methods *per se*. For this reason, previous publications[1–4] have emphasized the results of reaction studies and described only superficially the instrumentation used. This paper is written in the belief that more details of the long-path infrared technique may be of interest.

* Now with Scott Research Laboratories, P.O. Box 66, Perkasie, Pennsylvania.

Two quite similar cells were constructed using a base path length of 3 m. The first of these was completed in 1955 and used to study the important chemical reactions involving air pollutants. The second instrument, completed in 1956, was installed in a laboratory trailer and taken to southern California. It was used both for air analysis and for auto exhaust studies and is now at the University of California, Riverside, where it is being used in connection with studies of plant damage and eye irritation from air pollution.

REFLECTION SYSTEM

Both instruments are based on the multiple reflection system first described in 1942 by John White[5] and later modified by Herzberg and Bernstein.[6] This system is also used in the 10-meter cell offered commercially by the Perkin–Elmer Corporation. The basic scheme can be understood by reference to Figs. 1 and 2. The internal mirror system consists of

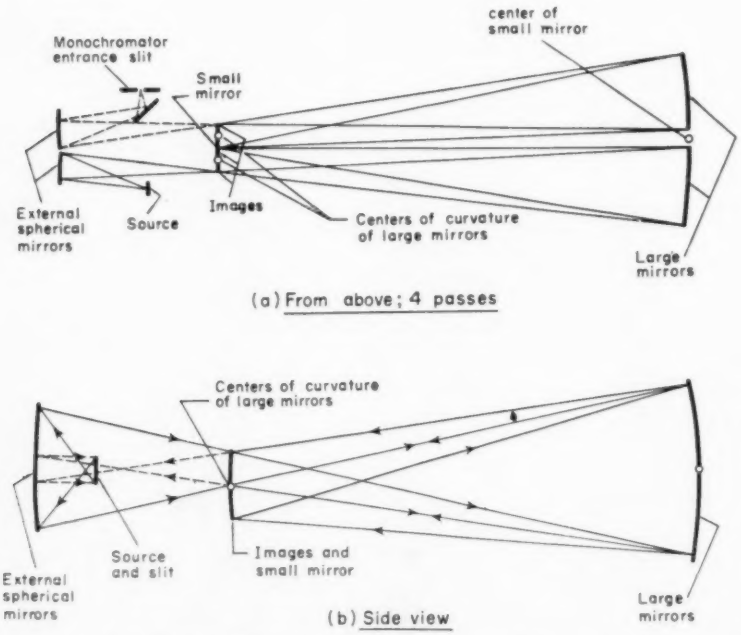

FIG. 1. Optical path in the multiple-reflection cell (not to scale)

three spherical mirrors, all of which have equal radii of curvature. Two are large mirrors (cut from 12½ in. diameter blanks) and are mounted at the right end of the cell with their centers of curvatures on the surface of the smaller spherical mirror at the left end of the cell, as shown by the small circles in Fig. 1. The center of curvature of this small mirror is between the two large mirrors and in the plane of their surfaces. The small mirror was cut from the side of one of the large mirrors to insure that it would have the same curvature.

An external spherical mirror forms an image of the source (a Nernst glower) just off the edge of the small mirror. The beam then diverges to fill the first of the two large mirrors at the right end of the cell. This mirror forms an image, on the surface of the small mirror, symmetrically placed about the center of curvature of this large mirror (see Fig. 2). The

Vol. 1 1961

small mirror in turn reflects the beam to fill the second large mirror. This mirror then forms an image of the source just off the edge of the small mirror so that the beam exists from the cell. Four passes are thus shown in Fig. 1(a).

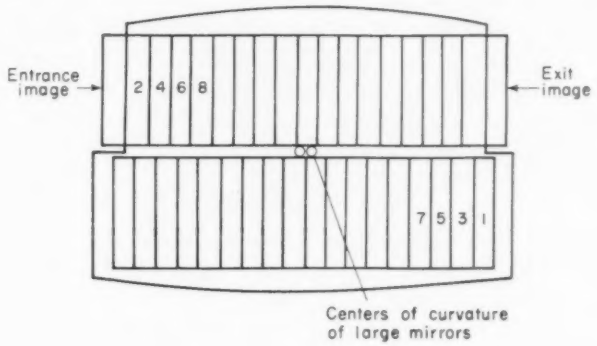

FIG. 2. Small mirror with thirty-five images (216 m path length)

By decreasing the separation between the centers of curvature of the two large mirrors (i.e., decreasing the angle between their surfaces) any integral multiple of four passes can be obtained. This is shown in Fig. 2 where thirty-five images appear on the small mirror. The numbers in Fig. 2 give the order in which the images are formed. In practice the path length is determined by counting the number of images on the small mirrors, multiplying by two, then adding two to account for the entrance and exit passes. These thirty-five images correspond to seventy-two passes of the beam through the cell. With a base path-length of 3 m (i.e., radius of curvature of mirrors = 3 m) seventy-two passes corresponds to a total path-length of 216 m.

The distance between the centers of curvature shown in Fig. 2 is equal to half the separation between successive even-numbered (or odd-numbered) images. As these centers are brought closer together the odd-numbered images move to the right while the even-numbered images move to the left, with higher-numbered images moving most rapidly. The former exit image then falls on the mirror and is reflected to form a new odd-numbered image on the lower left. This new image is in turn reflected to the upper right to form a new exit image. As the centers grow even closer, image No. 2 finally begins to over-step the edge of the mirror so that image 3 and all succeeding images become progressively narrower as the number of images is increased.

It is apparent that when many images are desired the edges of the small mirror which are adjacent to the entrance and exit images must be straight, parallel, only lightly bevelled, coated to the edge, and not obstructed by mirror mounts. Another critical feature is that the line joining the centers of curvature of the two large mirrors must be perpendicular to these entrance and exit images at the small mirror. If it is not, the rows of images will be tilted either up or down parallel to this line. When the horizontal separation between centers is small (i.e., at long path-lengths), a small vertical displacement of one of these centers will exaggerate the tilt of the rows of images and may throw the exit image far out of line.

Several interesting variations of this system may be mentioned. Suppose the entrance image is made narrower and the centers of curvature of the large mirrors are *both* moved upward to a horizontal line drawn through the centers of the upper row of images (see Fig. 2). This upper row of images will not move but the lower row (odd-numbered images) will move upward to nest alternately between the even-numbered images. This is the arrangement first described by White.[5] Another possibility would be to extend the surface of the small mirror to reflect the exit image back to form a new odd-numbered image at the lower left corner which could then be cut away to make this a new exit image placed directly below the entrance image; or these two modifications could be combined so that the entrance and exit images are adjacent to each other.

OPTICAL DESIGN

In order to record infrared spectra at long path-length the optics of the cell had to be designed rather carefully to avoid excessive loss of radiant energy. Both cells are used with Perkin–Elmer single-beam double-pass spectrometers having an effective aperture of f/4·5. A multiple-reflection cell with this aperture and a three-meter base path-length would require mirrors several feet in diameter. To keep this requirement within bounds it was necessary to magnify the image of the source by means of the spherical mirror used to reflect the beam into the cell. This limits the divergence of the beam inside the cell and makes it possible to use mirrors cut from 12½ in. diameter blanks.

To determine the size of the various mirrors the system was traced regarding the prism itself as the limiting aperture. A formula was derived which determines how large the beam on the large mirrors must be in order to just fill the spectrometer aperture (see Appendix)

$$H = R\left\{\frac{L}{S} + \frac{1}{M}\left[\frac{P}{F} + L\left(\frac{1}{F} + \frac{1}{S} - \frac{Z}{F^2}\right)\right]\right\} + ML$$

where H = height (or width) of beam on large mirror inside cell
R = distance between internal mirrors (base path)
L = slit height (or width)
M = magnification of image (image size in cell/image size on entrance slit)
P = prism height (or width)
Z = distance from parabolic mirror to prism plus twice the distance from the prism to the Littrow mirror
F = focal length of monochromator parabolic mirror
S = distance from monochromator slit to external spherical mirror.

This formula shows that the size of the beam on the large mirror depends not only on the magnification M but on the absolute value of the distance between the monochromator entrance slit and the external spherical mirror S. These relationships are plotted in Fig. 3 which shows the requisite height and width of the beam on the large mirror to fill the prism with light from the ends of the entrance slit (extreme ray) and from the center of the slit (central ray). This graph was an aid in selecting the parameters of the cell. A magnification of four was chosen with a slit-to-mirror distance, S, of about 400 mm so that the extreme ray could be carried by a mirror 12½ in. high. The small width of the beam permitted cutting off the sides to make a more compact system and to provide pieces of the same radius of curvature for the small mirror.

Vol. 1 1961

The size of the beam could have been further reduced either by making the distance, S, larger or by choosing a larger magnification, but the former would have made the external optics unwieldy and the latter would have made the images inside the cell excessively large. If the images are made too large the number required may not fit on the small mirror. When this happens, the demagnified image may not be wide enough to cover the wide entrance slits needed for sufficient energy at the longer paths. The size of the small mirror cannot be increased without limit since this would lead to excessive aberration in the images formed far from the centers of curvature of the large mirrors.

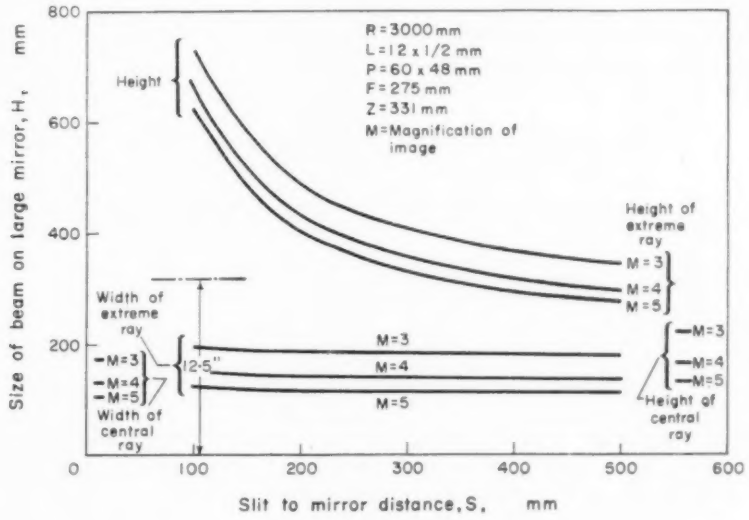

FIG. 3. Size of beam to fill prism

An alternative method of controlling the size of the beam inside the cell has been adopted for some of the double beam cells which have since been placed on the market. This involves placing field lenses just outside the entrance and exit images to focus the external mirror on the large internal mirror. These lenses are made of salt and serve also as entrance and exit windows for the cell.

An interesting feature of this optical system is illustrated in Fig. 1(a) where four passes of the beam through the cell are traced. The dotted lines show the extreme rays which will be accepted by the spectrometer. When these are traced back to the source it is found that a larger spherical mirror is required on the source side of the cell than on the monochromator side. This disparity is appreciable although not as great as indicated in the diagram.

OPTIMUM PERFORMANCE

An analysis of the multiple reflection cell shows that for the best signal-to-noise ratio, the path-length should not be increased beyond a certain optimum value. If reflection losses reduce the energy by one-half when the path is increased from 50 to 100 m they will also reduce the energy by the same fraction when the path is increased from 500 to 550 m, but in the first case the path-length is doubled while in the second it is increased by only 10

per cent. The optimum path-length can be derived by considering the amount of radiant power (P_a) removed from the beam at a given wavelength by an absorber present at a given concentration.

Then $P_a = P_0 K^{n-1} (1 - e^{-kcRn})$

where P_0 = radiant power of the beam without absorption and without losses that depend on path-length.

K = effective reflection coefficient of mirrors inside the cell
n = number of passes through cell
k = absorptivity of the absorber
c = concentration of the absorber
R = base path (distance between mirrors)

For weak absorptions

$$1 - e^{-kcRn} \cong kcRn$$

This approximation has only a minor effect on the result but simplifies the derivation somewhat.

Then

$$P_a = P_0 K^{n-1} kcRn$$

$$\frac{P_a}{P_0 kc} = K^{n-1} Rn$$

If the noise in the beam is small compared with the noise in the detecting system, then the optimum path-length will be that which makes P_a a maximum. Setting the derivative of $P_a/P_0 kc$ with respect to n equal to zero produces the condition:

$$K^n = 1/e$$

Thus the optimum path has been reached when the energy is reduced by reflection losses to e^{-1} of its initial value. In Fig. 4 $P_a/P_0 kc$ is plotted against the number of reflections for three different base path-lengths and a reflection coefficient of 0·975. In comparing these curves it should be recognized that several assumptions must be made viz.: (1) the energy carried by the cell without reflection losses or absorption is the same (i.e., P_0 is the same) for each value of base-length; (2) the sources are equally bright; (3) no consideration has been given to the spectrometer, the scanning time, resolution, time constant, etc. This treatment only considers the nature of the infrared beam given to the spectrometer for measurement.

It is apparent in Fig. 4 that performance of a multiple reflection cell decreases rather rapidly after the maximum is passed. Other things being equal the absorption signal is directly proportional to base path-length. Further calculation shows that a small increase in reflection coefficient would displace this optimum path-length toward the right and would lead to a marked improvement in cell performance.

It may also be noted that the presence of interfering absorbers (e.g., water vapor) in both the sample and blank will have the same effect as increased reflection losses. This will reduce the number of reflections and path-length for maximum absorption signal (i.e., shift the peaks of Fig. 4 to the left).

Vol. 1 1961

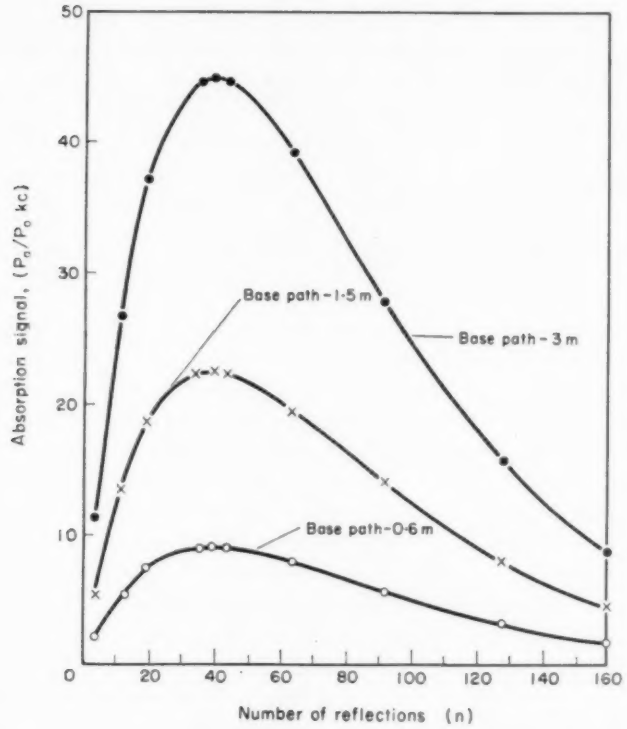

FIG. 4. Theoretical performance of long-path cells (reflection coefficient = 0·975)

Reflection coefficient can readily be measured by measuring the radiant power transmitted by the cell as a function of the number of reflections. The coefficient is then obtained from the slope of a plot of log radiant power vs. number of reflections. The internal mirrors in both cells originally were coated with gold by evaporation to provide a surface which combines reflectivity in the infrared with chemical inertness. The reflection coefficient was found to be 0·975 at the peak of the glower and at 9·6 μ. The standard aluminum–silicon monoxide coating was avoided because of the pronounced absorption of the silicon monoxide after many reflections. Later the gold was replaced with uncoated aluminum which proved just as reflective and more durable than the gold. No significant corrosion problems have been encountered.

In spite of the existence of an optimum path length for maximum absorption signal it has sometimes been found advisable to operate with a path length far in excess of the optimum. To make a weak absorption measurable at the optimum path would require depression of the zero so that only a portion of the transmission range is recorded (e.g. 75–100 per cent). But then the signal from a single-beam instrument with uncontrolled slits would quickly go off scale as the spectrum is scanned. Furthermore, if the sample contains water or carbon dioxide the bands of these compounds will go off scale if the zero is depressed.

Several double-beam systems have been constructed since these single-beam cells were built. These go a long way toward solving these problems. The 40-meter cells now offered

commercially by the Perkin–Elmer Corporation utilize this same optical system with $R = 1$ m. The scale expansion systems of modern double-beam spectrometers makes it possible to attain effective path lengths of hundreds of meters.

CO_2 AND H_2O INTERFERENCE

Experience with these cells has shown that atmospheric water vapor and carbon dioxide do not prohibit useful atmospheric analysis although they do make some regions of the infrared spectrum unusable and are a nuisance in others.

The spectrum as it appears with several hundred meters of air of normal humidity is as follows: Absorption is total in the carbon dioxide and water bands at about 2·9 μ but the air is sufficiently transparent at 3·4 μ so that weak CH absorption can be detected. This is especially true if a calcium fluoride prism is used. The region from 3·4 to about 3·9 μ, where characteristic aldehyde absorptions appear, is completely free of water and carbon dioxide absorptions. Absorption is total in the 4·3-micron band of carbon dioxide but the atmosphere is sufficiently transparent to reveal the carbon monoxide band at 4·66 μ. The absorption of naturally occurring nitrous oxide at 4·5 μ cannot be seen unless some of the atmospheric carbon dioxide is removed. The carbonyl region is opaque at hundreds of meters path-length but some energy is detectable in the center of the 6-micron water band. Between about 7·2 and 8 μ usable energy is transmitted although the water band is still strong. Between 8 and 9 μ the water band is troublesome but not a serious interference. The region 9–12 μ, where ozone, methanol, formic acid, ethylene, higher olefins, and many other absorbers have their strongest bands, is nearly free of interfering absorptions. With the trailer laboratory it was possible to identify and measure ozone in the Los Angeles atmosphere at concentrations down to 0·2 p.p.m.[2] Beyond 12 μ the water and carbon dioxide bands gradually increase in strength. The strong and characteristic acetylene band at 13·7 μ is about the last useful band detectable. The 15-micron carbon dioxide band makes the air opaque beyond about 14 μ.

MECHANICAL DESIGN

The laboratory and trailer cells differ somewhat in mechanical design. The two ends of the laboratory cell were mounted on separate frames and bolted into a concrete floor. This permitted complete alignment of the optical system after which an 18-in. diameter stainless steel tube could be rolled into place between the two ends. This system could be evacuated and filled with cylinder oxygen for photochemical experiments. For these experiments a high pressure mercury arc was used as light source.

In the trailer instrument the entire optical system is mounted on an iron framework. The 20-in. diameter body of the cell is bolted to this framework and has a flange at either end. The internal cell mirrors are mounted on gimbals bolted to these flanges as illustrated in Figs. 5 and 6. Adjustment of the large mirrors is quite critical, since these have an effective lever arm equal to the total path-length. As already mentioned, a small vertical separation of the centers of curvature will cause the rows of images on the small mirror to tilt. A small change in the horizontal separation of centers will change the path-length. Such changes can be caused by temperature changes in the mirror mounts.

The trailer instrument is also provided with artificial ultraviolet radiation to simulate sunlight. This is provided by eight "blacklite" fluorescent lamps mounted within the cell. When the interior surface of the stainless steel cell was polished these lamps provided

Vol. 1 1961

ol.
1
961

FIG. 5. Author adjusts mounts for large mirrors

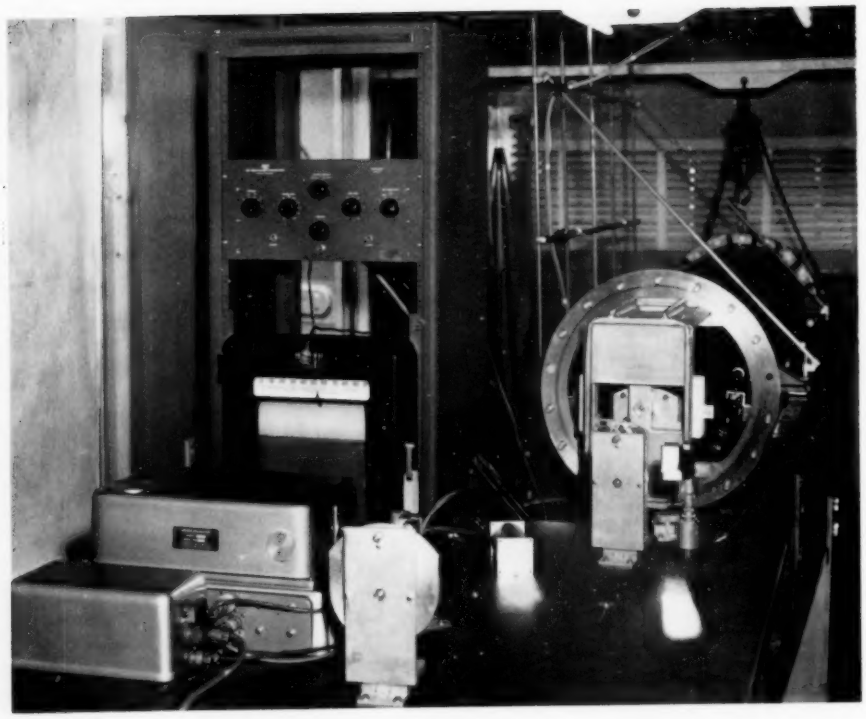

FIG. 6. General view of cell in mobile laboratory

radiation which would photolyze nitrogen dioxide about half as fast as bright sunshine. When the interior of the cell was lined with aluminum foil, photolysis was faster than in sunlight. Originally these lamps were mounted along either side of the cell. It was found, however, that schlieren effects from the warm lamp surfaces caused intolerable fluctuations in the infrared beam. When the lamps were moved upward 45° around the cell body this problem was completely eliminated.

Surface effects have not been a serious problem with these cells. Non-polar and unreactive materials such as aldehydes, alcohols, hydrocarbons, etc. will stay in the cell indefinitely.

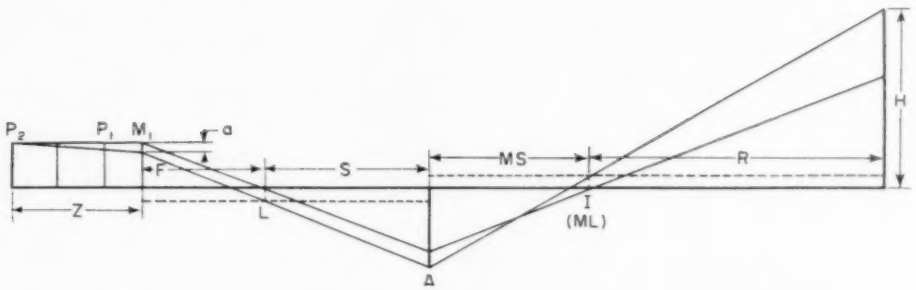

FIG. 7.

Acrolein, for example, was left over night in the cell at a concentration of 10 p.p.m. in air with no detectable loss. Under the best circumstances small concentrations of ozone are also stable in the cell. More polar and more reactive substances such as organic acids are subject to adsorption and desorption on the surfaces however.

Acknowledgements—Several members of the Chemical Kinetics and Spectroscopy Section of the Franklin Institute Laboratories made important contributions to the design and construction of the long-path cells. These include Rachel Franklin, Luther Conant, Louis Herczeg, and Richard Cavaliere. Edwin Bailey of the Astronomy Department of the Franklin Institute made the mirrors.

REFERENCES

1. HANST, P. L., E. R. STEPHENS, and W. E. SCOTT, Proc. API 35, III, 175–87 (1955). Reprinted in *J. Air Poll. Cont. Assoc.* **5**, 219 (1956).
2. SCOTT, W. E., E. R. STEPHENS, P. L. HANST, and R. C. DOERR, *Further Developments in the Chemistry of the Atmosphere*, Proc. API 37, III, 171–83 (1957).
3. STEPHENS, E. R., P. L. HANST, R. C. DOERR, and W. E. SCOTT, *Industr. Engng. Chem. (Industr.)* **48**, 1498 (1956).
4. STEPHENS, E. R., W. E. SCOTT, P. L. HANST, and R. C. DOERR, *Recent Developments in the Study of the Organic Chemistry of the Atmosphere*, Proc. API 36, III, 288–9 (1956), reprinted in *J. Air Poll. Cont. Assoc.* **6**, 159 (1956).
5. WHITE, J. U., *J. Opt. Soc. Amer.* **32**, 285 (1942).
6. BERNSTEIN, H. J., and G. HERZBERG, *J. Chem. Phys.* **16**, 30 (1948).

APPENDIX

Following is the derivation of the formula for determining how large the beam on the large mirrors must be in order to just fill the spectrometer aperture.

Refer to Fig. 7, and let

H = height (or width) of beam on large mirror inside cell
R = distance between internal mirrors (or image I at edge of mirror)
L = slit height (or width)
I = image of slit
M = magnification ($I/L = M$)
M_1 = parabolic mirror height (or width)
P_1, P_2 = prism height (or width)
Z = distance from parabolic mirror M_1 to prism, P_1, plus twice the distance from the prism to the Littrow mirror; i.e., M_1P_2
F = focal length of monochromator parabolic mirror M_1
S = distance from monochromator slit to external mirror (A = height of mirror)
a = separation of central ray and extreme ray on M_1

(For convenience and clarity, only one half the system has been shown in the figure, showing an extreme ray and a central ray.)

Draw a line parallel to the optic axis through the end of the image I from H to A. Then

$$\frac{H - ML}{A + ML} = \frac{R}{MS} \tag{1}$$

Draw a similar line through the end of L between A and M_1. Then

$$\frac{A - L}{M_1 - a + L} = \frac{S}{F}$$

$$M_1 = P(P_1, P_2) \text{ and } a = \frac{LZ}{F}$$

$$\frac{A - L}{P - LZ/F + L} = \frac{S}{F} \tag{2}$$

From (1): $$A = \frac{HMS - M^2LS - RML}{R} \tag{3}$$

From (2): $$A = \frac{SFP - SLZ + FSL + F^2L}{F^2} \tag{4}$$

By eliminating A from (3) and (4), and rearranging terms,

$$H = R\left\{\frac{L}{S} + \frac{1}{M}\left[\frac{P}{F} + L\left(\frac{1}{F} + \frac{1}{S} - \frac{Z}{F^2}\right)\right]\right\} + ML$$

Vol. 1 1961

Infrared Physics, 1961, Vol. 1, pp. 197–198. Pergamon Press Ltd., Printed in Great Britain.

COMPLETE LIQUEFACTION CRYOSTAT

H. P. WURTZ

Santa Barbara Research Center,
Goleta, California, U.S.A.

(*Received* 28 *July* 1961)

EXPLORATION of the longer wavelengths in the infrared spectrum has led to a need for miniature detector cooling devices. Of particular interest is the Joule–Thomson regenerative cryostat. As a result of this interest, considerable development work has been done to improve the reliability and versatility of this device. It is now used as an open-loop system in a number of infrared applications, and work is progressing on closed-loop operation.

Refrigeration of infrared detectors by Joule–Thomson cooling can, however, produce electrostatic noise in a system. At least one important source of the noise is the high velocity exhaust of partially liquefied gas from the Joule–Thomson throttle. This is evident from tests in which a cryostat is used to create a reserve of liquid in a detector dewar, and then shut off so that continued cooling is accomplished by the boiling of the residual liquid. In these tests the noise, if present, will drop to a value approaching the white noise of the system as soon as the cryostat flow stops. The problem has been partially solved by a number of techniques such as coatings in the detector dewar, and placement of absorbent materials between the detector and the cryostat. However, these methods often introduce other undesirable performance characteristics. And furthermore, experience has shown that finding the best method for a particular detector is often a matter of selection.

One of the most direct approaches to the problem of reducing the electrostatic noise lies in the direction of a cryostat design in which the cooler is capable of producing a low-velocity stream of completely liquefied gas. Such a cryostat has been developed and tested at Santa Barbara Research Center. The performance to date has been very satisfactory, and further testing is planned. The cooler is operated in the same manner as a conventional cryostat and no basic changes are necessary in the system. At 2000 p.s.i. gas pressure, the cryostat takes about 3 min to cool an average detector to liquid-nitrogen temperature. After start, cooling may be continued at 1000 p.s.i. supply pressure when room temperature ambient conditions prevail and the heat load is about 1 W. Flow rates under these conditions have been measured as low as 1 l./min. If the cooler is operated in a clear glass dewar at any pressure within its operating range, a uniformly low-velocity stream of liquid may be seen emerging from the throttle, whereas a conventional cryostat viewed in this manner will exhibit a high-velocity cone-shaped spray of liquid droplets. These effects are illustrated in Fig. 1 and Fig. 2, respectively.

The design of the cryostat which accomplishes this complete liquefaction is conventional in appearance and differs only in the throttle or Joule–Thomson valve arrangement. Conventional throttling methods have commonly been: orifices, porous plugs, or frictional losses in capillary heat exchanger tubing. The complete liquefaction throttling is done in

two steps. A primary throttle in the heat exchanger section partially drops the pressure from the gas supply, and the final expansion takes place at a secondary throttle near the cold end of the cryostat. The division of the expansion between these two throttles, and the location of the secondary throttle are the important parameters of the method.

Measurements of electrostatic noise in detectors cooled by these cryostats have been taken, and the results indicate that values comparable to those produced by boiling liquid are obtainable. The cryostat has therefore demonstrated the desirable characteristics of low electrostatic noise and low gas flow rates for economy in operation. In exchange for these advantages, we have had to accept a longer cool-down period and increased susceptibility to plugging due to gas contaminants. The latter problem, of course, can be alleviated by careful attention to the gas supply and by the use of selective filters. Depending on the availability of pure gas and the efficiency of the filters, it is possible to set the degree of throttling to achieve a low flow rate and reduction in electrostatic noise. Therefore, each system application may be tailored to yield the optimum balance of performance.

Vol.
1
1961

Vol.
1
1961

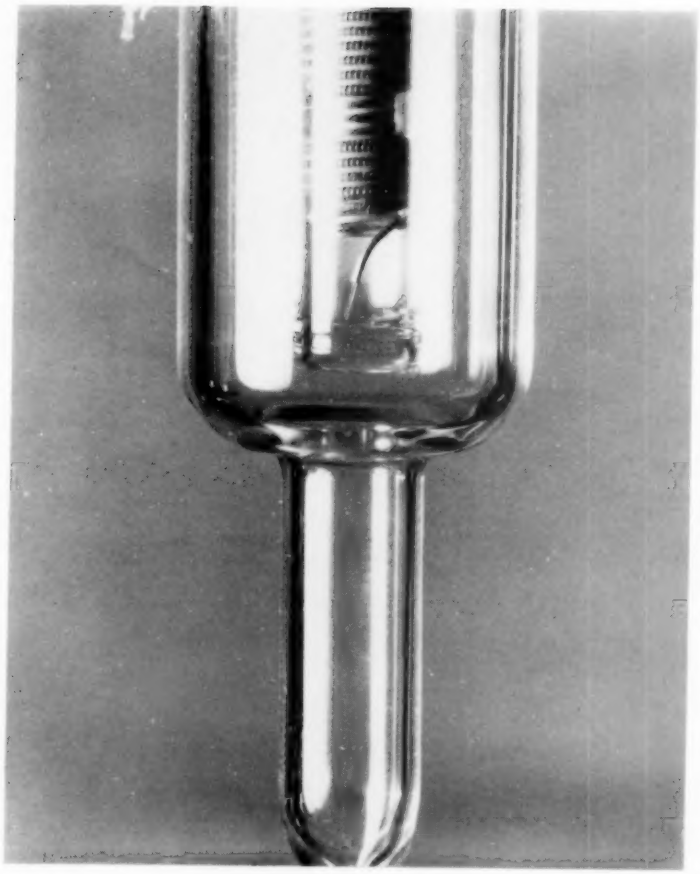

FIG. 1

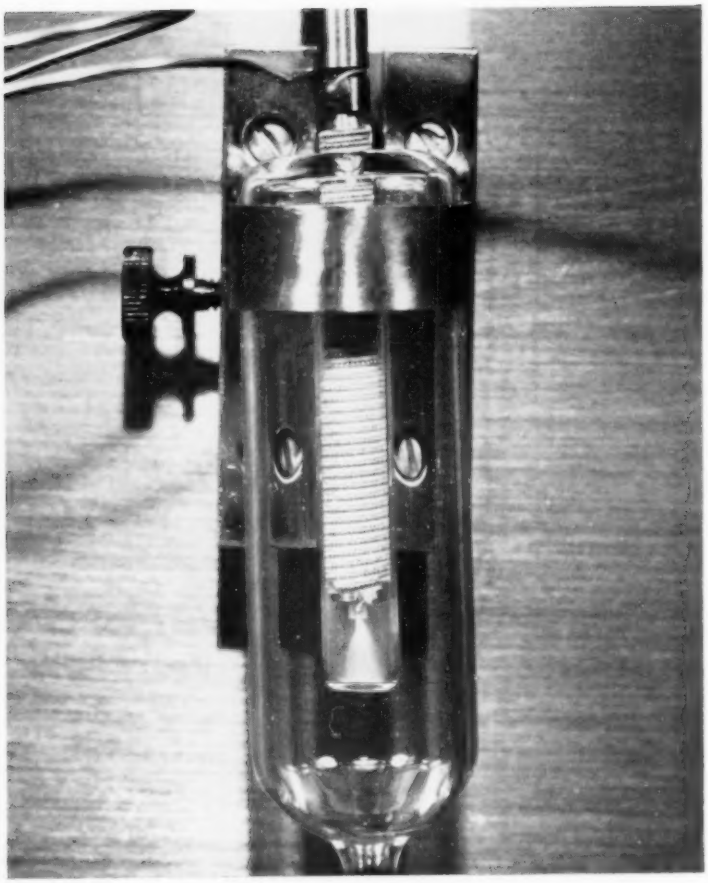

FIG. 2

Infrared Physics, 1961, Vol. 1, pp. 199–208. Pergamon Press Ltd., Printed in Great Britain.

RADIATION DAMAGE EXPERIMENTS ON PbS INFRARED DETECTORS

R. R. BILLUPS and W. L. GARDNER

Lincoln Laboratory,* Massachusetts Institute of Technology
Lexington, Mass., U.S.A.

(*Received* 21 *July* 1961)

Abstract—The purpose of the work reported in this paper was to determine the expected lifetime of PbS infrared detectors in the lower Van Allen radiation belt. Commercially available PbS cells were bombarded with high energy protons (7·5 MeV to 450 MeV) with the integrated proton flux ranging from 10^{10} protons/cm² to 10^{16} protons/cm². A comparison of the known information about the Van Allen belt and the experimental data obtained in this work indicates that PbS cells can function properly for at least 2 years in such an environment. Similar cells were also irradiated with neutrons. The changes in the PbS detector characteristics as a result of neutron irradiation are similar to the changes for proton bombardment and results show that these PbS cells can tolerate an integrated neutron flux of about 10^{15} nv_0t (thermal neutrons/cm²) without serious effects.

I. INTRODUCTION

THE purpose of the research work reported in this paper was to determine the expected lifetime of PbS detectors when exposed to the radiation environment existing in the Van Allen belt. Recent data indicates that the Van Allen belt radiation consists of high energy protons and electrons. Freden and White [1] measured proton energies ranging from 75 MeV to 700 MeV. These measurements were taken in the lower region of the Van Allen belt (~1200 km), and in this region the calculated proton flux is 10^3–10^4 protons/cm² sec. Van Allen [2] gives some tentative intensities of the proton and electron flux in the heart of the inner zone of the Van Allen belt (~3600 km), i.e., approximately 2×10^4 protons/cm² sec for protons with energies greater than 40 MeV, and approximately 1×10^7 electrons/cm² sec steradian for electrons with energies greater than 0·6 MeV.

The radiation level inside of a space package due to the electron flux would be small compared to that of the proton flux. Therefore, the main interest was the effects on PbS infrared detectors when bombarded with protons of comparable energies to those found in the Van Allen belt.

A continuous exposure to a proton flux density of 2×10^4 protons/cm² sec for one year would result in an integrated flux of $6{\cdot}3 \times 10^{11}$ protons/cm². The integrated flux for the same period of time would be less for any other than a circular equatorial orbit at approximately 3600 km altitude.

Since the main purpose of a PbS detector is to detect infrared radiation, a good measure of lifetime is the proton beam's influence on the responsivity of the detector. Responsivity is defined as a ratio of the voltage output of the cell to the infrared radiation input, i.e., V/W.

* Operated with support from the U.S. Army, Navy and Air Force.

The extent of the degradation that can be tolerated is determined by the design parameters of the system in which the PbS cell is used. Quite arbitrarily, a 50 per cent drop in responsivity will be considered the maximum allowable damage for purposes of defining the lifetime.

In our experiments, PbS cells were bombarded with protons with energies ranging from 7·5 MeV to 450 MeV and integrated flux values of from 10^{10} to 10^{16} protons/cm^2. PbS cells were also irradiated with neutrons and gamma-rays. It turns out that the type of damage to the PbS cells with neutron irradiation is similar to that resulting from proton bombardment. The integrated flux values were slightly higher, however, ranging from 10^{14} to 5×10^{17} neutrons/cm^2 (nv_0t).

II. TEST CONDITIONS

The cells used in these experiments were commercially available 1 mm × 1 mm chemically deposited PbS, manufactured by Infrared Industries. In general, the cells had a resistance ranging from 0·8 to 3 MΩ with a response time of approximately 250 μsec.

Characteristics such as resistance, signal-to-noise ratio, and responsivity of the cells were measured before and after exposure to nuclear radiation using the test set-up schematically shown in Fig. 1. The time elapsing between the final measurement of these characteristics and exposure to nuclear radiation was usually a day or less, depending on what had

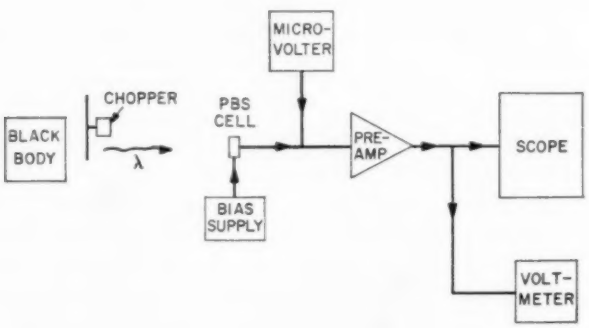

FIG. 1. Schematic of infrared test equipment.

to be done to prepare for the various runs. Measurements after exposure were made within a half-hour in most cases. The cells that were irradiated with neutrons, however, were fairly radioactive and in some cases measurements could not be taken for approximately 10 hr. Monitoring of the cell characteristics during exposure to nuclear radiation was not deemed necessary.

The characteristics were determined using a 500 °K blackbody. The radiant flux density was 10μW/cm^2 with a chopping frequency of 90 c/s. The band pass of the preamplifier was approximately 900 c/s. Under these operating conditions the initial signal-to-noise ratio was approximately 10 and the responsivity was about 2×10^3 V/W using a 45 V bias.

The proton experiments were made possible through the cooperation and assistance of various universities by permitting us to utilize the facilities at their cyclotron laboratories. The proton energies and location of these cyclotrons are: 7·5 MeV at the Massachusetts

Vol. 1 1961

Institute of Technology (MIT), 133 MeV at Harvard University, 240 MeV at the University of Rochester, and 450 MeV at the University of Chicago. The internal beam was used at the Chicago cyclotron with the beam intensity being determined by the resulting radioactivity of an aluminum target. The flux density during our experiments at Chicago was varied from 10^7 protons/cm^2 sec to 10^{12} protons/cm^2 sec. An external beam was used during our experiments at the other installations. At MIT and Harvard the beam was monitored with a faraday cup and at Rochester a counter telescope was used. The beam intensities at Rochester and Harvard were 8×10^6 protons/cm^2 sec and $3{\cdot}8 \times 10^9$ protons/cm^2 sec respectively. At MIT the beam intensity was varied from approximately 10^{10} protons/cm^2 sec to 2×10^{11} protons/cm^2 sec.

The facilities at the MIT Nuclear Engineering Laboratory were used for the neutron experiments. The neutron energy spectrum at the point in the reactor in which the experiment was conducted was not precisely known; however, there were principally thermal neutrons with a flux density of $5 \times 10^{12} nv_o$. The gamma-ray flux was 2×10^7 r/hr.

III. PROTON EXPERIMENT

The discovery of the Van Allen belt and subsequent work by Freden and White[1] in identifying the particles and their energies in the inner portion of the belt, has led to a considerable amount of activity to determine the effects on semiconductor devices when exposed to such radiation. Because there is insufficient data covering the entire radiation belt there have been attempts to extrapolate the known information at 1200 km to altitudes of 2000–3000 km. It is known, for example, that the proton flux density at 1200 km is

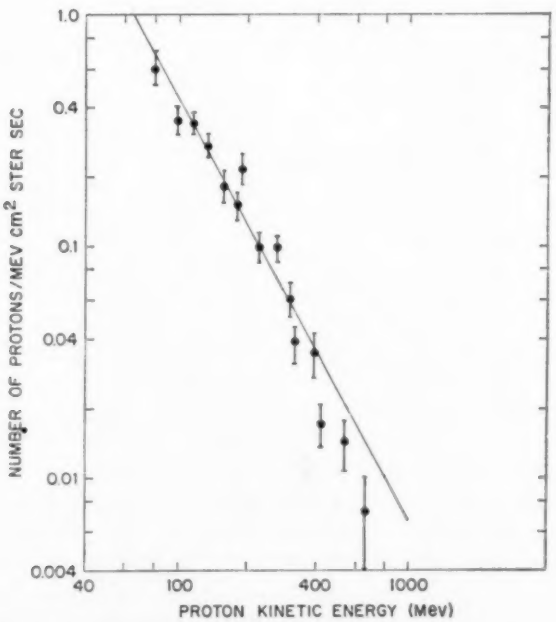

FIG. 2. The absolute energy spectrum of protons above 75 MeV in the lower Van Allen radiation belt at an altitude of 1200 km.[1]

somewhere between 10^3–10^4 protons/cm² sec. With the information[3] that the radiation intensity doubled for every 100 km increase in altitude to around 2200 km, the assumption was made that the increased radiation was due to an increase in proton flux, which led to very pessimistic predictions about the expected lifetime of semiconductor devices[4] when placed in the radiation belt. Some of the concern about humans and resulting radiation injury when placed in this belt were also based on this assumption.[5] However, a re-evaluation of the information has led to the conclusion that the increased radiation intensity as one goes up into the Van Allen belt is due to electrons rather than an increase in proton flux density.[6] It is also believed that the proton flux density does not go above 2×10^4 protons/cm² sec as one goes up into the belt. Van Allen[2] estimates that the proton flux density in the heart of the outer belt is approximately 10^2 protons/cm² sec.

The proton flux contains particles with measured energy values ranging from 80 MeV to 700 MeV. The density of particles is greatest at the lower energy portion with a rapid fall-off to a relatively low density above 200 MeV, Fig. 2.

As previously stated, the range of proton energies investigated in our work is from 7·5 MeV to 450 MeV. The effects on the PbS detector characteristics when exposed to such radiation are presented in Figs. 3–7. In the 7·5 MeV proton experiment the beam intensity ranged from approximately 10^{10} to 2×10^{11} protons/cm² sec and the cells were exposed

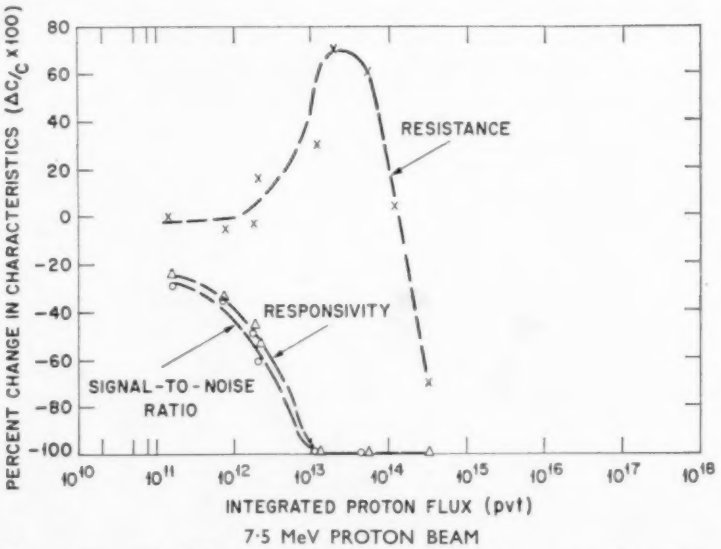

FIG. 3. Change in PbS characteristics due to 7·5 MeV proton bombardment.

for times varying from a fraction of a minute to a half-hour. This resulted in integrated flux values ranging from 10^{11} to 5×10^{14} protons/cm². As noted in Fig. 3, the PbS cells show a 50 per cent degradation in operation characteristics after having been exposed to an integrated flux of approximately 10^{12} protons/cm² (2 y in the heart of the inner Van Allen belt).

A constant flux density of $3{\cdot}8 \times 10^9$ protons/cm² sec was used during the 133 MeV experiment. Since the exposure time varied from 0·4 min to about 4 hr, the integrated flux values ranged from 10^{11} to $5{\cdot}4 \times 10^{13}$ protons/cm². A 50 per cent degradation in operating

characteristics is noted at approximately 10^{13} protons/cm^2 or approximately 20 y in the heart of the inner Van Allen belt, Fig. 4.

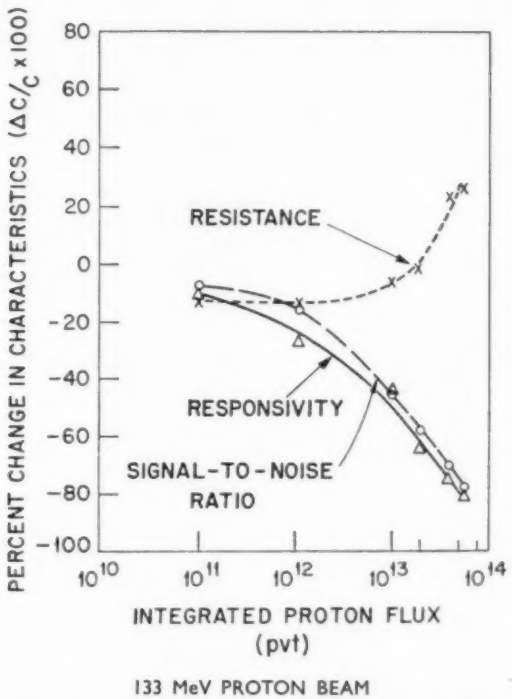

FIG. 4. Change in PbS characteristics due to 133 MeV proton bombardment.

The data for the 240 MeV proton experiment, presented in Fig. 5 does not extend far enough to show a 50 per cent degradation in operating characteristics. There is every reason to believe, however, that if this curve were extended it would follow the same general pattern exhibited by the other data and that an integrated flux of approximately 10^{13} protons/cm^2 would produce a 50 per cent drop in the responsivity of the PbS infrared detector.

The beam intensity for the 450 MeV proton experiment was varied from approximately 10^7 to 10^{12} protons/cm^2 sec. Exposure times of up to a half-hour resulted in integrated flux values ranging from 10^{10} to 8×10^{15} protons/cm^2. Once again, the effect on the PbS characteristics as a result of having been bombarded with 450 MeV protons is similar to that noted for the 7·5 MeV and 133 MeV proton experiments, Fig. 6. An integrated flux of slightly more than 10^{13} protons/cm^2 was needed to produce 50 per cent damage.

In general, the PbS cells completely recover their characteristics in a matter of hours if the damage is no greater than about 40 per cent. Otherwise, the recovery is at a very slow rate, unless the damage is complete (e.g., zero responsivity), and then it is permanent.

It is of interest to note that an integrated flux of 4×10^{10} protons/cm^2 with a 133 MeV proton beam caused the short-circuit current in silicon solar cells[7] to drop 25 per cent, while an integrated flux of approximately 10^{12} protons/cm^2 caused a 25 per cent drop in

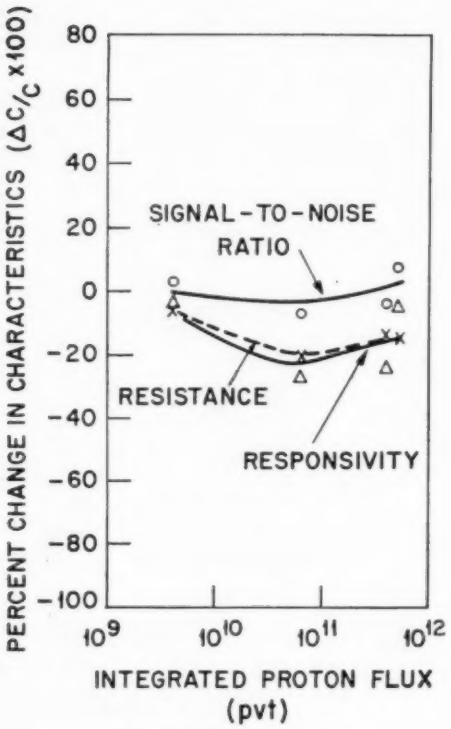

FIG. 5. Change in PbS characteristics due to 240 MeV proton bombardment.

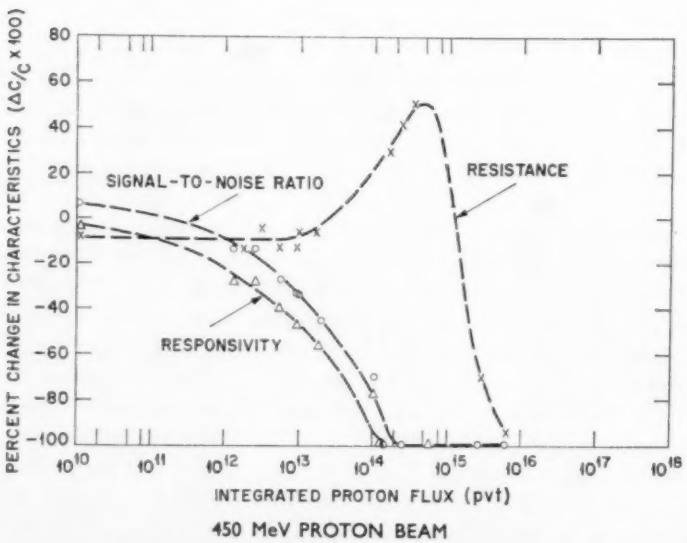

FIG. 6. Change in PbS characteristics due to 450 MeV proton bombardment.

Vol. 1 1961

the responsivity of PbS cells. This difference between PbS and Si is probably expected since the original number of defect-impurities is orders of magnitude higher in PbS. Also, W. C. Hulten[8] of the National Aeronautics and Space Administration conducted an experiment using the 240 MeV proton beam, concurrently with our experiments on PbS cells and noted, on the average, a permanent 40 per cent drop in gain of germanium transistors exposed to an integrated flux of $9{\cdot}3 \times 10^{11}$ protons/cm^2. The PbS cells showed less than 20 per cent change in responsivity for an integrated flux of 5×10^{11} protons/cm^2 and also they completely recovered.

IV. NEUTRON AND GAMMA-RAY EXPERIMENT

The length of time that PbS cells were exposed in the reactor to the mixed neutron/gamma-ray flux varied from 30 sec to 1 day, resulting in integrated flux density values ranging from 10^{14} nv_0t to slightly more than 10^{17} nv_0t. The results plotted in Fig. 7 clearly

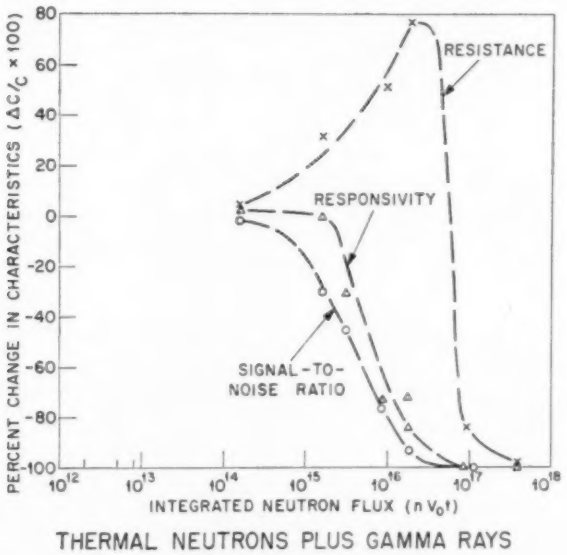

FIG. 7. Change in PbS characteristics due to neutron and gamma-ray irradiation.

indicate that a maximum integrated flux that these cells can tolerate is in the vicinity of 10^{15} nv_0t and 10^6 r. Figure 8, a composite of Figs. 3, 4, 6, and 7, points up the marked similarity in the type of damage suffered by the PbS cells when exposed to either a neutron or proton flux.

None of the characteristics of the cells receiving the greatest neutron irradiation (5×10^{17} nv_0t) have recovered at the end of a month and for cells receiving an integrated flux of about 10^{17} nv_0t, only the resistance has recovered. As a matter of fact the resistance has a tendency to over-recover, such that at the end of a month's time it was 2 to 3 times its original value. For lower values of integrated flux the PbS cells recovered; the length of time needed being dependent on the extent of the damage. Cells that were irradiated with an integrated flux of about 5×10^{15} nv_0t recovered in approximately a month.

The reported work on radiation damage to PbS deals with changes in the electrical characteristics that take place when PbS is exposed to neutron and gamma-ray irradiation. There is qualitative agreement between these data and the results discussed in this paper. For example, Levy[9] reported that the signal output of the PbS cells, and consequently

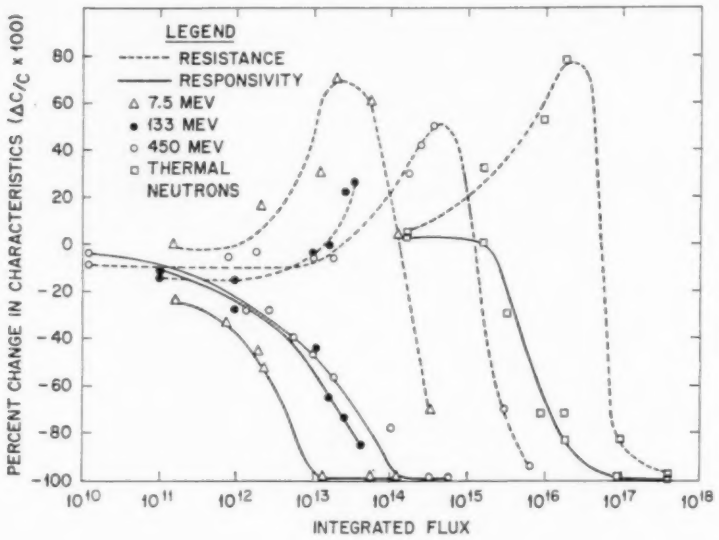

FIG. 8. A comparison of the neutron and proton experiments.

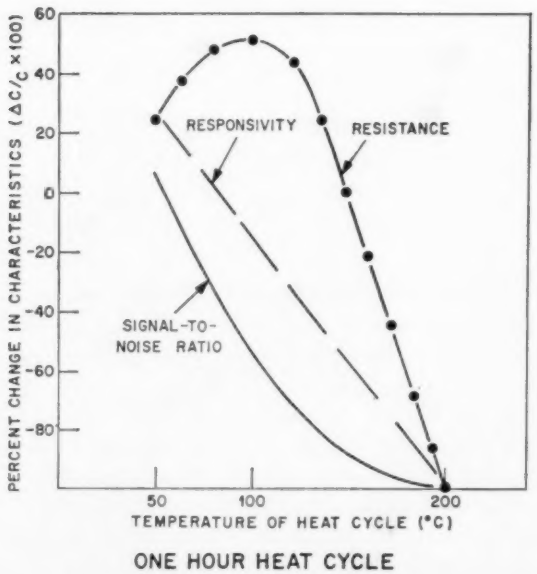

FIG. 9. The effect of heating PbS cells to various temperatures.

Vol. 1 1961

the signal-to-noise ratio, dropped to very low values as a result of exposure to an integrated flux of $1{\cdot}1 \times 10^{15}$ *nvt*. No data were given concerning the recovery of these cells.

Kutzscher[10] reported rather large changes in PbS characteristics after exposure to a total gamma-ray dose of 10^7 r or an integrated neutron flux of approximately 10^{13} *nvt*. In general, the noise and resistance increased while the responsivity and time constant decreased. In all cases, however, the cell characteristics returned to their original values within approximately a month.

V. HEATING EFFECTS

Early in these experiments it became evident that heating of the cells might be playing an important role in the observed changes of the PbS characteristics. Consequently, heat cycling experiments were performed with the results as noted in Fig. 9. Here, also, the cell characteristics were measured before and after, but not during the heat cycle. There is a marked similarity between these results and the change in characteristics due to nuclear irradiation.

Monitoring the temperature of the cells, while they were being bombarded with 7·5 MeV protons showed that the temperature did not go above 50 °C for a flux density of $1{\cdot}9 \times 10^{11}$ protons/cm² sec and an integrated flux of $3{\cdot}4 \times 10^{14}$ protons/cm². Obviously, as the flux density is lowered, the temperature rise of the PbS cell is less. The energy dissipated in the material being bombarded decreases as the energy of the bombarding particles increases, so that not as much of a temperature rise is to be expected for a similar flux density with higher energy protons.

A measurement of the temperature at the point in the reactor in which our neutron experiments were conducted indicated that the temperature does not go above 110 °C.

While the ambient temperature in the reactor might be influencing the neutron results slightly, it is quite clear that the results shown for the proton experiments are entirely due to radiation damage and not due to heating.

VI. CONCLUSIONS

A determination of the lifetime of PbS cells in the inner Van Allen belt on the basis of radiation damage versus integrated flux data presented in this paper would result in a conservative estimate. While it is true that it is the integrated flux and not the flux density, *per se*, that determines the amount of damage to the PbS cell, the fact remains that a low flux density makes it possible for the self-annealing process to be more effective. The experimental flux densities were up to eight orders of magnitude higher than that found in the Van Allen belt. Aside from diminishing the influence of the self-annealing process, such accelerated life-testing should not have any deleterious effects.

The 2×10^4 protons/cm² sec is presently accepted to be the flux density of protons of 40 MeV and up, so that the proton intensity at any given energy is obviously less than this value. The threshold energy value of protons able to penetrate a given vehicle housing is also a variable that has to be taken into account, since as previously pointed out the flux density per unit energy range is a function of the energy of the particles.

Any estimate of the lifetime of PbS cells, in the Van Allen belt, therefore, has to be tempered by the fact that the experimental conditions do not precisely conform to the radiation environment that PbS infrared detectors would see in an operational system. On the basis of the experimental data, the expected lifetime of the PbS cells should be

about 2 y (integrated flux of $1{\cdot}3 \times 10^{12}$ protons/cm^2). However, the factors mentioned above would seem to indicate that this estimate is a minimum value.

Of course the lifetime of all components for any orbit other than an equatorial orbit would be longer. The interesting question though is whether or not radiation damage in PbS cells due to periodic irradiation would be cumulative. The fact that these cells completely recover from slight damage suggests that such damage is not cumulative.

The neutron experiment indicates that an integrated flux of about 10^{15} $nv_o t$ can be tolerated without serious damage to a PbS infrared detector.

Acknowledgements—The acquisition of the data presented in this paper would have been impossible without the assistance and cooperation of Mr. L. Clark, Professor N. Wall, and Mr. E. White of MIT; Mr. A. Koehler of Harvard University; Dr. Heer and Mr. R. Mortenson of the University of Rochester; and Dr. N. Sugarman and Mr. J. Panontin of the University of Chicago.

Mr. E. Merrill's assistance in obtaining the data and in the data processing is also gratefully acknowledged.

REFERENCES

1. FREDEN, S. C. and R. S. WHITE, *Phys. Rev. Letters*, **3**, 9 (1959).
2. VAN ALLEN, J. A., *Report of the Space Science Board of the Nat. Acad. of Science-Nat. Res. Council*, Chap. VII, February (1960).
3. VAN ALLEN, J. A. and L. A. FRANK, *Nature, Lond.* **183**, 430 (1959).
4. POMEROY, D., *Proc. 2nd Conf. on Nuclear Radiation Effects on Semiconductor Devices, Materials and Circuits* p. 71. Cowan, New York (1959).
5. SCHAEFER, H. J., *Astronautics*, 36 (1960).
6. BALL, W., Hughes Aircraft, private communication.
7. BROWN, W., Bell Telephone Laboratories, work performed on contract AF 33(616)-6235 WADC.
8. HULTEN, W. C., Technical Note D-718, *Irradiation Effects of 22 MeV and 240 MeV Protons on Several Transistors and Solar Cells* (1960).
9. LEVY, G. F., R. R. FOUSE, and S. V. CASTNER, *Proc. 2nd Conf. on Nuclear Radiation Effects on Semiconductor Devices, Materials and Circuits*, p. 76. Cowan, New York (1959).
10. KUTZSCHER, E. W., *Proc. Inst. Radio Engrs.*, N.Y. **47**, 1520 (1959).

Vol. 1 1961

Infrared Physics, 1961, Vol. 1, pp. 209–211. Pergamon Press Ltd., Printed in Great Britain.

RECOMBINATION RADIATION AND PHOTOCONDUCTION EFFICIENCY IN LEAD SULPHIDE LAYERS

G. F. J. GARLICK and H. CHECINSKA*

Department of Physics, University of Hull, England.

(*Received* 2 *August* 1961)

Abstract—Correlation is found between the efficiency of infrared emission due to band to band transitions in lead sulphide layers and the photoconduction efficiency. Correlation is also found between the emission and the decay time for the photocurrent. Commercial cells with evaporated layers were studied. Good cells have decay times of the order of 300 μsec while bad cells have times of the order of 30–50 μsec. From comparison with estimated intrinsic life times in lead sulphide and from other considerations it is concluded that the efficiency of emission in such layers can approach 50 per cent. Considerable improvement in emission efficiency is obtained by cooling the layers, the photoconductivity efficiency approaching that for radiation noise limitation.

THE occurrence of infrared emission from lead sulphide layers in the 2·5 μ region when excited with shorter wavelength radiation was first reported by Galkin and Korolev in 1953.[1] The emission spectrum at room temperature and liquid air temperature was measured by Garlick and Dumbleton[2] and later the excitation spectrum was determined by Garlick and Fatehally.[3]

In his paper at the Atlantic City Conference on Photoconductivity in 1954, Petritz[4] provided an analysis of the relations between lifetime and photoconduction sensitivity in which he showed that the limit of detection was set by the radiative recombination life time of carriers. In the discussion which followed that paper, Rose concluded that lead sulphide cells should be good infrared emitters. This is so as shown by the work referred to above. Moss in the same discussion[4] gave an estimate of intrinsic lifetime in lead sulphide of the order of 300–400 μsec, the usual lifetime of cells being of the order of 100 μsec.

We have recently been able to compare the photoconduction and radiative emission characteristics of a number of commercial lead sulphide cells at room temperature and have found correlation between high sensitivity, high emission efficiency, and long carrier lifetimes. The results are reported and discussed below.

EXPERIMENTAL ARRANGEMENTS

The cells were excited by a tungsten lamp using filters which transmitted radiation between 1 and 1·8 μ. The total emission band was measured by use of a selected lead sulphide cell or in some cases a lead telluride cell and a germanium filter, transmitting radiation of wavelengths greater than 1·8 μ. Tests for stray light signals etc. were made by substituting a magnesium oxide surface for the lead sulphide layer under investigation. Such signals

* On study leave from the Technical University of Warsaw.

were found to be negligible. Photoconductivity response was measured at 1·8 μ for all the cells using monochromatic radiation. Radiation in all experiments was chopped at 800 c/s and a narrow band 800 c/s amplifier, rectifier and meter or pen recorder used as the measuring system. For measurement of photocurrent decay the cells were excited with repetitive light pulses of a few μsec duration, the amplified cell response being displayed on an oscilloscope screen and photographed.

EXPERIMENTAL RESULTS

Figure 1 shows the relation between photoconductivity response and infrared emission efficiency. Each point represents the mean value for one cell designated by a number or

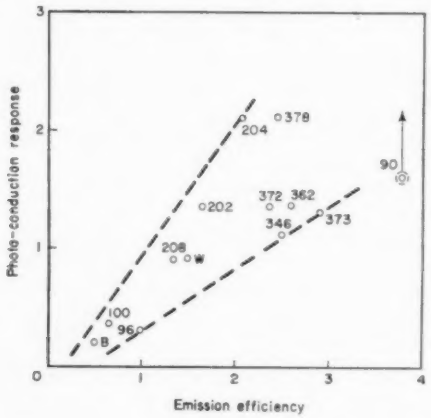

FIG. 1. Relation between photoconduction response and infrared emission efficiency (axes in arbitrary units). Numbers and letters specify individual cells.

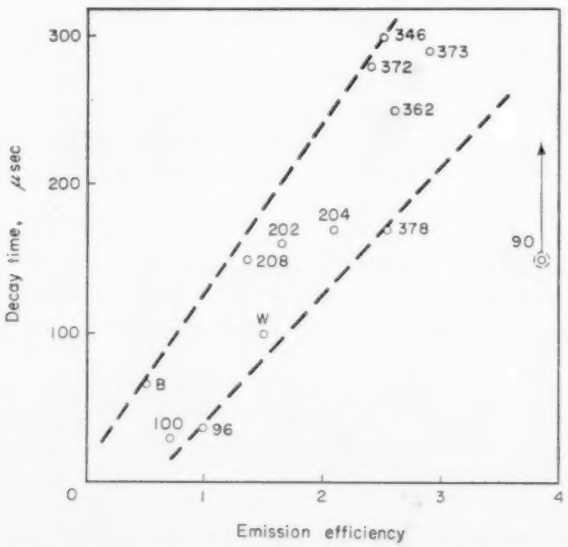

FIG. 2. Relation between photocurrent decay time and infrared emission efficiency (latter in arbitrary units).

Vol. 1 1961

letter. It will be seen that there is a definite correlation between radiative recombination and photoconduction efficiency. The cell No. 90 was a little exceptional as it had a very small sensitive spot in its layer and this made any experimental setting difficult as far as photoconduction was concerned. Such sensitivity over all the interelectrode region, as for the normal cells, would push up the position of this cell point to a place within the limits shown. Figure 2 shows the correlation between the emission efficiency and the carrier lifetime (time to decay to half initial value) obtained from the measurement of photocurrent decay. Omitting the cell No. 90, one can see that as expected from theory [4] the very poor cells have short carrier lifetimes ($\sim$50 μsec). The good cells have lifetimes between 150 and 300 μsec. The best of these would appear to reach the limit of Moss's estimates [4] and so the absolute efficiency of emission must be in the neighbourhood of 50 per cent. Estimates of absolute efficiency are difficult to obtain with accuracy and our best attempts give between 10 and 50 per cent. However, it is certain that lead sulphide layers are as efficient infrared emitters as some of the best phosphors emitting in the visible region.

In these experiments the "dark" noise of the cells showed little correlation with the photoconduction efficiency. In all cases the noise was a factor of at least 8 above the amplifier noise. It was found that cell No. 90 had a very low noise level and this suggests, together with the other remarks on noise above, that barriers in the layer must be the chief noise sources. Cell No. 90 has only a very limited region of photoconduction sensitivity characteristic of poor barrier conditions, but the emission would be characteristic of the whole layer. The latter was evident in all cells since while a relative steady emission signal was recorded for light incident on various parts of the evaporated layer the photoconductivity was sensitive to the incidence of the light on the inter-electrode region, as might be expected.

No extensive measurements have yet been made on these cells at lower temperatures than room temperature but evidence obtained indicates that as in previous studies [3] the emission efficiency and the decay time increase markedly with fall in temperature. This suggests that trapping of one kind of carrier increases the life time and probability of radiative recombination of the other carriers. In chemically deposited layers sensitised for photoconduction and infrared emission by heat treatment in an oxidising atmosphere the effect of trapping is more marked. Efficiencies of photoconduction and infrared emission are about the same as those for the commercial cells made by evaporation techniques.

These experiments are of a preliminary nature but indicate the importance of a study of radiative recombination in investigations of the optimum performance of infrared photoconductors.

Acknowledgement—We are much indebted to Messrs. Mullard Ltd. for the loan of lead sulphide cells for these experiments.

REFERENCES

1. Galkin, L. N., and N. V. Korolev, *Dokl. Akad. Nauk S.S.S.R.* **92**, 529 (1953).
2. Garlick, G. F. J., and M. J. Dumbleton, *Proc. Phys. Soc.* B. **67**, 442 (1954).
3. Garlick, G. F. J., and R. A. Fatehally, *Solid State Physics in Electronics and Telecommunications*, Vol. IV, p. 1. Academic Press, New York (1960).
4. Petritz, R. L. *Photoconductivity Conference*, p. 49, John Wiley, New York (1956).

Infrared Physics, 1961, Vol. 1, pp. 212–224. Pergamon Press Ltd., Printed in Great Britain.

AN EXPERIMENTAL STUDY OF ENERGETIC PROTON RADIATION EFFECTS ON IRI LEAD SULFIDE INFRARED DETECTORS*

R. P. DAY, R. A. WALLNER and E. A. LODI

Lockheed Aircraft Corporation Missiles and Space Company,
Sunnyvale, California, U.S.A.

(*Received* 1 *August* 1961)

Abstract—The effects of 12 MeV protons on IRI PbS detectors were measured dynamically for both integrated flux (protons/cm²) and flux (protons/cm² sec). The integrated flux reached $6{\cdot}4 \times 10^{12}$ protons/cm² and the flux ranged between 10^3 and 4×10^8 protons/cm² sec. The detectors exhibited no rate (flux) effects. Recoverable damage occurred for integrated fluxes of about 6×10^{11} protons/cm². Additional investigations included long term bias effects, and vacuum effects. The results of the investigation show that detector orbit lifetimes for proton damage for 12 MeV protons are on the order of 3 y.

Vol.
1
1961

INTRODUCTION

EXPERIMENTAL studies of the effects of energetic particles on infrared detector performance are necessary because of the anticipated use of these detectors in satellites which will pass through the Van Allen radiation zones. Representative neutron and gamma radiation work is listed in the bibliography.[1–8] These studies have shown that pronounced effects occur for specific doses of both gamma and neutron irradiation but little work has been done to determine the extent of proton radiation damage.

At the start of the program described in this paper, there was little evidence concerning the effects of proton irradiation on detectors and other satellite components. Therefore, a broad program was initiated to ascertain the effects of satellite environment on infrared detectors and other components. This paper describes the experimental results of a study of 12 MeV proton effects on PbS detectors.

Satellite environmental studies are concerned with penetrating radiation effects, therefore it is necessary to discuss the important aspects of the Van Allen Belt trapped radiation. The energetic particle radiation trapped in the geomagnetic field has been shown to consist actually of two belts formed by the interaction of various particles with the earth's magnetic field: (1) a hard proton component (proton belt), probably formed by strong cosmic rays from space, centered at about 11×10^3 km from the earth's magnetic axis;[9, 10] and (2) an electron component (electron belt), composed of protons and electrons from the sun, centered at about 22×10^3 km from the earth's magnetic axis.[11–14] The electron belt extends through the region occupied by the proton belt.[15] An estimate of the proton

* This report is part of the detector behavior study being conducted by Subsystems G, LMSC, under U.S. Contract No. AF 04(647)-564.

particle radiation trapped in the proton belt has been summarized by Dessler[16] and is partially reproduced in Table 1.

It is impossible to duplicate exactly the energy spectrum of the Van Allen belt with one accelerator because most accelerators produce protons in a limited energy range. Therefore, radiation experiments of this kind must be performed for different energies on different accelerators and the results collated.

TABLE 1. PROTON RADIATION TRAPPED IN THE PROTON BELT

Proton radiation	Flux (p/cm² sec)	Particle energy
Auroral protons (altitudes above 100 km)	Normally 10^4 to 10^6 with $E > 100$ MeV	Integral spectrum for 100 keV $< E <$ 800 keV. Varies between E^{-1} and $E^{-3.3}$
Van Allen protons ($\pm$ 40° from integral invariant equator, altitudes from 10^3 to 8×10^3 km)	Up to about 10^4	$E^{-0.8}$ integral spectrum above 40 MeV. No radiation observed with $E > 700$ MeV
Solar flare protons—relativistic	Usually 10 to 10^2 occasionally to 10^4	$E > 1$ BeV and usually less than 10 BeV
Solar flare protons—non-relativistic	Usually 10^2 but occasionally to about 10^4	From 30 to 300 MeV, E^{-1} to E^{-6} integral spectrum. For a typical large solar flare event, initial integral spectrum might be represented by 3×10^{10} E^{-4} protons cm^{-2} sec^{-1}, where E is proton energy in MeV. This spectrum should not be applied below 30 MeV
Cosmic rays (interplanetary space)	2 ± 0.3 for $E > 40$ MeV (near maximum of sunspot cycle)	$E^{-1.5}$ integral spectrum for $E > 10$ BeV
Cosmic ray albedo, or "splash albedo" (within 10 earth radii)	1 near top of atmosphere	1–10 MeV

PROGRAM AND OBJECTIVES

The objectives of the study reported on in this paper were (1) to determine the change in the infrared performance of specific detectors for 12 MeV protons and (2) to determine possible limitations of use for these detectors in the trapped proton zone.

The program consisted of the irradiation of Infrared Industries PbS detectors and the dynamic measurement of their infrared performance. The dynamic measurements consist of the simultaneous infrared and proton irradiation of the detectors and the dynamic measurement of their infrared performance. Both flux (protons/cm² sec) and integrated flux (protons/cm²) effects were investigated at various chopping frequencies. Secondary investigations were to determine the effects of vacuum and long term bias on these detectors.

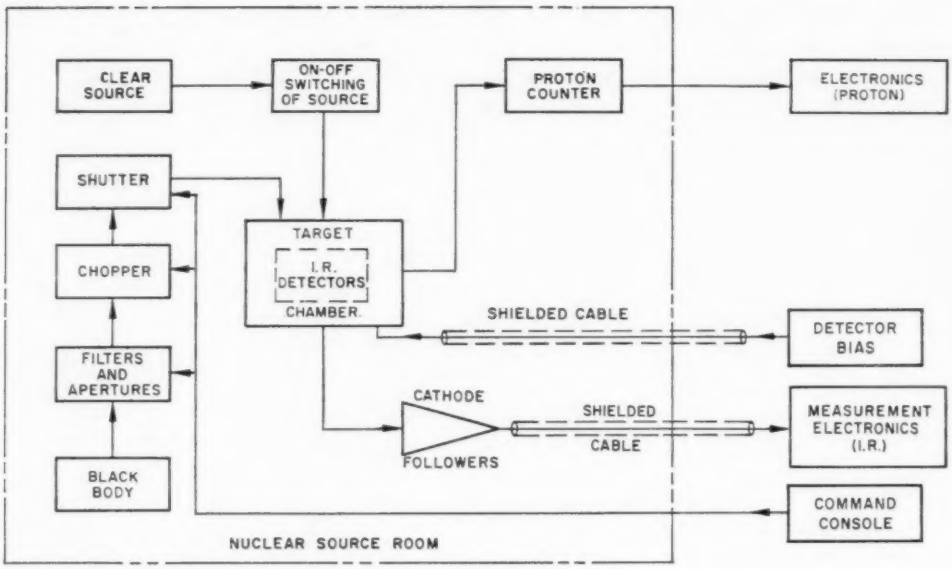

FIG. 1. System block diagram.

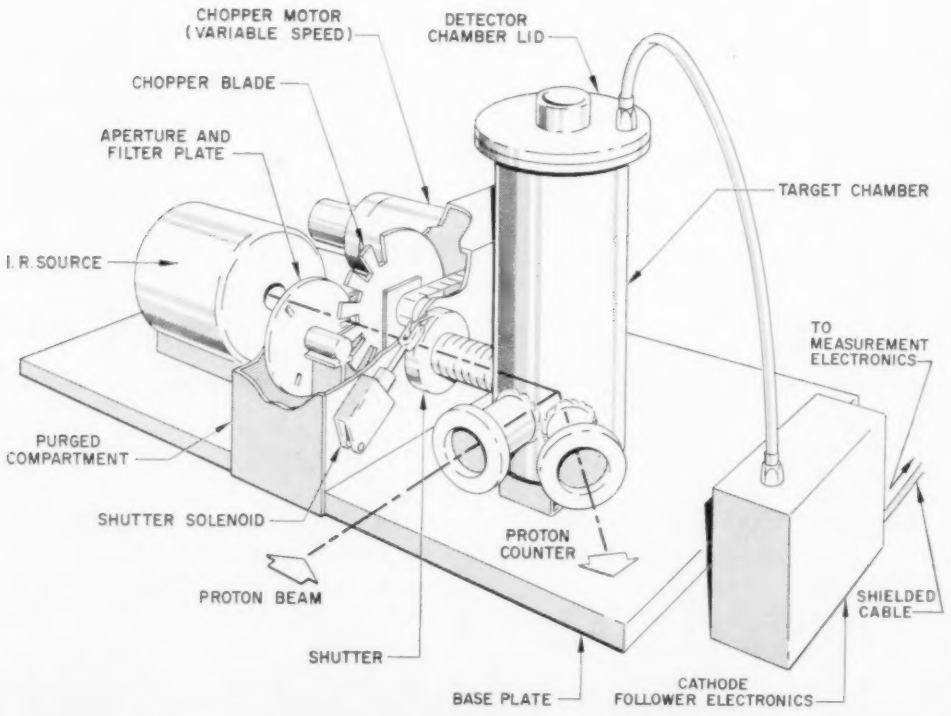

FIG. 2. Assembly drawing for infrared detector evaluation.

Vol. 1 1961

EQUIPMENT

A block diagram of the overall infrared measurement system is shown in Fig. 1. The measurement and calibration equipment were located in the cyclotron room about 75 ft from the control console. The calibrations were performed remotely through the long cables because of the radiation hazard at the cyclotron beam exit.

Figure 2 is an assembly drawing of the infrared detector evaluation equipment.

Infrared Equipment

The blackbody source shown in Fig. 2 is operated at 600 °C and is located 49·5 cm from the detectors located on the coolant chamber arm. The aperture plate limits the energy from the blackbody and has three adjustable apertures, two of which are covered by selected radiation filters. Filter–aperture combinations may be remotely switched into position. Each aperture is adjustable in width to normalize the energy from each filter-aperture combination.

The slit boundaries for each of the apertures and the variable speed chopper blade pass through a common center so that the modulated signal approximates a square wave. Signal and noise measurements are facilitated with the remotely operated shutter.

The infrared beam enters the exposure tank through a vacuum sealed sapphire window.

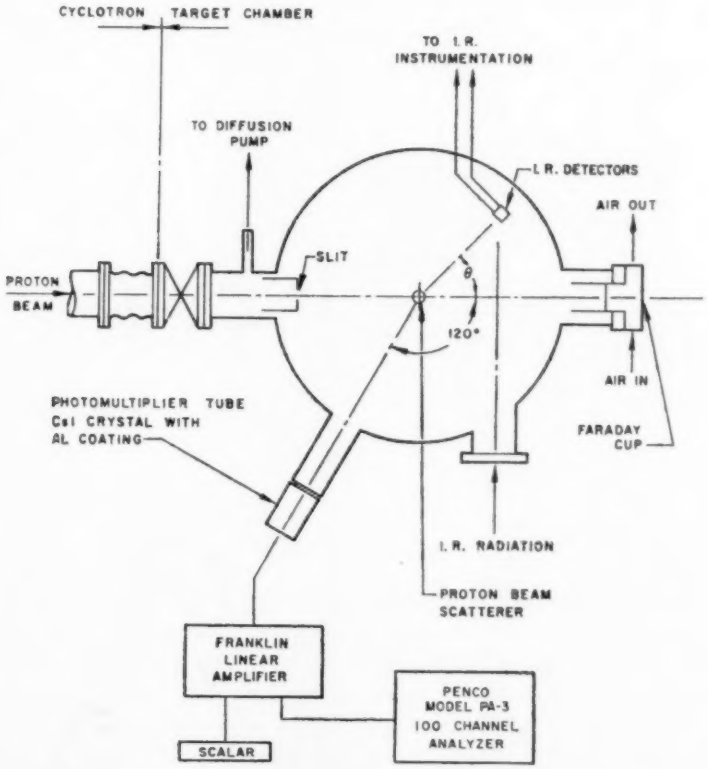

FIG. 3. Schematic diagram showing proton irradiation of cell.

Beam scattering is reduced inside the chamber by baffles. The entire infrared system is light tight and may be purged if necessary.

The target chamber is schematically shown in Figs. 3 and 4. The coolant-chamber arm, with the detectors mounted, is positioned at the point labeled IR detector in Fig. 3 during a proton experiment or during an infrared calibration. The detector coolant tank is designed to maintain the detectors at any temperatures from 100 °C to −196 °C. Up to 20 of the PbS detectors could be accommodated on the removable arm attached to the bottom of the coolant tank.

Nuclear Equipment

Basically the nuclear equipment consisted of the target chamber, equipment to monitor and control the proton beam, and the vacuum equipment with adaptors so the equipment could be attached to the accelerator. The target chamber is shown in Figs. 3 and 4. A gold

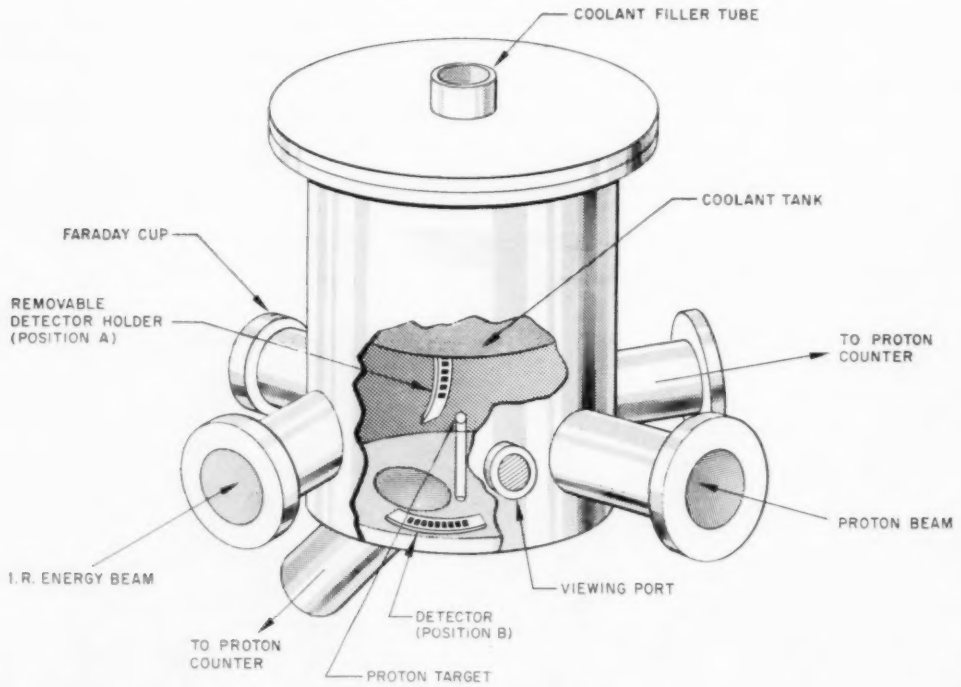

Fig. 4. Schematic diagram of IR detector target chamber.

target was used to scatter the proton beam so that the flux on the detectors could be decreased to the point where it would be compatible with the fluxes encountered in the Van Allen belt with little or no change in the proton energies. An air-cooled Faraday cup was used to collect and dissipate the proton energy not scattered by the gold target. After passing through the beam defining slits, the proton beam was about 7 mm in diameter.

The integrated proton flux was measured periodically by turning off the beam.

The proton flux was measured with scintillation counters at low flux levels and by beam current measurements at the higher flux levels. The integrated flux was measured when the

Vol. 1 1961

beam was turned off by reading the integrated count on the scaler. The proton energy distribution was measured with a 100 channel analyzer. Proton fluxes at the detectors were calculated from Rutherford scattering formulas.

INFRARED DETECTORS

Two types of IRI PbS detectors (Infrared Industries Inc.) were used in this study; they were designated by the manufacturer as type 101 and type Z. The type 101 detector has a protective coating of a quarter wave thickness of silicon monoxide. The detector sensitive area is 0·0638 by 0·0425 cm or 0·0029 cm². The type Z detector has a thick (0·7 mm) covering of quartz over the sensitive area which is 0·399 cm by 0·030 cm or 0·0123 cm². The PbS film is estimated to be 1 to 2 μ thick.

CALIBRATION PROCEDURE

All calibrations are done with the detectors located on the coolant chamber arm. The electronics are calibrated by inserting a test signal of known amplitude at the preamp input. The calibration signal is adjusted in frequency until all four of the fixed frequency tuned voltmeters are calibrated. The detectors drive cathode followers which in turn drive the preamp through the long cables. Each cathode follower is adjusted to a gain of exactly 0·5 and the tubes are all aged for minimum drift. Through the entire experimental sequence no drift was observed in the cathode followers.

At the completion of the calibration of the electronics, the detectors are calibrated

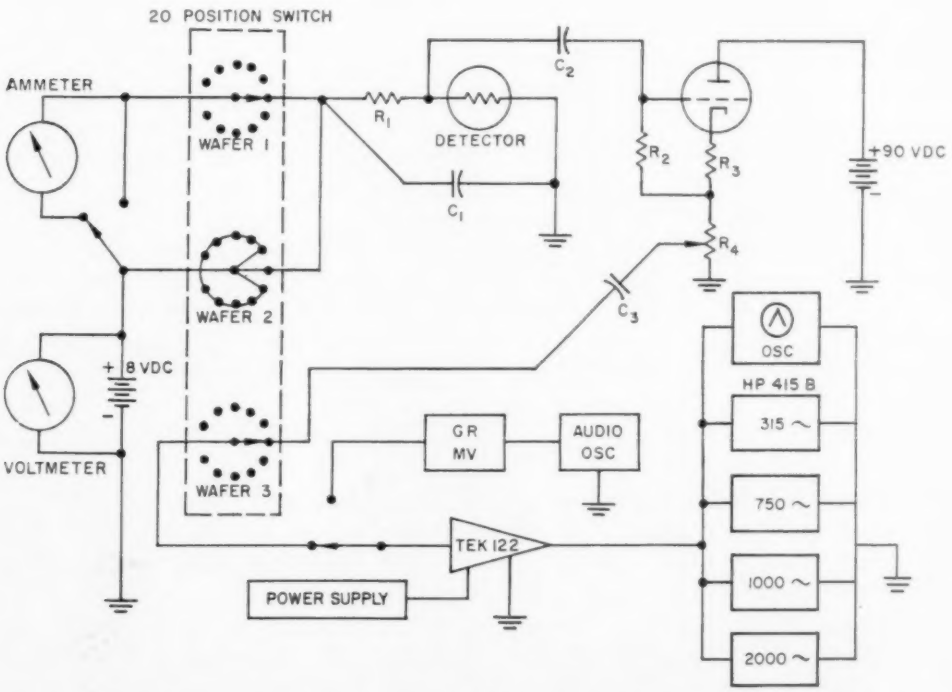

FIG. 5. Schematic diagram of an individual detector electrical measurement circuit.

sequentially. Signal measurements are made at each center frequency of the tuned voltmeters by adjusting the chopper frequency. The shutter is then closed and the noise is read at each frequency and the detector bias conditions are recorded. The sequence continues until all detectors have been calibrated. During long exposures calibrations of the electronics are performed periodically and the chopper is readjusted to the center frequency of the voltmeters if required. The center frequencies (and noise bandwidths) are 315(25), 750(37), 1000(49), and 2000(107) c/s.

The switching circuit shown schematically in Fig. 5 allows the sequential measurement of each detector while the other detectors are kept biased. Three long cables (75 ft each) are used to bring the signals from the cathode followers to the measurement console, provide detector bias from the measurement console, and to provide power and commands from the infrared measuring equipment in the cyclotron room.

All low level circuits are battery operated and isolation transformers and heavy grounding buses are also used to eliminate spurious signal sources. The vicinity of the cyclotron abounds in electrical interference. By following these procedures measurements were able to be made where the peak to peak value of any periodic (observed on an oscilloscope) interference was no more than twice the peak to peak value of the detector noise, and generally was less. Detector support arm temperatures were measured with thermocouples.

Vol. 1 1961

EXPERIMENTAL PROCEDURE

Normally the cyclotron was available for a period of 16 hr. The first 4 hr were required to align and calibrate the proton beam. The remaining time was used for irradiation and was divided into two parts so that if effects were noted during the first part of a run, a second set of detectors could be exposed under the same conditions in the second part of the experiment. If no effects were noted the initial experiment was continued for the remainder of the irradiation time.

Usually 2 or 3 detector arms were taken to the irradiation site. One set of detectors was used as control detectors and the second set (s) were irradiated. The control detectors were exposed to neither proton irradiation nor vacuum.

To minimize the possibility of not observing rapid self-annealing after damage, detectors 1 and 2 were measured frequently during and after each proton exposure; the other channels were measured whenever experimental conditions permitted. At the beginning of an irradiation, the proton beam was held to low levels to avoid overshooting possible thresholds. To decrease the total irradiation time, the flux was increased as the irradiation continued.

RESULTS

There are two dynamic experiments reported in this paper. Others are planned and will be reported later. The purpose of the first experiment was to determine flux effects. The flux ranged between 10^3 and 6×10^5 protons/cm^2 sec without producing an observable effect. The integrated flux reached 3×10^9 without an effect.

The second experiment was to determine integrated flux effects. The initial part of the experiment confirmed the results of the first experiment. As the integrated flux reached higher values a proton effect was observed. The details of the results are discussed below for each experiment separately.

First Experiment, 4–5 April 1960

In this initial investigation of rate effects, the infrared and nuclear instrumentation operated satisfactorily. For the fluxes and integrated fluxes already mentioned, there was no observable effect in either signal or noise caused by proton irradiation. A total of 12 detectors were irradiated. The type 101 detectors exhibited a slight increase in signal after being subjected to the accelerator vacuum; the type Z detectors exhibited no increase. This difference in response is attributed to the different vacuum responses of the detector protective coverings. There was no change in either bias current or bias voltage and no temperature changes were noted. Thus, it was concluded that there was no 12 MeV proton rate effect for fluxes between 10^3 and 6×10^5 protons/cm² sec and there was no effect for integrated fluxes of 3×10^9 protons/cm².

Second Experiment, 20–21 June 1960

Integrated flux effects were investigated in this experiment. Ten detectors were mounted on an arm located at the bottom of the storage reservoir 45° (forward scattering) from the incident proton beam on a 3 in. radius from the gold scatterer. There were 5 of each type of detector alternately spaced on the arm. Six detectors were also placed on the bottom of the exposure tank on a 4·77 in. radius from the scatterer with three detectors of each type alternately spaced on the arm; these detectors received a lesser integrated flux and were placed outside of the infrared beam so that dynamic infrared measurements were not made.

Dynamic measurements showed that definite degradations occurred for both types of detectors at integrated fluxes of about 6×10^{11} protons/cm². Typical detector results are shown in Figs. 6 (type 101) and 7 (type Z). The noise results have been normalized to a noise bandwidth of 8 c/s with the assumption that the detector noise is white within our measuring bandwidths. Note that infrared calibrations were taken 164 min prior to the start of irradiation and before the detectors were subjected to a vacuum. The next calibration,

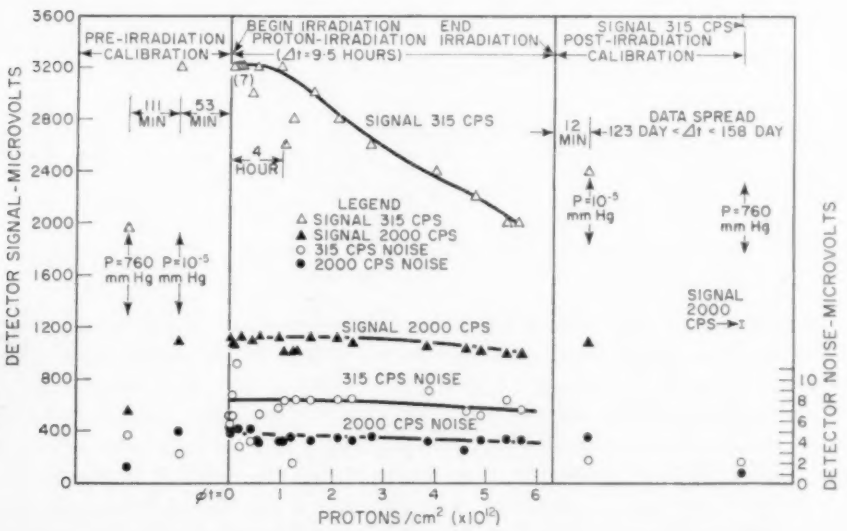

FIG. 6. Experimental signal and noise data for detector type 101-31 (20–21 June, 1960).

taken 53 min before the first proton beam, was at a pressure of 5×10^{-5} mm of Hg. The average signal increase ranged from 1·5 to 2 times higher for the latter calibration. The effect of high vacuum on these detectors is briefly described later.

The probable explanation for this effect is that the detector performance had deteriorated because of uncontrollable storage conditions at the accelerator prior to the irradiation. The signal improvement because of the vacuum apparently improved the surface state and contributed to a return to the previous photoconductivity. This vacuum improvement was noted for both types of detectors indicating that the vacuum isolation achieved by quartz coverings is by no means complete.

The possibility of overshooting integrated flux thresholds in the beginning of the experiment was avoided by irradiating for very short times initially. Two detectors were monitored continuously during this period to ascertain the occurrence of any changes during the exposure time. Figures 6 and 7 show that there was no effect for integrated fluxes less than about 10^{11} protons/cm^2.

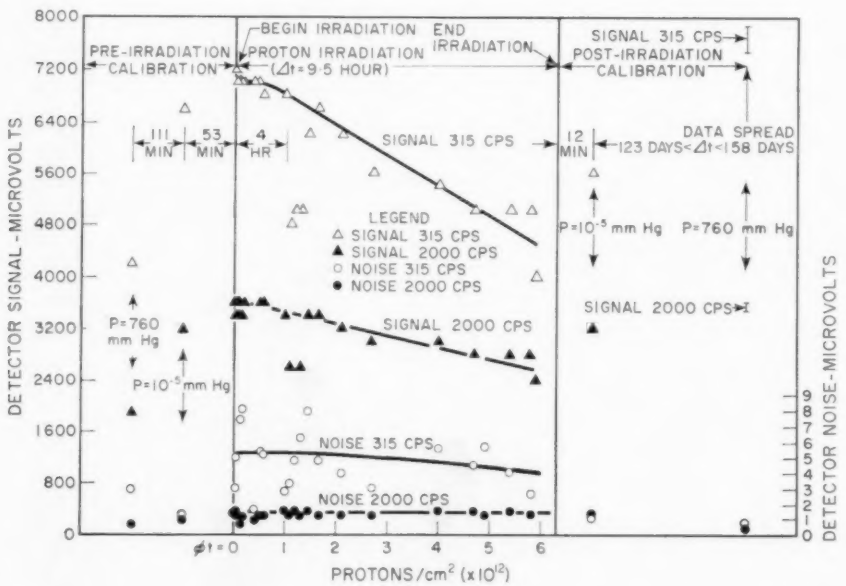

FIG. 7. Experimental signal and noise data for detector type Z-32 (20–21 June, 1960).

The IR measuring system was periodically calibrated and the calibration readings were essentially the same as those taken before the initial proton exposure. At an integrated flux of about 6×10^{11} protons/cm^2, a general degrading of the signal voltage began and continued throughout the remainder of the irradiation. The signal noise, signal to noise, and time constant for the various chopping frequencies and the dark resistance data are listed in Table 2 for the type 101 detectors and in Table 3 for the type Z detectors.

Note that recovery for the detectors shown in Figs. 6 and 7 occurs immediately after the proton beam is turned off. The recovery continues until the detector completely recovers. It is likely that there is an integrated flux where permanent non-recoverable

Vol. 1 1961

damage will take place. This point was not reached with the integrated fluxes reached in this experiment.

Tables 2 and 3 show that the signal voltages for the type 101 detectors decreased in the range of 12–37 per cent from the beginning of irradiation to the end of irradiation for 2000 and 315 c/s chopping frequencies, respectively, while the type Z detectors exhibited a 13–24 per cent change when compared to the values before proton exposure. The noise measurements were made by visually integrating the voltmeter fluctuations over a short time so that one might expect rather large variations. The noise data for both types of detectors are erratic probably because of the short integration time and the noise caused either by proton irradiation or some other wide band influence.

The data in Tables 2 and 3 show that there was degrading of the detector signal beginning at an integrated flux of about 6×10^{11} protons/cm^2, and that the 315 c/s measurements were more affected than the 2000 c/s measurements. The interpretation of the noise data is not straightforward for the reasons already stated. It is clear, however, that $1/f$ type noise is present in these detectors.

A vacuum calibration was performed 12 min after the final proton beam exposure. The signal showed a definite recovery in this short period. This same self-annealing effects was noted for each detector after the end of a proton exposure. Figures 6 and 7 show the post calibration data taken over a 158 day period after the irradiation; the standard deviation

TABLE 2. NORMALIZED IRI LEAD SULFIDE DETECTOR TYPE-101 DATA FOR 12 MEV PROTON IRRADIATION

	Modulation frequency (c/s)	Data at ϕt_1 / Data at ϕt_0 $\times 100$ (%)*	Data at ϕt_2 / Data at ϕt_0 $\times 100$ (%)†	Change in data due to protons (%)‡
Signal data	315	98·7 ± 6·0	61·5 ± 4·2	37·2 ± 10·2
	750	97·8 ± 3·9	67·9 ± 4·0	29·9 ± 8·8
	1000	100·7 ± 2·5	68·9 ± 3·0	31·8 ± 5·5
	2000	103·2 ± 4·4	90·8 ± 7·9	12·4 ± 12·3
Noise data	315	215·2 ± 15·8	135·6 ± 6·8	79·6 ± 22·6
	750	69·4 ± 12·8	59·3 ± 2·7	10·1 ± 15·5
	1000	75·4 ± 2·8	81·2 ± 8·2	(+) 5·8 ± 11·0
	2000	69·3 ± 3·7	72·4 ± 4·4	(+) 3·1 ± 8·1
Signal/noise data	315	45·9 ± 11·0	45·4 ± 11·0	0·5 ± 32·8
	750	140·9 ± 16·7	114·5 ± 7·6	26·4 ± 24·3
	1000	133·6 ± 5·3	84·8 ± 11·2	48·8 ± 16·5
	2000	148·9 ± 8·1	125·4 ± 12·3	23·5 ± 20·4
Time constant data	—	92·1 ± 5·1	79·8 ± 4·0	12·3 ± 9·1
Dark resistance data	No change noted			

* where ϕt_0 is the integrated flux at time zero, i.e. 0 protons/cm^2
where ϕt_1 is the integrated flux at the beginning of effect, i.e., 6×10^{11} protons/cm^2
† where ϕt_2 is the integrated flux at the end of the experiment, i.e., $6{\cdot}32 \times 10^{12}$ protons/cm^2
‡ where (+) indicates an increase

Table 3. Normalized IR1 Lead Sulfide Detector Type-Z Data for 12 MeV Proton Irradiation

	Modulation frequency (c/s)	Data at ϕt_1 / Data at ϕt_0 × 100 (%)*	Data at ϕt_2 / Data at ϕt_0 × 100 (%)†	Change in data due to protons (%)‡
Signal data	315	95·0 ± 1·5	71·2 ± 1·4	23·8 ± 2·9
	750	95·4 ± 2·8	72·7 ± 4·2	22·7 ± 7·0
	1000	98·8 ± 2·1	72·3 ± 2·9	26·5 ± 5·0
	2000	100·7 ± 4·3	87·6 ± 6·7	13·1 ± 11·0
Noise data	315	111·1 ± 1·4	68·4 ± 14·1	42·7 ± 15·5
	750	93·2 ± 7·1	73·3 ± 8·5	19·9 ± 15·6
	1000	90·9 ± 3·7	93·9 ± 18·0	(+) 3·0 ± 21·7
	2000	104·4 ± 2·8	114·6 ± 2·6	(+) 10·2 ± 5·4
Signal noise data	315	85·5 ± 2·9	104·1 ± 15·5	(+) 18·6 ± 18·4
	750	102·3 ± 9·9	99·2 ± 12·7	3·1 ± 22·6
	1000	108·7 ± 5·8	77·0 ± 20·9	31·7 ± 26·7
	2000	96·4 ± 7·1	60·0 ± 9·3	36·4 ± 16·4
Time constant data	—	102·4 ± 3·3	93·1 ± 6·9	9·3 ± 10·2
Dark resistance data	No change noted			

* where ϕt_0 is the integrated flux at time zero, i.e., 0 protons/cm²
where ϕt_1 is the integrated flux at the beginning of effect, i.e., 6×10^{11} protons/cm²
† where ϕt_2 is the integrated flux at the end of the experiment, i.e., $6{\cdot}23 \times 10^{12}$ protons/cm²
‡ where (+) indicates an increase

for these readings under controlled environmental conditions is shown as a vertical line. These final calibrations were taken with no vacuum.

It is noted that if the detectors were exposed to a much larger integrated proton flux they would probably be sustained permanent damage as was reported by Billups [8] and that their recovery rate is probably dependent on the extent of damage.

The detectors located at the bottom of the tank were not calibrated at the cyclotron. If any damage had occurred the detectors had fully recovered by the time they were again measured at the LMSC laboratory. The integrated flux for these detectors varied from $1{\cdot}3 \times 10^{12}$ to 4×10^{11} protons/cm² because each detector was located at a different scattering angle.

No trend was observable for the reported integrated fluxes in the dark resistance measurements. Tables 2 and 3 give data for apparent time constants. The time constant is computed from signal versus chopping frequency curves. The time constant is defined in terms of the frequency where the detector response is 3 dB down. The time constants shows a 20 per cent decrease at the end of the irradiation experiment. The time constants are partially affected by vacuum and by the proton beam and generally recovers to its pre-irradiation value for the integrated fluxes encountered.

For this experiment no spectral measurements were made and the detectors were measured only at one temperature. The additional capability is available and may be used in future experiments.

Vol. 1 1961

ADDITIONAL EXPERIMENTAL INVESTIGATIONS

To make sure that instrumentation difficulties did not cause the effect observed in the proton experiment, additional laboratory measurements were made to determine possible effects. These additional measurements were: (1) changing electronic bias voltages, (2) maintaining long term bias on the detectors, and (3) subjecting the detectors to vacuum while making dynamic measurements.

The bias voltage changes on the electronic preamps produced no output signal change for a 10 per cent supply voltage variation. This is not unexpected and it is certain that supply voltages did not vary more than this amount during the exposure times. The d.c. bias was maintained on the detectors for an 11-day period. During the first 5 or 6 days some variation was noted then there was no change in the signal for the remaining test period.

A vacuum study was conducted because of the large increase in signal observed during the second irradiation experiment which was attributed to the detector's being placed in a vacuum. It was impossible to duplicate the environment encountered immediately before the proton irradiation so the detectors used in the vacuum study were maintained under normal laboratory environment. The brief study showed that for these detectors no effect occurred from atmospheric pressure to about 5×10^{-3} mm Hg. At this point there was a decrease in signal until about 1×10^{-4} mm Hg. The signal then increased until the limit of the vacuum system's capability was reached, $3{\cdot}5 \times 10^{-5}$ mm Hg. The detectors were maintained at each pressure for about a half hour in this experiment; when the cyclotron pressure was reached (5×10^{-5} mm of Hg) the detectors were maintained at this pressure for times simulating the time the detectors were evacuated during irradiation experiments. During this time the signal did not change but remained at its higher level indicating that the film had probably become sufficiently decontaminated. Thus the effect observed in the cyclotron was not due to a long term vacuum effect but to proton effects.

CONCLUSIONS

As a result of these first experiments the following conclusions have been reached.

1. The signal recovery begins as soon as the proton beam is turned off.
2. The time constant decreases as the signal decreases.
3. There is no noise increase for flux to 6×10^5 protons/cm^2 sec.
4. There was no observed dark resistance change.
5. The percentage signal decrease is less at 2000 c/s than at 315 c/s.
6. The signal is rate independent up to at least 4×10^8 protons/cm^2 sec.
7. Integrated flux threshold for signal change is about 6×10^{11} protons/cm^2.
8. The detector infrared performance is affected by vacuum and other environmental effects making exact repeatable absolute measurements difficult.
9. Environmental effects other than proton effects may produce even greater changes.
10. The quartz detector covering (0·7 mm thick) provides greater protection than the thin film of silicon monoxide.

Note: the conclusions are for proton energies of 12 Mev, for a flux ranging between 10^3 and 4×10^8 protons/cm^2 sec, and for an integrated flux less than $6{\cdot}4 \times 10^{12}$ protons/cm^2.

RECOMMENDATIONS FOR FUTURE IRRADIATION EXPERIMENTS

1. Pre-calibrations and post-calibrations should be performed at irradiation facility if practicable. Preferably, calibrations should be days in duration.

2. Future experiments should include additional vacuum, spectral, bias, and temperature investigations.
3. Dynamic experiments are preferred; care must be taken to reduce spurious signals caused by intense accelerator fields.
4. Continuous data recording systems should be used in dynamic experiments to obtain more data and to eliminate reading and copying errors. Personnel fatigue through long experiments is a factor.
5. Experiment should be designed to make use of punched card data reduction. Determining statistical effects is greatly facilitated by machine computations.

RECOMMENDATIONS FOR SATELLITE OPERATION

1. More data is needed for all energetic particles at various energies. Investigations should include other environmental effects such as vacuum, temperature, long term bias, etc.
2. A system design should consider the possibility of exploiting less severe percentage signal degradation at higher chopping frequencies.
3. For greatest stability the detectors should be left biased.
4. If possible, include inflight infrared calibration for detectors.
5. Consider the effects of secondary particle production caused by interaction of high energy primary particles with satellite skin and other shielding.

Vol. 1 1961

REFERENCES

1. JUNGA, F. A., and R. S. KROGSTAD, *Nuclear Radiation Effects on Infrared Materials and Components Part II*, Lockheed Missiles and Space Division, LMSD-5929, Sunnyvale, Calif., (1960).
2. BISBEE, J., *Effects of Nuclear Radiation on IRI PbS Detectors*, Baird-Atomic, Inc., Memorandum, Cambridge, Mass. (1959).
3. BISBEE, J., *Further Radiation Tests on IRI PbS Detectors*, Baird-Atomic, Inc., Cambridge, Mass. (1959).
4. READY, J. F., *Gamma Irradiation Effects on Infrared Detector*, Honeywell Research Center, Hopkins, Minn.
5. ENSLOW, G. F., F. A. JUNGA, and W. W. HAPP, *Gamma Radiation Effects in Silicon Solar Cells*, Lockheed Missiles and Space Division. LMSD-5137, Sunnyvale, Calif. (1958).
6. WILLARDSON, R. K., F. J. REID, J. H. CAHN, L. W. AUKERMAN and E. M. MOODY, *Theoretical and Experimental Studies Concerning Radiation Damage in Selected Compound Semiconductors*, Battelle Memorial Institute, 8th Interim Progress Report, Columbus, Ohio (1959).
7. BARJON, R., *C. R. Acad. Sci., Paris*, **248**, 83 (1959).
8. BILLUPS, R. R.. and W. L. GARDNER, *Radiation Damage Experiments on PbS Infrared Detectors*, Massachusetts Institute of Technology, Lincoln Laboratory, 26 G-0002, Lexington, Mass. (1961).
9. FREDEN, S. C., and R. S. WHITE, *Phys. Rev. Letters*, **3**, 11 (1959).
10. FAN, C. Y., P. MEYER, and J. A. SIMPSON: *First International Space Science Symposium*, Amsterdam, North Holland (1960).
11. VAN ALLEN, J. A., *J. Geophys. Res.*, **64**, 1683 (1959).
12. VERNOV, S. N., A. E. CHUDAKOV, P. V. VAKULOV, and YU. I. LOGACHEV, *Dokl. Akad. Nauk S.S.S.R.*, **4**, 338 (1959).
13. WALT, J., L. F. CHASE, Jr., J. CLADIS, W. L. IMHOF, and D. J. KNECHT, *First International Space Science Symposium*, Amsterdam, North Holland (1960).
14. ARNOLDY, R.. R. HOFFMAN, and J. R. WINCKLER, *First International Space Science Symposium*, Amsterdam, North Holland (1960).
15. HOLLY, F. R., and R. G. JOHNSON, *J. Geophys. Res.*, **65**, 771 (1960).
16. DESSLER, A. J., *Satellite Environment Handbook* (Ed. by F. S. Johnson), Lockheed Missiles and Space Division, LMSD-895006, Sunnyvale, Calif., 3,1 to 3,35 (1960).

Infrared Physics, 1961, Vol. 1, pp. 225–226. Pergamon Press Ltd., Printed in Great Britain.

BOOK REVIEW

Calculation of the Brightness of Light in the Case of Anisotropic Scattering E. M. FEIGELSON, M. S. MALKEVICH, S. YA. KOGAN, T. D. KORONATOVA, K. S. GLAZOVA, and M. A. KUZNETSOVA. Academy of Sciences, U.S.S.R. Press, Moscow 1958. Translated from the Russian by Consultants Bureau, Inc., New York, 1960. $8.00.

AN INCREASING number of scientific papers are being published in recent years, both in this country and abroad, on the problem of diffuse transmission and reflection of sunlight on planetary atmospheres. This renewed interest in the subject stems partly from the fact that its theoretical aspect reduces to a non-trivial mathematical problem which can be solved numerically by means of present-day high-speed computers. On the other hand, the advent of the space age makes it imperative to develop the theory in all details in order to meet new engineering requirements and, more important still, to take full advantage of the excellent new platforms made available for the optical investigation of the terrestrial and other planetary atmospheres.

In the quantitative-theoretical realm, the model of the terrestrial atmosphere, which considers only Rayleigh scattering and Lambert reflection at the surface, but with complete results based on multiple scatterings, including the degree and plane of polarization of the emergent light, is now available for the plane parallel case, mainly with the publication of detailed tables by Z. Sekera and collaborators (1960). These authors used the method of solution developed by S. Chandrasekhar (1950). A similar treatment of more realistic models corresponding to turbid atmospheres, where the gaseous medium contains optically significant amounts of particles of a diameter comparable to the wavelength of the incident radiation, is lacking. Such models have to be considered, not only in the terrestrial case, but also in those of Venus and Mars, for example, which are known to have more or less turbid atmospheres.

In this latter problem, the work under review, published as No. 1 of the *Transactions of the Soviet Institute of Atmospheric Physics*, represents a useful contribution. Its six authors set out to solve the following particular case: What is the angular distribution and total flux of radiation emerging from the "top" and "bottom" of a two-layered, plane-parallel atmosphere, over a Lambert surface, illuminated by parallel radiation (sunlight) incident from various fixed directions with respect to the vertical. This model differs from the Rayleigh case mentioned above in several important aspects, to wit: (a) The model is not homogeneous in scattering properties. In the lower layer these differ radically from the Rayleigh case, so that the flux scattered by a unit volume into the forward hemisphere is much greater than that scattered into the backward hemisphere. In the upper layer the scattering is more symmetrical with only a small deviation from the Rayleigh pattern. (b) The scattering mechanism does not introduce polarization, hence the degree and plane of polarization of the emergent light are not determined as in the Rayleigh model. (c) Multiple scatterings are taken into account in a limited way, especially for large optical thicknesses. In other aspects, the two models are quite similar.

The method of solution, described in Chap. 1, is straightforward in that the characteristic scattering pattern is normalized and expanded in a series of Legendre polynomials which are functions of the scattering angle alone. This makes it possible to separate the dependence on zenith angle from that on the azimuth and the solution can be written in terms of a trigonometric series involving the azimuth measured from the plane containing the sun. The technique of explicit successive approximations was used rather than Chandrasekhar's solution which is based on the invariance principles of Ambartsumian. The former method, although laborious, has the advantage that the effect of successive orders of scattering can be evaluated.

The authors of the present work certainly deserve credit for undertaking the painstaking calculations involved and presenting their results in detailed numerical tables covering some forty pages. These are especially interesting since, in the choice of characteristic scattering functions, discussed in Chap. 2, the authors made an effort to fit the best available experimental data on actual conditions in the atmosphere. For the lower layer, several characteristic functions were used, with a progressively higher degree of anisotropy or asymmetry with respect to 90° scattering (the functions are axially symmetric).

Chapter 3 is devoted to a discussion of the results by means of numerous good diagrams and illustrative tables. The effects of asymmetrical scattering on the downward and upward diffuse intensities and total fluxes are interesting. It is regrettable that the authors were not able to compare their results with those of the Rayleigh model, some of which were available in published form before 1958. The neglect of

polarization is a serious shortcoming. However, especially in the most turbid and asymmetric cases treated, the new results should give a good idea of the general features of the intensity and total flux.

In general, the work under review should be considered as a first step in the correct direction, in that a detailed treatment of a clear-cut model was accomplished. Judging from the translation available to us, the presentation is clear and coherent. There are of course some points which may be criticized. For example, the relation of optical thickness to geometrical height above the ground is misleading in that the ground is represented by zero optical thickness. A Legendre expansion of only eleven terms was used. This is more than anything in the published literature, however, it is not quite sufficient to reproduce the measured anisotropy. The ratio of forward- to back-hemisphere fluxes in the characteristic function is not a sufficient criterion in matching the experimental data. It is also important to match the intensity gradient in the region of small scattering angles. The authors were apparently limited in the number of terms in the Legendre expansion by the use of slow desk computers. The same must be true in limiting the successive iterations to three or four. Also, the degree of turbidity is not clearly defined and the relative importance of Rayleigh versus non-Rayleigh scattering cannot be assessed. The bibliography is somewhat incomplete.

As far as infrared physics is concerned, the work under review has only limited applications, mainly because only perfect scattering, without true absorption, is considered. Even so, in the near infrared, in regions where there are no molecular absorption bands, the results will give a general idea of the contribution of scattering to the infrared skylight in a sunlit, turbid atmosphere, provided the measured or estimated infrared characteristic functions are matched by those used by the authors.

Although we are unable to compare the text with the original in Russian, the translators seem to have done a very creditable job. The English text reads smoothly, the terminology is correct, and the presentation of mathematical symbols and expressions excellent. The addition of figure titles would have greatly facilitated the reading, but their absence must be due to the original.

The Rand Corporation D. DEIRMENDJIAN.

Vol. 1 1961

Vol.
1
961